DO NOT TAKE FROM LIBRARY
AUG
Copy 2

# THE PHYSICAL REVIEW

VOLUME 48 | Second Series | NUMBER 3

AUGUST 1, 1935

Published for the
AMERICAN PHYSICAL SOCIETY
by the
AMERICAN INSTITUTE OF PHYSICS
Incorporated
LANCASTER, PA., AND NEW YORK, N. Y.

# THE AMERICAN PHYSICAL SOCIETY


## OFFICERS OF THE SOCIETY

R. W. WOOD, *President*
The Johns Hopkins University
Baltimore, Maryland

F. K. RICHTMYER, *Vice President*
Cornell University
Ithaca, New York

W. L. SEVERINGHAUS, *Secretary*
Columbia University
New York, New York

G. B. PEGRAM, *Treasurer*
Columbia University
New York, New York

JOHN T. TATE, *Editor*
University of Minnesota
Minneapolis, Minnesota

L. B. LOEB, *Local Secretary for the Pacific Coast*
University of California
Berkeley, California


# THE PHYSICAL REVIEW


## BOARD OF EDITORS

JOHN T. TATE, *Editor*

J. W. BUCHTA, *Assistant Editor*

*Associate Editors*

K. K. DARROW
J. C. HUBBARD
A. E. RUARK
A. ELLETT
L. A. TURNER
G. E. UHLENBECK
W. V. HOUSTON
R. S. MULLIKEN
I. I. RABI


THE PHYSICAL REVIEW, which was established in 1893, is a journal of experimental and theoretical physics. It is published for the American Physical Society by the American Institute of Physics Incorporated. There are two volumes annually with twelve issues in each volume.

**Manuscripts** for publication should be submitted to John T. Tate, University of Minnesota, Minneapolis, Minnesota.

**Proof and all correspondence** concerning papers in the process of publication, should be addressed to the Editorial Secretary, American Institute of Physics, 11 East 38th Street, New York, New York.

**Subscription price:** United States and Possessions and Canada, $15.00; Foreign, $16.50. Subscriptions and orders for back numbers should be addressed to Prince and Lemon Streets, Lancaster, Pennsylvania, or to the American Institute of Physics, 11 East 38th Street, New York, New York.

**Advertising** is not accepted for the *Physical Review* but attention is called to the *Review of Scientific Instruments with Physics News and Views*, a companion publication of the Institute, and a medium through which the field of physics can be reached most effectively. Rates and other information will be furnished on request to the Editorial Secretary.

**Changes of address** and complaints of failure to receive the *Physical Review*, in the case of members of the American Physical Society, should be addressed to the Treasurer; in the case of other subscribers, to the Editorial Secretary. New copies can be sent free in response to complaints of non-delivery only if notice of non-delivery is received within three months of date of issue.


The Physical Review is published semi-monthly at Prince and Lemon Streets, Lancaster, Pennsylvania.

Entered at the Post Office at Lancaster, Pennsylvania, as second class matter.

Acceptance for mailing at special rate of postage provided for in section 1103, Act of October 3, 1917, authorized September 6, 1926.

THE
PHYSICAL REVIEW
A Journal of Experimental and Theoretical Physics
VOL. 48, NO. 3 AUGUST 1, 1935 SECOND SERIES

# The Radioactivity of the Earth's Crust and Its Influence on Cosmic-Ray Electroscope Observations Made Near Ground Level

ROBLEY D. EVANS,* *Massachusetts Institute of Technology* AND RUSSELL W. RAITT, *California Institute of Technology*
(Received May 21, 1935)

Radium analyses of 23 rock specimens from the scene of cosmic-ray observations made by R. A. Millikan and his coworkers discloses a linear relationship between the average radium content of the terrain and the local gamma-ray ionization in the cosmic-ray electroscope. Ionization due to soft gamma-radiation stimulated in the earth's crust by the impact of cosmic rays, or due to the reflection of cosmic rays by the earth's crust is therefore negligible, and the ratio of thorium to uranium is approximately constant in the materials examined. A local gamma-ray ionization of 5.5 ion pairs per sec. per cm³, in air at one atmosphere pressure, is normally associated with a content of 1.0 $\times 10^{-12}$ g Ra per g rock in the neighboring terrain. It is shown that the gamma-ray ionization $n$ ion pairs per cm³ per sec., at $h$ cm above a broad radioactive surface is $n=(2\pi\rho mK/\mu_1)G_{\mu h}$, where $G_{\mu h}=\int_1^\infty z^{-2}e^{-\mu h z}dz$, $\mu_1/\rho$ is the mass absorption coefficient and $m$ the Ra concentration of the emitter, $\mu$ is the gamma-ray absorption coefficient of air, and $K$ is Eve's number. Application to the experimental data suggests that the Th/U ratio is the order of 5 to 10 for many common geological materials.

## INTRODUCTION

THE extra-terrestrial origin of the penetrating radiation now called cosmic rays was first demonstrated by Gockel,[1] who discovered that the residual ionization in a sealed electroscope at first decreased but then increased markedly as the instrument was raised away from the earth's surface. The initial decrease shows that a part of the residual ionization is of terrestrial origin. Whereas the bulk of this terrestrial radiation was believed to be due to gamma-radiation from radioactive elements in the earth's crust, Millikan[2] suggested that experiments were needed to demonstrate whether an appreciable fraction of this radiation was due to soft secondary rays stimulated by the cosmic rays or to cosmic rays reflected or scattered back by the earth's crust. That practically all of the terrestrial radiation is due to gamma-rays from rocks in the earth's crust has now been demonstrated by ground level and airplane comparisons of the ionization in unshielded electroscopes with the ionization in similar electroscopes shielded only from below by lead.[3] Further evidence is furnished by the cloud-chamber photographs of Anderson[4] and Blackett and Occhialini,[5] which show a pronounced distribution maximum for cosmic-ray tracks entering from vertically overhead, and also show very few tracks entering the apparatus from below. The present observations also support the conclusion that all of the terrestrial radiation is due to gamma-rays from the earth's crust, by corre-

* Experimental work done as National Research Fellow, University of California, Berkeley, 1932–1934.

[1] Gockel, Physik. Zeits. **11**, 280 (1910); Hess, Physik. Zeits. **12**, 998 (1911); **13**, 1084 (1912); Kolhörster, Physik. Zeits. **14**, 1153 (1913); Millikan and Bowen, Phys. Rev. **27**, 353 (1926).

[2] Millikan and Cameron, Phys. Rev. **28**, 851 (1926).

[3] Anderson, Millikan, Neddermeyer and Pickering, Phys. Rev. **45**, 352 (1934).

[4] Anderson, Phys. Rev. **44**, 406 (1933).

[5] Blackett and Occhialini, Proc. Roy. Soc. **A139**, 699 (1933).

TABLE I. *Description and geographical origin of the samples, local gamma-radiation in ion pairs per cm³ per sec. at 30 atmospheres of air, and radium content of the geological samples in g Ra per g of specimen.*

| DESCRIPTION | SPECIMEN NUMBER | LOCAL GAMMA-RADIATION | RADIUM CONTENT |
|---|---|---|---|
| Gravel. Top of Pike's Peak, Colorado. | C1 | 97 | $0.41\times10^{-12}$ |
| Gravel. Roadway on Mt. Manitou, Colorado. | C2 | 97 | 0.25 |
| Deep glacial rubble. Churchill, Manitoba. | C3 | 32 | 0.33 |
| Glacial sand. Churchill, Manitoba. | C4 | 32 | 0.44 |
| Gravel. Windy Point, Colorado. | C5 | 98 | 0.52 |
| Granite. Churchill, Manitoba. | C6 | 12 | 0.23 |
| Red Granite. Pike's Peak, Colorado. | C7 | 97 | 1.52 |
| Hard granite outcrop. 30 ft. stone in Red River, Winnipeg, Manitoba. | C8 | 45 | 0.19 |
| Granite. Mt. Manitou, Colorado. | C9 | 97 | 1.34 |
| Gravel. Superior pits, Minneapolis, Minn. | C10 | 32 | 0.48 |
| Limestone. Quarry in Minneapolis, Minn. | C11 | 34 | 0.60 |
| Quartzose sandstone. Zion Canyon, Utah. | C12 | 25 | 0.32 |
| Granite boulder. Glen Cove, Colorado. | C13 | 135 | 1.83 |
| Soil. Ellendale, North Dakota. | C14 | 42 | 0.78 |
| Soil. Felts Field, Spokane, Washington. | C15 | 47 | 0.68 |
| Limestone. Cormorant Lake, Manitoba. | C16 | 6 | 0.11 |
| Limestone. Riverside, California. | C17 | 14.5 | 0.32 |
| Kaibab limestone. Rocky point with railing, North Rim, Grand Canyon, Colorado. | C18 | 24 | 0.95 |
| Acidic lava. Arequipa, Peru. | C19 | 148 | 1.75 |
| Rhyolitic lava. Crucero Alto, Peru. | C20 | 60 | 2.38 |
| Quartzite. Crucero Alto, Peru. | C21 | | 0.20 |
| Limestone. Cormorant Lake, Manitoba. | C22 | 6 | 0.12 |
| Quartz-mica schist. Inside railroad tunnel, San Gabriel Canyon, Cal. | C23 | 73 | 0.20 |

lating the measured radium content of certain rocks with the soft gamma-radiation observed in a cosmic-ray electroscope operated on or near these rocks.

## DESCRIPTION OF SPECIMENS

All of the rock specimens were furnished by R. A. Millikan and his co-workers, and represent samples of the rocks or soil underlying the electroscope at the scene of the cosmic-ray observations which they have made during the past four years. A brief description of the specimens and the location of the stations is given in Table I.

## LOCAL GAMMA-RADIATION *vs.* RADIUM CONTENT

The intensity of the local gamma-radiation at each of these sites was determined by comparing the discharge rates for the unshielded electroscope with the rate when the electroscope was completely surrounded by a lead shield 7.64 to 10 cm thick. Corrections were of course made[6] for the fact that the lead shield absorbs some (24 to 39 percent, depending on altitude) of the cosmic radiation while absorbing practically all (97.6 percent) of the local gamma-radiation.

The field specimens of local geological material were ground to about 60 mesh and 3 to 5 g samples analyzed for radium by the emanation method, employing the direct-fusion furnace and double ionization-chamber technique.[7] Two or more duplicate analyses were made on nearly every specimen, and individual values seldom varied from the mean value by as much as $0.05\times10^{-12}$ g Ra per g. Sample variations of this magnitude are to be expected on statistical grounds because of the local concentration of radium in the grains of certain heavy mineral constituents of the samples. As is to be expected, these sample variations are considerably smaller in the fine grained materials than in coarse grained igneous or conglomerate samples. Those specimens which are free from limestone and opal were analyzed by Raitt with Evans' earlier apparatus[8] at the California Institute of Technology. These two independent sets of data are in splendid agreement as is shown by Fig. 1.

Table I presents the local gamma-ray ionization found by Millikan and his co-workers as observed in, or else reduced to, a 15 cm diameter steel electroscope filled with air at 30 atmospheres pressure. The average radium content of the field specimen is given in g Ra per g of material.

[6] Millikan and Cameron, Phys. Rev. **28**, 851 (1926); **37**, 235 (1931).

[7] Evans, Rev. Sci. Inst. **6**, 99 (1935).

[8] Evans, Rev. Sci. Inst. **4**, 223 (1933).

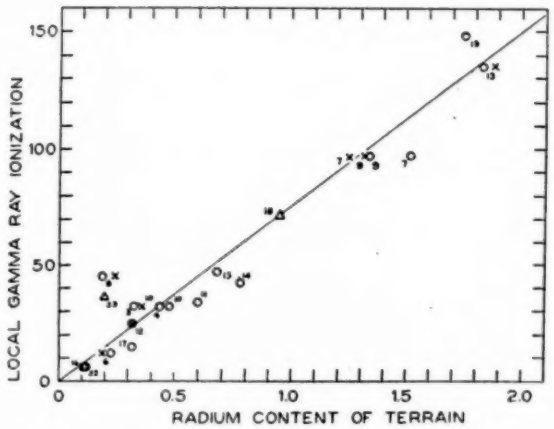


FIG. 1. Ionization due to soft local radiation *vs.* radium content of specimens of the surrounding rocks or soil. Ionization is in ion pairs collected per sec. per cm³ in air at 30 atmospheres. Radium content is in $10^{-12}$ g Ra per g material. Analyses marked ○ or △ are by Evans, × by Raitt.

The local gamma-ray ionization is due to the combined effect of all the gamma-emitters in the uranium, actinium and thorium series. The thorium content of ordinary rocks is usually several times greater than the uranium content, and hence the thorium series gamma-rays are at least as strong as those from the uranium series. McCoy and Henderson[9] found 1 g Ra to be the gamma-ray equivalent of $6.85\times10^{6}$ g Th, hence 1 g U and its decay products is slightly more active than 2.3 g Th and its decay products in the production of gamma-ray ionization. The radium content of a rock body is proportional to the total uranium series gamma-rays emitted by that body. But in a series of rock bodies the radium content can only be proportional to the *total* gamma-radiation if the ratio of the thorium to uranium content is constant. The close correlation here found between the total gamma-radiation and the radium content, shown in Fig. 1, indicates that in at least 15 of the samples in this series the thorium-uranium ratio does not vary widely.

Fig. 1 omits four of the specimens found in Table I for the following reasons. Samples C1, C2 and C5 are gravels from the Pike's Peak area, whose radium content shows no agreement with the local gamma-radiation at these stations. This fact prompted inquiries which confirmed the radioactive evidence that these materials are not really indigenous to their areas, but are thin surface layers which were hauled into their present site during road building operations. At Crucero Alto, the rocks in the neighborhood of the cosmic-ray station are a mixture of C20 and C21, mostly the latter. The local gamma-radiation corresponds to a mixture of 73 percent C21 and 27 percent C20, which is in agreement with the field notes on the terrain, but cannot be readily plotted in Fig. 1.

In all but two cases, the electroscope stood about a foot or two above the surface of a rather flat area, hence subtended on earthward solid angle of nearly $2\pi$. For C18, however, the electroscope was on a narrow rocky point jutting out from the rim of the Grand Canyon, and subtended a solid angle of only about $2\pi/3$ steradians, and for C23 the electroscope was inside a mountain tunnel and subtended nearly $4\pi$ steradians. In plotting Fig. 1, triangular points are shown for these two stations to indicate that the observed local radiation has been corrected for solid angle.

The local radiation for C23 and C8 is about 2.5 to 3 times the value expected from the radium content if the thorium-uranium ratio is the same as for the other samples in the series. This suggests that these two specimens are either not truly representative of the average rock in their vicinity or else that they have a higher thorium-uranium ratio than the other members of the series.

Employing the newly developed technique[10] for counting alpha-rays emitted from the surface of rocks, Dr. Gladys Finney made a preliminary estimate of the Th/U ratio for C8, 11, 18 and 23. The numerical values depend upon the alpha-ray stopping power of the rock, which was inferred from the known radii of plechroic halos in various minerals. Under such assumptions the Th/U ratios obtained from measurements on flat polished surfaces ground onto the solid specimens indicate that C11 and C18 have the same Th/U ratio, while C8 has 2.8 times and C23 has 3.3 times as high a Th/U ratio as C11 and C18. The high Th/U ratios thus indicated for C8 and C23 bring their local gamma-radiation into agreement

[9] McCoy and Henderson, J. Am. Chem. Soc. **40**, 1316 (1918).

[10] Evans, Finney, Kip and Mugele, Phys. Rev. **47**, 791 (1935).

TABLE II. *Average radium content of the classified samples.*

| NUMBER OF SPECIMENS | CLASSIFICATION | G RADIUM PER G SPECIMEN LIMITS | G RADIUM PER G SPECIMEN AVERAGE |
|---|---|---|---|
| 1 | Quartz-mica schist | $0.20\times10^{-12}$ | $0.20\times10^{-12}$ |
| 1 | Quartzite | 0.20 | 0.20 |
| 4 | Limestones | 0.11 to 0.60 | 0.29 |
| 1 | Sandstone | 0.32 | 0.32 |
| 2 | Glacial sand and rubble | 0.33 to 0.44 | 0.38 |
| 4 | Gravels | 0.25 to 0.52 | 0.41 |
| 2 | Soils | 0.68 to 0.78 | 0.73 |
| 1 | Kaibab limestone | 0.97 | 0.97 |
| 5 | Granites | 0.19 to 1.83 | 1.02 |
| 2 | Peruvian Lavas | 1.75 to 2.38 | 2.06 |
| Total 23 | All specimens | 0.11 to 2.38 | $0.70\times10^{-12}$ |

with that of the other specimens. It must be emphasized, however, that this alpha-ray method for Th is still in a state of development and that absolute Th values are uncertain, although there can be no doubt that the relative values for Th/U given above are essentially correct. No field specimen in this series was large enough to permit confirming these Th/U values by the $\gamma$-ray methods recently developed by Evans and Mugele.[11]

The radium content of the sample of Kaibab limestone C18 is much higher than for most limestones, but is certainly correct as it was checked by a variety of alternative analytical techniques, employing both solution and direct-fusion methods. This result is in accord with the rather large contamination, by sand and other silicates, noticeable in the Kaibab formation.

There are six simultaneous criteria for a linear relationship between the local gamma-radiation from the earth and the radium content of a small sample of rock or earth, taken near the cosmic-ray electroscope.

(1) The sample is truly a representative specimen of all the neighboring and underlying terrain.
(2) The ratio of the thorium to the uranium content is the same in each specimen of the series.
(3) Radioactive equilibrium exists between thorium, uranium, actinouranium and their individual decay products.
(4) No new strong gamma-radioactive element is present in the rocks which is not a member of one of the three known radioactive families.
(5) No appreciable gamma-radiation is produced in the rocks by cosmic-ray bombardment.

[11] Evans and Mugele, Phys. Rev. **47**, 427 (1935).

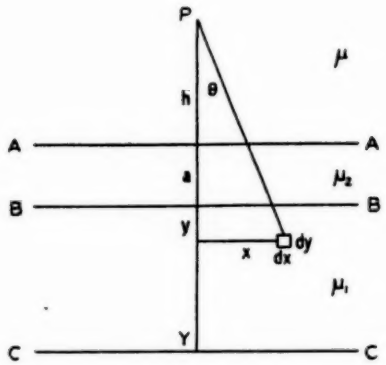


FIG. 2. Geometry for Eqs. (1) to (4).

(6) No appreciable fraction of the cosmic rays incident on the earth's crust are reflected or scattered back toward celestial space.

Criteria 4, 5 and 6 may be regarded as established by the data of Fig. 1 and Table I. Criterion 2 is obeyed by most of the specimens, and the constancy of the Th/U ratio thus disclosed is of considerable geochemical interest. The ratio is not sufficiently constant, however, to lend strong support to belief in a generic relationship between the uranium and thorium families, moreover such a belief is embarrassed by the existence of radioactive ores bearing either thorium or uranium exclusively.

The cosmic-ray electroscope is here shown to be a geophysical instrument which is useful for rapid radioactive surveying, even where no radioactive ore bodies are involved.

Bearing in mind that the number of specimens in each petrographic classification is small, and that therefore the average values cannot be regarded as universally applicable, it is of interest to compute the average radium content of each class of material which entered the present investigation. These averages are shown in Table II.

## THEORY OF GAMMA-RAY IONIZATION FROM LARGE RADIOACTIVE BODIES

The gamma-ray ionization above a flat radioactive solid such as a region of the earth's surface may be computed as follows. For greater generality, consider the ionization $n$ produced at the point $P$, Fig. 2, located $h$ cm above the plane surface $AA$ of a nonradioactive absorbing layer $a$

cm thick, which overlies the radioactive solid $BB-CC$. Let the thickness of this radioactive material be $Y$ cm, its density $\rho_1$, g cm$^{-3}$, its Ra content $m$ g Ra per g, and its effective absorption coefficient $\mu_1$ cm$^{-1}$. Let $\rho_2$ and $\mu_2$ be the density and absorption coefficient of the absorber, and $\mu$ the absorption coefficient of the medium above $AA$ (air in the present application).

The ionization $dn_1$ ion pairs per cm$^3$ per sec. at $P$ due to the Ra in the volume element $2\pi xdxdy$ formed by rotating $dxdy$ about the vertical $y$ axis is:

$$dn_1=\frac{2\pi xdxdy\rho mK}{(h+a+y)^2+x^2}e^{-\mu_1 y/\cos\vartheta}e^{-\mu_2 a/\cos\vartheta}e^{-\mu h/\cos\vartheta}, \tag{1}$$

where $K$ is a proportionality constant.

We now change variables by substituting $z=1/\cos\vartheta$, and then integrate over the region $1\leqslant z\leqslant\infty$ which is equivalent to $0\leqslant\vartheta\leqslant\pi/2$. From the geometry of Fig. 2, $x=(h+a+y)\tan\vartheta$, and by substitution of the new variable $z$ we find:

$$n_1=2\pi\rho mK\int_1^\infty z^{-1}e^{-(\mu_2 a+\mu h)z}dz\int_0^Y e^{-\mu_1 yz}dy \tag{2}$$

$$=(2\pi\rho mK/\mu_1)\int_1^\infty\{z^{-2}e^{-(\mu_2 a+\mu h)z}-z^{-2}e^{-(\mu_1 Y+\mu_2 a+\mu h)z}\}dz. \tag{3}$$

A table of the integral $G_b=\int_1^\infty z^{-2}e^{-bz}dz$ was given by Gold,[11a] whose values are shown in Fig. 3. From Eq. (3) and Fig. 3 one may compute the gamma-ray ionization for the general case, such as for specimens C1, C2 and C5 where the absorbing layer is also radioactive.

In the special case which applies to most of the specimens, $a=0$ and $Y=\infty$. We therefore have:

$$n=(2\pi\rho mK/\mu_1)G_{\mu h}. \tag{4}$$

Eve's number[12] $K$ is evaluated by noticing that for any radiation which is exponentially absorbed the ionization $n$ ion pairs per cm$^3$ per sec. at a distance $r$ cm from a source of unit strength will be $n=Ke^{-\mu r}/r^2$ in a medium whose absorption coefficient is $\mu$ cm$^{-1}$. The total ionization produced by such a unit source will be

$$N=\int_0^\infty 4\pi r^2 ndr=4\pi K\int_0^\infty e^{-\mu r}dr$$

$$=4\pi K/\mu \text{ ion pairs per sec.}$$

Eve's number $K$ depends upon temperature pressure and ionization chamber wall materials, and is not accurately known, but is approximately $60/4\pi\times10^9$ ion pairs per sec. per cm for the gamma-rays from Ra $(B+C)$ in equilibrium with 1 g of Ra. (For $\mu N$ in air Eve gives $50\times10^9$; Hess 61 and $72\times10^9$; Moseley and Robinson $73\times10^9$. Reitz gives $K=4.3\times10^9$ for RaC in free air at 0° and 760 mm, or up to $6.8\times10^9$ in an iron ionization chamber with 3 mm thick walls.)[13]

The mass absorption coefficient $\mu_1/\rho$ is not accurately known for geological specimens but has a value somewhere near or between 0.034 (McClelland[14]) and 0.065 cm$^2$ g$^{-1}$ (Behounek[15]). Since $\mu$ is the order of $6\times10^{-5}$ cm$^{-1}$ for air, any observations made within a few meters of the earth's surface will correspond to $\mu h\to0$, hence $G_{\mu h}\to1$. If we substitute $G=1$, $\mu_1/\rho=0.06$, $K=6.8$

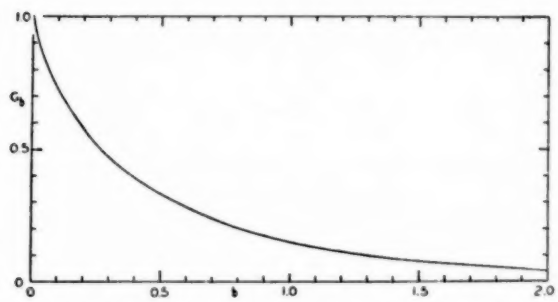


FIG. 3. Values of the integral $G_b=\int_1^\infty z^{-2}e^{-bz}dz$ for $0\leqq b\leqq2$. For larger $b$, some values are:

| $b$ | 2 | 3 | 4 | 5 | 6 |
|---|---|---|---|---|---|
| $G_b$ | 0.03754 | 0.01064 | 0.00320 | 0.00099 | 0.00032 |

The series $G_b=e^{-b}(1/b-2/b^2+3!/b^3-4!/b^4+\cdots)$ represents the integral asymptotically.

[11a] E. Gold, Proc. Roy. Soc. **A82**, 43 (1909).

[12] Eve, Phil. Mag. **22**, 551 (1911); **27**, 394 (1914); Rutherford, Chadwick and Ellis, *Radiations from Radioactive Substances* (1930), p. 496.

[13] A. S. Eve, Phil. Mag. **12**, 189 (1906); **22**, 551 (1911); **27**, 394 (1914); V. F. Hess, Akad. Wiss. Wien, Ber [IIa] **122**, 1053 (1913); H. G. J. Moseley and H. Robinson, Phil. Mag. **28**, 327 (1914); A. W. Reitz, Zeits. f. Physik **69**, 259 (1931).

[14] Eve, Phil. Mag. **21**, 26 (1911).

[15] Behounek, Zeits. f. Physik **79**, 590 (1932).

$\times 10^9$, and $m = 1 \times 10^{-12}$ g Ra per g in Eq. (4) we obtain $n = 0.7$ ion pairs per cm³ per sec., for the ionization near the ground[16] due to the penetrating gamma-rays of RaC from material containing $10^{-12}$ g Ra per g. The softer gamma-rays from higher members of the uranium series will increase this value to about unity, but accurate data are not available.

This theoretical ionization value is to be compared with the observations plotted in Fig. 1. Incomplete saturation[17] of the ion current permits only 13.8 times[18] as many ions to be collected in air at 30 atmospheres as at 1 atmosphere pressure. Consequently, the data of Fig. 1 show that the radioactive content of average terrestrial materials, be they granites, limestones, sandstones, rubble or soil, will cause a gamma-ray ionization[19] of about 5.5 ion pairs per sec. per cm³ in air at a pressure of one atmosphere when the terrain contains $1.0 \times 10^{-12}$ g Ra per g.

Recalling[9] that the gamma-rays from 2.3 g Th and its decay products are nearly as effective as those from 1 g U and its decay products, it is readily seen that the Th/U ratio must be between 5 and 10 in order to account for the 5.5 ion pairs per cm³ per sec. observed in the cosmic-ray electroscope. More accurate knowledge of $K$ and $\mu_1/\rho$ may alter this figure somewhat, but there is here clear support for the view that the Th/U ratio is considerably greater than the value 2.5 which has been used by Holmes and others.[20]

Entirely independent measurements on another suite of rock samples[10] has confirmed this high Th/U ratio. This conclusion has considerable geophysical importance because it shows that the thorium series is more important than the uranium series in such questions as geological age measurements based on helium ratios in common materials, and in geothermal problems concerning earth movements and the earth's internal heat.

### Acknowledgments

This research was originally initiated by R. A. Millikan at the California Institute of Technology, where it followed the carbonate-fusion investigations by J. Lloyd Bohn[21] and E. M. McMillan,[22] and was a part of Professor Millikan's cosmic-ray research program, supported by a grant from the Carnegie Corporation of New York. Completion of the experimental phases awaited the recent final development of the direct-fusion furnace technique[23] in the laboratories of the University of California, where the able assistance of Mr. Fred Ludecke and Mr. Arthur Kip was of great value.

[16] The variation of ionization with altitude is given by Eq. (4) and Fig. 3. Thus at 200 meters above ground level $\mu h = ca.$ 1.3 and the ionization will amount to about 10 percent of its value at the earth's surface. Similar considerations make it possible to compute the terrestrial gamma-ray corrections for balloon and airplane observations.

[17] I. S. Bowen, Phys. Rev. **41**, 24 (1932).

[18] R. A. Millikan, Phys. Rev. **39**, 397 (1932).

[19] This value, of course, corresponds to measurements made in a particular detecting instrument. Secondary and transition effects due to the walls of the instrument cause the observed value to differ somewhat from the corresponding ionization in free air; see A. W. Reitz, Zeits. f. Physik **69**, 259 (1931) and E. J. Workman, Phys. Rev. **43**, 859 (1933). Moreover, in free air near land areas there will be the order of 1 ion pair per cm³ per sec. of additional ionization due to alpha-rays from Rn, Tn and their decay products in the air itself.

[20] A. Holmes, *Radioactivity and Earth Movements*, Trans. Geol. Soc. Glasgow **18**, III, 559 (1928–29; published 1931).

[21] Bohn, Ph.D. Thesis, California Institute, (1927); J. Frank. Inst. **210**, 461 (1930).

[22] McMillan, M.S. Thesis, California Institute (1928).

[23] Evans, Rev. Sci. Inst. **6**, 99 (1935).

# Ionization Currents Produced by Radon, RaA and RaC′ in Cylindrical Ionization Chambers

ROBLEY D. EVANS, *Massachusetts Institute of Technology*

(Received May 21, 1935)

A general theoretical equation is derived for the ionization produced in cylindrical ionization chambers by Rn and its decay products. Where $dv/dt \equiv$volts per sec. discharge, $j \equiv$fractional saturation of the ion current, $C \equiv$electrostatic capacity in cm, $A \equiv$curies of Rn present at time $t=0$, $\lambda_1 \equiv$decay constant of Rn, $1/\mu \equiv$stopping power of the gas in the ionization chamber, $d \equiv$cm diameter and $h \equiv$cm height of the chamber, and $t \geq 3$ hr.:

$$dv/dt = 5.3\times 10^8 (j/C)(3.57 - 5.00\mu/h - 3.47\mu/d + 5.48\mu^2/hd) A e^{-\lambda_1 t}$$

when $d$ and $h$ are greater than twice $6.60\mu$ cm, the range of the RaC′ alpha-ray. Experimental confirmation employing standard radium solutions is described. Where either $C$ or $A$ is known, the other may be computed, therefore Rn ionization may be employed for absolute capacity measurements. General equations are also derived for alpha-ray ionization (1) above a plane surface due to a homogeneous radioactive substance below the plane, and (2) a radioactive substance uniformly distributed on a wire normal to the plane, and (3) for the ionization outside a dihedral right angle enclosing a homogeneous radioactive substance.

## I. INTRODUCTION

THE convenience and structural simplicity of the cylindrical ionization chamber has led to its general adoption for the measurement of the ionization produced by the alpha-radiation from radioactive gases. The mathematical problem of predicting the net observable ionization produced by alpha-emitters in a cylindrical ionization chamber has long defied exact analysis. This is partly because of the geometrical complications, such as the presence of sharp corners, the lack of symmetry and the inhomogeneous fields at the ends, and partly because of inadequacies in the theory of the ionization by alpha-particles in a confined region bounded by absorbing walls. The desired analytical expression relates $dv/dt$, the rate of voltage discharge of the ionization-chamber-electrometer system, to its total electrostatic capacity, $C$; the height, $h$, and diameter, $d$, of the ionization chamber; the stopping power, $1/\mu$, of the gas in the chamber, and the amount, $A$, of radioactive material present. Thus:

$$dv/dt = (A/C) f(h, d, \mu) \qquad (1)$$

and the mathematical problem is the determination of $f(h, d, \mu)$.

An expression such as Eq. (1) is useful as (a) giving confirmation of and confidence in emanation measurements, (b) providing an absolute radium or radon calibration for laboratories possessing no precision radium standard but capable of making electrostatic capacity measurements, (c) providing an easy and accurate means of measuring electrostatic capacity in laboratories possessing a standard radium solution (d) providing a means of making accurate quantitative determinations of yields in atomic disintegration experiments if the products are alpha-active.

Equations analogous to Eq. (1), for the case of Rn and its alpha-emitting decay products RaA and RaC′ in a parallel plate condenser have been given by Flamm and Mache,[1] Siegl[2] and others, while the case of the spherical ionization chamber has been treated by Lind,[3] Mund[4] and Glockler and Heisig.[5]

Empirical expressions for Rn, and for Rn, RaA and RaC′ in equilibrium in cylindrical ionization chambers were given by Duane[6] and Duane and Laborde,[7] and these have been widely used.[8] Evans[9] combined some of Duane and Laborde's data with a preliminary theory to

[1] Flamm and Mache, Akad. Wiss., Wien, Ber. [II *a*], **121**, 227 (1912).
[2] Siegl, Akad. Wiss., Wien, Ber. [II *a*] **134**, 11 (1925).
[3] Lind, J. Phys. Chem. **16**, 564 (1912).
[4] Mund, J. Phys. Chem. **30**, 890 (1926).
[5] Glockler and Heisig, J. Phys. Chem. **35**, 2478 (1931).
[6] Duane, Comptes rendus **1**, 581 (1905); J. de phys. et rad. **4**, 605 (1905).
[7] Duane and Laborde, Comptes rendus **1**, 1421 (1910).
[8] Schmidt and Nick, Physik. Zeits. **14**, 199 (1912); Mache and Meyer, Physik. Zeits. **13**, 320 (1912); Berndt, Ann. d. Physik **38**, 958 (1912); Ramsey, Am. J. Sci. **40**, 309 (1915); Gockel, *Die Radioaktivität von Boden und Quellen*, Vieweg (1914), p. 102; Lester, Am. J. Sci. **44**, 225 (1917); Zlatarovic, Akad. Wiss., Wien, Ber. [II *a*] **129**, 59 (1920), etc.
[9] Evans, Thesis, Calif. Institute of Tech. (1932), p. 62.

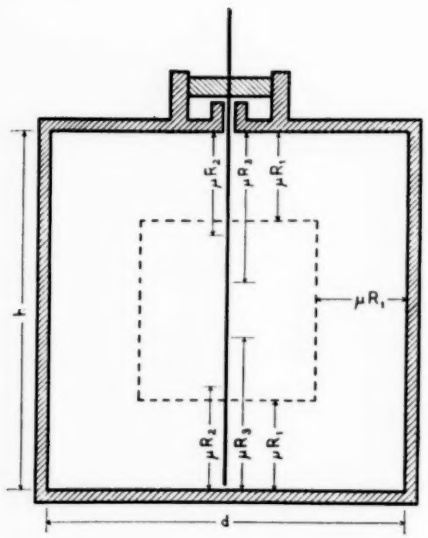


FIG. 1. Schematic cylindrical ionization chamber.

derive a semi-empirical formula for cylindrical ionization chambers in which the ionization from the solids, RaA and RaC′, and the gaseous Rn were treated independently. In the treatment given below, $f(h, d, \mu)$ is evaluated entirely analytically, and the results are confirmed by direct experiments.

Fig. 1 illustrates the typical cylindrical ionization chamber considered in the following analysis. The center electrode is a wire of sufficiently small diameter to occupy a volume which is negligible in comparison with the rest of the chamber. The center wire is charged negatively, hence collects[10] the positively charged[11] atoms of RaA as they are formed by the decay of Rn in the chamber.

$R_1$, $R_2$, $R_3$ are the ranges of the Rn, RaA and RaC′ alpha-particles in air at 0°C and 760 mm Hg, and $\mu R_1$, $\mu R_2$, $\mu R_3$ are their ranges in the gas filling the ionization chamber. An alpha-particle from Rn emitted within a distance of $\mu R_1$ from any wall of the chamber and directed toward that wall will lose some of its energy by absorption in the wall. To determine what ionization is produced inside the chamber by Rn alpha-particles we must evaluate the ionization lost in the wall, and deduct this from the total maximum ionization which would be produced if all the energy were dissipated in ionizing the gas in the chamber. Similar corrections must be derived for those RaA and RaC′ alpha-particles which are emitted from the lower or upper portion of the center wire and strike an end wall. To avoid overlapping, the theory is here derived only for chambers in which the diameter and height exceed twice the range of the RaC′ alpha-particle.

For generality, we derive the dependence of the ionization current on time elapsed (a) after introducing Rn into a cylindrical ionization chamber, and (b) after withdrawing Rn from a chamber in which it had previously come to transient equilibrium with its decay products.

## II. Accumulation of RaA and RaC′

When Rn is introduced into an ionization chamber its disintegration gives rise to the successive solid decay products RaA, RaB, RaC, RaC′, RaD, etc. For the present work the 0.04 percent of RaC traversing the RaC″ branch is entirely negligible. Of these decay products only RaA and RaC′ emit alpha-particles, and the half-life of RaD is so long (25 yrs.) that its decay products are negligible. We have therefore to consider the number of alpha-particles per sec., $N_1$, $N_2$, $N_3$, from Rn, RaA, RaC′ respectively, as a function of time, where, at $t=0$, $N_1=Z$ and $N_2=N_3=0$. The general expressions for the number of atoms of any of the decay products as a function of time constitute the familiar Case I of Rutherford's treatises, and the general equations,[12] given by Bateman,[13] need only to be multiplied by the decay constants of the products involved to give $N_1$, $N_2$, $N_3$. In this way, substituting for the decay constants: $\lambda_{Rn}=2.097\times10^{-6}$ sec.$^{-1}$, $\lambda_{RaA}=3.79\times10^{-3}$ sec.$^{-1}$, $\lambda_{RaB}=4.31\times10^{-4}$ sec.$^{-1}$, $\lambda_{RaC}=5.86\times10^{-4}$ sec.$^{-1}$, $\lambda_{RaC'}=ca.10^{6}$ sec.$^{-1}$, as given by Rutherford,[12] we obtain:

$$N_1=Ze^{-\lambda_{Rn}t} \tag{2}$$

$$N_2=1.00054Z(e^{-\lambda_{Rn}t}-e^{-\lambda_{RaA}t}) \tag{3}$$

$$N_3=1.0089Z(e^{-\lambda_{Rn}t}-0.0232e^{-\lambda_{RaA}t}-4.26e^{-\lambda_{RaB}t}+3.28e^{-\lambda_{RaC}t}). \tag{4}$$

[10] Dadourian, Am. J. Sci. **19**, 16 (1905); Kovarik and McKeehan, Bull. Nat. Research Council **10**, 140 (1925).
[11] McGee, Phil. Mag. **13**, 1 (1932).
[12] Rutherford, *Radioactivity* (1905), p. 332; Rutherford, Chadwick and Ellis, *Radiations from Radioactive Substances* (1930), p. 11.
[13] Bateman, Proc. Camb. Phil. Soc. **15**, 423 (1910).

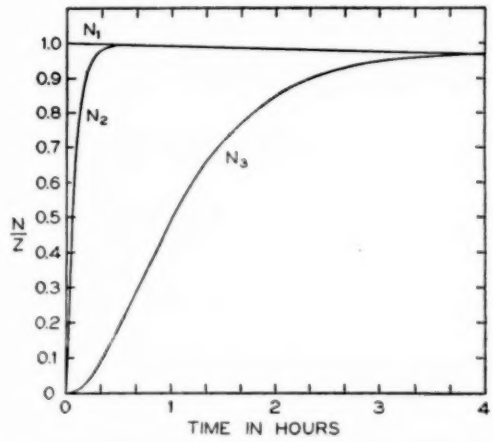


FIG. 2. Rate of emission of alpha-particles from Rn, ($N_1$), and accumulating decay products, RaA, ($N_2$), and RaC', ($N_3$), in terms of emission from Rn at $t=0$. See Eqs. (2), (3), (4).

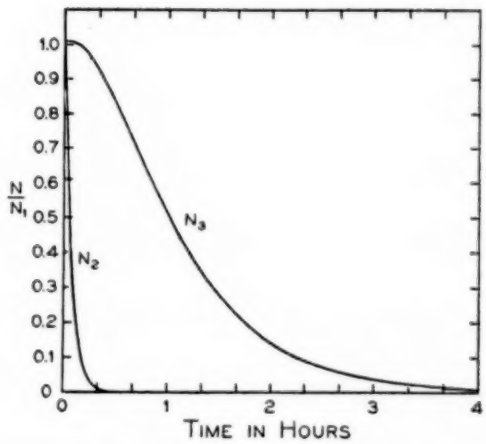


FIG. 3. Rate of emission of alpha-particles from RaA, ($N_2$), and RaC', ($N_3$) after removing a Rn source giving $N_1$ alpha-particles per sec. at $t=0$.

The numerical values for Eqs. (2), (3), (4) are given in Fig. 2.

## III. Decay of RaA and RaC'

If, after transient equilibrium has been established between Rn and its decay products through RaC', the Rn is suddenly removed, then the number of alpha-particles per sec. $N_2$ and $N_3$, from RaA and RaC', respectively, may be expressed in terms of the number of Rn alpha-particles per sec., $N_1$, at the moment previous to withdrawing the Rn from the ionization chamber. $N_2$ and $N_3$ may be computed from Bateman's[14] equations or from Meyer and Schweidler's[15] table, by multiplying the amount of each element, as given by these equations or tables, by the decay constant of the element. It can be seen that the mean life of RaC' is so short that the rate of emission of RaC' alpha-particles is equal to that of RaC, which facilitates computation. Fig. 3 shows $N_2$ and $N_3$, the rate of emission of RaA and RaC' alpha-particles after the removal of a Rn source giving $N_1$ alpha-particles per sec. at $t=0$, transient equilibrium having been present.

[14] A serious misprint in the original general equations for decay (reference 13) has avoided correction for twenty years. In Rutherford, Chadwick and Ellis (reference 12) p. 14, the coefficient $d$ of Eq. (13) should be multiplied by $1/\lambda_4$.

[15] Meyer and Schweidler, *Radioaktivität* (1927), p. 437.

## IV. Ionization by Rn in Cylindrical Ionization Chambers

When a small amount of Rn is added to the gas in a cylindrical brass ionization chamber all the Rn remains uniformly distributed throughout the entire volume of the chamber. We have verified this by withdrawing samples of gas from a chamber and examining the resulting change in ionization.

The ionization losses due to absorption of alpha-particles in the walls can be computed by regarding the wall as the outer boundary of a homogeneous radioactive material and computing the ionization outside this boundary.[16] Exact integrals for the alpha-particle ionization, $q$, per cm$^2$ above the plane surface of a radioactive solid emitting $N$ alpha-particles per sec. per cm$^3$ have been given by Evans.[17] If $R$ is the range of the alpha-particle in air at 0°C and 760 mm Hg, $R\mu$ is its range in the radioactive source, $k$ the total number of ion pairs per alpha-particle, then

$$q=\epsilon k N R\mu \qquad (5)$$

where $\epsilon$ is a dimensionless coefficient, increasing slightly with $R$, and having values between 0.114 and 0.150 for all known alpha-particles from Sm ($R=1.06$ cm) to ThC' ($R=8.17$ cm).

Considering, for the moment, all the walls of

[16] R. W. Raitt, personal communication, June, 1933.

[17] Evans, Phys. Rev. **45**, 29 (1934).

the cylindrical chamber of volume, $V$ cm³, as plane surfaces of total area, $S$ cm², and writing subscripts 1 to indicate numerical values for Rn alpha-particles, the total ionization absorbed by these walls is:

$$i_1 = \epsilon_1 k_1 N_1 R_1 \mu S/V \qquad (6)$$

where $N_1$ is the total number of Rn alpha-particles per sec. in the entire chamber, hence $N_1/V$ represents the Rn alphas per cm³.

The actual curvature of the walls leads to two small and oppositely directed correction terms which, for practical measurements, cancel each other. On the one hand the curvature decreases the effective fractional volume of radioactive source, which is within $R\mu$ cm of the wall, from $R\mu S/V = 2R\mu(1/h+2/d)$ to $2R\mu(1/h+2/d - 2R\mu/d^2)$. This correction has its maximum value for small chambers, where it corresponds to about 5 percent of the Rn ionization, or 2.5 percent of the ionization from Rn and its decay products. On the other hand the wall curvature increases the wall area which can be hit from any point radially distant less than $R\mu$ cm from the wall. This fractional increase is about $1 - d \sin^{-1}(2(b^2-y^2)^{\frac{1}{2}}/d)/2(b^2-y^2)^{\frac{1}{2}}$ where $d$ is the diameter of the chamber, $b$ the length of track inside the chamber and $y$ the perpendicular distance from the origin of $b$ to the chord which defines the hypothetical plane replaced by the actual curved wall. Without practical error, we may say that these two effects of wall curvature exactly cancel each other, leaving Eq. (6) as the Rn ionization absorbed by the walls.

The corners of the chamber give rise to a small but appreciable correction. This can be evaluated by computing the ionization produced outside a dihedral right angle by a radioactive source within, and bounded by, the angle. Since this computation has general applications to all finite, bounded radioactive sources, where it is the "edge correction," its derivation will be given. In Fig. 4, an element of volume, in the radioactive source bounded by the dihedral right angle $AOB'$, emits alpha-rays uniformly in all directions. Those which emerge above the plane $AA'$ cause ionization above this plane which is exactly described by Eq. (5), where $q$ is taken as the total ionization above $AA'$ per cm of length (into the plane of the paper) of the dihedral edge, $O$, and where the effective cross sectional area of the source (in the plane of Fig. 4) for emission of alpha-rays capable of emerging from $AA'$ is $(R\mu)^2$. Consideration of this ionization is indicated in Fig. 4 by circles on the alpha-ray tracks. Similarly those which emerge to the right of the plane $BB'$ are described by Eq. (5) and are indicated in Fig. 4 by dots on the alpha-ray tracks. The ionization from these two plane edges is already included in Eq. (6), because $S$ is taken as the total inside surface of the ionization chamber.

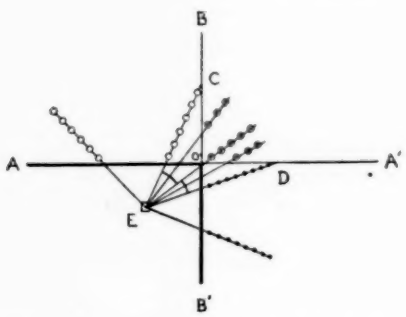


FIG. 4. Schematic cross section describing corrections for ionization outside a dihedral right angle $AOB'$ bounding a homogeneous radioactive source.

Inspection of Fig. 4 shows that alpha-particles emergent above $AA'$ and to the right of $BB'$ have been counted twice, as indicated by the dotted circles. We must therefore compute the ionization represented by these track elements and deduct it from the ionization described by Eq. (6).

As shown in the next section, the general expression for the corner correction is $i' = \psi N k R^2 \mu^2$ ion pairs per sec. per cm of edge where $\psi$ is a dimensionless coefficient. As in the case of the side walls, the curvature of the corner exerts two oppositely directed influences, one due to reduction of effective volume, the other to increased effective surface exposed to each volume element, which cancel each other. Each of these two corrections represents, in this case, a maximum of only about 0.6 percent of the total Rn ionization in small chambers, where curvature effects are most pronounced. The total effective length of the corners at the top and bottom of the chamber is $2\pi d$, therefore the Rn ionization absorbed by the walls is:

$$i_1 - i_1' = \epsilon_1 k_1 N_1 R_1 \mu (S/V) - \psi_1 k_1 N_1 R_1^2 \mu^2 (2\pi d/V) \qquad (7)$$

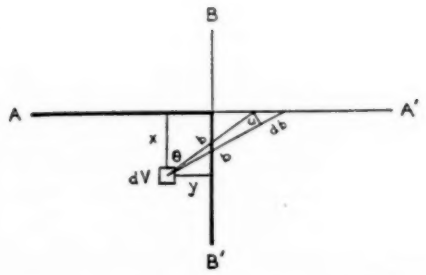


FIG. 5. Geometry for Eqs. (10) to (15) giving ionization outside a dihedral right angle.

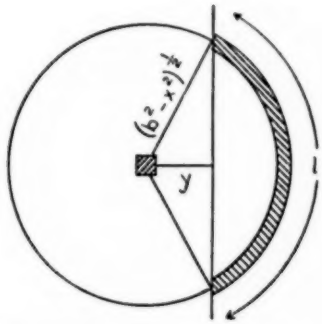


FIG. 6. Geometry for Eqs. (10) to (15), in the $AA'$ plane of Fig. 5.

and the total net ionization by Rn is $I_1=N_1k_1-(i_1-i_1')$ ion pairs per sec. Substituting $S=\pi d^2/2+\pi hd$, and $V=\pi hd^2/4$, we have for the Rn ionization:

$$I_1=N_1k_1\{1-2\epsilon_1R_1\mu(1/h+2/d)+8\psi_1R_1^2\mu^2/hd\}. \quad (8)$$

As shown in the next section $\psi$ for Rn $(=\psi_1)=0.0208$, and from Table I of reference 17, $\epsilon_1=0.143$, $R_1=3.91$ cm, $k_1=1.55\times10^5$ ion pairs per Rn alpha-particle. Hence, in general, for Rn ionization in a cylindrical ionization chamber:

$$I_1=1.55\times10^5N_1\{1-1.12\mu(1/h+2/d)+3.54\mu^2/hd\}\text{ ion pairs per sec.} \quad (9)$$

## V. Alpha-Particle Ionization Outside a Dihedral Right Angle

As shown in Section IV, the ionization from the dotted and circled alpha-ray track ends in Fig. 4 constitutes the corner correction required for all cases involving a homogeneous radioactive source confined within the dihedral right angle $AOB'$. This ionization may be computed by adding the contribution from alpha-rays emerging from the plane of $AA'$ to the right of $BB'$ (those within the angle $OED$) to those alpha-rays emerging from the plane of $BB'$ above $AA'$ (those within the angle $OEC$). From symmetry these two are equal, hence, for analysis, rays emerging within the angle $OED$ will be considered.

In Fig. 5, take the $x$ and $y$ coordinates of the volume element $dV=dxdydz$, as shown, with $dz$ normally into the plane of the page. We first find the total number, $dn$, of alpha-rays emerging in the angle $OED$, of Fig. 4, which have ranges below $AA'$ of between $b$ and $b+db$ cm. Since the stopping power of the source is $1/\mu$, and since the stopping power may be taken as constant over the entire region $AA'BB'$ without loss of generality, the ionization produced above $AA'$ by each of these rays is the same as that produced along the path of an alpha-ray in air at 0°C and 760 mm Hg between a point $b/\mu$ cm from the origin of the ray and the end of the ray. If $\varphi(r)$ is the specific ionization in ion pairs per cm of path in air at 0°C and 760 mm Hg at a distance $r$ from the origin of the "standard" alpha-ray, then the ionization above $AA'$, per cm of depth in $z$, equals $dn\int_{b/\mu}^{R}\varphi(r)dr$, and the total ionization, $i'$, for all values of $b$ from 0 to $R\mu$, and for all rays emergent in both the angles $OED$ and $OEC$, i. e., for all dot-circled rays in Fig. 4, is:

$$i'=2\int_{b=0}^{b=R\mu}dn\int_{b/\mu}^{R}\varphi(r)dr. \quad (10)$$

The evaluation of $dn$ follows the geometry of Figs. 5 and 6. The number of alpha-rays per sec. emitted in all directions from the volume element $dV$ is $Ndxdydz$, where $N$ is the number of alpha-rays per sec. per cm$^3$. The fraction of these rays which emerge from the plane $AA'$ to the right of $BB'$ is $ul/4\pi b^2$, where $l$ is the length of the arc of emergence of rays which have ranges below $AA'$ lying between $b$ and $b+db$ cm. From geometry, $u=db\ \cot\theta=\{x/(b^2-x^2)^{\frac{1}{2}}\}db$, and $l=2(b^2-x^2)^{\frac{1}{2}}\cos^{-1}\{y/(b^2-x^2)^{\frac{1}{2}}\}$. Hence the number of rays originating in $dV$, and emerging above $AA'$ and to the right of $BB'$ (i. e., within the angle $OED$) with ranges between $b$ and $b+db$ below $AA'$ is $(ul/4\pi b^2)NdV=(Nx/2\pi b^2)\cos^{-1}\{y/(b^2-x^2)^{\frac{1}{2}}\}dbdxdydz$, and the total number of such rays, per cm depth in $z$, is:

$$dn=\frac{Ndb}{2\pi}\int_0^1 dz\int_b^0 dy\int_{(b^2-y^2)^{\frac{1}{2}}}^0 \frac{x}{b^2}\cos^{-1}\frac{y}{(b^2-x^2)^{\frac{1}{2}}}dx \quad (11)$$

$$=(N/6\pi)bdb. \quad (12)$$

Substituting Eq. (12) in Eq. (10) we have for the ionization dot-circled in Fig. 4:

$$i'=(N/3\pi)\int_0^{R\mu} bdb\int_{b/\mu}^R \varphi(r)dr. \quad (13)$$

The point $b$ along the path of the actual alpha-ray, in a medium of uniform (i.e., independent of $r$) stopping power $1/\mu$, corresponds in specific ionization to the point $r$ along the path of a standard alpha-ray in air at 0°C and 760 mm Hg when $r=b/\mu$. Making this substitution in Eq. (13), we have:

$$i'=(N\mu^2/3\pi)\int_0^R rdr\int_r^R \varphi(r)dr, \quad (14)$$

which is valid for media of any $\mu$.

*Lemma.* By partial integration of the left side of Eq. (15) and integration by parts of the right side, it may be shown that if $n$ and $\varphi$ are any functions of $r$, $n=n(r)$, $\varphi=\varphi(r)$, then, provided that $n(a)=0$,

$$\int_a^R dn\int_r^R \varphi dr=\int_a^R n\varphi dr. \quad (15)$$

Eq. (14) may therefore be transformed with the aid of the lemma of Eq. (15), resulting in:

$$i'=(N\mu^2/6\pi)\int_0^R r^2\varphi(r)dr, \quad (16)$$

which may be written:

$$i'=\psi NkR^2\mu^2, \quad (17)$$

where $\psi$ is a dimensionless coefficient and, like $\epsilon$ of Eq. (5), depends slightly on $R$. For $R=3.91$ cm (Rn), graphical integration employing $\varphi(r)$ as found by Henderson[17, 18] given $\psi_1=0.0208$. If the approximate analytical expression[17] $(\frac{2}{3})kR^{-\frac{1}{2}}(R-r)^{-\frac{1}{2}}$ is substituted for $\varphi(r)$, the integration may be carried out analytically, and leads to the approximate value, $\psi_\infty=3/40\pi=0.0238$, which is the limiting value for very long alpha-rays.

[18] G. H. Henderson, Phil. Mag. **42**, 538 (1921).

Eq. (15), with suitable values for $\psi$, describes completely the edge or corner corrections applicable to all finite radioactive sources of the type considered here. In practical cases it must be combined with Eq. (5), as was done in deriving Eq. (7).

## VI. Ionization Due to RaA and RaC′

As pointed out in Section I the negatively charged center wire of the cylindrical ionization chamber of Fig. 1 is assumed to collect all the RaA atoms resulting from the disintegration of Rn. Since the mean life of RaA is very long compared with the time required for collecting this ion from its place of origin in the gas, all the RaA alpha-rays, as well as those from RaC′, are regarded as emitted from the surface of the center wire. If a small fraction of the RaA should be collected on the walls of the chamber, the difference in the energy absorbed by the end wall would be negligible, as the equations have the same form, differing only by a term representing the wall curvature. Because the emission is random in direction, half of the RaA and RaC′ alpha-rays will be absorbed in the center wire. Of the remaining rays, those emitted within a distance $R_2\mu$ for RaA, and $R_3\mu$ for RaC′, of an end wall, and directed toward that wall, will lose some of their energy in the wall.

The method of analytical evaluation of this energy is identical for the RaA and RaC′ rays. Assuming that the radioactive source (say RaA) is uniformly distributed along the surface of a wire normal to, and just reaching the plane $DD'$ of Fig. 7, we need to evaluate the ionization appearing above the plane $DD'$, which, in this case, is the energy absorbed by the wall. If the wire is $h$ cm long and emits $N_2$ alpha-rays per sec. in all directions, hence $N_2/2$ which can be effective in producing ionization below the plane

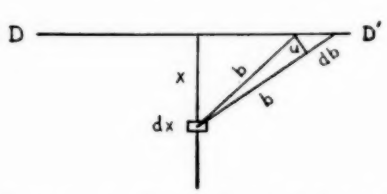


Fig. 7. Geometry for Eqs. (18) to (24) describing ionization above $DD'$ due to alpha-particles emitted from a wire normal to $DD'$.

$DD'$, then in an element of length, $dx$, there will be $(N_2/2h)dx$ alpha-rays effectively emitted. The fraction of those emitted from a depth, $x$, below $DD'$ which have the range element between $b$ and $b+db$ below $DD'$ is $2\pi(b^2-x^2)^{\frac{1}{2}}u/4\pi b^2 = (x/2b^2)db$, and the number of such rays is $(N_2/2h)(x/2b^2)dbdx$ from the depth $x$, or $(N_2/8h)db$ from all depths between $x=0$ and $x=b$. Every ray in such a group produces ionization above $DD'$ equal to $\int_{b/\mu}^{R}\varphi(r)dr$, where $r$, as in Section V is measured on the path of a standard alpha-ray in air at 0°C and 760 mm, and $1/\mu$ is the stopping power of the material in the region below $DD'$. The total ionization above $DD'$, due to rays having all possible values of $b$ from $b=0$ to $b=R\mu$ is

$$i=(N_2/8h)\int_0^{R\mu}db\int_{b/\mu}^{R}\varphi(r)dr \qquad (18)$$

and substituting $r=b/\mu$ as for Eq. (14), and applying the lemma of Eq. (15) we find

$$i=(N_2\mu/8h)\int_0^{R}dr\int_r^{R}\varphi(r)dr$$

$$=(N_2\mu/8h)\int_0^{R}r\varphi(r)dr \qquad (19)$$

$$\equiv(N_2\mu/2h)\epsilon kR, \qquad (20)$$

where $\epsilon$ is the dimensionless coefficient defined by Eqs. (19) and (20), and appearing in Eq. (5), and is obtained by graphical integration[17] of Eq. (19). The RaA ionization lost by absorption in the two end walls is, therefore, $2i_2$, where the subscript 2 refers to RaA, and the ionization produced in the gas of the cylindrical ionization chamber by RaA is

$$I_2=(N_2k_2/2)-(N_2\mu/h)\epsilon_2k_2R_2$$
$$=\tfrac{1}{2}N_2k_2(1-2\epsilon_2\mu R_2/h) \qquad (21)$$

and, similarly, the ionization in the chamber, due to RaC′ is

$$I_3=\tfrac{1}{2}N_3k_3(1-2\epsilon_3\mu R_3/h), \qquad (22)$$

where the subscripts 3 refer to RaC′ values of $N$, $R$, $k$ and $\epsilon$. From Table I of reference 17, $\epsilon_2=0.144$, $R_2=4.48$ cm, $k_2=1.70\times10^5$ ion pairs per RaA alpha-ray; and $\epsilon_3=0.148$, $R_3=6.60$ cm, and $k_3=2.20\times10^5$ ion pairs per RaC′ alpha-ray. Substituting in Eqs. (21) and (22) we obtain:

$$I_2=0.85\times10^5N_2(1-1.29\mu/h) \qquad (23)$$

$$I_3=1.10\times10^5N_3(1-1.95\mu/h)$$

ion pairs per sec. (24)

## VII. Total Ionization Due to Rn+RaA +RaC′

The ionization currents actually observed in the cylindrical ionization chamber are due to the combined effects of the alpha-rays from Rn and its alpha-emitting decay products RaA and RaC′. Other sources of ionization such as that due to beta-rays from RaB and RaC, and that due to electrons liberated from the walls by the alpha-rays which strike the walls, are negligible in comparison. The total alpha-ray ionization, $I$, is the sum of $I_1$, $I_2$ and $I_3$ of Eqs. (9), (23) and (24).

A small additive correction must be made for the ionization produced by the recoil atoms. For elements near RaA, momentum considerations show that the recoil atom has 2.0 percent as much energy as the associated alpha-ray. Most of this recoil energy produces ionization, but a small fraction of it may be dissipated in elastic molecular collisions without ionization. Bearing in mind that the density of ionization due to a recoil atom exceeds that due to an alpha-ray, it is probable that there is more recombination of ions, and a correspondingly lower saturation, in the ionization produced by recoil atoms. We may safely say that $1.5\pm0.5$ percent should be added to the alpha-ray ionization to account for recoil energy. Because the recoil tracks are very short there will be no significant wall correction in their case. Every Rn alpha-ray gives rise to an effective recoil atom, and those RaA and RaC′ alpha-rays which are directed into the center electrode each produce a recoil atom which can ionize the gas. The correction for recoil therefore increases the first term of Eqs. (9), (23) and (24) from 1 to $1.015\pm0.005$, as shown in Eq. (26).

With ordinary collecting potentials of several hundred volts across the chamber, some recombination of ions will occur in the dense columnar

ionization due to the alpha-rays. The relative saturation, $j$, discussed in Section VIII, is the fraction of the total ionization, $I$, which is actually observed. If $C$ is the electrostatic capacity of the ionization-chamber-electrometer system in cm, $e$ the electronic charge, $4.77\times10^{-10}$ e. s. u., and $dv/dt$ the discharge rate in volts per sec. then:

$$dv/dt=300jeI/C \tag{25}$$

and

$$I\equiv I_1'+I_2'+I_3'$$
$$=1.55\times10^5N_1\{1.015-1.12\mu(1/h+2/d)$$
$$+3.54\mu^2/hd\}+0.85\times10^5N_2\{1.015-1.29\mu/h\}$$
$$+1.10\times10^5N_3\{1.015-1.95\mu/h\}. \tag{26}$$

During the accumulation or decay periods discussed in Sections II and III, Rn is not in equilibrium with RaA nor RaC′, and $N_1$, $N_2$ and $N_3$ are the functions of time described by Eqs. (2), (3), (4) and Figs. 2 and 3. For the brass ionization chambers used in the experimental phases of this investigation $h=d=6$ in. $=15.24$ cm. The chambers were filled with nitrogen at 22°C and 760 mm Hg, hence, from the Bragg-Kleeman rule, $\mu=1.09$. Substituting these values in Eq. (26) we have:

$$I=(1.24N_1+0.79N_2+0.97N_3)\times10^5. \tag{27}$$

Fig. 8 shows the dependence of $I$ on time for both accumulation and decay. The experimental points, plotted on Fig. 8 for comparison with the theory, show statistical fluctuations about the mean value because of the small quantity of Rn employed in these tests ($19.66\times10^{-12}$ curie). Reliable ionization values for small values of $t$ are difficult to observe because of the possibility of the presence of heavy ions in chamber, due to filling, which require several minutes for collection. The shape of these theoretical curves is not strongly dependent on $h$ and $d$, since these must exceed $2R_3\mu$ for the cases treated by the theory. The agreement in Fig. 8 between theory and experiment is entirely satisfactory, but a more critical test is offered by observing the total equilibrium ionization due to a known amount of Rn, as is done in Section IX.

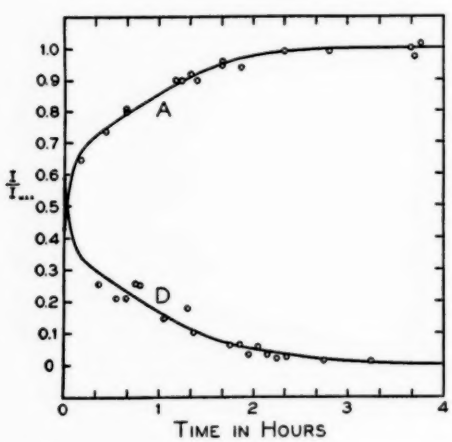


FIG. 8. Ionization in a brass chamber, $h=d=15.24$ cm, $\mu=1.09$, for (A) Rn plus accumulating RaA and RaC′, and (D) decay of RaA and RaC′ after withdrawing Rn.

## VIII. Relative Saturation of Alpha-Ray Ionization Current in Cylindrical Ionization Chambers

Brössler[19] measured the degree of saturation achieved by various collecting potentials in cylindrical ionization chambers containing large amounts of Rn and its decay products, finding the saturation also dependent on the amount of Rn. If $J$ is the saturated ion current in e. s. u. per sec., $i$ the observed ion current in e. s. u. per sec., $E$ the potential on the chamber in volts, and $k$, $K$, constants, Brössler found, for a chamber in which $h=30$ cm, $d=25$ cm, center electrode 0.6 cm diameter and RaA and RaC′ collected on the wall:

$$i=J(1-e^{-Ek}) \tag{28}$$

$$J^2k^5=K \tag{29}$$

where $K=4.44\times10^{-11}$ e. s. u.$^2$ sec.$^{-2}$ volt$^{-5}$ for $J<100$ e. s. u. per sec., and $K=4.57\times10^{-11}$ for $J>100$. At $J=100$, Brössler gave $k=0.0013512$. The measurements were presumably made with air in the ionization chamber.

For small quantities of Rn, such as are met in the Rn analysis of ordinary materials, Brössler's data predict $j=i/J=1.000$, which is not in agreement with observations. Brössler's data should, therefore, not be extrapolated beyond the range of his measurements, i.e. $10\leq J\leq210$ e. s. u. per sec.

[19] Brössler, Akad. Wiss., Wien, Ber. [II $a$] **129**, 47 (1920).

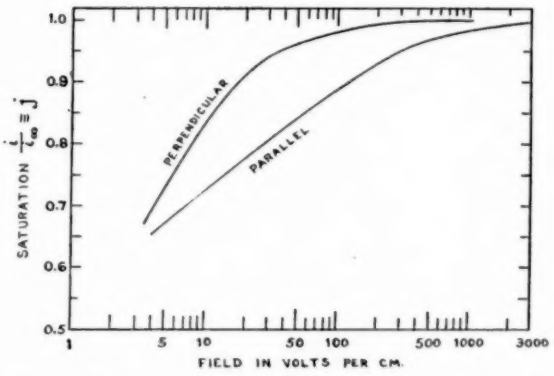


FIG. 9. Saturation of alpha-ray ionization in air at 760 mm Hg for rays (I) parallel to the collecting field, (II) perpendicular to the collecting field. (Moulin.[20])

Moulin[20] measured the relative saturation of alpha-particle ionization when the path of the ray is (a) parallel to the collecting field, (b) perpendicular to the collecting field. Measurements were made in air, $CO_2$ and $H_2$. Moulin's values for air are plotted in Fig. 9. The minimum value of the average collecting field in a cylindrical ionization chamber may be computed by neglecting end effects. Where $E$ is the potential between the wall of diameter $d$ and the center electrode of diameter $a$, and $r$ is the radial distance from the axis of the chamber to a volume element $2\pi r dr$ in area and of unit length, the minimum volumetric average field, $(dE/dr)_{av}$, in the chamber is:

$$\left(\frac{dE}{dr}\right)_{av} = \left\{\int_{a/2}^{d/2} \frac{E}{\log_e d/a} \cdot \frac{1}{r} \cdot 2\pi r dr\right\} \Big/ \frac{\pi}{4}(d^2-a^2)$$

$$= 4E/(d+a)(\log_e d/a). \qquad (30)$$

From Eq. (30) and Fig. 9 the minimum value of the saturation, $j$, may be computed for any cylindrical chamber by taking a mean value from curves I and II of Fig. 9 as describing a uniform mixture of all possible angles between the alpha-rays and the collecting field gradient. For the present chambers, at $E=300$ volts, $(dE/dr)_{av}$ $=18.7$ volts/cm, hence $j>0.84$.

Since $j$ also varies with the chemical nature of the gas in the chamber (for example, $j$ is low[21] for $CO_2$, high for very pure $N_2$), it is preferable to make a direct measurement of $j$ in any ionization-chamber-electrometer system which is being calibrated for precision measurements. This is best done by observing the ionization, $I$, at various values of $E$, and extrapolating a graph of $I/E$ *vs.* $I$ to $I/E=0$, $(E=\infty)$. For approximate use, $j$ is usually between 0.87 and 0.93 in cylindrical chambers filled with $CO_2$, air or nitrogen at 760 mm Hg, where $d$ and $h$ are between 30 and 15 cm, and $E$ is 300 volts. The saturation, $j$, at $E=300$ volts was found to be $90\pm1$ percent in the present chambers.

## IX. Capacity Calibrations for Ionization Chambers

The ionization chambers used in the present experiments were connected in the double-chamber differential circuit regularly employed[22] for the measurement of small quantities of Rn. Direct capacity calibrations were made by adding small cylindrical condensers of identical cross section but of various lengths (and hence of known differences in capacity) to the central system and observing the fractional change in capacity. Quantitative observations of the ratios of the several capacities so produced were made by several independent methods.[22b] (A) By observing the potentials induced on the central system (center electrodes of ionization chambers and string electrometer fiber) when the potential on one ionization chamber is suddenly changed by a known voltage. (B) By observing the rates of discharge of the central system with one ionization chamber evacuated, the other radiated with gamma-rays. (C) By observing the rates of discharge of the central system when Rn plus decay products is used as the ionizing agent in one of the chambers.

The method (A) is a development of the inductive method, usually credited to Harms,[23] but used over a decade earlier by Lebedew.[24] It has been used by many subsequent observers[25]

[20] Moulin, Ann. de Chem. et Phys. **21**, 550 (1910); **22**, 26 (1911).

[21] Hess and Hornyak, Akad. Wiss., Wien, Ber. [II *a*] **129**, 661 (1920).

[22] Evans, (a) Phys. Rev. **39**, 1014 (1932); Rev. Sci. Inst. **4**, 223 (1933); (b) **6**, 99 (1935).

[23] F. Harms, Physik. Zeits. **5**, 47 (1904).

[24] Lebedew, Wied. Ann. **44**, 289 (1891). Kohlrausch, *Physical Measurements* (1894), p. 380.

[25] Siegl, Akad. Wiss., Wien, Ber. [II *a*] **134**, 11 (1925); Halledauer, Akad. Wiss., Wien, Ber. [II *a*] **134**, 39 (1925); Steinke, Zeits. f. Physik **48**, 647 (1928); Schindler, Zeits. f. Physik, **72**, 625 (1931); J. Clay, Zeits. f. Physik **78**, 250 (1932); H. Lampe, Zeits. f. Physik **79**, 254 (1932).

and has been shown to agree with electrodynamic methods to 1 part in 1000 by Lampe.[25] Using the inductive principle, a null method can be employed by which capacities may be compared with a standard capacity to 1 part in $10^6$.

The numerical results from the three methods (A)(B)(C) are in agreement, within the respective probable errors of measurement, and indicate a total capacity of 16.4 cm for the double ionization-chamber string-electrometer apparatus, when the electrometer is at zero sensitivity. As was shown independently by Raitt[26] and by Sienkiewicz[27] and Benndorf[28] the effective capacity of a string electrometer rises with sensitivity. In the present apparatus, when $v$ volts are applied to the electrometer plates, and $s$ is the resulting sensitivity of the electrometer in divisions per volt, the effective capacity, $C$, is given by:

$$C=16.4(1+1.0\times10^{-5}\,vs). \tag{31}$$

An analogous equation holds for all similar electrometer systems.

There is a fourth method for measuring the capacity, $C$, of the electrometer system. Assuming the validity of the present theoretical treatment of the ionization in cylindrical chambers by Rn and its decay products, we measure (a) the equilibrium ionization, $dv/dt$, due to a known amount of Rn, and (b) the relative saturation, $j$, of this ionization current. Then employing Eqs. (25) and (27), or Eq. (33) we can compute $C$. The Rn for these tests was released from a portion of a standard radium solution, most generously furnished by Professor S. C. Lind, which was prepared[29] from pure $RaCl_2$ which had been compared, by the gamma-ray method, with the international radium standard by the U. S. Bureau of Standards. The Rn was released from a solution containing $19.66\times10^{-12}$ g Ra by boiling in a glass apparatus[30] developed for the routine analyses of liquid specimens having very low Ra content. The mean of a large number of such Rn calibrations, made over a period of two years in connection with routine analyses of feebly radioactive materials, leads to a value for $C$ which is in complete agreement with the direct measurements by the three methods of the preceding paragraph. Because of the normal statistical fluctuations resulting from the use of a feeble Ra solution,[31] the probable error is about $\pm1$ percent.

## X. General Equation for Radon Calibration of a Cylindrical Ionization Chamber

Eqs. (25) and (26) may now be combined and simplified to describe the ionization current produced by Rn and RaA+RaC′ in transient equilibrium. If $A$ curies of Rn are introduced into the cylindrical ionization chamber at time $t=0$, and the rate of discharge, $dv/dt$ volts per sec., is observed at time $t\geq3$ hr., when transient equilibrium is practically established, then $N_1=3.7\times10^{10}Ae^{-\lambda_1 t}$, where $\lambda_1$ is the decay constant[32] of Rn, $7.551\times10^{-3}$ hr.$^{-1}$, and $N_2=1.00054N_1$, $N_3=1.0089N_1$, and

$$I=10^5N_1(3.57-5.00\mu/h-3.47\mu/d+5.48\mu^2/hd) \tag{32}$$

$$dv/dt=300jeI/C=5.3\times10^8(j/C)(3.57-5.00\mu/h-3.47\mu/d+5.48\mu^2/hd)Ae^{-\lambda_1 t}. \tag{33}$$

Eq. (33) is the general equation for the Rn calibration of any cylindrical ionization chamber having $d\geq2\mu R_3$ and $h\geq2\mu R_3$, and is the solution of Eq. (1).

## Acknowledgments

The assistance of Russell W. Raitt and Ben Holzman, of the California Institute of Technology, and of Arthur Kip, Fred Ludecke and Raymond Mugele of the University of California in various experimental phases of this investigation is deeply appreciated. Grateful acknowledgment for hospitality and support is also made to the Physics Department of the University of California, where the present theoretical treatment was begun during the author's tenure as National Research Council Fellow.

[25] R. W. Raitt, personal communication, Dec. 16, 1932.
[27] Sienkiewicz, Physik. Zeits. **34**, 376 (1933).
[28] Benndorf, Physik. Zeits. **34**, 335 (1933); Akad. Wiss., Wien, Ber. [II a] **142**, 175 (1933).
[29] Lind and Roberts, J. Am. Chem. Soc. **42**, 1170 (1920).
[30] Evans, Phys. Rev. **46**, 328 (1934); Rev. Sci. Inst. **6**, 99 (1935).
[31] v. Schweidler, Physik. Zeits. **14**, 198 (1931); T. Ehrenfest, Physik. Zeits. **14**, 675 (1913).
[32] A useful table of $e^{-\lambda_1 t}$ is given in Meyer and Schweidler, *Radioaktivität* (1927), p. 419. Because of a misprint the value of $e^{-\lambda_1 t}$ for $t=3$ hr. should be 0.9776, instead of 0.9786, as there given.

# Double Electron Transitions in X-Ray Spectra

F. BLOCH, *Stanford University*

(Received May 2, 1935)

Elementary processes are considered, in which simultaneous transitions of an inner and an outer atomic electron result in the emission of one single light quantum. Considering the nuclear distance of the inner electron as small compared to that of the outer electron, formulae are developed for the probability of double transitions by dipole radiation. The occurrence of the Cu $K\alpha_3$ satellite is given as a possible illustration of the case, where the inner transition alone occurs by dipole emission; a special consideration applies in this connection to the probability of simultaneous inner ionization and outer excitation. For the case of a forbidden inner transition, the simultaneous emission of a light quantum and an outer electron (radiative Auger effect) is discussed.

## 1. INTRODUCTION

THE possibility of double electron transitions in x-ray spectra was first suggested by Richtmyer[1] in connection with the occurrence of the so-called "satellites" of x-ray spectral lines. According to his theory, the satellite line is due to the simultaneous transition of an inner and an outer electron from a higher to a lower energy level, so that the energy of the emitted quantum is the sum of both energy differences, while for the "parent" line only the transition of the inner electron should be responsible. An alternative explanation of the satellites has been given by Wentzel[2] and Druyvesteyn,[3] who attribute their appearance to the possibility of double ionizations of inner shells.

A quantitative theoretical justification of the double transition hypothesis has in the first place to explain a considerable probability of a simultaneous excitation of an outer electron and an ionization of an inner shell while for the double ionization a sufficiently frequent occurrence of such processes has to be explained.

Whereas it seems at first that at least one of these two theories must be wrong, one has to consider the possibility that both have a certain but different range of applicability. Indeed, the experimental evidence rather leads to the conclusion that one has to assume *different* mechanisms according to whether one considers the satellites of $K$ or $L$ lines. While the former occur only in the spectra of comparatively light elements, the latter show an irregular dependence[4] on the atomic number $Z$, being absent in the range from about $Z=50$ to $Z=70$, but occurring both for lower and higher atomic numbers.

Recently Coster and Kronig[5] have succeeded in giving a satisfactory explanation of the $L$ satellites both as to their great intensities and their peculiar dependence on $Z$. They have to be understood as the result of a special process of double ionization, due to the Auger emission of an $M$ electron and the simultaneous radiationless transition of an $L$ electron from $(2p)$ to $(2s)$.

It is clear, however, that such an explanation cannot account for the satellites of the $K$ series, and it seems to us that here, indeed, Richtmyer's point of view has to be taken into consideration. Some time ago, Ramberg[6] published arguments against the double transition theory, coming to the conclusion that such transitions should be expected to be far too improbable to account for the observed intensity of the $K\alpha$ satellites. In his considerations, however, decisive features are omitted which, as we will see, bring the theoretical intensity of the satellites quite close to the observed order of magnitude. Our main objection applies against his argument, that the ratio of the probabilities of double excitation (i.e., simultaneous ionization of the $K$ shell and excitation of an outer level) to single excitation (i.e., mere ionization of the $K$ shell) should be of the same order of magnitude as those of double transition to single transition. This would imply that the square of the latter ratio should give approximately the intensity ratio of satellite to parent line and would indeed turn out to be of far too

[1] F. K. Richtmyer, J. Frank. Inst. **208**, 325 (1929).
[2] G. Wentzel, Ann. d. Physik **66**, 437 (1921).
[3] M. J. Druyvesteyn, Zeits. f. Physik **43**, 707 (1927).
[4] F. K. Richtmyer and S. Kaufman, Phys. Rev. **44**, 605 (1933).
[5] D. Coster and R. de L. Kronig, Physica **2**, 1, 13 (1935).
[6] E. G. Ramberg, Phys. Rev. **45**, 389 (1934).

small an order of magnitude. Although, however, as Ramberg points out, both double excitation and double transition involve the coupling of an inner with an outer electron, there is nevertheless a radical difference between the two processes, making the former far more probable than the latter. While in the double transition the inner electron merely changes between two inner levels, for the double excitation an inner electron is completely removed, thus in a nonadiabatic process changing approximately the effective atomic number $Z^*$ of an outer electron into $Z^*+1$. As we will point out later for the case of the Cu $K\alpha$ satellite, this has as a consequence that *if* the $K$ electron is removed, there is not a small probability but almost *certainty* that at least one of the outer electrons will be excited; thus we understand also why in this case the satellite is found on the short wavelength side of the parent line and that there are not, as Ramberg would expect, two corresponding satellites on both sides, the more intense one lying on the long wavelength side.

We believe also that there are other cases of double transitions. A particularly interesting one is associated with the occurrence of "forbidden" lines, and is brought to evidence by recent observations of Ross.[7] This mechanism can roughly be described in the following way: Instead of performing a forbidden radiative transition the atom is able to emit simultaneously a light quantum and an outer electron. The total system (consisting of inner + outer electron) can thus radiate by dipole emission (instead of quadrupole emission, as in the case of the forbidden line) and emit a continuum on the long wavelength side of the forbidden line, this type of "satellite" being more intense than the weak "parent" line.

A more quantitative discussion of the processes here considered would necessitate very accurate knowledge of atomic eigenfunctions and involve a great amount of numerical integration. We will restrict ourselves in the next sections to pointing out the main characteristics of the most interesting cases and estimating their probability under special conditions.

## 2. Probability of Double Transitions

We consider an inner electron 1 and an outer electron 2, assuming that the orbital dimensions of 1 shall be small compared with those of 2; in this case the eigenfunctions of 1 and 2 will overlap only very little, so that their exchange can be neglected. The presence of other atomic electrons shall be taken into account only insofar as they modify the potential field, in which 1 and 2 move, and as those transitions of 1 and 2 shall be excluded that lead to states occupied by any of the other electrons. This means that as "zero order" atomic eigenfunction we assume a function that can be written as a product of functions, each of them depending only on the coordinates of one electron.

Calling $\mathfrak{r}_1$ and $\mathfrak{r}_2$ the position vectors of electron 1 and 2 with components $(x_1y_1z_1)$ and $(x_2y_2z_2)$, respectively, we may expand the interaction energy of 1 and 2 in terms of the coordinates of 1 in the form:

$$e^2/|\mathfrak{r}_1-\mathfrak{r}_2| = e^2/r_2+v(\mathfrak{r}_1, \mathfrak{r}_2)=e^2/r_2+v'(\mathfrak{r}_1, \mathfrak{r}_2)+v''(\mathfrak{r}_1, \mathfrak{r}_2), \tag{1}$$

where

$$v'(\mathfrak{r}_1, \mathfrak{r}_2)=e^2(\mathfrak{r}_1\mathfrak{r}_2)/\mathfrak{r}_2^3 \tag{2}$$

contains the terms that are linear, and

$$v''(\mathfrak{r}_1, \mathfrak{r}_2)=e^2/2[3(x_1x_2+y_1y_2+z_1z_2)^2/r_2^5-r_1^2/r_2^3] \tag{3}$$

contains the terms that are quadratic in the coordinates of 1, higher order terms being neglected. The term $e^2/r_2$ in (1) has to be taken as part of the nonperturbed potential of electron 2, representing the screening due to the presence of electron 1. The coupling energy $v=v'+v''$ shall be considered as a small perturbation. The nonperturbed eigenfunctions of 1 and 2 shall be generally designated by $u_\mu(1)$, $u_m(2)$, respectively, the corresponding energy levels by $E_\mu$ and $E_m$. Keeping only the terms linear in the matrix elements of $v$, we can write the eigenfunction of the initial state

[7] F. Bloch and P. A. Ross, Phys. Rev. **47**, 884 (1935).

$$\psi_{\alpha a}(1,2)=u_\alpha(1)u_a(2)-\sum_{\mu,\ m\pm\alpha,\ a}\frac{v_{\mu m,\ \alpha a}}{E_\mu+E_m-E_\alpha-E_a}u_\mu(1)u_m(2) \tag{4}$$

and that of the final state

$$\psi_{\beta b}(1,2)=u_\beta(1)u_b(2)-\sum_{\mu,\ m\pm\beta b}\frac{v_{\mu m,\ \beta b}}{E_\mu+E_m-E_\beta-E_b}u_\mu(1)u_m(2). \tag{4a}$$

We may assume furthermore, that not only the orbital dimensions of 1 shall be small compared with those of 2, but also, that the orbital dimensions of the final state $\beta$ of electron 1 shall be small compared with those of the initial state $\alpha$. In this case, the coupling energy $v$ will practically act only on the initial state $\alpha$, $a$ and for the final state $\beta$, $b$, we can, instead of (4a) write approximately

$$\psi_{\beta b}(1,2)=u_\beta(1)u_b(2). \tag{5}$$

The emission of a light quantum with frequency

$$\nu=(E_\alpha+E_a-E_\beta-E_b)/h$$

will be mainly due to a radiative transition of 1. According to the general rules of the quantum theory of radiation[8] the probability for such a transition will then be proportional to the absolute square of

$$I_{\beta b}{}^{\alpha a}=\int\psi^{\alpha a*}\exp(i\mathbf{k}\mathbf{r}_1)(\mathbf{n},\operatorname{grad}_1)\psi_{\beta b}d\tau_1 d\tau_2, \tag{6}$$

where $\mathbf{n}$ is a unit vector, perpendicular to the direction of propagation of the emitted quantum and $\mathbf{k}$ its vector of propagation; $(\mathbf{n}\ \operatorname{grad}_1)$ stands for

$$n_x\partial/\partial x_1+n_y\partial/\partial y_1+n_z\partial/\partial z_1$$

and $d\tau_1$, $d\tau_2$ are the elements of the configuration space of 1 and 2, respectively. Using the expressions (4) and (5) and taking the functions $u(2)$ as orthogonal and normalized, we find for the "parent" line

$$I_\beta{}^\alpha=\int u_\alpha{}^*(1)\exp(i\mathbf{k}\mathbf{r}_1)(\mathbf{n},\operatorname{grad}_1)u_\beta(1)d\tau_1 \tag{6a}$$

and for the "satellite"

$$I_{\beta b}{}^{\alpha a}=\sum_\mu\frac{v_{\alpha a,\ \mu b}}{E_\alpha+E_a-E_\mu-E_b}\int u_\mu{}^*(1)\exp i(\mathbf{k}\mathbf{r}_1)(\mathbf{n},\operatorname{grad}_1)u_\beta(1)d\tau_1. \tag{6b}$$

The difference of frequency $\Delta\nu=(E_b-E_a)/h$ between parent line and satellite will always be so small that their intensity ratio will be given by the ratio of the absolute squares of (6a) and (6b). The discussion of (6a) and (6b) offers two entirely different aspects, according to whether the parent line is allowed or forbidden and they shall therefore be treated separately.

**(a) Parent line allowed**

If $l_\mu$ is the angular momentum (measured in units $h/2\pi$) of a state $\mu$ of electron 1, the well-known selection rules imply in this case that $l_\alpha-l_\beta=\pm1$. Similarly, in (6b) there will noticeably occur only states $\mu$, for which $l_\mu-l_\beta=\pm1$. Both conditions together lead to the selection rule $l_\alpha-l_\mu=0,\ \pm2$. We may now split the matrix elements, occurring in (6b) into two parts, writing

$$v_{\alpha a,\ \mu b}=v'_{\alpha a,\ \mu b}+v''_{\alpha a,\ \mu b} \tag{7}$$

with

$$v'_{\alpha a,\ \mu b}=\int u_\alpha{}^*(1)u_a(2)v'(\mathbf{r}_1,\mathbf{r}_2)u_\mu(1)u_b(2)d\tau_1 d\tau_2 \tag{7a}$$

and

$$v''_{\alpha a,\ \mu b}=\int u_\alpha{}^*(1)u_a(2)v''(\mathbf{r}_1,\mathbf{r}_2)u_\mu(1)u_b(2)d\tau_1 d\tau_2, \tag{7b}$$

[8] Cf. e.g., G. Wentzel, *Handbuch der Physik*, 24, part 1, p. 743 f.f.

using for $v'$ and $v''$ the expressions given in (2) and (3). Since (7a) contains the coordinates of 1 *linearly*, it leads only to a result different from zero, if $l_\alpha - l_\mu = \pm 1$. This condition contradicts the selection rule $l_\alpha - l_\mu = 0, \pm 2$, stated above and means that for the case of an allowed parent line, the terms (7a) will give *no* contribution to (6b). On the contrary, since $v''$ contains the coordinates of 1 in the *second* power, (7b) will generally be different from zero for $l_\alpha - l_\mu = 0, \pm 2$.

We can therefore write (6b) in the form

$$I_{\beta b}{}^{\alpha a} = \sum_\mu \frac{v''_{\alpha a,\ \mu b}}{E_\alpha + E_a - E_\mu - E_b} \int u_\mu{}^*(1) \exp(i\mathbf{k}\mathbf{r}_1)(\mathbf{n}, \operatorname{grad}_1) u_\beta(1) d\tau_1. \tag{8}$$

The energy differences $E_\alpha - E_\mu$ of inner atomic levels will be big, compared with the outer atomic difference $E_a - E_b$, so that we will get a considerable contribution to the sum (8) only from the term $\mu = \alpha$, which simplifies our expression to

$$I_{\mu b}{}^{\alpha a} = \frac{v''_{\alpha a,\ \alpha b}}{E_a - E_b} \int u_\alpha{}^*(1) \exp(i\mathbf{k}\mathbf{r}_1)(\mathbf{n}, \operatorname{grad}_1) u_\beta(1) d\tau_1. \tag{8a}$$

Comparing (8a) with (6a) we find finally for the intensity ratio of satellite to parent line

$$|I_{\beta b}{}^{\alpha a}|^2 / |I_\beta{}^\alpha|^2 = |v''_{\alpha a,\ \alpha b}|^2 / (E_a - E_b)^2. \tag{9}$$

In the following section we shall discuss this formula for the case of the Cu $K\alpha_3$ satellite.

**(b) Parent line forbidden**

We will consider here only the special case of a forbidden line, for which $l_\alpha - l_\beta = 0, \pm 2$, so that (6a) vanishes. The situation is here just the inverse of case (a); the condition $l_\mu - l_\beta = \pm 1$ which is still necessary for the nonvanishing terms in (6b) implies here $l_\alpha - l_\mu = \pm 1, \pm 3$, a selection rule, which is only compatible with the terms (7a) but not with (7b). We obtain therefore

$$I_{\beta b}{}^{\alpha a} = \sum_\mu \frac{v'_{\alpha a,\ \mu b}}{E_\alpha + E_a - E_\mu - E_b} \int u_\mu{}^*(1) \exp(i\mathbf{k}\mathbf{r}_1)(\mathbf{n}, \operatorname{grad}_1) u_\beta(1) d\tau_1. \tag{10}$$

The main difference between (10) and (8) has to be seen in the circumstance that here the term with $\mu = \alpha$ gives no contribution, since the average value of the coordinates of 1 in the state $\alpha$ vanishes. The sum has therefore to be extended over "intermediate" states $\mu$ of the electron 1, different from $\alpha$. Now the exclusion-principle formulated in the antisymmetry of the zero order eigenfunction demands that only such states $\mu$ shall be taken as are not occupied by any other electron and we have to investigate what possibilities there are left for $\mu$. One of them is that $\mu$ refers to one of the optical levels of the atom; but the corresponding terms in (10) will generally appear with such small numerators and such big denominators that their contribution is negligible. Another possibility is $\mu = \beta$. The state $\beta$ has certainly to be supposed unoccupied since otherwise it could not be the final state for electron 1; however, for $\mu = \beta$ the integral in (10) vanishes. The only remaining possibility is that $\mu$ refers to the state $a$, left unoccupied by the transition of electron 2 from $a$ to $b$. This term will give the main contribution to (10), if the orbit of state $a$ lies in deeper regions of the atom than those of optical levels. This assumption can and shall be made for further simplifications; it is not in contradiction to the distinction of "inner" and "outer" electrons, introduced in the beginning of this section since this distinction demands only the smallness of the orbital dimensions of $\alpha$, compared with those of $a$. Omitting in (10) all terms, except the one with $\mu = \alpha$, we find thus

$$I_{\beta b}{}^{\alpha a} = [v'_{\alpha a,\ ab}/(E_\alpha - E_b)] \int u_a{}^*(1) \exp i(\mathbf{k}\mathbf{r}_1)(\mathbf{n}, \operatorname{grad}_1) u_\beta(1) d\tau_1. \tag{11}$$

Instead of comparing the probability of such a double transition with the forbidden single transition $\alpha \rightarrow \beta$, it is more convenient to compare it with that of the single transition $a \rightarrow \beta$. Using (6a), we find for their ratio

$$R = |I_{\beta b}{}^{\alpha a}|^2 / |I_{\beta}{}^{a}|^2 = |v'_{\alpha a,\, \alpha b}|^2 / (E_a - E_b)^2. \tag{12}$$

In a paper, recently published with Ross,[7] we gave an illustration of case (b), applying to the continuum, observed on the long wavelength side of $K\beta_5$ of molybdenum. Here the final state $b$ of the outer electron 2 has to be considered to lie in the continuous part of the energy spectrum, corresponding to an ejection of this electron. Instead of a well-defined satellite, we get then a continuous band; the separation of its short wavelength end from the parent line is given by the ionization energy of the ejected electron. Neglecting the binding forces, acting on the ejected electron (which is a good approximation except for the immediate neighborhood of the short wavelength limit of the continuum) we find from (12) for the relative intensity of the continuum lying within a frequency range $d\nu$:

$$dR = (8\pi m k_2 d\nu / h(I_a + E)^2) \overline{|e^2 \int u_\alpha{}^*(1) u_a{}^*(2) [(\mathbf{r}_1 \mathbf{r}_2)/r_2{}^3] u_a(1) \exp i(\mathbf{k}_2 \mathbf{r}_2) d\tau_1 d\tau_2|^2}. \tag{13}$$

In this formula the horizontal line refers to the averaging over the different directions of the vector $\mathbf{k}_2$ with absolute value

$$k_2 = (2\pi/h)(2mE)^{\frac{1}{2}}.$$

$E = h\nu_{\alpha,\beta} - h\nu - I_a$ is the kinetic energy of the ejected electron with mass $m$, $\nu_{\alpha,\beta}$ the frequency of the forbidden parent line and $I_a$, $I_\alpha$ the ionization energies of the initial states of inner and outer electrons, respectively.

The details of the intensity distribution represented by (13) depend sensitively on the special shape of the eigenfunction $u_a(2)$. As general features, we may mention: vanishing for $E = 0$ (short wavelength limit of the continuum) rapid approach of a maximum and slow falling off towards longer wavelengths.

The ratio of the total intensity of the continuum to that of the line $a \rightarrow \beta$ can be estimated to be of the order of magnitude

$$\int dR \leqq (e^4/E_a{}^2)(r_i/r_0{}^2)^2, \tag{14}$$

$r_i$ and $r_o$ being the radius of the initial orbits of inner and outer electrons, respectively.

### 3. Intensity of the Cu $K\alpha$ Satellite

The general formula (9) for the intensity ratio of a satellite to its strong parent line cannot be evaluated without further assumptions. We want to estimate its order of magnitude for the special case of the satellite $K\alpha_3$ of the Cu $K\alpha_1$ line, which has been carefully investigated by DuMond and Hoyt;[9] its separation from the parent line $K\alpha_1$ corresponds to an energy difference of about 35 e.v. The outer electronic configuration of Cu is of the type $(3d)^{10}\ (4s)^1$, the $4s$ electrons in the solid state being probably conduction electrons. After having removed one inner electron, the $3d$ electrons have to be compared with those of Zn, the element with the next higher atomic number; their ionization energy, the first ionization potential of the doubly ionized Zn equals 40 e.v.[10] Considering the $4s$ electrons in the metal as practically free, it seems therefore plausible to assume that Cu $K\alpha_3$ is due to a previous excitation of a $3d$ electron and emission of a $1s$ electron and a subsequent transition $2p,4s \rightarrow 1s,3d$.

As already indicated in the introduction, we want first to show that the simultaneous excitation of a $3d$ electron and a transition $1s \rightarrow \infty$ has a considerable probability; in fact, the expression

[9] J. W. M. DuMond and A. Hoyt, Phys. Rev. **36**, 799 (1930). The following considerations shall be regarded as an illustration of a possible double electron transition. That they cannot claim general validity is shown by the work of Coster and Thijssen on one of the $K$ satellites of sulfur.

[10] Bacher and Goudsmit, *Atomic energy states*, page 525.

(9) has to be multiplied by this probability in order to obtain the true intensity ratio of satellite to parent line. Let $u_{b'}$ and $u_b$ be the normalized eigenfunctions of one and the same $3d$ state in Cu and Zn, respectively. Then the probability that after having suddenly removed an inner electron, the electron will still be in its original $3d$ state, is obviously given by

$$1-\epsilon=|\int u_{b'}^{*}, u_b d\tau|^2.$$

$\epsilon$ is then the probability that the electron is *not* found in its original but in an excited state since all states with lower energy are occupied by other electrons. For the estimation of $\epsilon$ we assume that both states $b'$ and $b$ can be described by hydrogenic functions, but with different effective atomic numbers $Z^{*'}$ and $Z'$. We thus find for $l=Z$, $n=3$

$$\epsilon=1-[4Z^{*'}Z^{*}/(Z^{*'}+Z^{*})^2].^{7}$$

$Z^{*}$ and $Z^{*'}$ we choose such, that they account for the observed ionization energy of $3d$ electrons of $Zn^{++}$ and $Cu^{+}$ respectively, the former being 40, the latter 20.2 e.v.[11] We obtain so

$$Z^{*}=3(40/13.5)^{\frac{1}{2}}=5.2, \quad Z^{*'}=3(20.2/13.5)^{\frac{1}{2}}=3.7$$

and $$\epsilon=0.2.$$

This means that for a specified one of the 10 $3d$ electrons there is a chance of about 1/5, that after having removed one inner electron we will find it in an excited state. Excluding the possibility that more than one of these electrons will be excitated, we have now to ask for the probability of having *any* one of them excited. Calling, for the moment, $g$ the number of such equivalent electrons, we find for this probability

$$P=g\epsilon/(g-1)\epsilon+1$$

or with $g=10$, $\epsilon=0.2$, $P=5/7$. (15)

It is true that the assumptions which have led to this result, especially that of hydrogenic eigenfunctions, can give only rough approximations; nevertheless we may state that it is perfectly understandable that there is practical certainty for an outer excitation, the value (15) being rather close to unity and therefore only a satellite on the short wavelength side is observed. Of course we cannot exclude the possibility of a corresponding long wavelength satellite, but in any case we would expect it to be considerably weaker than the one on the short wavelength side.*

For the intensity ratio $R$ of satellite to parent line, we have now

$$R=P|I_{\beta b}^{\alpha a}|^2/|I_{\beta}^{\alpha}|^2,$$

where in our case $\alpha$ stands for $(2p)$, $\beta$ for $(1s)$, $a$ for $(4s)$, $b$ for $(3d)$. Since we only want to estimate the order of magnitude, we will leave out all factors of order of magnitude 1, and using (9), write $R$ in the approximate form

$$R\leqq(e^4/(E_a-E_b)^2)[(r_i)^2/(r_0)^3]^2,$$

where $r_i$ is of the order of magnitude of the radius of the $2p$ orbit, $r_0$ of the order of magnitude of the radius of either $4s$ or $3d$ of the doubly ionized Zn. From the corresponding ionization energies, we may assume

$$r_i\leqq a_0/8, \quad r_0\leqq a_0/2,$$

$a_0$ being the Bohr radius. Taking furthermore for $E_b-E_a$ the energy, indicated by the separation from satellite to parent line, i.e., $E_b-E_a=35$ e.v. $\leqq 3I_0$ where $I_0$ is the ionization energy of hydrogen, we find approximately

$$R\leqq(1/8)^4/9(1/2)^6=1/576. \qquad (16)$$

This result is only about a factor 3 times smaller than the observed ratio $R=1/180$, but it is naturally very unsure, because of the high power in which all possible errors appear. It shows, however, at least for the case of the Cu $K\alpha_3$ satellite, that the observed intensity lies entirely within the scope of the order of magnitude, theoretically to be expected and makes it plausible that here, indeed, we are faced with an emission by double electron transition.

[11] Reference 10, p. 180.

* If inner and outer excitation would *always* occur together, the satellite corresponding to the transition

$$2p(3d)^{10}\rightarrow 1s(3d)^{9}4s$$

could of course not be observed, because the initial state would never be realized. One may object that nevertheless there should be a long wavelength satellite

$$2p(3d)^{9}\rightarrow 1s(3d)^{8}4s.$$

It seems plausible, however, that the removal of a second (and even more so of a third, etc.) electron from the $3d$ level should occur with considerably smaller probability, so that this satellite should be expected to be quite weak. Besides it should not be exactly opposite to the long wavelength satellite discussed above.

# The Size and Arrangement of Bismuth Microcrystals Formed from Vapor

C. T. LANE, *Sloane Physics Laboratory, Yale University*

(Received April 29, 1935)

The magneto-resistance of films of bismuth, deposited on glass and mica, has been measured at room and liquid-air temperatures and for various angles between the film normal and the magnetic field ($H=16{,}000$). The ratio $\Delta R_{-180°C}/\Delta R_{+20°C}$ rises steeply for thicknesses between 0.1 $\mu$ and 0.4 $\mu$ and then much more gradually to a thickness of 4$\mu$. The thermal coefficient of resistance shows no corresponding anomaly. X-ray analysis shows all the films to be composed principally of small crystals with (111) parallel to the backing. $\Delta R$ varies with the direction of $H$, the current remaining always in one direction in the film, as predicted, from experiments on monocrystals for such an assembly. The bearing of these results on the structure of metallic films is briefly discussed.

## INTRODUCTION

ALTHOUGH there is a voluminous literature on the subject of metallic films, a wide divergence of opinion exists with regard to their actual structure. Some writers suppose that metallic films of thickness about 1$\mu$ or less possess no regular crystalline structure; other authors take the opposing stand that such films possess the normal lattice of the bulk material. Still another view is that, depending on the conditions of preparation, thin films are initially amorphous but may be converted into normal structure by appropriate heat treatment.[1] A rather significant point seems to be that most films reported to be amorphous are produced by cathode sputtering and the unavoidable gas in the apparatus may form unstable compounds which break down on heating.[2] In particular, an investigation by Gross[3] on evaporated Bi films indicates that such films consist of minute crystallites, having the normal Bi lattice, the average size increasing as the film thickness increases. Further he finds that films less than about 1$\mu$ thick possess fiber structure, thicker ones have a random orientation of the crystallites. Kirchner[4] has more recently investigated very thin bismuth films (0.01$\mu$ and less) by means of electron diffraction. He finds that such films possess a fiber structure with the (111) plane parallel to the backing substance. The lattice constant deduced agrees with that determined by x-rays.

Experiments on colloidal powders of Bi have shown that above a certain critical particle size (about 1$\mu$) the negative magnetic susceptibility is nearly constant, below this limit it decreases as the particle size is reduced. Ehrenfest[5] and Raman[6] have advanced the hypothesis that the very large diamagnetism of Bi is due to long electron paths and the above experiments substantiate this view and fix the dimensions of such paths at about 1$\mu$. A comparison between well-known experimental facts relating to the magnetic susceptibility and the magneto-resistance in Bi suggests that they have a common origin, possibly the long paths just mentioned.

If we accept the view that progressively thinner films possess progressively smaller crystallites, we should expect, on the basis of the above, the magneto-resistance to show a sharp discontinuity at some critical film thickness. To test this idea the following investigation was undertaken.

## TECHNICAL METHODS

All the films used in this experiment were produced by evaporation of the Bi metal in high vacuum, and deposited on glass or mica backings. The arrangement of the evaporating apparatus is shown in Fig. 1. *A* is a cylindrical furnace, with a rectangular slot approximately 4×0.5 cm cut in the wall; *BB* are two copper ends. The heating units consist of Mo wire wound on mica forms lying in three grooves running lengthwise along the tube. Over the tube and windings is placed a heavy copper cylinder. The material of the tube is German "Sillimantin—R Masse." The three heating units are connected in parallel between the blocks *BB*. One of the electrical input leads (*L*) is water-cooled. The lower part of the

[1] J. Kramer, Ann. d. Physik [5] **19**, 37 (1934).
[2] W. Büssem, F. Gross, Zeits. f. Physik **86**, 135 (1933).
[3] F. Gross, Zeits. f. Physik **64**, 520, 537 (1930).
[4] F. Kirchner, Zeits. f. Physik **76**, 576 (1932).
[5] P. Ehrenfest, Physica **5**, 388 (1925).
[6] C. V. Raman, Nature **123**, 945 (1929).

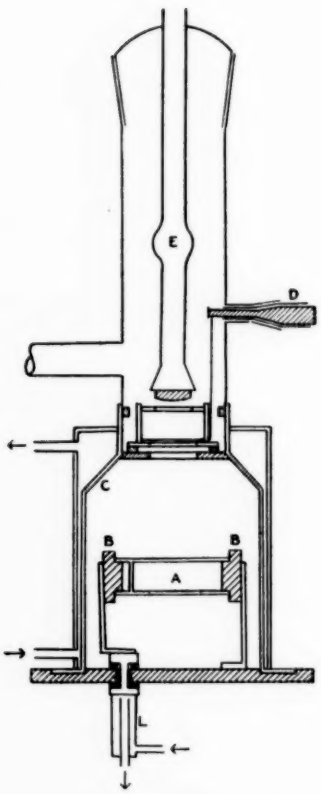


FIG. 1. Apparatus for producing thin bismuth films.

apparatus consists of a copper tube ($C$) also water-cooled. The molecular beam is collimated by three slits and the second one has a "trap-door" arrangement actuated from $D$, so that the time of deposit can be accurately controlled. The backing material, on which the film is deposited, is fixed to $E$, which consists of a copper-to-glass seal. In this way the backing surface may be cooled with liquid air if desired. During evaporation a vacuum of about $10^{-5}$ mm Hg is maintained in the apparatus.

The films were all about $0.5\times 2$ cm$^2$, with a thick deposit of metal at each end and were clamped between brass blocks mounted on a lavite block. This gave satisfactory electrical contact.

For measurements at low temperatures a thermostat similar to the one employed by Foëx and Forrer[7] for magnetic susceptibility investigations was constructed. This gave a continuous variation in temperature from $-180$°C to $+20$°C and was economical to use. The magnetic field was produced by a large Weiss water-cooled magnet. The field over the surface of the film was constant at about 16,000 gauss in all the experiments. A Wheatstone bridge arrangement was used to measure the electrical resistance. The film thickness was determined in the usual manner by weighing. A small goniometer was employed which permitted the rotation of the film in the magnetic field about any one of three mutually perpendicular axes.

[7] G. Foëx and R. Forrer, J. de physique [6] **7**, 180 (1926).

## PROCEDURE AND RESULTS

The conventional method of expressing magneto-resistance is by the ratio $\Delta r/r$ where $\Delta r$ is the increase in $r$ when the magnetic field is applied and, as Gross[3] has already shown, this ratio when plotted against film thickness has a rather ill-defined discontinuity between 1 and $2\mu$. Unfortunately such a curve tells us nothing about any possible discontinuities in the magneto-resistance, since it has long been known that the resistance $r$ itself is a discontinuous function of film thickness. Gross explains the form of his $\Delta r/r$ *versus* thickness curve on this basis. We can, however, as will presently appear, proceed in a somewhat different manner. In Fig. 2 is plotted the ratio of the field free resistance at any temperature $T$ to that at $+20$°C for a number of films of widely different thicknesses. The points are seen to cluster reasonably well about a smooth curve, indicating that the temperature coefficient of resistance, in the range studied, is very approximately independent of the thickness of the film. The ratio

$$\frac{(\Delta r/r)_{T_1}}{(\Delta r/r)_{T_2}} \propto \frac{(\Delta r)_{T_1}}{(\Delta r)_{T_2}}$$

is therefore a measure of the temperature dependence of the magneto-resistance. In Fig. 3 this ratio has been plotted against film thickness, the two temperatures chosen being $-180$°C and $+20$°C, respectively. A sharp discontinuity is seen to occur at about $0.4\mu$ and the ratio is seen to extrapolate to somewhere near unity at zero film thickness. Unit ratio means temperature independence. A possible explanation of this result is given in the discussion.

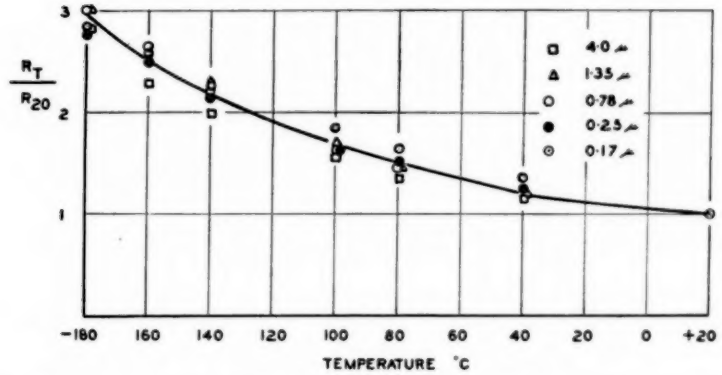


FIG. 2. Relation between field free resistance and temperature for various films.

In order to gain some additional information regarding the crystalline structure of the films under investigation, both magnetic and x-ray tests were made. The x-ray analysis was carried out using Mo radiation, the film being set at the appropriate Bragg angle for reflection from the (111) plane of Bi. A typical photograph is reproduced in Fig. 4 for a film about $2\mu$ thick and shows a definite fiber structure. Analysis of the picture shows the (111) plane to be parallel to the backing, with the (200) and (220) planes also giving reflections. It was not found possible to obtain photographs of the very thinnest films tested, because of the small amount of scattering matter present. Films $3$–$4\mu$ in thickness also showed the same fiber structure, in disagreement with Gross who reported films of this thickness to have a random orientation of crystallites.

It has long been known that the magneto-resistance of Bi single crystals is anisotropic and Stierstadt[8] in a number of recent papers has reported extensive measurements for Bi monocrystals. This suggests a convenient way to determine the orientation of the crystallites in the film. Hence three sets of experiments, in which films were rotated in a magnetic field, were undertaken. Hereafter an axis perpendicular to the plane of the film is referred to as the [111] axis.

(1) As the film was rotated about an axis parallel to *H* (the magnetic field), the current and [111] axis being kept mutually perpendicular to

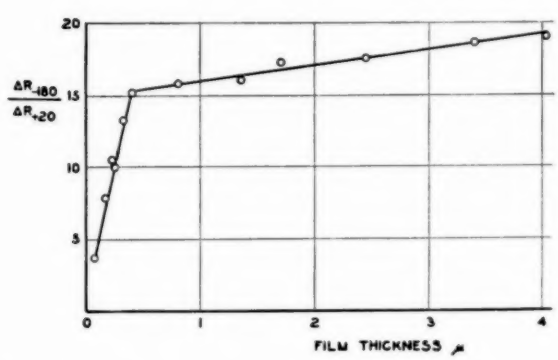


FIG. 3. Relation between temperature dependence of magneto-resistance and film thickness.

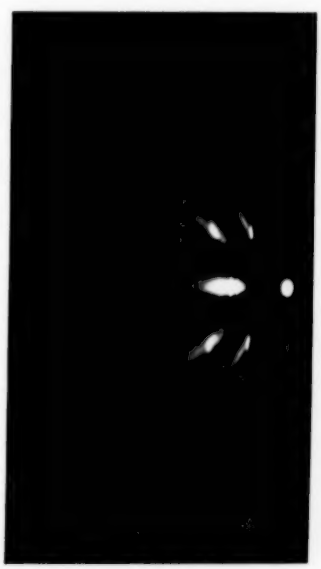

FIG. 4. Bragg photograph of $1.8\mu$ Bi film. Film set with its normal at 84° 21′ to incident beam.

[8] O. Stierstadt, Zeits. f. Physik **80**, 636; **85**, 310, 697 (1933); **87**, 687 (1934).

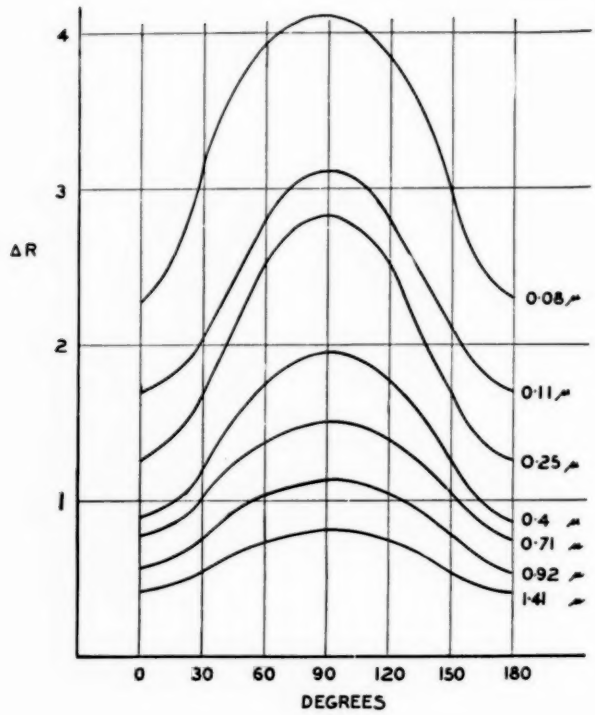


FIG. 5. Relation between magneto-resistance and magnetic field direction for various films.

$II$, no variation in $\Delta R$ was found. This is typical of a polycrystalline aggregate.

(2) As the film was rotated about the [111] axis with the latter always perpendicular to the magnetic field, $\Delta r$ was found to vary harmonically in a way which was again entirely typical of a polycrystalline aggregate.

(3) As the film was rotated about the current as axis, the latter remaining always perpendicular to $II$, $\Delta r$ varied in a characteristic manner as shown in Fig. 5. Now these curves are identical with those found for a monocrystal with [111] $\perp II \perp$ current rotated about the current as axis.[8*] Further the form of the curve is seen to be independent of the film thickness.

## DISCUSSION

The first fact which emerges from these experiments is that all the films within the range $0.1\mu$ to $4\mu$ are definitely crystalline. The curves in Fig. 5 alone rule out any possibility of an amorphous structure. Further the x-ray photographs and the magnetic experiments show that all the films possess a fiber structure with (111) parallel to the plane of the backing (Exp. 3), the orientation being otherwise random (Exps. 1 and 2). This disagrees with Gross' statement that only films less than $1\mu$ thick possess fiber structure.

A possible explanation of Fig. 2 is as follows. In the introduction we have already outlined the Ehrenfest-Raman theory and some salient experimental tests of it. Now it is well known that the susceptibility (and magneto-resistance) of Bi is strongly temperature-dependent in the solid state, but temperature-independent in the liquid. This forcibly suggests that the temperature dependence has its origin in the large orbits, since the sharp decrease in susceptibility at fusion means that the large orbits no longer exist in the liquid phase. Hence as the particle size is reduced below the critical value the magneto-resistance should become more and more nearly temperature-independent approaching complete temperature-independence for infinitely small particles (corresponding to the liquid phase). Now the ratio plotted in Fig. 2 is a measure of the

[8*] Fig. 7, p. 315 of the second paper. In Stierstadt's notation $\varphi = 0$ is the same as our $\varphi = 90$.

temperature dependence of the magneto-resistance plotted against film thickness; it shows a discontinuity in slope at a certain critical film thickness, and the curve extrapolates approximately to the value unity (temperature independence) for zero particle size.

It is not possible to say accurately what the particle diameter corresponding to a given film thickness is, since the relationship between these two quantities is not accurately measurable. Gross, on the basis of his x-ray measurements, finds that the average particle diameter is around 25 percent greater than the film thickness. We should not, of course, expect all the particles in a given film of "uniform" thickness to be equal in size, but rather the particles should possess a statistical distribution of sizes, the average dimensions depending on the thickness of the film in question. For this reason, probably, the curve in Fig. 2 shows a slow rise in value above the critical point. The susceptibility of colloidal powders shows the same effect for the same reason.

In connection with the foregoing, an observation by Goetz[9] should be mentioned. He has found that in films of bismuth produced by slow evaporation, the backing being below 100°C, the first few thousand layers (several $\mu$) have a microcrystalline structure. Succeeding layers on the other hand have a macrocrystalline structure consisting of parallel growths of small individual columns of triangular or rhombohedral cross section. He suggests, on the basis of some observations by the writer[10] on the susceptibility of bismuth films, that this microcrystalline structure has a lower susceptibility than the macrocrystalline structure, and since the actual crystal structure of all the layers is most probably the same as the bulk metal, the difference between these two structures must be one of average particle size only. The method used by Goetz to observe these two structures was that of reflected polarized light and a microscope. The film thickness at which the microcrystalline structure merges into the macrocrystalline as found by Goetz (several $\mu$) does not agree with the present observations which finds this transition at about $0.5\mu$. Since the transition as determined by the experiments on colloidal powders is at about $1\mu$ the present work seems to be in somewhat better agreement, although, as has been mentioned, it is somewhat difficult to make any definite statements about particle size on the basis of film thickness. However, the magnetic method used here should, *a priori*, be much more delicate than any microscopical method since the particle size, as we know from the work on powders, wields a great influence on the magnetic properties.

The present work suggests that two interesting effects should be present in colloidal powders. We have already pointed out the experimental evidence all points to the conclusion that, as far as bismuth is concerned, the phenomena of magneto-resistance and diamagnetic susceptibility both have a common origin. For instance, the temperature dependence of the two effects, in bulk material, is completely analogous. Thus as the temperature is raised from $-180$°C up through the melting point the diamagnetic susceptibility decreases up to the melting point whence upon liquefaction it suddenly drops to a very small value which is thereafter temperature independent. The magneto-resistance does precisely the same thing. Hence one should expect that the temperature dependence of susceptibility of thin films, or colloidal powders, should follow the same course as has been found for the magneto-resistance. In other words the function $(\chi_{-180°C})/(\chi_{+20°C})$ *versus* particle size should have somewhat the same form as Fig. 2. No results on this point have, to the writer's knowledge, been published up to the present.

Secondly, the curves in Fig. 5 indicate that particles below the critical size are still anisotropic as far as the magneto-resistance is concerned and hence, from what has been said above, such particles should also show an anisotropic diamagnetism.

This effect has already been found, experimentally, by Goetz, Faessler and Focke[11] in the case of graphite, which, of course, is very similar in its magnetic behavior to bismuth.

[9] A. Goetz, Nature **132**, 206 (1933).
[10] C. T. Lane, Nature **130**, 999 (1932).

[11] A. Goetz, A. Faessler and A. B. Focke, Phys. Rev. **39**, 553 (1932); A. Goetz and A. Faessler, Phys. Rev. **40**, 1053 (1932).

Finally, in connection with the first-mentioned effect to be expected, the case of carbon black is of interest. The diamagnetic susceptibility of this substance is virtually temperature independent[12] and Warren[13] has found, on the basis of x-ray examination, that it consists of graphite of extremely small particle size.

It is a privilege to thank Professor L. W. McKeehan for many helpful discussions during the progress of this work. I am indebted to Yale University for a Sterling Fellowship during the tenure of which this work was done.

[12] M. Owen, Ann. d. Physik [4] **37**, 657 (1912).
[13] B. E. Warren, J. Che n. Phys. **2**, 551 (1934).

AUGUST 1, 1935 PHYSICAL REVIEW VOLUME 48

# Dilatations in Rochelle Salt

IRWIN VIGNESS, *University of Minnesota*
(Received April 23, 1935)

The inverse piezoelectric effect of Rochelle salt has been studied by means of mechanical dilatometers. The dilatation of a crystal along a direction 45° to the *b* and *c* axes and 90° to the *a* axis, caused by an electric field impressed in a given direction along the *a* axis, has been found, in general, not to be the same as the dilatation caused by an equal field impressed in the opposite direction. This indicates a permanent electric polarization within the crystal. A prolonged application of voltage along the *a* axis slowly changes this "permanent" polarization, which gives rise to an inverse piezoelectric fatigue effect, and is associated with the fatigue effect as observed by Valasek. Oscillograms showing the rate of deformation of a Rochelle salt crystal were taken. The forms of these curves, for small distortions of the crystal or small applied fields along the *a* axis, are in approximate agreement with the exponential type as required by the theory of Schulwas-Sorokin and Posnov. The relaxation times varied from zero at the Curie points to a maximum approximately midway between the critical temperatures. The thermal expansion of Rochelle salt along the three crystallographic axes was determined through the upper critical temperature. No discontinuities were observed, but a change in the rate of expansion occurred at the Curie point for the *b* and *c* axes.

IT has been shown[1] that there is a one to one relation between the change of lattice constant, as measured by x-rays, and the corresponding change of external dimensions as measured by means of a microscope. The effect of x-rays on a Rochelle salt crystal is not a negligible factor. Besides the ordinary yellow coloring of the crystal, due to the x-rays, there occurs a roughening of its surface. A crystal placed in a dry atmosphere will normally become coated with a white dehydrated salt. This will not form where an intense x-ray beam impinges. Thin aluminum foil fastened to a surface of a crystal will tend to disappear under the action of an x-ray beam. Crystals completely painted with a solution of celluloid in amyl acetate, so as to form an impervious coating, had small amounts of liquid form between the crystal and the coating after long exposure to x-rays. These indicate a gradual disintegration of the crystal.

[1] Vigness, Phys. Rev. **46**, 255 (1934).

For x-rays, from a copper target excited at 10 ma and 28 kv, incident on the crystal, there was a change of the lattice spacing, (021) planes, of the order of $10^{-5}$ cm per cm per minute, the rate of which decreased as the time of exposure increased. The reflected spectrum lines broadened as the time of exposure to the x-rays increased, which indicated increasing imperfections in the crystal structure. It was found inadvisable to use a given crystal after it had been exposed to x-rays of the above intensity more than 20 hours.

As mechanical or optical measurements of strain are equivalent to x-ray measurements, there appeared to be no reason for adhering to the x-ray method if more suitable means could be found.

## DILATOMETERS

The dilatometers constructed are shown in Fig. 1. In type *b* the crystal, *A*, was fastened at one end to a hard rubber support by means of celluloid dissolved in amyl acetate, hard rubber

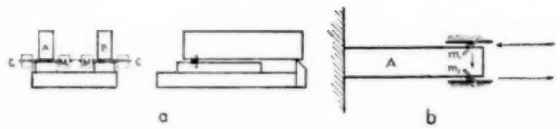


FIG. 1. Dilatometers. $A$ is a material whose coefficient of expansion is being measured. $B$ is a material whose coefficient of expansion is known. $M_1$, $M$, $m_1$, $m_2$ are mirrors attached to needles. The arrows in Fig. $b$ refer to the path of light. $C_1$ and $C$ are counterweights.

was used for insulating purposes, the other end of the crystal rolled on two needles as illustrated. Thin sheet rubber was stretched tightly over portions of the surfaces that would otherwise make contact with the needles. This was to insure no slippage and was necessary for all experiments involving a sudden application of an electric field causing a rapid change in length of the crystal.

The second dilatometer ($a$ of Fig. 1) was used only in measuring the thermal expansion of the crystal. Except for the needles and mirrors all parts were constructed of brass. A very similar instrument of quartz was recently described by Clark Williams.[2] The mirrors, $M_1$ and $M$, are caused to rotate by the material whose thermal expansion is being studied and by a standard sample, respectively; from the differences in their rotation the differences in their rate of expansion can be determined. Motions or expansions of the rest of the apparatus cancel out. The material used in $B$ was brass, the composition of which was 1/3 zinc and 2/3 copper; the coefficient of expansion[3] for this material is $18.3\times10^{-6}$. A small lateral scratch was made on both $A$ and $B$ to make a reference line of contact with the knife-edge support. The surfaces upon which the needles roll are made flat and polished. With needles 0.06 cm in diameter and with the distance from the mirrors to the scale 150 cm the amplification per unit length of the crystal, for the type $a$, is about 5000, for type $b$ there is twice this amplification.

## ASYMMETRY OF INVERSE PIEZOELECTRIC RESPONSE

Voigt[4] has shown that for a crystal of the symmetry of Rochelle salt the relations connecting the six strain components and electric field reduce to

$$y_z=d_{14}E_x; \qquad z_x=d_{25}E_y; \qquad x_y=d_{36}E_z;$$

$y_z$, $z_x$ and $x_y$ are strain components, $d_{ij}$ the piezoelectric moduli and $E_x$, $E_y$, $E_z$ the electric field components along the respective axes. For voltage applied along the $a$ axis the change in length per unit length of a crystal, along a direction $r$, which is perpendicular to the $a$ axis, is

$$\Delta r/r=d_{14}mnE_x,$$

where $m$ and $n$ are the direction cosines of $r$ with respect to the $y$ and $z$ axes.

The above equation shows that the direction of maximum piezoelectric expansion or contraction of a Rochelle salt crystal is in a direction 45° to the $b$ and $c$ axes and 90° to the $a$ axis; crystals were therefore cut with $r$ along this direction. Tin foil electrodes fastened to the crystal by means of Canada balsam xylol solution were used.

That the inverse piezoelectric effect is not the same for the voltage applied in one direction, along the $a$ axis of the crystal, as it is for the same voltage applied in the opposite direction is shown in Fig. 2. A check of the values of strain for corresponding voltages and temperatures shows good agreement between the x-ray and dilatometer measurements.[1] Staub[5] shows a similar lack of symmetry between the change of positive and negative fields along the $a$ axis (actually along a line perpendicular to the (111) planes, which is quite equivalent for purposes of comparison) and the change of the intensity of an x-ray beam reflected from the (111) planes. The

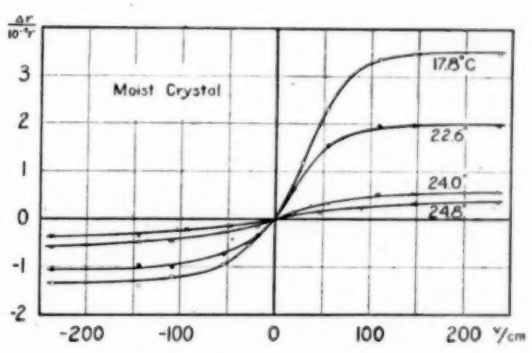


FIG. 2. Nonsymmetrical response of a crystal to voltages impressed in opposite directions along the $a$ axis.

[2] Clark Williams, Phys. Rev. **46**, 1011 (1934).
[3] International Critical Tables, Vol. 2, page 469.
[4] Voigt, *Lehrbuch der Kristallphysik*, Chapter 8, Leipzig (1910).
[5] Staub, Helv. Phys. Acta **7**, 3 (1934).

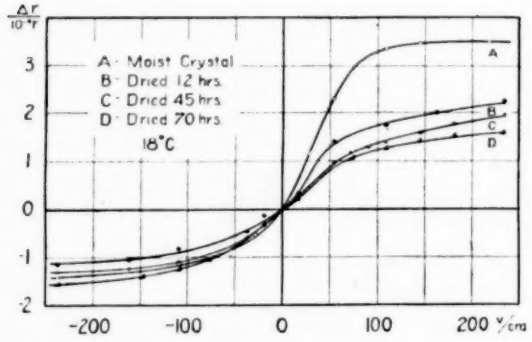


FIG. 3. Inverse piezoelectric displacement as a function of the moisture content of the crystal.

shapes of the curves show that there is not a linear relation between the change in lattice spacing and the change of intensity of the reflected x-ray beam.

The effect of drying a crystal is shown in Fig. 3. The crystal was initially moist and $CaCl_2$ was placed in the crystal chamber for the time indicated. For the dry crystal the inverse piezoelectric strain was quite symmetrical but smaller, on the average, than for the moist crystal.

## POLARIZATION AND FATIGUE EFFECT. RELAXATION TIMES

A very prominent characteristic of Rochelle salt crystals is the sluggishness with which the deformation of the crystal takes place when small voltages are applied along the active axis,[5, 6] or when the electric field is removed from this axis. The measurement of the final deformation is made additionally difficult by a gradual creep that may persist for hours.

Rochelle salt crystals about $3.5\times1.5\times0.5$ cm were used in dilatometer type *b* (Fig. 1), the greatest dimension was in a direction 45° to the *b* and *c* axes and the smallest was along the *a* axis. Because of surface conductivity it was not found practicable to keep a saturated solution of Rochelle salt in the chamber containing the crystal, as short circuits would gradually develop between the electrodes of the crystal when voltages were applied for long periods of time. For measurements involving the long applications of voltage $CaCl_2$ was kept in the crystal chamber unless otherwise stated, but in no case

[6] Schulwas-Sorokin and Posnov, Phys. Rev. **47**, 175 (1935).

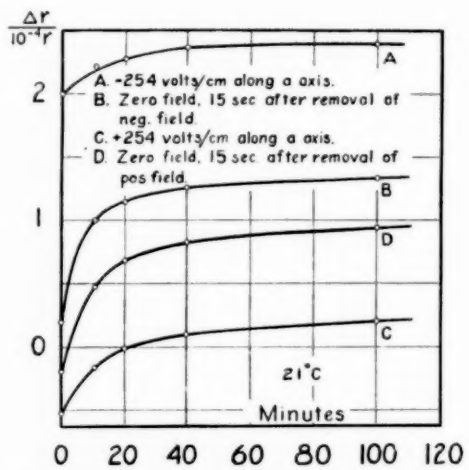


FIG. 4. Gradual polarization of a crystal due to a field of −254 volts per cm along the *a* axis applied continuously, except for short intervals of time necessary to apply a change in voltage and to determine the corresponding change in length of the crystal.

were crystals used if they exhibited any physical evidence of dehydration. Kobeko and Kurtschatov[7] state that there is no fatigue effect[8] if liquid (saturated Rochelle salt solution) electrodes are used, and Staub[5] gives the time of relaxation as strongly dependent on the dryness of the crystal. The results given here will correspond to those obtained from a "dry" crystal.

The effect of an application of an electric stress along the *a* axis for a considerable period of time is illustrated in Fig. 4. Previous to this experiment the crystal from which these data were derived had been subjected to an electric stress of +254 volts per cm for several hours. The direction that is called positive is arbitrary. The field was reversed in direction at zero time on the graph, and its effect on the inverse piezoelectric effect, as a function of the time of its application, was studied. It is to be noted that a gradual polarization of the crystal takes place which slowly changes the zero field length of the crystal. The electric field is removed for about 15 seconds for the determination of the length at zero field. This gradual change in the zero field length of the crystal corresponds to a change in a "permanent" polarization of the dielectric. The longer an electric stress is applied in a given

[7] Kobeko and Kurtschatov, Zeits. f. Physik **66**, 192 (1930).

[8] By the fatigue effect[9] is meant that as the time of charge of a condenser (Rochelle salt dielectric) is made longer, the quantity discharged in a given time becomes less.

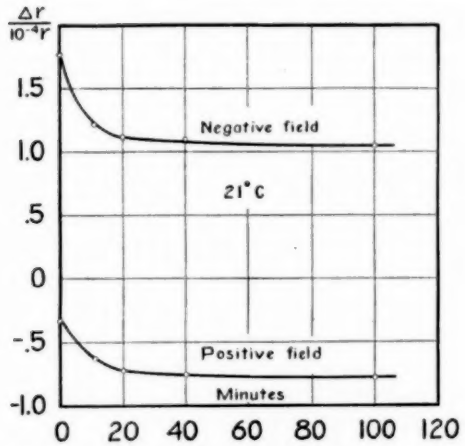


FIG. 5. Fatigue effect. Inverse piezoelectric response due to a negative and positive electric field of 254 volts per cm along the $a$ axis. An electric field of $-254$ volts per cm has been applied for the time indicated on the abscissa, except during the time the voltage was changed in order to determine the inverse piezoelectric response.

direction along the $a$ axis, the less will be the deformation caused by a removal of this voltage, and the greater will be the deformation caused by a removal of a field applied a short time (15 seconds) in the opposite direction. This is the fatigue effect[9] expressed in terms of the deformation of the crystal and is illustrated in Figs. 4 and 5.

The rate of change of deformation of a crystal is shown in Fig. 6. In general the rate of relaxation, caused by a removal of the electric field, is less than the rate of deformation caused by electric fields greater than 30 volts per cm. An analysis of curves of these types shows that the sluggishness of the crystal decreases from a maximum, approximately midway between the Curie points, to zero at the Curie points. If a large voltage (greater than 100 volts per cm) is applied along the $a$ axis, the crystal deforms very rapidly to a point that appears very near saturation; but a creep may begin after this initial deformation that is caused by a gradual change in the permanent polarization of the crystal. For small values of field (less than 40 volts per cm) it is predicted by Schulwas-Sorokin and Posnov[6] that these curves will be of a simple exponential type.

The first of the oscillograms illustrate very markedly the difference in the inverse piezoelectric response to positive and negative electric fields of equal magnitudes along the $a$ axis. The ordinate scale for all the curves of Fig. 6 is the same.

Schulwas-Sorokin and Posnov suppose that the motion of an electric dipole with respect to the lattice can be represented by the equation

$$v\dot{x}_4+c_{44}x_4=M_4,$$

where $v$ is a constant of viscosity, $c_{44}$ an elastic constant, $x_4$ is the shear strain, and $M_4$ is the applied mechanical stress (shear, corresponding to $x_4$). There would be a similar equation for an applied electric stress. The electric field is assumed to be zero. The equation is obviously correct only for small values of stress, as it assumes that the final value of displacement is a linear function of the stress. This is approximately true (Fig. 2) if the stress is limited to the equivalent of 40 volts per cm.

For the relaxation times as are represented from data derived from curves of the type shown in Fig. 6, we have assumed that $M_4$ and the electric field are zero; i.e., we remove the stress, thus

$$v\dot{x}_4=-c_{44}x_4.$$

The displacement $\Delta r/r$ is proportional to the strain $x_4$, as the displacement is in a direction 45°

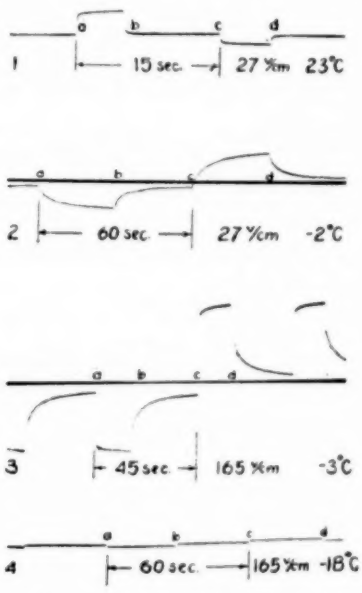


FIG. 6. Oscillograms of the dilatation of a crystal as a function of time. An electric field is applied along the $a$ axis at $a$, this field is removed and the crystal faces short circuited at $b$, the field is applied in the opposite direction at $c$, and at $d$ the field is again made zero.

[9] Valasek, Phys. Rev. **24**, 560 (1924).

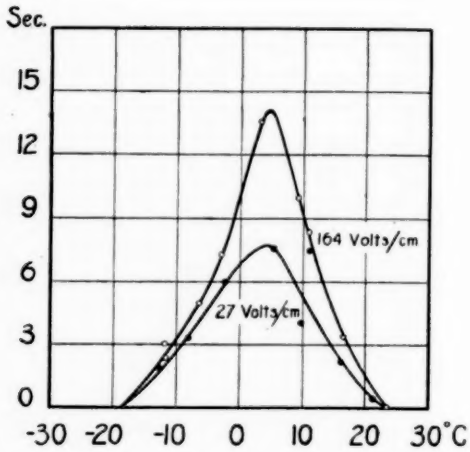


FIG. 7. Relaxation times.

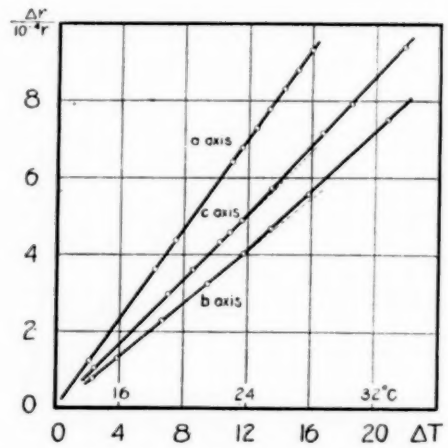


FIG. 8. Thermal expansion of a Rochelle salt crystal along the three crystallographic axes.

to the $b$ and $c$ axes. Therefore in Fig. 7 it is assumed that

$$\Delta r/r = Ke^{-t/\theta},$$

which is a solution of the above equation. The constants have been adjusted to fit the relaxation curves of the type shown in Fig. 6. These curves plotted on semilogarithmic paper appear as fairly straight lines except for the steepest portion of the curves, where the rate of deformation is too great. In Fig. 7 the time constant, $t=\theta$, has been plotted as a function of the temperature. From the experimental data there appear to be three relaxation times of quite different orders of magnitude. A very short time, which makes the crystal suitable for microphones or loudspeakers, a time of the order of a few seconds, which is represented in Fig. 7, and a time in the order of minutes, which is apparent in the fatigue effect and which is illustrated in Figs. 4 and 5.

## THERMAL EXPANSION

Valasek[10] has determined the temperature coefficient of expansion along the three crystallographic axes of Rochelle salt and states that no abnormal change in the rate of expansion was observed at the critical points.

The dilatometer, type $a$ Fig. 1, was used to determine the rate of expansion through the upper critical temperature. No elaborate precautions were made in order that the absolute magnitude of the coefficient of expansion might be determined, though the values should be correct within two percent. Temperature was measured by means of a thermometer placed in the crystal chamber. It was found necessary to wait approximately one hour after the thermometer had reached a steady value before a measurement of the expansion of the crystal could be taken. This meant that the time necessary for the apparatus to come to an equilibrium temperature was about 6 hours.

From data of the type shown in Fig. 8 the coefficients of expansion along the three principal axes are found to be

| | |
|---|---|
| $a=58.3\times10^{-6}$ | From +12°C to +35°C |
| $b=35.5\times10^{-6}$ | From +12°C to +24°C |
| $=39.7\times10^{-6}$ | From +24°C to +35°C |
| $c=42.1\times10^{-6}$ | From +14°C to +24°C |
| $=43.6\times10^{-6}$ | From +24°C to +34°C. |

This shows a change in the rate of expansion along the $b$ and $c$ axes at the upper Curie point. The anomaly of the specific heat at the upper critical temperature[11, 12] leads one to expect a corresponding anomaly in the coefficient of expansion.[12]

In conclusion I wish to express my sincere appreciation to Dr. Joseph Valasek, under whom I have been privileged to work, and Dr. Henry A. Erikson, chairman of the department of physics, for their helpful advice and for their assistance in obtaining the materials necessary for this work.

[10] Valasek, Phys. Rev. **20**, 639 (1922).

[11] Kobeko and Nelidow, Physik. Zeits. d. Sowjetunion **1**, 382 (1932).

[12] Rusterholz, Helv. Phys. Acta **8**, 39 (1935).

# Radiative Capture of Protons by Carbon

G. BREIT AND F. L. YOST, *Department of Physics, University of Wisconsin*

(Received June 4, 1935)

In previous notes[1] we have reported results of calculations which show that the probability of $\gamma$-ray radiation is sufficiently high to make the reaction $C^{12}+H^1\rightarrow N^{13}+\gamma$ a probable one. It turned out that the theoretical yield is larger than that observed by a factor of roughly 1000. As in all intensity calculations the overlapping of wave functions in the initial and final states is of primary importance and the theoretical result is sensitive to this overlapping. The apparent discrepancy between calculation and experiment may be taken to indicate that the interaction between $C^{12}$ and $H^1$ is not represented sufficiently well by a potential function which is constant inside $C^{12}$ and is Coulombian outside of it. In order to decrease the theoretical yield one has to change the potential in such a way as to decrease the region in which the initial and final wave functions overlap or else one must shift the region towards smaller radii. The $\gamma$-ray yield expected in the bombardment of $Be^9$ by protons is calculated for a nuclear radius of $0.318\times10^{-12}$ cm and a well 9 MEV deep. It increases more slowly with the voltage than the observed intensity indicating a deeper nuclear well. A simple discussion of the method of complex eigenwerte is applied to the properties of wave functions near resonance.

## 1. General Relations for Capture in a Central Field

A PARTICLE of mass $M_1$ and charge $Z_1e$ traveling with velocity $v$ is incident on another particle of mass $M_2$ and charge $Z_2e$ supposed to be initially at rest. The particles repel each other according to the inverse square law of force when they are separated by distances $r>r_0$. Inside $r_0$ the force is supposed to remain central but to change into an attractive one. The system is transformed as usual into a separable system in which the coordinates of the common center of mass and the relative coordinates of the two particles can be treated independently of each other. The kinetic energy of the center of mass is constant and the factor of the wave function which involves the relative coordinates satisfies a Schrödinger equation for a single particle with mass

$$\mu=M_1M_2/(M_1+M_2). \tag{1}$$

The kinetic energy of relative motion is $(\mu/M_1)T$ where $T=(\frac{1}{2})M_1v^2$ is the kinetic energy of the incident particle. The plane wave which represents $v$ particles $Z_1$, $M_1$ per second per cm$^2$ traveling along the $Z$ axis is described in the reference system of the center of mass by $e^{ikz}$ where

$$k=\mu v/\hbar \tag{2}$$

and $x$, $y$, $z$ are the relative coordinates of particle 1 with respect to particle 2.

If the field were Coulombian also inside $r=r_0$ the plane wave would be modified by the field into[2]

$$e^{ikz}\rightarrow\sum_0^\infty(2L+1)i^LP_L(\cos\theta)e^{i\sigma_L}F_L(\rho)/\rho;$$
$$\rho=kr,$$
$$\sigma_L=\arg\Gamma(L+1+i\eta); \tag{3}$$
$$\eta=1/ka=Z_1Z_2e/\text{“}137\text{”}v.$$

Here $F_L$ is the solution of

$$[d^2/d\rho^2+1-2\eta/\rho-L(L+1)/\rho^2]F_L=0, \tag{4}$$

which is regular at $\rho=0$ normalized so as to be asymptotic to a sine wave of unit amplitude at $\rho=\infty$. The deviation of the field from the inverse square law modifies (3) into

$$e^{ikz}\rightarrow\sum_0^\infty(2L+1)i^LP_L(\cos\theta)e^{i\sigma_L}\bar{F}_L(\rho)/\rho, \tag{5}$$

where $\bar{F}_L$ is the solution of the radial equation in the changed field for the azimuthal number $L$ normalized to be asympototic to a sine function of unit amplitude at $\rho\rightarrow\infty$ and regular at $\rho=0$. The radial equation is (4) for $r>r_0$ and

$$[d^2/d\rho^2+1+(2/\mu v^2)U-L(L+1)/\rho^2]\bar{F}_L=0;$$
$$r<r_0, \tag{4'}$$

where $U$ is the potential energy inside the “potential well.”

[1] G. Breit and F. L. Yost, Phys. Rev. **46**, 1110 (1934); **47**, 508 (1935).

[2] N. F. Mott and H. S. W. Massey, *The Theory of Atomic Collisions* (Oxford University Press, 1933), Chapter III.

The incident wave in accordance with Eq. (5) consists of a superposition of states with different orbital angular momenta $L$. The transition probability from any of these states to a lower stable state can be calculated by the formula

$$\frac{64\pi^4\nu^3}{3hc^3}\sum_n\{|\mathfrak{M}_{mn}{}^x|^2+|\mathfrak{M}_{mn}{}^y|^2+|\mathfrak{M}_{mn}{}^z|^2\}, \quad (6)$$

where $\mathfrak{M}$ is the dipole moment due to the relative displacement of the two particles and $m$, $n$ are, respectively, the magnetic quantum numbers of the incident and bound state. Eq. (6) is well known for two stationary states and the matrix elements entering it are supposed to be calculated by using wave functions normalized to unity. Introducing a fundamental volume $V$ one has to divide expression (5) by $V^{\frac{1}{2}}$ and using that expression in (6) one obtains the transition probability when the incident state corresponds to $v/V$ particles/sec./cm$^2$. The number of captures which occur per second due to a single nucleus exposed to the bombardment of $N$ particles/sec./cm$^2$ will be defined as $N\sigma$ and $\sigma$ will be called the collision cross section. Using (6) in the above manner one obtains therefore $v\sigma/V$. This amounts to using (5) directly in the calculation of matrix elements and equating the result to $v\sigma$. Due to any term with a definite $L$ in (5) it is possible to obtain a transition to a lower stable term having azimuthal quantum number $L+1$ or $L-1$. We let the radial wave function of the stable state be $R$ and we normalize it so as to have

$$\int_0^\infty R^2r^2dr=1. \quad (7)$$

Performing the angular integrations in (6) one finds

$$\sigma_{L,\ L\pm1}=\frac{256\pi^5e^2\nu^3}{3hc^3v}(L+\tfrac{1}{2}\pm\tfrac{1}{2})A^2\cdot k^{-2}\left|\int\bar{F}_LRr^2dr\right|^2 \quad (8)$$

$$=30.3(c/v)A^2k^{-2}\lambda^{-3}\left|\int\bar{F}_LRr^2dr\right|^2(L+\tfrac{1}{2}\pm\tfrac{1}{2}),$$
$$A=(M_2Z_1-M_1Z_2)/(M_1+M_2). \quad (8')$$

It is often desirable to express $\bar{F}_L$ inside the barrier as a multiple of a function $\bar{u}$ having unit amplitude at $r=r_0$ and proportional to $\bar{F}_L$. One can determine the value of $\bar{F}_L$ at $r=r_0$ in terms of the logarithmic derivative of $\bar{F}_L$ at $r=r_0-0$ and the values of $F_L$ and $G_L$ at $r=r_0$. Here $G_L$ is the solution of Eq. (4) which is asymptotic to $\cos[\rho-L\pi/2-\eta\ln 2\rho+\sigma_L]$ while $F_L$ is asymptotic to $\sin[\rho-L\pi/2-\eta\ln 2\rho+\sigma_L]$. Requiring that for $r>r_0$, $\bar{F}_L$ be expressible as a linear combination of $F_L$ and $G_L$ and that for large $\rho$ the function $\bar{F}_L$ should consist of $F_L$ and a term in $e^{i\rho}$ one satisfies the condition of having (5) equal to a sum of the modified plane wave (3) and a set of diverging waves. It is found by an easy calculation that

$$\bar{F}_L=(F_L/(1-F_LG_L\delta_L-iF_L{}^2\delta_L))_{r=r_0}\cdot\bar{u}, \quad (9)$$

$$\delta_L=(F_L'/F_L-\bar{F}_L'/\bar{F}_L)_{r=r_0}, \quad (9')$$

where the last differentiations are with respect to $\rho$. The connection with usual formulas of the theory of anomalous scattering is given by the asymptotic form of $\bar{F}_L$:

$$\bar{F}_L\sim e^{iK_L}\sin[\rho-L\pi/2-\eta\ln 2\rho+\sigma_L+K_L], \quad (10)$$

where $K_L$ is determined by

$$e^{2iK_L}=[(1-F_LG_L\delta_L+iF_L{}^2\delta_L)/(1-F_LG_L\delta_L-iF_L{}^2\delta_L)]_{r=r_0}. \quad (10')$$

The phase $K_L$ is the usual phase shift which is responsible for anomalous scattering.[3] Formula (9) determines the amplitude of $\bar{F}_L$. The main contributions to $\sigma$ come usually from the region inside the nuclear radius $r_0$ and a comparable region $r_0<r<3r_0$. Inside $r<r_0$ the shape of $\bar{u}$ is determined by (4') and for $r>r_0$ the function $\bar{u}$ can be usually determined sufficiently accurately by approximate methods. The quotient $\bar{F}_L/\bar{u}$ requires the knowledge of $F_L$ and $G_L$. It is possible to express $F_L$ in the following way:[4]

[3] H. M. Taylor, Proc. Roy. Soc. **A134**, 103 (1931); **A136**, 605 (1932).

[4] Th. Sexl, Zeits. f. Physik **81**, 163 (1933); J. A. Wheeler, F. L. Yost and G. Breit, in preparation for publication.

$$F_L = C_L \rho^{L+1} \Phi_L;$$

$$C_L = \frac{2^L}{(2L+1)!}\{2\pi\eta[L^2+\eta^2][(L-1)^2+\eta^2]\cdots[1+\eta^2]/[e^{2\pi\eta}-1]\}^{\frac{1}{2}},$$

$$G_L = D_L\{[\rho^{-L}+a_{-L+1}\rho^{-L+1}+\cdots+0\cdot\rho^{L+1}+a_{L+2}\rho^{L+2}+\cdots]+[p\ln 2\rho+q]F_L/C_L\},$$

$$(2L+1)C_L D_L = 1; \quad p = \frac{2^{2L+1}}{(2L)!(2L+1)!}[L^2+\eta^2][(L-1)^2+\eta^2]\cdots[1+\eta^2]\eta, \tag{11}$$

$$q = p\left[\frac{L}{L^2+\eta^2}+\cdots+\frac{1}{1+\eta^2}-\left(1+\frac{1}{2}+\cdots+\frac{1}{2L+1}\right)+2\gamma+\text{R.P.}\frac{\Gamma'(-i\eta)}{\Gamma(-i\eta)}\right]$$

$$+(-)^{L+1}\frac{2^L}{(2L)!}\sum_{n=-L}^{L}\frac{2^n}{(L+n)!(L-n+1)}\text{I.P.}\,(i\eta+n-1)\cdots(i\eta-L).$$

Here $\Phi_L$ is a power series in $\rho$ the first term of which is 1 and $\gamma$ is Euler's constant. The above form of $F$, $G$ was worked out by Wheeler and the tables the computation of which was begun by him were used for the values of $\Phi_L$ and the second power series entering $G_L$. Introducing

$$\Psi = rRk^{-\frac{1}{2}}, \quad \int \Psi^2 d\rho = 1,$$

we have $$\sigma = B^2\sigma_0,$$

$$\sigma_0 = 30.3(c/v)A^2k^{-5}\lambda^{-3}F_L^2 \times \left|\int_0^\infty \rho\Psi\bar{u}d\rho\right|^2(L+\tfrac{1}{2}\pm\tfrac{1}{2}), \tag{12}$$

$$B^2 = \{1/[(1-F_LG_L\delta_L)^2+F_L^4\delta_L^2]\}_{r=r_0}. \tag{12'}$$

If $F_LG_L\delta_L = 1$ there is resonance of the nucleus to the $L$ component of the incident wave. In this case $F_L^2B^2 = G_L^2(kr_0)$, which is large for high barriers on account of the presence of $e^{2\pi\eta}-1$ in $D_L$. The functions $F_L$, $G_L$ satisfy $F_L'G_L - F_LG_L' = 1$. Using this relation the condition for resonance can be expressed as

$$\bar{F}_L'/\bar{F}_L = G_L'/G_L, \tag{13}$$

which shows together with $B^2 = G_L^2(kr_0)$ that resonance is obtained when the function $\bar{F}_L$ has the proper phase to join itself on to the irregular solution $G_L$ at $r = r_0$.

Although it is convenient to define the resonance velocity arbitrarily as that velocity of incident particles for which $F_LG_L\delta_L = 1$ it should be remembered that neither $B^2$ nor $\sigma$, considered as functions of the velocity, have maxima precisely when this condition is satisfied. Thus the maximum of $B^2F_L^2$ should be reached at slightly lower velocities. For sharp resonance however the condition used is sufficiently accurate.

If resonance is sharp then the observed yield in thick targets is primarily due to the captures of particles retarded by the stopping power of the target to approximately the resonance velocity. The yield can be then calculated approximately by integrating the contributions which result from (12) in the neighborhood of resonance. The quantity $1-F_LG_L\delta_L$ can be then supposed to vary linearly with the energy in the energy range giving important contributions around resonance. Changes in all other quantities entering $\sigma$ will be neglected in this approximation, and their values at resonance will be used. According to the 3/2 power law of variation of range with the kinetic energy $T$ the distance $dl$ laid off by the particle in the target while the energy changes by $dT$ is $dl = (3/2)ldT/T$. By means of this relation and (12) it is found that the number of captures per $N_1$ incident particles bombarding a target having $N_2$ nuclei per cm$^3$ is

$$Y = (3\pi/2)(\Delta T/T)N_1N_2l_0\sigma_0/F_L^4\delta_L^2, \tag{14}$$

where $l_0$ is the range of particles having the resonance velocity and $\Delta T$ is one-half of the half value breadth of resonance so that the resonance curve is represented by $1/[(\Delta T)^2+(T-T_0)^2]$. For high barriers the dependence of $Y$ is most critical with respect to $\Delta T/T$ and the factors $1/F_L^4\delta_L^2$ as well as the $F_L^2$ involved in $\sigma_0$. The

two last factors together give a net factor $G_L^2$ so that $Y$ is proportional to $G_L^2(\Delta T/T)$. Here $G_L^2$ increases with the barrier height but $\Delta T/T$ decreases and the net effect will be seen to leave $Y$ nearly independent of the barrier height.

## 2. Relations Between Wave Functions Near Resonance

It was shown by Casimir[5] that Gamow's use of solutions exponentially decaying with time and exponentially increasing with distance can be interpreted as an approximation to a straightforward calculation by means of wave packets and that the actual solution satisfies the necessary conditions of finiteness at infinite distances. The same fact together with relations between wave functions near resonance was previously reported by one of us.[6] In view of the fact that the method used allows one to see the connection between capture and spontaneous disintegration most clearly it is described below.

We consider solutions of the radial equation

$$d^2\Psi/dr^2+(2m/\hbar^2)(E-V)\Psi=0 \qquad (15)$$

and we suppose that at infinity the function $V$ decreases with $r$ faster than $1/r$. This restriction is of a purely mathematical character because at sufficiently large distances the Coulombian field can be changed into a more rapidly decreasing one without changing the physical results. We shall also require that the function $V$ is such as to allow regular solutions for $\Psi$. Otherwise the function $V$ can be arbitrary. The energy $E$ is supposed to be positive. Asymptotically for large $r$ we have

$$\Psi(E)=Ae^{-ikr}+Be^{+ikr}, \quad k=(2mE)^{\frac{1}{2}}/\hbar. \qquad (16)$$

If $\Psi$ is defined in the neighborhood of $r=0$ by the value of its first nonvanishing derivative $C$ the differential Eq. (15) establishes its values for all $r$ and hence the coefficients $A$, $B$ are determined as functions $A(C, E)$, $B(C, E)$. Physical applications should be made with real $E$. It is nevertheless useful to examine the functions $A$, $B$ also for complex $E$. Gamow's complex eigenwerte method simply amounts to making use of the properties of $A$, $B$ as functions of $E$ in the neighborhood of the root of

$$A(C, E)=0. \qquad (16')$$

A root of this equation we call $E_0-i\lambda\hbar/2$ where $E_0$, $\lambda$ are real. The constant $\lambda$ has no relation to the wavelength which it stood for in the first section and will be interpreted as the disintegration constant. For real $C$, $E$ the function $\Psi$ must be real and hence

$$B=A^* \quad (E \text{ real}). \qquad (16'')$$

The roots of (16′) are therefore complex, and $\lambda\neq 0$. As in Gamow's paper one shows that for small $|\lambda|$ only $\lambda>0$ need be considered. For real $E$ close to $E_0$ and for small $\lambda$ one may expand by Taylor's series around $E_0-i\lambda\hbar/2$

$$\begin{aligned} A(E)&=(E-E_0+i\lambda\hbar/2)(dA/dE)_{A=0};\\ B(E)&=(E-E_0-i\lambda\hbar/2)(dA/dE)^*_{A=0}. \end{aligned} \qquad (17)$$

By using these values in (16) it follows that for large $r$

$$\overline{|\Psi|^2}=2|(dA/dE)_{E=0}|^2[(E-E_0)^2+(\lambda\hbar/2)^2]. \qquad (17')$$

For small $r$ the function $\Psi$ varies only slowly with $E$ and this is particularly so if there is a "well" at small $r$ in the potential $V$. Thus according to (17′) the relative probability of the particle being in the region of small $r$, i.e., inside the nucleus, is proportional to

$$1/[(E-E_0)^2+(\lambda\hbar/2)^2]. \qquad (18)$$

This shows that half value breadth is $\lambda\hbar$ while the quantity $\Delta T$ of the first section is $\lambda\hbar/2$.

Superposing solutions (16) one obtains a wave packet

$$\Psi=\int_0^\infty \Psi(E)e^{-iEt/\hbar}f(E)dE \qquad (19)$$

and one can arrange $f(E)$ so as to have $\Psi$ initially vanish at $r=\infty$. Approximately this is accomplished by

$$f(E)=(\lambda\hbar/2\pi)/[(E-E_0)^2+(\lambda\hbar/2)^2]. \qquad (19')$$

The calculation of the function (19) by using (16), (19′) is easily made approximately by using $K-K_0\cong(E-E_0)/\hbar v_0$ where $v_0$ is the velocity at

[5] H. Casimir, Physica **1**, 193 (1934); cf. also H. Bethe, Ann. d. Physik **4**, 443 (1930).
[6] G. Breit, Phys. Rev. **40**, 127 (1932).

resonance and by changing the range of integration from $0\to\infty$ into $-\infty\to+\infty$. The integration reduces then to

$$\int_{-\infty}^{+\infty} e^{-ixt'/\hbar}[x-i\lambda\hbar/2]^{-1}dx=0(t'>0);$$
$$=2\pi i e^{\lambda t'/2}(t'<0)$$

or

$$\int_{-\infty}^{+\infty} e^{-ixt'/\hbar}[x+i\lambda\hbar/2]^{-1}dx=$$
$$-2\pi i e^{-\lambda t'/2}(t'>0); \quad =0(t'<0).$$

It is found that in the region where (16) holds

$$\Psi=B(E_0-i\lambda\hbar/2)\exp\left[-i(E_0t-mv_0r)/\hbar\right.$$
$$\left.-\lambda(t-r/v_0)/2\right] \quad (t>r/v_0), \quad (20)$$
$$\Psi=0 \qquad\qquad (t<r/v_0),$$

where

$$B(E_0-i\lambda\hbar/2)=-i\lambda\hbar(dA/dE)^*_{A=0} \quad (20')$$

in accordance with the fact that (17) applies for complex as well as real values of $E$. Similarly for small $r$ one finds, using (19′) and the fact that $\Psi(E)$ is practically independent of $E$ in the region where $f(E)$ is appreciable:

$$\Psi=\Psi(E_0)\exp\left[-iE_0t/\hbar-\lambda t/2\right]. \quad (20'')$$

Eqs. (20), (20″) show that to within the approximations made Gamow's solution represents the wave packet in the region $r<v_0t$ but that for $r>v_0t$ the wave packet gives zero probability of finding the particle. In higher approximations the head of the wave packet at $r=v_0t$ becomes rounded off and for $r>v_0t$ there is a finite though small probability of finding the particle.

Eq. (18) shows that one may define $E_0$ as that real energy for which the probability of the particle being inside the nucleus is a maximum taken relatively to the probability of its being very far away. Eqs. (17), (19), (19′) show that the wave packet which is represented by Gamow's solution contains stationary states with different energies and that the relative probabilities of these energies vary in proportion with the same resonance factor (18) which determines the relative probabilities of capture for particles of these energies; in comparing relative probabilities of particles of different energies we use the same amplitude at $r=\infty$ for all energies.

According to Gamow's conservation theorem argument one can determine the disintegration constant by

$$\lambda=v|B(E_0-i\lambda\hbar/2)|^2/$$
$$(\int|\Psi(E_0)|^2dr)_{E=E_0-i\lambda\hbar/2}, \quad (21)$$

where the integral is to be taken only through the nucleus. Here the numerator represents the number of particles leaving the nucleus and the denominator similarly represents the number of particles in the nucleus. This formula of Gamow's is often inconvenient in applications because it presupposes the knowledge of the solution of the wave equation for complex energies. Using Eq. (17) we have

$$B(E_0-i\lambda\hbar/2)=2B(E_0). \quad (21')$$

Substituting this into Eq. (21) we see that

$$\lambda=v/\int|\bar{G}|^2dr, \quad (21'')$$

where $\bar{G}$ is the solution of the wave equation for a *real* energy normalized so as to be asymptotic to a sine function of unit amplitude at $\infty$. Remembering that $\Delta T=\lambda\hbar/2$ we also have

$$\Delta T/T=1/\int|\bar{G}|^2d\rho; \quad (\rho=mvr/\hbar). \quad (22)$$

The above general properties of wave functions near resonance are seen to be verified by the special functions used in section 1. Thus according to Eq. (17) the phase of the function at resonance differs by $\pi/2$ from what it is far away from resonance and this is in agreement with Eq. (10).

### 3. Applications

By means of Eq. (22) we change Eq. (14) into

$$Y=142.8N_1N_2l_0(L+\tfrac{1}{2}\pm\tfrac{1}{2})A^2(c/v)k^{-5}\lambda^{-3}$$
$$\times|\int_0^\infty\rho\Psi\bar{G}d\rho|^2/\int\bar{G}^2d\rho, \quad (23)$$

where $\lambda$ again stands for the wavelength. For $r>r_0$, $\bar{G}$ is identical with $G_L$ and for $r<r_0$ it is the continuation of $G_L$ in the field $U$. As has been shown in connection with Eq. (13) this continuation is regular at $r=r_0$ at resonance. The integral in the denominator is to be extended only

through the nucleus. The function $\overline{G}$ is the only quantity in this formula which contains the energy of the incident particle exponentially. It occurs with equal powers in the numerator and denominator of $Y$ and as a result $Y$ depends on the energy much less critically than the disintegration yield away from resonance. The $\Delta T/T$ is proportional in its order of magnitude to $e^{-2\pi\eta}$ while $\sigma_0/F_L{}^4\delta_L{}^2$ is the collision cross section at resonance and it behaves as $F_L{}^{-2}$ and is of the order $e^{2\pi\eta}$. At resonance the collision cross section increases in the same ratio as the width of the resonance region decreases. This property is seen to be general and not confined to radiative captures. We may, therefore, expect observable yields of nuclear reactions in cases of resonance even though the exponential factors describing the probability of penetrating a nuclear barrier should be very small.

The expected probability of radiative capture was calculated for carbon with several values of the nuclear radius and of the depth of the potential well. Only a certain range of values comes into consideration because mass defects indicate that the energy released in the capture of a proton by $C^{12}$ is of the order of 6 or 7 MEV. It is therefore necessary to have the radius and the depth such as to allow an $s$ level at $E\leqq -6$ MEV. At the same time it is necessary to account for resonance to incident protons at about 0.5 MEV. Supposing that the process occurs as a transition $L=1\rightarrow L=0$, only certain radii and depths will give simultaneously the correct position of the bound $s$ level and of the virtual $p$ level. For simplicity we have supposed that the $1s$ and $2p$ levels are responsible for the transition so as to have no nodes inside the nucleus for the wave function, either in the initial or in the final state. Similarly the potential energy $-U$ inside the nucleus was taken to be constant. This corresponds to the usual treatment of radioactive nuclei and although actually $U$ may vary, an approximate idea about the probability of the process is obtainable with such a model. Letting $r_0\times 10^{12}=0.33$, 0.41, 0.52 cm we found by trial that the corresponding values of $U$ which had to be used in order to obtain resonance to the first $p$ level at 564 kv are 21.4, 13.4, 8.3 MEV. The energy of the $s$ level calculated with these values of $r_0$ and the corresponding values of $U$ is approximately $-10$, $-6.5$, $-4.0$ MEV and it is seen that $r_0=0.41\times 10^{-12}$ cm, $U=13.4$ MEV fit the requirement of correct binding energy best.

For any of these radii and depths resonance is sharp and the direct calculation of $1-FG\delta$ and $F^2\delta$ in the vicinity of resonance is troublesome. Eq. (23) is more suitable. Since it was supposed in deriving it that Eq. (22) is at least approximately valid we have verified the latter by comparison with approximate direct calculations in which the values of $F$, $G$, were used. For the latter calculations $1-FG\delta$ and $F^2\delta$ were computed for $T=224$, 356, 564, 894 kv and the rate of change of $1-FG\delta$ at 564 kv was compared with $F^2\delta$. The quantity $F^2\delta$ varies sufficiently rapidly to make its change through the resonance region appreciable but not very serious and we used the value of $F^2\delta$ at maximum resonance in estimating the resonance width. We obtain for $\Delta T/T$ by Eq. (22) $1.63\times 10^{-2}$ and by direct estimate $1.44\times 10^{-2}$ for $r_0=0.31\times 10^{-12}$ cm. For $r_0=0.41\times 10^{-12}$ cm the agreement is worse, Eq. (22) giving $2.5\times 10^{-2}$ and direct estimate $2.0\times 10^{-2}$. It could be expected that for broader resonance Eq. (22) will be less accurate. In both cases the agreement is sufficiently good to warrant the application of Eq. (22) to the calculation of the yield.

Formulas (14), (23) give the yield expected in thick targets on the supposition that only particles with nearly the resonance velocity need be considered. This assumption is justified for the theoretical model used here as may be seen by comparing the collision cross section at resonance with that at other voltages. Thus for $U=13.4$ MEV, $r_0=0.41\times 10^{-12}$ cm the approximate values of $\sigma$ are given below:

| $T=224$ kv | 356 kv | 564 kv | 894 kv |
|---|---|---|---|
| $\sigma=6.1\times 10^{-31}$ | $1.8\times 10^{-29}$ | $5.0\times 10^{-28}$ | $9.8\times 10^{-29}$ cm$^2$. |

At the resonant voltage the effective collision cross section is $4.2\times 10^{-26}$ cm$^2$ and is appreciably higher than the other values listed above. In the above tabulation changes in $\int r^2R\bar{u}dr$ with voltage were neglected, being relatively unimportant because $\bar{u}$ is primarily determined by the depth and width of the potential well rather than the kinetic energy of the incident proton.

The values of $F$, $G$, $FG\delta$, $F^2\delta$ and $\int\rho\Psi\bar{u}d\rho$ for different $r_0$ and $U$ are listed in Table I for different voltages. The latter as well as the values

TABLE I. *γ-ray yield per proton as a function of energy of incident particle and radius of bombarded nucleus.*

| $T$ | $F'/F$ | $F$ | $G$ | $FG\delta$ | $F^2\delta$ | $\int\rho\Psi\bar{u}d\rho$ | $Y$ per proton |
|---|---|---|---|---|---|---|---|
| | $r_0=0.33\times10^{-12}$ cm | | | $U=21.4$ MEV, | | | |
| 894 | 3.525 | .02664 | 6.727 | 1.036 | 0.00410 | | |
| 564 | 4.494 | .00962 | 14.43 | .994 | .000663 | 0.267 | $7.3\times10^{-7}$ |
| 356 | 5.699 | .002876 | 37.82 | .971 | .000074 | | |
| 224 | 7.212 | .0006735 | 127.0 | .956 | | | |
| | $r_0=0.41\times10^{-12}$ cm | | | $U=13.4$ MEV | | | |
| 894 | 2.837 | .04465 | 5.03 | 1.073 | 0.010 | | |
| 564 | 3.640 | .01626 | 10.48 | 1.002 | .00155 | 0.371 | $2.66\times10^{-7}$ |
| 356 | 4.640 | .00488 | 27.12 | .967 | .000182 | | |
| 224 | 5.880 | .001147 | 90.40 | .942 | | | |
| | $r_0=0.52\times10^{-12}$; $U=8.3$ MEV | | | | | | |
| 894 | 2.281 | .0754 | 3.81 | 1.135 | 0.0225 | | |
| 564 | 2.952 | .02778 | 7.56 | 1.006 | .00369 | 0.525 | $0.85\times10^{-7}$ |
| 356 | 3.784 | .00840 | 19.18 | .944 | .00041 | | |
| 224 | 4.818 | .00198 | 63.1 | .907 | | | |

of $r_0$ were chosen so as to be able to use the tables for $F$ and $G$ without interpolation. The values of $Y$ also listed in Table I were obtained with $l_0=6.96\times10^{-4}$ cm for 564 kv while $1.136\times10^{23}$ was used as the number of carbon atoms per cm³. The values of $\Delta T/T$ used for $Y$ were $1.036\times10^{-2}$ for $r_0=0.33\times10^{-12}$ cm, $1.44\times10^{-2}$ for $r_0=0.41\times10^{-12}$ cm, $1.90\times10^{-2}$ for $r_0=0.52\times10^{-12}$ cm. The values of $Y$ for these three radii correspond to $4.6\times10^{6}$, $1.7\times10^{6}$, $0.54\times10^{6}$ captures per microampere. The decrease of $Y$ with increase of nuclear radius is due to a large extent to an increase in the wavelength of the emitted γ-ray. The energy of the $s$ level increases as $r_0$ and so does the wavelength of the γ-ray. The wavelengths used for the three radii were $1.21\times10^{-11}$ cm, $1.89\times10^{-11}$ cm, $3.07\times10^{-11}$ cm.

According to Hafstad and Tuve[7] and to Crane and Lauritsen[8] the observed yield is due to resonance which takes place at about 425 kv. The observations of Cockcroft, Gilbert and Walton[9] are consistent with the existence of resonance but speak for a somewhat higher value of the resonance energy. The difference between the 564 kv used in the calculations and the true experimental energy is not certain and cannot be very significant because according to formula (23) the yield does not vary critically with the barrier. This is also indicated by the fact that our calculated yields decrease with the radius.

The observed yield as estimated by Hafstad and Tuve is one in $10^{10}$ incident protons. Among the radii which we tried $r_0=0.41\times10^{-12}$ cm seems to be the most acceptable because the corresponding binding energy corresponds most closely to the expected 6 or 7 MEV. The theoretical yield for this radius is 2700 times greater than the observed yield and it is thus quite possible to explain the formation of radioactive $N^{13}$ as due to radiative capture of the proton. The discrepancy between theory and experiment indicates that the model used is only a poor approximation to reality and this could have been expected because both the assumption that the field acting on the proton is central and that this field has the particular shape used by us are open to question. As in all intensity calculations the transition probability is proportional to the square of the matrix element for the displacement and is therefore sensitive to the degree of overlapping of the initial and final state. By increasing $U$ at small $r$ one can contract the wave function of the bound $s$ state towards small $r$ without affecting the $p$ function of the incident state nearly as much. Almost any desired result can be obtained by this means and the theoretical value can be decreased to the experimental one. It is questionable, however, whether such forcing of theory to experiment has much meaning because the assumption of the central nature of the field is also questionable.

According to Massey and Mohr[10] who follow a discussion of Taylor and Mott[11] one may expect dipole radiation to be absent on the Heisenberg Majorana theory of nuclear binding forces. According to Bethe and Peierls,[12] however, dipole radiation is expected on either the Heisenberg Majorana or the Wigner theory. It is clear without calculation that a dipole moment exists in our special problem and a more detailed calculation which we omit here shows that the exchange interaction does not essentially modify the possibility of dipole radiation.

The revised masses of Bethe[13] give 1.0032 for the difference between the masses of $C^{13}$ and $C^{12}$ instead of the previously supposed 1.0003 which

[7] L. R. Hafstad and M. A. Tuve, Phys. Rev. **47**, 506, 507 (1935).
[8] C. C. Lauritsen and H. R. Crane, private communication.
[9] J. D. Cockcroft, C. W. Gilbert and E. T. S. Walton, Proc. Roy. Soc. **A148**, 225 (1935).
[10] H. S. W. Massey and C. B. O. Mohr, Proc. Roy. Soc. **A148**, 225 (1935).
[11] H. M. Taylor and N. F. Mott, Proc. Roy. Soc. **A138**, 665 (1932).
[12] H. Bethe and R. Peierls, Proc. Roy. Soc. **A148**, 146 (1935).
[13] H. Bethe, Phys. Rev. **47**, 633 (1935).

followed from Aston's value 12.0036 for $C^{12}$ and King and Birge's value 13.0039 for $C^{13}$. This change when used for an estimate of the mass of $N^{13}$ lowers the estimated frequency of the $\gamma$-ray to about 3 MEV with 0.0014 for the kinetic energy of the positrons in $N^{13}\rightarrow C^{13}+e^+$ and neglecting the mass of the neutrino. The nuclear radius has to be increased and the depth of the well must be decreased to fit this $\gamma$-ray wavelength. The estimated yield is decreased by approximately a factor of 3.

According to Hafstad and Tuve there is a strong indication of a fine structure of the resonance of carbon to protons. If this were due to the proton magnetic moment we would expect the fine structure to have the same order of magnitude as though the proton obeyed Dirac's equation. The discontinuity in the potential energy will be expected to give rise to a doublet splitting of the order of

$$\Delta W=\int_{R-0}^{R+0} II'G^2dr$$

where $II'=(\mu_0/1840)^2(2L+1)dU/rdr$ which amounts to $(2L+1)(v^2/4c^2)G^2U/\int_0^\infty G^2d\rho$. Multiplying the result by 3 in order to take into account the fact that the magnetic moment of the proton is greater than would be expected on Dirac's theory one still has an energy difference of the order of only 700 volts which is much less than the observed structure of about 70 kv. The structure may however be accounted for by the coupling between movable parts of the $C^{12}$ nucleus or else by the simultaneous presence of two or more "wells" for the incident proton. As is well known, the interaction of two equal wells in molecules gives rise to a doublet structure and a similar phenomenon may be imagined to take place here.

**Application to $Be^9+H^1$**

Applying the above formulas to the $\gamma$-rays emitted in the bombardment of $Be^9$ by protons we obtain the following values of $(c/v)(F^2/k^2)/(1-FG\delta)^2$ for $r_0=0.318\times10^{-12}$ cm and $U=9$ MEV:

| $T=$ | 99.8 | 158.2 | 250.7 | 397.3 | 629.7 | 998.0 | 1582 kv |
|---|---|---|---|---|---|---|---|
| $(c/v)(F^2/k^2)/(1-FG\delta)^2=$ | $2.3\times10^{-29}$ | $2.1\times10^{-28}$ | $1.21\times10^{-27}$ | $4.8\times10^{-27}$ | $1.43\times10^{-26}$ | $3.5\times10^{-26}$ | $7.6\times10^{-26}$cm². |
| $\bar\sigma/\sigma=$ | | | .28 | .33 | .38 | .43 | |

The above numbers are nearly proportional to $\sigma$ because the part of $\bar u$ which matters is in the "well" and is nearly independent of $T$. Plotting the logs of above values against $T^{-\frac{1}{2}}$ one obtains nearly a straight line. Approximating the graph by a series of straight lines one determines for each $T$ the coefficient $b$ for the approximation $\sigma=e^{-b/\sqrt{T}}$. Using the 3/2 power law and this approximation we obtain by integration the ratio $\bar\sigma/\sigma$ where $\bar\sigma$ is the effective cross section for thick targets defined by $\bar\sigma\cdot x=\int_0^x\sigma(x)dx$ where $x$ is the distance inside the target measured from the face. The approximate values of $\bar\sigma/\sigma$ are also tabulated above. The values of

$$S=(c/v)F^2k^{-2}(1-FG\delta)^{-2}(\bar\sigma/\sigma)(T/397.3)^{\frac{1}{2}}$$

should be proportional to the observed yield and are compared below with the observed $\gamma$-ray yield on an arbitrary scale. The observations are due to Tuve and Hafstad and were kindly made available to us before publication. The

| $T$ | 600 | 700 | 800 | 900 | 920 | 1000 kv |
|---|---|---|---|---|---|---|
| $10^{25}S$ | .9 | 1.7 | 2.8 | 4.3 | — | 6.0 |
| Experimental ray yield | .3 | .5 | 1.2 | 5.0 | 6.7 | — |

experimental yield increases much faster from 700 to 900 kv than the theoretical. This suggests a deeper well and perhaps the approach of resonance around 1 MEV which, however, has not been found so far.

# The Formation of Electron-Positron Pairs by Internal Conversion of γ-Radiation

MORRIS E. ROSE AND GEORGE E. UHLENBECK, *University of Michigan*

(Received June 19, 1935)

The production of an electron and positron by the spherical γ-wave emitted from a nucleus has been considered on the basis of different approximation methods (Section II, III, IV), which yield simple closed formulae for the probability of the process. Regarding the nucleus as a Hertzian oscillator, both the dipole and quadripole radiation are treated. The approximate methods, which may be classified according to which of a certain set of parameters (the momenta of the particles, $\alpha Z$, and eventually the ratios of these) are to be considered small, form a consistent scheme (§6, where also the case of the plane γ-wave is discussed). A discussion of the qualitative features of the angular and energy distribution is given (§7 and §8) and a comparison is made with the rigorous treatment of the problem by Jäger and Hulme (§9). This shows that both the differential and total internal conversion coefficient may be computed with a fair degree of accuracy by the combined use of the Born and the Schrödinger approximation results.

## I. INTRODUCTION

**1.**

THE Dirac theory of the positron[1] describes the formation of an electron-positron pair by γ-radiation near a nucleus as a kind of photoelectric effect. The absorption of a γ-quantum of energy $\geqq 2mc^2 = 10^6$ ev raises an electron in an occupied negative energy state to a state in the positive continuum, the "hole" left in the negative energy spectrum together with the electron in the positive state constitute the positron-electron pair. For the case that the γ-radiation is a plane wave, calculations, with approximate wave functions for the probability of the process have been made by Oppenheimer and Plesset, Bethe and Heitler and others.[2] For the case of a spherical γ-wave emitted by the nucleus, with which we shall be concerned here, there exist the calculations of Oppenheimer and Nedelsky,[3] where the Born approximation is used, and those of Jäger and Hulme,[4] in which the exact solutions of the Dirac equations for a Coulomb field have been used. Because of the lengthy numerical computations necessary in the exact theory, we have gone back to approximate methods which give simple closed formulae. We have especially examined the consistency of these methods. By comparing the results with those of Jäger and Hulme one can then obtain an idea concerning the range of applicability of these approximate methods, which may be also of value in other related problems.

**2.**

The calculation of the probability for pair formation can in all cases be reduced to the evaluation of the matrix elements of the perturbation due to the radiation. We write the Dirac equation for the electron in a Coulomb field with a nuclear charge $\alpha^{\frac{1}{2}}Z$.[5]

$$i\partial\psi/\partial t = \{(\boldsymbol{\alpha}\cdot\mathbf{p}) + \beta + \alpha Z/r - \alpha^{\frac{1}{2}}\mathfrak{H}\}\psi. \qquad (1)$$

Here $\mathfrak{H}$ is the perturbation of the radiation field:

$$\mathfrak{H} = H e^{-ikt} + \text{compl. conj.},$$
$$H = V + (\boldsymbol{\alpha}\cdot\mathbf{A}), \qquad (2)$$

$k$ is the frequency which in our units is the same as the energy of the photon of this frequency; $V$ and $\mathbf{A}$ are the space parts of the scalar and vector potentials. In accordance with the results of Hulme, Taylor and Mott[6] for the atomic

[1] P. A. M. Dirac, Proc. Roy. Soc. **133**, 60 (1931).

[2] J. R. Oppenheimer and M. Plesset, Phys. Rev. **44**, 53 (1933) (nonrelativistic approximation); H. Bethe and W. Heitler, Proc. Roy. Soc. **146**, 83 (1934) (Born approximation, influence of screening); G. Racah, Nuovo Cimento **11**, 3 (1934) (Born approximation); Y. Nishina, S. Tomonaga and S. Sakata, Suppl. Sc. Pap. I. P. C. R. **24**, 1 (1934) (nonrelativistic and Born approximation).

[3] J. R. Oppenheimer and L. Nedelsky, Phys. Rev. **44**, 948 (1933).

[4] J. C. Jäger and H. R. Hulme, Proc. Roy. Soc. **148**, 708 (1935).

[5] In the following we will always use rational relativistic units. In this system the unit of energy is $mc^2$, of momentum $mc$ and of length the Compton wavelength $\hbar/mc$. Equations in ordinary units may be written in these units by replacing $\hbar$, $m$ and $c$ by unity and the electron charge $e$ by $\alpha^{\frac{1}{2}}$, where $\alpha$ is the fine structure constant $e^2/\hbar c$. This $\alpha$ is not to be confused with the Dirac matrices $\alpha_x$, $\alpha_y$, $\alpha_z$, collectively denoted by $\boldsymbol{\alpha}$.

[6] H. R. Hulme, Proc. Roy. Soc. **138**, 643 (1932); H. M. Taylor and N. F. Mott, Proc. Roy. Soc. **138**, 665 (1932).

internal conversion, we will consider the case of the electric quadripole wave as well as that of the electric dipole wave. The fields are given by (omitting from each potential a constant factor having the meaning of a moment, since it does not enter in the final results):

Electric dipole:

$$V=(1/r)e^{ikr}(i-1/kr)\cos\vartheta;$$
$$A_z=(i/r)e^{ikr},\quad A_x=A_y=0. \tag{3}$$

Electric quadripole:[7]

$$V=(1/r)e^{ikr}\{2P_2(\cos\vartheta)(1+3i/kr-3/k^2r^2)+1\},$$
$$A_z=(3/r)e^{ikr}(1+i/kr)\cos\vartheta,\quad A_x=A_y=0. \tag{4}$$

Applying the usual method of variation of constants the solution of (1) may be expressed in terms of the probability amplitudes $a_n(t)$ of the various states. At time $t=0$ the electron is in a negative energy state $W_0$, so that $a_n(0)=\delta_{n0}$. One finds then from (1) for the probability $|a_n|^2$ that the electron be in state $W_n$ at the time $t$:

$$|a_n|^2=4\alpha|(n|H|0)|^2\frac{\sin^2(W_n-W_0-k)t/2}{(W_n-W_0-k)^2}, \tag{5}$$

using the Dirac notation for the matrix elements. One has now to sum $|a_n|^2$ over the spin, energy and direction of momentum (or quantum numbers corresponding thereto) of both particles. The summation over the energy of one of the particles will give then as usual the conservation of energy. The manner in which the summation has further to be carried out will depend on the type of wave functions used. We will distinguish between three cases.

(*a*) *Both particles are represented by plane waves at infinity.* This is most convenient when the Born approximation or parabolic coordinate wave functions are used. To obtain the energy distribution a summation of (5) over the direction of the momenta and over the spin has to be carried out. The result is:

$$\sigma(W_+)dW_+=dW_+(2\alpha/(2\pi)^5n)(p_+p_-W_+W_-/k)\iint d\Omega_-d\Omega_+\sum_{s_+}|(\mathbf{p}_-s_-|H|\mathbf{p}_+s_+)|^2. \tag{A}$$

Here quantities referring to the electron are denoted by the index $-$ and those referring to the positron by the index $+$;[8] $d\Omega_-$, $d\Omega_+$ are elements of solid angle of the direction of emission of the two particles. The matrix element has to be formed with wave functions normalized to one particle per unit volume. The four term summation over the spin variables $s_-$ and $s_+$ reduces to twice a two term sum over one, say $s_+$, because although there is a preferred direction (the $z$ axis) there is no preferred sense. Finally $nk$ is the number of $\gamma$-quanta which in unit time are emitted by the nucleus; $n$ depends on the type of radiation;

$n=4/3$ for electric and magnetic dipole,
$n=12/5$ for electric quadripole.

(*b*) *Both particles represented by spherical waves at infinity.* This is most convenient in the case of the nonrelativistic approximation. Because the Dirac equations for a central field are separable *only* in polar coordinates,[9] this will also be the natural representation when the exact wave functions are used. Here the integration over the direction of the momenta is replaced by a summation over the azimuthal and magnetic quantum numbers of both particles. The energy distribution is then:

[7] We have taken the $z$ direction along the multipole axis and we will also take the axis of quantization in this direction. That this is no loss in generality can be shown by averaging the results for an arbitrarily orientated multipole field over all directions of its axes. In the same way one shows that our restriction in (4) to a zonal quadripole is not essential. In the strict development of the electromagnetic field of an oscillating charge distribution there appears together with the electric quadripole the so-called magnetic dipole terms:

$$A_z=\sin\vartheta\sin\varphi(1+i/kr)(1/r)e^{ikr}$$
$$A_y=-\sin\vartheta\cos\varphi(1+i/kr)(1/r)e^{ikr}\qquad V=A_x=0 \tag{4a}$$

which we shall also consider (cf. H. M. Taylor and J. B. Fisk, Proc. Roy. Soc. **146**, 178 (1934)).

[8] The energy $W_0$ and momentum $\mathbf{p}_0$ of an electron in a negative energy state are related to the corresponding quantities for a positron by $W_0=-W_+$ and $\mathbf{p}_0=-\mathbf{p}_+$.

[9] This is the reason why the internal conversion problem is simpler than the problem of pair formation by a plane wave.

$$\sigma(W_+)dW_+ = dW_+(4\alpha/\pi n)(W_+W_-/p_+p_-k)\sum_{l_+m_+}\sum_{l_-m_-}\sum_{s_+}|(l_-m_-s_-|H|l_+m_+s_+)|^2. \tag{B}$$

For the fields (3), (4) or (4a) there will be selection rules which eliminate the summation over one set of quantum numbers $l$ and $m$. The matrix element has here to be formed with wave functions normalized to one particle in a sphere of unit radius.

(*c*) *One particle represented by a plane wave and the other by a spherical wave at infinity.* This we will use in order to determine the form of the energy distribution curve at the ends, that is when one of the particles receives almost all the energy of the $\gamma$-quantum. In the case that the positron is represented by a plane wave at infinity the energy distribution is:

$$\sigma(W_+)dW_+ = dW_+(\alpha/2\pi^3 n)(p_+W_+W_-/p_-k)\int d\Omega_+\sum_{l_-m_-}\sum_{s_+}|(l_-m_-s_-|H|\mathbf{p}_+s_+)|^2. \tag{C}$$

By interchanging the indices + and − one obtains the formula for the case that the electron is represented by a plane wave. Integration over $W_+$ from 1 to $k-1$ yields the total internal conversion coefficient $\sigma$.

## II. The Born Approximation

### 3.

For light nuclei or for high energies of the particles we can neglect the nuclear field and take for the wave functions plane waves. The criterion for the validity of this approximation is that the Born parameters $\alpha Z/p_+$ and $\alpha Z/p_-$ are both small compared to unity. Then

$$\psi_\pm = u_\pm[\exp \mp i(\mathbf{p}_\pm\cdot\mathbf{r})]$$

and the amplitudes $u_+$ and $u_-$ are:

$$u_-^{(1)} = \left(\frac{1+W_-}{2W_-}\right)^{\frac{1}{2}}\begin{vmatrix} -\dfrac{p_{-z}}{1+W_-} \\ -\dfrac{p_{-x}+ip_{-y}}{1+W_-} \\ 1 \\ 0 \end{vmatrix}, \qquad u_-^{(2)} = \left(\frac{1+W_-}{2W_-}\right)^{\frac{1}{2}}\begin{vmatrix} -\dfrac{p_{-x}-ip_{-y}}{1+W_-} \\ \dfrac{p_{-z}}{1+W_-} \\ 0 \\ 1 \end{vmatrix}, \tag{6a}$$

$$u_+^{(1)} = \left(\frac{1+W_+}{2W_+}\right)^{\frac{1}{2}}\begin{vmatrix} 1 \\ 0 \\ -\dfrac{p_{+z}}{1+W_+} \\ -\dfrac{p_{+x}+ip_{+y}}{1+W_+} \end{vmatrix}, \qquad u_+^{(2)} = \left(\frac{1+W_+}{2W_+}\right)^{\frac{1}{2}}\begin{vmatrix} 0 \\ 1 \\ -\dfrac{p_{+x}-ip_{+y}}{1+W_+} \\ \dfrac{p_{+z}}{1+W_+} \end{vmatrix}. \tag{6b}$$

The superscripts (1) and (2) refer to the two spin directions. Oppenheimer and Nedelsky[3] have given the results for the energy distribution for the electric dipole and quadripole. We shall here outline the method of calculation. The matrix element in (A) will have the form:

$$(\mathbf{p}_-s_-|H|\mathbf{p}_+s_+) = (u_-^*u_+)\int[\exp -i(\mathbf{P}\cdot\mathbf{r})]Vd\tau + (u_-^*\alpha_z u_+)\int[\exp -i(\mathbf{P}\cdot\mathbf{r})]A_z d\tau,$$

in which $\mathbf{P}=\mathbf{p}_-+\mathbf{p}_+$ and $V$ and $A_z$ are given by (3) or (4). The angular integrations are elementary and lead to radial integrals of the form:

$$\int_0^\infty J_{l+\frac{1}{2}}(Pr)e^{ikr}r^{\nu+\frac{1}{2}}dr,$$

where $P=|\mathbf{P}|$ and $l$ and $\nu$ are integers. These may diverge at infinity. One has then, as in the derivation of the Rutherford scattering formula using the Born approximation, to introduce a convergence factor $\exp(-ar)$ and after the integration set $a=0$. One obtains in the case of the dipole:

$$|(\mathbf{p}_-s_-|H|\mathbf{p}_+s_+)|=(16\pi^2/k^2(k^2-P^2)^2)\{P_z^2|u_-^*u_+|^2+2P_zkR(u_-^*u_+)(u_+^*\alpha_zu_-)+k^2|u_-^*\alpha_zu_+|^2\},$$

where $R$ denotes "real part of." Using (6a) and (6b), summing over the spin of one of the particles and carrying out in (A) the integrations over all the angles but the one between $\mathbf{p}_+$ and $\mathbf{p}_-$, designated by $\theta$, we obtain the angular distribution. Writing $J(\theta, W_+)$ for the number of pairs per unit energy range and per unit solid angle, one finds:

$$J(\theta, W_+)=\frac{\alpha}{4\pi^2k^3}p_-p_+\left\{\frac{k^2}{(q^2-p_+p_-\cos\theta)^2}+\frac{W_+^2+W_-^2}{(q^2-p_+p_-\cos\theta)}+1\right\}, \tag{7}$$

where $q^2=1+W_+W_-$. The energy distribution is given by:

$$\sigma(W_+)=2\pi\int_0^\pi J(\theta, W_+)\sin\theta d\theta=(\alpha/\pi k^3)\{2p_+p_-+(W_+^2+W_-^2)\log b\}, \tag{$D_1$}$$

$$kb=1+W_+W_-+p_+p_-.$$

When $k$ is large one finds for the total internal conversion coefficient:

$$\sigma=\int_1^{k-1}\sigma(W_+)dW_+\leqq(2\alpha/3\pi)(\log 2k-\tfrac{3}{5})+O(1/k). \tag{8}$$

The calculation for the quadripole is quite analogous and one finds:

$$J(\theta, W_+)=\frac{\alpha}{4\pi^2k^3}p_+p_-\left\{\frac{k^2}{(q^2-p_+p_-\cos\theta)^2}+\frac{p_+^2+p_-^2}{(q^2-p_+p_-\cos\theta)}\right.$$
$$\left.+\frac{1}{3k^2}(16W_+W_--3k^2)-\frac{8}{3k^2}(q^2-p_+p_-\cos\theta)\right\}, \tag{9}$$

$$\sigma(W_+)=(\alpha/3\pi k^5)\{8p_+p_-(W_+W_--1)+3k^2(p_+^2+p_-^2)\log b\}, \tag{$Q_1$}$$

$$\sigma=(2\alpha/3\pi)(\log 2k-61/30)+O(1/k). \tag{10}$$

A discussion of these results will be given in section V.[10]

## III. The Schrödinger Approximation

**4.**

When the energy of the $\gamma$-quantum is so small that throughout the entire allowed energy range $p_+\ll1$, $p_-\ll1$ and when further $\alpha Z\ll1$ the so-called Schrödinger approximation of the Dirac wave functions may be used. Then:

---

[10] It has been suggested by Taylor and Fisk, Reference 7, for the process of atomic internal conversion that one should perhaps consider besides the electric quadripole the magnetic dipole terms. We have therefore carried out the calculation of the pair formation by this field (Eq. 4a) and find:

$$\sigma(W_+)=(\alpha/\pi k^3)(p_+^2+p_-^2)\log b.$$

This is slightly smaller than $Q_1$, so that since the magnetic dipole moment is almost certainly much smaller than the electric quadripole moment, the contribution from this source may be neglected.

$$\psi_-^{(1)}=\begin{vmatrix} \frac{i}{2}\frac{\partial u_-}{\partial z} \\ \frac{i}{2}\left(\frac{\partial u_-}{\partial x}+i\frac{\partial u_-}{\partial y}\right) \\ u_- \\ 0 \end{vmatrix}, \qquad \psi_-^{(2)}=\begin{vmatrix} \frac{i}{2}\left(\frac{\partial u_-}{\partial x}-i\frac{\partial u_-}{\partial y}\right) \\ -\frac{i}{2}\frac{\partial u_-}{\partial z} \\ 0 \\ u_- \end{vmatrix}, \tag{11a}$$

$$\psi_+^{(1)}=\begin{vmatrix} u_+ \\ 0 \\ -\frac{i}{2}\frac{\partial u_+}{\partial z} \\ -\frac{i}{2}\left(\frac{\partial u_+}{\partial x}+i\frac{\partial u_+}{\partial y}\right) \end{vmatrix}, \qquad \psi_+^{(2)}=\begin{vmatrix} 0 \\ u_+ \\ -\frac{i}{2}\left(\frac{\partial u_+}{\partial x}-i\frac{\partial u_+}{\partial y}\right) \\ \frac{i}{2}\frac{\partial u_+}{\partial z} \end{vmatrix}. \tag{11b}$$

The superscripts again denote the two directions of the spin. The elements occurring as derivatives will be referred to as the small components since they enter with a coefficient $1/c$ (not apparent in our units). The $u_-$ and $u_+$ are solutions of the Schrödinger equation:

$$\Delta u_\pm+(p_\pm^2\mp 2\alpha Z/r)u_\pm=0. \tag{12}$$

The solution of (12) for the electron in a state of the continuous spectrum ($W_->1$) is:[11]

$$u_-=N_\Omega P_l^m(\vartheta,\varphi)f_l^-(p_-r),$$

where the angular normalization factor is:

$$N_\Omega=((2l+1)/4\pi)^{\frac{1}{2}}(l+m)\,!^{-\frac{1}{2}}(l-m)\,!^{-\frac{1}{2}}.$$

Of the radial wave function $f_l^-(p_-r)$ we shall need only the expansion around the origin:

$$f_l^-(p_-r)=N_l^-r^l\left\{1-\frac{\alpha Z}{l+1}r+\frac{2\alpha^2Z^2-(l+1)p_-^2}{2(l+1)(2l+3)}r^2+\cdots\right\}. \tag{13}$$

Normalizing to one particle in a sphere of unit radius, we get:[12]

$$|N_l^-|^2=e^{\pi\alpha Z/p_-}(2p_-)^{2l+2}|\,\Gamma(l+1+i\alpha Z/p_-)\,|^2/2(2l+1)\,!^2 \tag{14}$$

The corresponding expressions for the positron may be obtained from these by changing the sign of $Z$ and replacing the index $-$ by $+$. From the expressions for the electromagnetic fields (3) and (4) one can show that the matrix elements in (B) will vanish unless the following selection rules are fulfilled:

| | | |
|---|---|---|
| for the dipole | $\lvert l_--l_+\rvert=0,\ 2,$ | $\lvert m_--m_+\rvert=0,\ 1,\ 2;$ |
| for the quadripole | $\lvert l_--l_+\rvert=1,\ 3,$ | $\lvert m_--m_+\rvert=0,\ 1,\ 2.$ |

For the internal conversion, first considering the dipole, it is evident from the normalization factors (14) that transitions involving high $l$'s will introduce the parameters of smallness, $p_+$ and $p_-$ to a high power. Indeed a calculation shows that it is necessary to consider only the $s-s$ transition and the large components in the wave functions to get the main contribution. Then:

[11] We omit here the index $-$ on the $l$ and $m$.
[12] See e.g. H. Bethe, *Handbuch der Physik*, Vol. 24-1, p. 292.

$$(0, 0, \tfrac{1}{2}|H|0, 0, \tfrac{1}{2}) = \int \psi_-^{(1)} \alpha_z A_z \psi_+^{(1)} d\tau = i \int_0^\infty r e^{ikr} f_0^- f_0^+ dr,$$

only the vector potential and the wave functions with parallel spin contributing. Because $f_0^- f_0^+$ varies slowly compared to the oscillations of exp $(ikr)$ the main contribution to the integral comes from a region near the origin. We may therefore insert for $f_0^-$ and $f_0^+$ the first term of (13). In fact one sees that the terms in (13) involving higher powers of $r$ would give contributions of higher order in $p_+$, $p_-$ and $\alpha Z$; therefore it would be inconsequent to include these terms. Thus:

$$\sum_{l_- m_-} \sum_{l_+ m_+} \sum_{s_+} |(l_- m_- s_- |H| l_+ m_+ s_+)|^2 \cong |(0, 0, \tfrac{1}{2}|H|0, 0, \tfrac{1}{2})|^2 \cong |N_0^-|^2 |N_0^+|^2 / k^4, \tag{15}$$

where as before we have introduced a convergence factor exp $(-ar)$ in the integrand and after integration set $a=0$. The energy distribution is then from (B):

$$\sigma(W_+) dW_+ = dW_+ \frac{48\pi\alpha^3 Z^2 W_+ W_-}{k^5 (e^{2\pi\alpha Z/p_+} - 1)(1 - e^{-2\pi\alpha Z/p_-})}. \tag{16}$$

To be consistent with the approximation here considered one should further replace $W_+$ and $W_-$ by 1 and $k$ by 2, so that:

$$\sigma(W_+) dW_+ = dW_+ \frac{3\pi\alpha^3 Z^2}{2(e^{2\pi\alpha Z/p_+} - 1)(1 - e^{-2\pi\alpha Z/p_-})}. \tag{$D_2$}$$

The calculation for the quadripole involves the $s-p$ and $p-s$ transitions. It is also necessary to consider the small components in those terms where they are multiplied with a large component. We will give only the result:

$$\sigma(W_+) dW_+ = dW_+ \frac{20\pi\alpha^3 Z^2}{3k^5} \left(1 - \frac{4}{k} + \frac{12}{k^2}\right) \frac{W_+ W_- (p_+^2 + p_-^2 + 2\alpha^2 Z^2)}{(e^{2\pi\alpha Z/p_+} - 1)(1 - e^{-2\pi\alpha Z/p_-})}. \tag{17}$$

Or again replacing $k$ by 2:[13]

$$\sigma(W_+) dW_+ = dW_+ \frac{5\pi\alpha^3 Z^2}{12} \frac{p_+^2 + p_-^2 + 2\alpha^2 Z^2}{(e^{2\pi\alpha Z/p_+} - 1)(1 - e^{-2\pi\alpha Z/p_-})}. \tag{$Q_2$}$$

By using polar coordinate wave functions as in (B) it is impossible to obtain an angular distribution of the particles formed. For this one has to use wave functions which behave like plane waves at infinity as in (A). In the Schrödinger approximation this can be done by means of the well-known parabolic coordinate wave functions.[14] It is then found that in this approximation the distribution function $J(\theta, W_+)$ is independent of $\theta$. For a discussion of these results see section V.

## IV. Endpoint Formulae

### 5.

It is possible to find an expression for the energy distribution near the ends of the curve, that is, when one of the particles receives almost all the energy of the $\gamma$-quantum, by taking for the fast particle plane wave functions (6) and for the slow particle Schrödinger approximation wave functions (11). In case the positron is the fast particle the parameters of smallness are therefore $\alpha Z/p_+$, $p_-$ and $\alpha Z$. Then for the dipole we need only to consider the electron in an $s$ state. The square of the matrix element in (C) summed over the spin $s_+$ becomes:

---

[13] The corresponding result for the magnetic dipole is 3/5 of $Q_2$. Cf. footnote 10.

[14] Cf. Bethe, *Handbuch der Physik*, Vol. 24-1, p. 299.

$$\sum_{s_+}|(0,0,s_-|II|\mathbf{p}_+s_+)|^2=(2\pi^2/k)|N_0^-|^2\{1-[(k^2-4)/k^2]\cos^2\theta_+\},$$

where $\theta_+$ is the angle between $\mathbf{p}_+$ and the $z$ axis. Consistently with our development in powers of $p_-$ we have set $p_+^2\leqq k(k-2)$ and $W_+\leqq k-1$. Inserting in (C) and integrating over $\theta_+$ one obtains:

$$\sigma(W_+)dW_+=dW_+2\alpha^2Z(k^2+2)p_+/k^4(1-e^{-2\pi\alpha Z/p_-}). \tag{$D_3$}$$

Upon interchanging $p_+$ and $p_-$ and changing the sign of $Z$ we get the formula for the case that the positron is the slow particle:

$$\sigma(W_+)dW_+=dW_+2\alpha^2Z(k^2+2)p_-/k^4(e^{2\pi\alpha Z/p_+}-1). \tag{$D_3'$}$$

For the quadripole we have again to consider only the slow particle formed in an $s$ state. It suffices to give the result for the positron the fast particle:

$$\sigma(W_+)dW_+=dW_+2\alpha^2Z(3k^2+8)p_+^3/3k^6(1-e^{-2\pi\alpha Z/p_-}). \tag{$Q_3$}$$

The case in which the electron is the fast particle is to be obtained as before.

## V. Structure and Discussion of the Formulae

### 6. Consistency of the approximation methods

In the foregoing we have given the energy distribution for the electric dipole and quadripole in three different regions of approximation:

$$D_1 \text{ and } Q_1 \text{ for: } \alpha Z/p_+,\ \alpha Z/p_-\ll 1,$$

$$D_2 \text{ and } Q_2 \text{ for: } p_+,\ p_-,\ \alpha Z\ll 1,$$

$$D_3 \text{ and } Q_3 \text{ for: } \alpha Z/p_+,\ p_-,\ \alpha Z\ll 1.$$

That these approximation methods be consistent with each other it is necessary that the following limit equations be fulfilled:

$$\lim_{p_+,\ p_-\to 0} D_1=\lim_{\alpha Z/p_+,\ \alpha Z/p_-\to 0} D_2,\quad \lim_{p_-\to 0} D_1=\lim_{\alpha Z/p_-\to 0} D_3,\quad \lim_{\alpha Z/p_+\to 0} D_2=\lim_{p_+\to 0} D_3 \tag{18}$$

and the corresponding equations with $Q_1$, $Q_2$ and $Q_3$. Reference to the results given for $\sigma(W_+)$ in II, III and IV shows that all six limit equations are satisfied and therefore, that there are no non-uniformities in the approximation scheme.

It is of interest to consider in this connection whether a similar situation exists in the case of the problem of pair formation by plane $\gamma$-radiation. The result for the differential cross section using the Born approximation as given by Bethe and Heitler[15] becomes (in our units) when $p_+$ and $p_-$ are made small:

$$\sigma(W_+)dW_+=dW_+(\alpha^3Z^2/6)p_+p_-(p_+^2+p_-^2). \tag{19}$$

The Schrödinger approximation has been considered by Oppenheimer and Plesset[2] using parabolic coordinates and taking only the big components in the wave functions. The result is:[16]

$$\sigma(W_+)dW_+=dW_+\frac{\pi^2\alpha^5Z^4}{3}\frac{p_+^2+p_-^2+2\alpha^2Z^2}{(e^{2\pi\alpha Z/p_+}-1)(1-e^{-2\pi\alpha Z/p_-})}. \tag{20}$$

---

[15] Reference 2, p. 90, Eq. (21). The + sign in front of the third line in this equation has to be changed to a − sign.

[16] A correction by a factor two has been made here (see Fermi and Uhlenbeck, Phys. Rev. **44**, 510 (1933)). The same result (20) follows, using polar coordinates and considering again only the big components for the $s$–$p$ and $p$–$s$ transitions, which give the largest contribution.

When $\alpha Z/p_+$ and $\alpha Z/p_-$ are small, (20) reduces to one-half of (19). However, we believe (20) is not correct, since, using parabolic coordinates one can show that the small components as well as the next approximation to the large ones give contributions of the same order of magnitude. A result different from (20) has been given by Nishina, Tomonaga and Sakata:[2]

$$\sigma(W_+)dW_+ = dW_+ \frac{\pi^2\alpha^5 Z^4}{8} \frac{(16/3)(p_+^2+p_-^2)+\alpha^2Z^2(4+\pi^2/2)}{(e^{2\pi\alpha Z/p_+}-1)(1-e^{-2\pi\alpha Z/p_-})}. \tag{21}$$

This *does* reduce to (19) if $\alpha Z/p_+$ and $\alpha Z/p_-$ are small. We have not been able to check this formula.[17] We have made a nonrelativistic calculation using the wave functions of Sommerfeld and Maue.[18] They are an expansion of the Dirac wave functions for the Coulomb field in powers of $\alpha Z$ and may be written:

$$\psi = \{f_0 + i(\boldsymbol{\alpha}\cdot\boldsymbol{G})\}u,$$

where, if one uses parabolic coordinates, $f_0$ is the solution of the scalar Schrödinger equation in these coordinates and the $u$'s are the columns given in (6). The term with $\boldsymbol{G}$ is the first order correction and is proportional to $\alpha Z$. Using $f_0$ only one gets the Oppenheimer-Plesset result. However the correction term, even in the nonrelativistic limit, gives a contribution of the same order of magnitude. We find then:

$$\sigma(W_+)dW_+ = dW_+ \frac{2\pi^2\alpha^5 Z^4}{3} \frac{p_+^2+p_-^2+\alpha^2Z^2}{(e^{2\pi\alpha Z/p_+}-1)(1-e^{-2\pi\alpha Z/p_-})}, \tag{22}$$

which has the correct limit.

## 7. Angular distribution

It is readily seen that for both the electric dipole and quadripole at each energy $W_+$ the angular distribution $J(\theta, W_+)$ as given by (7) and (9) is a monotonically decreasing function of $\theta$, so that there is always a tendency for the particles to be emitted in the *same* direction. This is most marked at the middle of the energy distribution, i.e., $W_+ = W_- = k/2$ (see Fig. 1). As $p_+$ or $p_-$ approach zero the emission becomes more and more spherically symmetric. All these properties may be seen in a qualitative manner from the matrix element which governs the angular distribution, that is

$$(\mathbf{p}_-s_-|H|\mathbf{p}_+s_+) \sim \int d\tau \exp(ikr - i(\mathbf{p}_+ + \mathbf{p}_-)\cdot\mathbf{r}). \tag{23}$$

In the exact theory one may expect that the same qualitative features are true with the exception that the strongest parallel emission ($\theta = 0$) will be shifted away from the center toward higher positron energies. The angular distribution will in fact qualitatively depend on a matrix element of the form (23) where now $p_+$ and $p_-$ are functions of $r$. For each energy

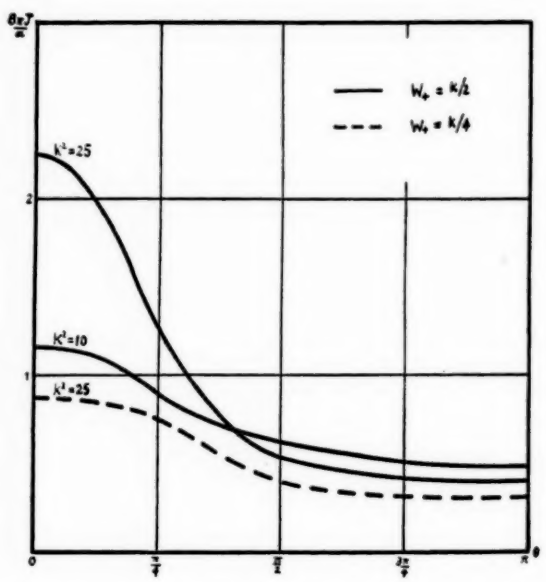


FIG. 1. Angular distribution for the dipole in the Born approximation.

[17] The angular distribution (see their Eq. (1)) does not upon integration over the angles give (21) (=their Eq. (2)).

[18] A Sommerfeld and A. W. Maue, Ann. d. Physik **22**, 629 (1935).

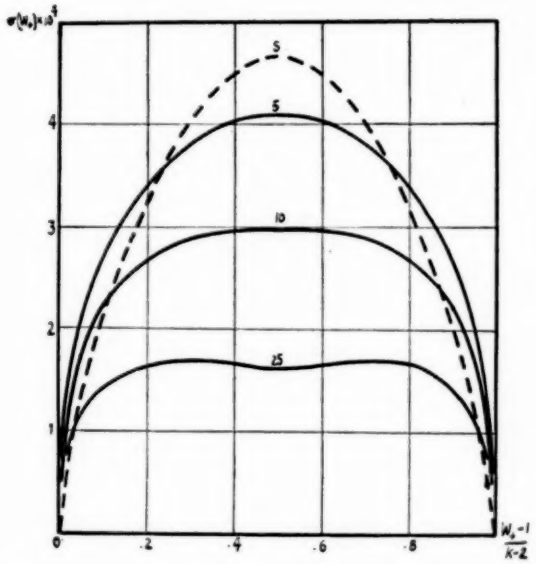


FIG. 2. Energy distribution for the dipole in the Born approximation. The numbers affixed to the curves refer to the value of $k$. In the statistical distribution $S$, computed for $k=5$ a constant multiplicative factor has been chosen so that the areas under this curve and under the corresponding Born curve are the same.

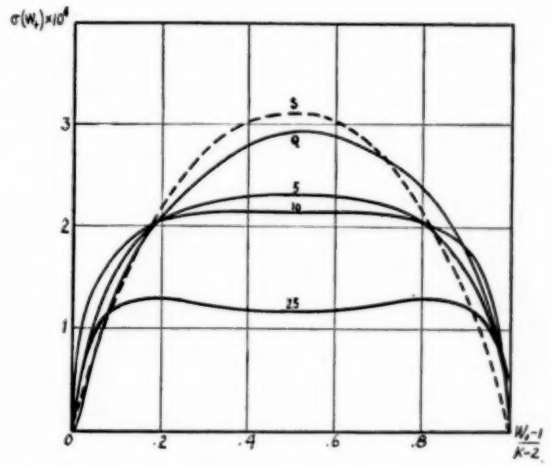


FIG. 3. Energy distribution for the quadripole. The curves marked 5, 10, 25 are the Born approximation distribution for those values of $k$. The curve $Q$ is the Schrödinger approximation (17) for $k=5$, $Z=6$ while the statistical distribution $S$, $k=5$ has the same area as $Q$.

the parallel emission will preponderate over the antiparallel emission ($\theta=\pi$) and this contrast will be greatest when $p_+(r)=p_-(r)$ for then the integrand oscillates the least. Since the main contribution comes from $r\leqq 1$, i.e., the Compton wavelength, then when $p_-(1)=p_+(1)$ the difference of the energies of electron and positron at infinity will be about $2\alpha Z$. That is, the maximum preponderance of the parallel over the antiparallel emission may be expected to occur at a point of the energy distribution which is displaced from the center toward higher positron energies by an amount $2\alpha Z$, i.e., 0.6 MEV for $Z=80$.

For any fixed value of $W_+$ Eqs. (7) and (9) show that the angular distribution as a function of the energy of the $\gamma$-quantum $k$ will become more and more spherically symmetric as $k$ approaches 2. This will also be true in the exact theory, and is in accord with the result mentioned in the Schrödinger approximation.

For increasing $k$ the parallel emission increases while the antiparallel emission decreases so that the maximum at $\theta=0$ becomes more and more sharp. In fact for large $k$ the average value of $\theta$ is:

$$\bar{\theta}\sim(\log 2k)^{-\frac{1}{2}}.$$

This holds for both dipole and quadripole fields. Indeed from (7) and (9) it follows that for large $k$ the angular distributions and therefore the energy distributions and the total internal conversion coefficients for both fields become asymptotically equal as may be verified from $(D_1)$, $(Q_1)$ and (8), (10). This of course is to be expected, since the pairs are formed in a region around $r\geqq 1$ which for increasing $k$ will lie more and more in the radiation zone of the multipole field. In this radiation zone the field strengths $E$ and $H$, normalized so as to give unit energy flux, will become the same for all multipoles and therefore the probability for pair formation for $k$ large become the same. The asymptotic forms of (7), $(D_1)$ and (8) will therefore be valid independently of the Born approximation and for all multipole fields.

## 8. Energy distribution

In the interpretation of all the expressions found for the energy distribution it is well to distinguish between two factors. The first may be called the statistical factor and is simply proportional to the volume in phase space of the particle formed.[19] In our case where the

[19] Cf. G. E. Uhlenbeck and S. Goudsmit, *Zeeman Jubilee Papers*, Nijhoff, The Hague, 1935, p. 201.

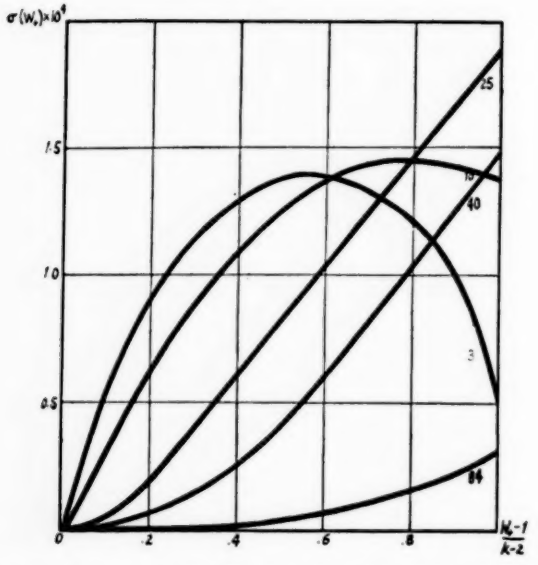


FIG. 4. Energy distribution for the dipole in the Schrödinger approximation for $k=2.2$. The numbers affixed to the curves refer to the value of $Z$.

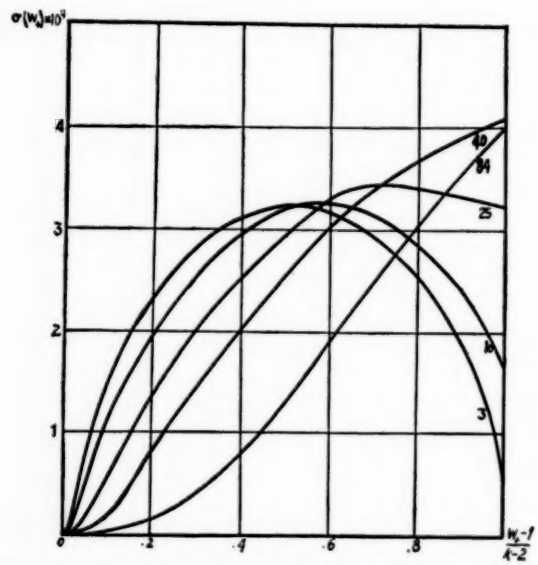


FIG. 5. Energy distribution for the dipole in the Schrödinger approximation for $k=3$ and the values of $Z$ indicated.

energy is distributed between two particles with no conservation of momentum this factor becomes $\sim W_+W_-p_+p_-$. The second factor, which is the more interesting one, is characteristic of the mechanism of the process. We will refer to it as the "mechanism factor." It will depend essentially on the matrix element of the pair-producing field. The division into these two factors is quite evident in (A) for example.

In Figs. 2 and 3 we have given the energy distribution for different values of $k$ for both the dipole and quadripole as follows from the Born approximation formulae $D_1$ and $Q_1$.[20] As is to be expected the curves are symmetrical between the two particles; since the nuclear field has been neglected there is physically no difference between the particles. For energies below $k \leqq 5$ the form of the distribution is given almost exactly by the statistical factor, so that the mechanism factor is practically constant. For higher $k$ the distribution becomes flatter than the statistical factor and eventually develops a minimum at the center, just as the distribution in the case of the plane $\gamma$-wave.[21] This is probably due to the spin of the particles since in the Pauli-Weiszkopf theory[22] such a minimum does *not* appear.

In Figs. 4 and 5 we have given the energy distribution for two values of $k$ and several values of $Z$ as follows from the Schrödinger approximation formula (16) for the dipole. Because of the influence of the nuclear field, which is contained in the mechanism factor and is expressed by $|N_0^-|^2|N_0^+|^2$ (see Eq. (15)), the distribution is no longer symmetrical. This factor $|N_0^-|^2|N_0^+|^2$ is the product of the densities of the two particles at the nucleus and for large $Z$ or small $k$ essentially determines the form of the distribution. Expressing the repulsion of the positron by the nucleus $|N_0^+|^2$ will be small and will make the distribution function vanish exponentially when $p_+$ goes to zero. Due to the attraction of the electron by the nucleus, expressed by $|N_0^-|^2$ the distribution will be finite at the other end. As a consequence for large $Z$ or small $k$ the distribution function will be monotonically increasing with $W_+$. For smaller $Z$ or larger $k$ the curve will develop a maximum which shifts more and more to the center, and approaches the statistical distribution. This is evident from

[20] Among the $\gamma$-rays found for light elements there are several of energies around $k=5$, 10 and 25. For example, $_5B^{11}$ (2.4 MEV, $k=4.7$), $_6C^{13}$ (2.7 MEV, $k=5.3$), $_6C^{12}$ (5.5 MEV, $k=10.8$), $_8O^{16}$ (5.4 MEV, $k=10.6$), $_3Li^7$ bombarded with protons ($\sim$12 MEV, $k=24$).

[21] Bethe and Heitler, Reference 2, Fig. 5.

[22] W. Pauli and V. Weiszkopf, Helv. Phys. Acta **7**, 709 (1934).

(16) and (17) when $\alpha Z/p_+$ and $\alpha Z/p_- \ll 1$. It becomes therefore similar to the Born approximation distribution for small $k$ (cf. Fig. 3). For a particular value of $k$ and $W_+$ the probability as a function of $Z$ will have a maximum which occurs at larger $Z$ the greater $W_+$. This is due to the interplay of the densities $|N_0^-|^2$ and $|N_0^+|^2$ which are increasing and decreasing functions of $Z$, respectively.

The behavior of the distribution function near the ends as given by the endpoint formulae in section IV is qualitatively the same as that found from the Schrödinger approximation, since they also contain the density factors. One might hope that especially at the important end of the distribution, i.e., $W_- \leqq 1$, $(D_3)$ and $(Q_3)$ would give quantitatively better results. Comparison with the exact theory (see §9) shows that this is *not* the case, $(D_3)$ and $(Q_3)$ giving too large values. This must mean that replacing the positron wave function by a plane wave overestimates its "interference effect" on the probability. At the other end of the distribution, i.e., $W_+ \leqq 1$, $(D_3')$ and $(Q_3')$ give the same behavior as the Schrödinger approximation. The strong exponential decrease of the distribution function at this end must be expected to be generally valid.

### 9. Comparison with the exact theory of Jäger and Hulme

Using the exact Dirac wave functions for the Coulomb field Jäger and Hulme have given the theory for the internal conversion process for both the dipole and the quadripole. They have obtained numerical results for $\sigma(W_+)$ at five points on the energy range in the case $k=3$, $Z=84$. Fig. 6 shows the comparison of these results with the corresponding Schrödinger approximation curves.[23]

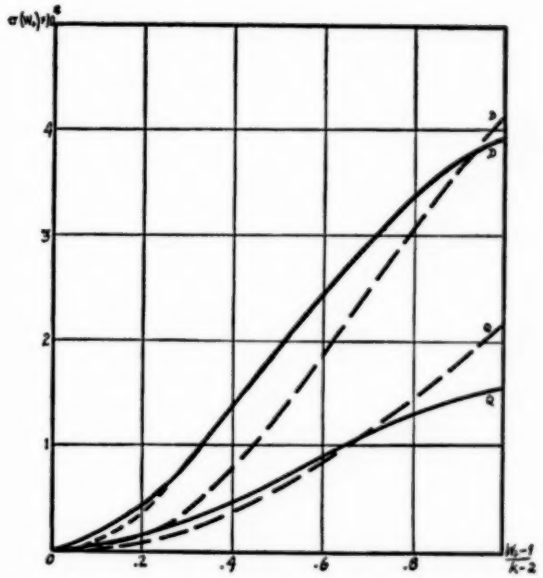


FIG. 6. Energy distribution for $k=3$, $Z=84$, in the exact theory (full lines) and in the Schrödinger approximation (dashed lines). The dipole and quadripole curves are designated by $D$ and $Q$, respectively.

The agreement is no doubt partly accidental. This becomes clear if one tries to improve the Schrödinger approximation formulae (16) and (17) by removing the restriction $\alpha Z \ll 1$. This can be done by using the exact Dirac wave functions, developing in $p_+$ and $p_-$ only and considering just those transitions which give the main contribution. These correspond to the $s-s$ (dipole) and $s-p$, $p-s$ transitions (quadripole) in the Schrödinger approximation. The result in case of the dipole for the sum of the matrix elements in (B) is quite analogous to (15). One gets from this sum:

$$|M_-|^2 |M_+|^2 (\Gamma^2(2\gamma_0)/k^{4\gamma_0}), \qquad (24)$$

where $\gamma_0=(1-\alpha^2Z^2)^{\frac{1}{2}}$ and $|M_-|^2$, $|M_+|^2$ are radial normalization factors:

$$|M_-|^2=\frac{(1+W_-)(2p_-)^{2\gamma_0}e^{\pi\alpha ZW_-/p_-}|\Gamma(\gamma_0+i\alpha ZW_-/p_-)|^2(\gamma_0+1)^2}{4W_-\Gamma^2(2\gamma_0+1)}$$

and $|M_+|^2$ is to be obtained from this by changing the sign of $Z$ and by replacing $-$ by $+$. The difference in the dependence on $k$ between (15) and (24) is due to the fact that in

[23] The lowest value of $W_+$ which Jäger and Hulme have computed is $W_+=1.25$. In accordance with what has been pointed out concerning the behavior of the distribution function near $W_+=1$, we believe it more plausible to extrapolate their curve towards $W_+=1$ as we have indicated by the dotted curve.

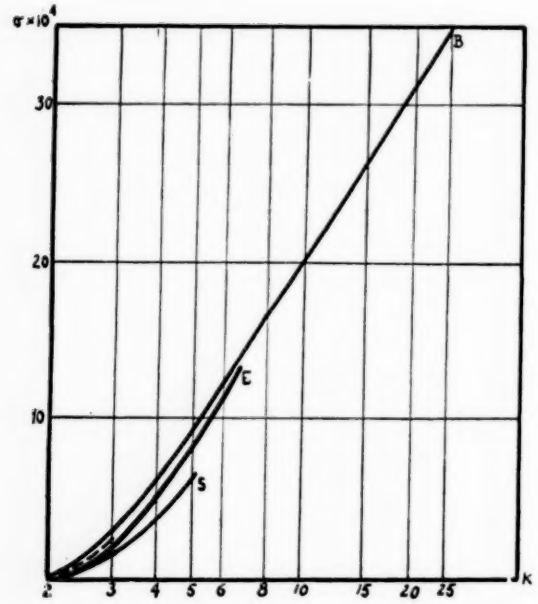


FIG. 7. Total internal conversion coefficient for the dipole. $B$ is the Born approximation curve, $E$ the curve of Jäger and Hulme and $S$ the Schrödinger approximation result all for $Z=84$. The dotted curve is the Schrödinger approximation curve for $Z=10$.

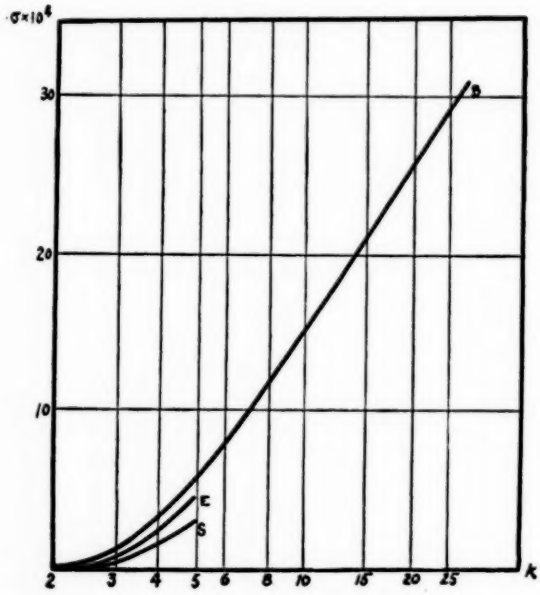


FIG. 8. Total internal conversion coefficient for the quadripole, $Z=84$.

the exact theory the wave functions considered behave like $r^{\gamma_0-1}$ at the origin. Combining (24) with (B) one obtains an expression for the energy distribution which for $\alpha Z \ll 1$ becomes the same as (16). This might be expected to give better numerical results. Actually this is *not* the case; the $\alpha Z$ arbitrary distribution lies entirely below that obtained from (16). The infinity of the wave functions at the origin, expressed in the $k$-dependence, does tend to increase the results but this is entirely overcome by the fact that the positron normalization factor $|M_+|^2$ is so much smaller than the non-relativistic $|N_0^+|^2$. Of course it is not surprising that the $\alpha Z$ arbitrary distribution lies completely below the true one of Jäger and Hulme, since one has also to consider other transitions. It appears then that the overestimate of the positron normalization factor $|N_0^+|^2$ in the Schrödinger approximation rather accidentally compensates for the neglect of the other transitions.

One may expect that in a certain range of energy this compensation will always be more or less the case. Since in addition the Schrödinger approximation formulae (16) and (17) have the right qualitative behavior, we believe that for $k$ say up to 5 and for all $Z$, (16) and (17) will give also quantitative results correct within a fair degree of accuracy. For $k$ larger than 5 and $Z$ small (say $\leq 20$) the Born approximation will no doubt give nearly correct results. For large $Z$ however, the Born approximation even for values of $k$ as high as 6 or 7 will probably not give the correct form of the energy distribution, although the total area $\sigma$ may be given quite accurately.

### 10. The total internal conversion coefficient

In Figs. 7 and 8 we have given the total internal conversion coefficient as a function of $k$ both for dipole and quadripole. The Born approximation result has been computed by graphical integration from $(D_1)$ and $(Q_1)$.[24] The Schrödinger approximation results have been obtained in the same way from (16) and (17). For $k$ near 2 (16) and (17) can be integrated analytically, giving:

$$\sigma \leqq (3/4)\alpha^2 Z g^3 e^{-2\pi\alpha Z/g},$$

$$\sigma \leqq (5/12)\alpha^4 Z^3 g^3 e^{-2\pi\alpha Z/g},$$

respectively, if $g^2=2(k-2)$. This shows the be-

[24] We have not made use of the asymptotic formulae (8) and (10) since the approach to them is very slow.

havior for $k$ near 2; for large $k$ (8) and (10) show that $\sigma$ increases like log $k$.

These results have to be compared with the results of Jäger and Hulme which are also indicated in the figures. They have given curves for the dipole up to $k=7$ and for the quadripole up to $k=5$ in the case $Z=84$. One sees again that by the combined use of the Born and Schrödinger approximation results the total internal conversion coefficient may be obtained for all $k$ and all $Z$ to within a fair degree of accuracy, say of the order 15 percent.

---

AUGUST 1, 1935 PHYSICAL REVIEW VOLUME 48

# The Spectrum of Molybdenum V

M. W. TRAWICK, *Department of Physics, Cornell University*

(Received June 15, 1935)

The spectrum of Mo V has been excited in a vacuum spark and photographed with a vacuum spectrograph. With the aid of the irregular doublet law applied to the Sr I-like isoelectronic sequence, lines involving combinations of $4d^2\,{}^3(FP)$, $4d5s\,{}^{1,3}D$, $4d5d\,{}^1(PD)$, and $4d5d\,{}^3(DF)$ with $4d5p\,{}^{3,1}(F^\circ D^\circ P^\circ)$ and $4d4f\,{}^3(G^\circ F^\circ)$, and lying in the spectral region from 2100A to 400A have been identified. Estimates of the absolute term values have been made from a Moseley diagram.

THE spectra of the first four elements in the Sr I-like isoelectronic sequence have been classified by various investigators; Sr I by Russell and Saunders and by others,[1] Y II by Meggers and Russell,[2] Zr III by Kiess and Lang,[3] and Cb IV by Gibbs and White[4] and, more fully, by Lang.[5] The present paper extends the sequence to include Mo V.

The spectrum of Mo V was excited in a vacuum spark between solid metal electrodes and photographed with a vacuum spectrograph containing a concave grating of 150-cm radius of curvature and ruled with 15,000 lines per inch. The vacuum spark between aluminum electrodes furnished the standard lines, either those of aluminum itself or those of nitrogen and oxygen brought out in the discharge.

Higher order lines were carefully noted. The lines of Mo IV and Mo VI which lie in the region investigated (2100A to 400A) were sorted out on the basis of the classifications by Eliason[6] and by the author.[7]

The identification of the multiplet transitions $4d5p\,{}^3(F^\circ D^\circ P^\circ)$ into $4d^2\,{}^3(FP)$ and $4d5s\,{}^3D$ furnished the key to the classification of the triplet lines. First, the triplet transition $4d5s\,{}^3D - 4d5p\,{}^3(F^\circ D^\circ P^\circ)$ was looked for with the help of a linear extrapolation of the wave numbers of the corresponding lines for the preceding members of the sequence. Fig. 1 is a diagram showing the relative positions of the lines in these multiplets. In this diagram, only the stronger lines, in general, are connected from one element to the next.

Since there was a large number of lines in the region of the spectrum occupied by the lines of the $4d5s\,{}^3D - 4d5p\,{}^3(F^\circ D^\circ P^\circ)$ multiplets, it was only by finding lines lying in the region of $4d^2\,{}^3F - 4d5p\,{}^3(F^\circ D^\circ P^\circ)$ (as indicated by the linear extrapolation of wave numbers) and having the same wave number separations as the lines of the $4d5s - 4d5p$ transition that a solution of the problem was obtained. Difficulty in identifying these latter lines was experienced because

[1] Saunders, Astrophys. J. **56**, 73 (1922); Russell and Saunders, Astrophys. J. **61**, 39 (1925).
[2] Meggers and Russell, Bur. Standards J. Research **2**, 733 (1929).
[3] Kiess and Lang, Bur. Standards J. Research **5**, 305 (1930)
[4] Gibbs and White, Phys. Rev. **31**, 520 (1928).
[5] Lang, Phys. Rev. **44**, 325 (1933). Also, private communication to Professor R. C. Gibbs.
[6] Eliason, Phys. Rev. **43**, 745 (1933).
[7] Trawick, Phys. Rev. **46**, 63 (1934).

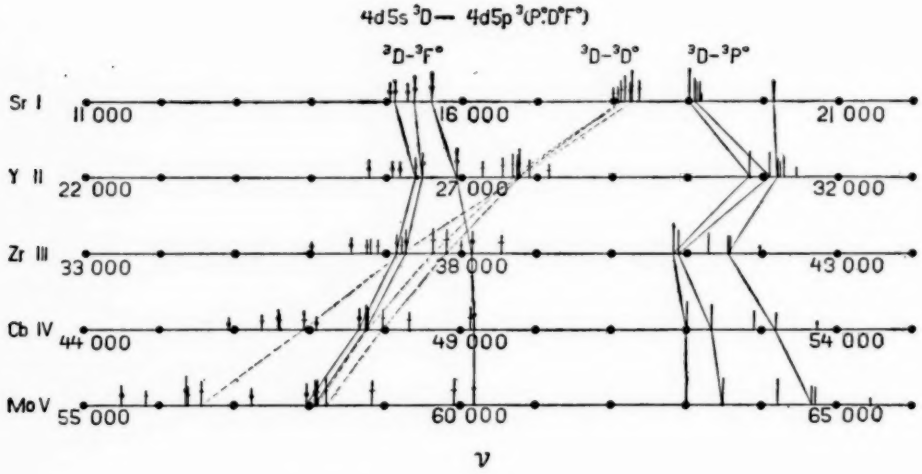


FIG. 1. Displacement of multiplets.

TABLE I. *Classified lines of Mo V.*

| λ(A) | Int. | ν(cm⁻¹) | Classification |
|---|---|---|---|
| 2159.30 | 0*d* | 46,311.3 | $4d5s\ ^3D_3 - 4d5p\ ^1F°_3$ |
| 2081.83 | 5*d* | 48,034.6 | $4d5s\ ^3D_2 - 4d5p\ ^1F°_3$ |
| 1848.59 | 0 | 54,095.3 | $4d5s\ ^3D_2 - 4d5p\ ^1P°_1$ |
| 1823.98 | 0 | 54,825.2 | $4d5s\ ^3D_1 - 4d5p\ ^1P°_1$ |
| 1801.49 | 5 | 55,509.6 | $4d5s\ ^3D_3 - 4d5p\ ^3F°_2$ |
| 1790.91 | 4 | 55,837.5 | $4d5s\ ^3D_2 - 4d5p\ ^3D°_1$ |
| 1774.35 | 9 | 56,358.7 | $4d5s\ ^3D_3 - 4d5p\ ^3F°_3$ |
| 1773.79 | 4*d* | 56,376.4 | $4d5s\ ^3D_3 - 4d5p\ ^3D°_2$ |
| 1767.77 | 7 | 56,568.4 | $4d5s\ ^3D_1 - 4d5p\ ^3D°_1$ |
| 1756.83 | 2*d* | 56,920.7 | $4d5s\ ^3D_3 - 4d5p\ ^1D°_2$ |
| 1756.33 | 1 | 56,936.9 | $4d5p\ ^3P°_0 - 4d5d\ ^3D_1$ |
| 1749.02 | 2 | 57,174.9 | $4d5s\ ^1D_2 - 4d5p\ ^1F°_3$ |
| 1747.22 | 7 | 57,233.8 | $4d5s\ ^3D_2 - 4d5p\ ^3F°_2$ |
| *1725.15 | 6 | 57,966.0 | $4d5s\ ^3D_1 - 4d5p\ ^3F°_2$ |
| 1722.40 | 2 | 58,058.5 | $4d5p\ ^3P°_1 - 4d5d\ ^3D_2$ |
| 1721.67 | 7 | 58,083.1 | $4d5s\ ^3D_2 - 4d5p\ ^3F°_3$ |
| 1721.20 | 7 | 58,099.0 | $4d5s\ ^3D_2 - 4d5p\ ^3D°_2$ |
| 1718.09 | 7 | 58,204.2 | $4d5s\ ^3D_3 - 4d5p\ ^3D°_3$ |
| 1705.25 | 0 | 58,642.4 | $4d5s\ ^3D_2 - 4d5p\ ^1D°_2$ |
| 1699.75 | 7 | 58,832.2 | $4d5s\ ^3D_1 - 4d5p\ ^3D°_2$ |
| 1684.16 | 00 | 59,376.8 | $4d5s\ ^3D_1 - 4d5p\ ^1D°_2$ |
| 1668.67 | 6 | 59,928.0 | $4d5s\ ^3D_2 - 4d5p\ ^3D°_3$ |
| 1661.23 | 9 | 60,196.4 | $4d5s\ ^3D_3 - 4d5p\ ^3F°_4$ |
| 1644.74 | 6 | 60,799.9 | $4d5p\ ^3D°_3 - 4d5d\ ^3D_3$ |
| 1643.12 | 2 | 60,859.8 | $4d5p\ ^1D°_2 - 4d5d\ ^1D_2$ |
| 1622.55 | 0 | 61,631.4 | $4d5p\ ^3D°_3 - 4d5d\ ^3D_2$ |
| 1596.73 | 0 | 62,628.0 | $4d5p\ ^3D°_2 - 4d5d\ ^3D_3$ |
| 1586.91 | 8 | 63,015.5 | $4d5s\ ^3D_3 - 4d5p\ ^3P°_2$ |
| 1581.34 | 6 | 63,237.5 | $4d5s\ ^1D_2 - 4d5p\ ^1P°_1$ |
| 1575.85 | 2 | 63,457.8 | $4d5p\ ^3D°_2 - 4d5d\ ^3D_2$ |
| 1574.71 | 8 | 63,503.8 | $4d5s\ ^3D_2 - 4d5p\ ^3P°_1$ |
| 1572.96 | 3 | 63,574.4 | $4d5p\ ^3D°_2 - 4d5d\ ^3D_1$ |
| 1559.70 | 3 | 64,114.9 | $4d5p\ ^1D°_2 - 4d5d\ ^1P_1$ |
| 1556.78 | 6 | 64,235.2 | $4d5s\ ^3D_1 - 4d5p\ ^3P°_1$ |
| 1546.13 | 4 | 64,677.6 | $4d5s\ ^3D_1 - 4d5p\ ^3P°_0$ |
| 1544.65 | 4 | 64,739.6 | $4d5s\ ^3D_2 - 4d5p\ ^3P°_2$ |
| 1538.75 | 0 | 64,987.8 | $4d5s\ ^1D_2 - 4d5p\ ^3D°_1$ |
| 1528.80 | 3 | 65,410.8 | $4d5p\ ^1P°_1 - 4d5d\ ^1D_2$ |
| 1527.44 | 0 | 65,469.0 | $4d5s\ ^3D_1 - 4d5p\ ^3P°_2$ |
| 1521.51 | 1 | 65,724.2 | $4d5p\ ^3D°_1 - 4d5d\ ^3D_2$ |
| 1518.86 | 3 | 65,838.9 | $4d5p\ ^3D°_1 - 4d5d\ ^3D_1$ |
| 1487.18 | 0 | 67,241.4 | $4d5s\ ^1D_2 - 4d5p\ ^3D°_2$ |
| 1475.19 | 2 | 67,787.9 | $4d5s\ ^1D_2 - 4d5p\ ^1D°_2$ |
| 1456.35 | 3 | 68,664.8 | $4d5p\ ^1P°_1 - 4d5d\ ^1P_1$ |
| 1447.78 | 00 | 69,071.3 | $4d5s\ ^1D_2 - 4d5p\ ^3D°_2$ |
| 1399.14 | 3 | 71,472.5 | $4d5p\ ^1F°_3 - 4d5d\ ^1D_2$ |
| 1189.96 | 2 | 84,036.4 | $4d5p\ ^3F°_4 - 4d5d\ ^3F_3$ |
| 1169.34 | 4 | 85,518.3 | $4d5p\ ^3F°_3 - 4d5d\ ^3F_2$ |
| 1157.85 | 4*d* | 86,367.0 | $4d5p\ ^3F°_2 - 4d5d\ ^3F_2$ |
| 1148.53 | 8*d* | 87,067.8 | $4d5p\ ^3F°_4 - 4d5d\ ^3F_4$ |
| 1137.97 | 6*d* | 87,875.8 | $4d5p\ ^3F°_3 - 4d5d\ ^3F_3$ |
| 1127.07 | 0 | 88,725.0 | $4d5p\ ^3F°_2 - 4d5d\ ^3F_3$ |
| 1099.97 | 0 | 90,911.6 | $4d5p\ ^3F°_3 - 4d5d\ ^3F_4$ |
| 730.27 | 1 | 136,936 | $4d^2\ ^3P_2 - 4d5p\ ^3F°_2$ |
| 729.23 | 1 | 137,131 | $4d^2\ ^3P_1 - 4d5p\ ^3D°_1$ |
| 725.77 | 8 | 137,785 | $4d^2\ ^3P_0 - 4d5p\ ^3D°_1$<br>$4d^2\ ^3P_2 - 4d5p\ ^3F°_3$ |
| 721.86 | 8 | 138,534 | $4d^2\ ^3P_1 - 4d5p\ ^3F°_2$ |
| 717.36 | 3 | 139,400 | $4d^2\ ^3P_1 - 4d5p\ ^3D°_2$ |
| 716.19 | 7 | 139,628 | $4d^2\ ^3P_2 - 4d5p\ ^3D°_3$ |
| 698.33 | 2 | 143,199 | $4d^2\ ^3P_2 - 4d5p\ ^3P°_1$ |
| 692.32 | 6 | 144,442 | $4d^2\ ^3P_2 - 4d5p\ ^3P°_2$ |
| 690.59 | 6 | 144,804 | $4d^2\ ^3P_1 - 4d5p\ ^3P°_1$ |
| 688.47 | 6 | 145,250 | $4d^2\ ^3P_1 - 4d5p\ ^3P°_0$ |
| 687.52 | 3 | 145,450 | $4d^2\ ^3P_0 - 4d5p\ ^3P°_1$ |
| 684.75 | 5 | 146,039 | $4d^2\ ^3P_1 - 4d5p\ ^3P°_2$ |
| 676.42 | 6 | 147,837 | $4d^2\ ^3F_4 - 4d5p\ ^3F°_3$ |
| 672.24 | 6 | 148,756 | $4d^2\ ^3F_3 - 4d5p\ ^3F°_2$ |
| 671.37 | 6 | 148,949 | $4d^2\ ^3F_2 - 4d5p\ ^3D°_1$ |
| *668.39 | 10 | 149,613 | $4d^2\ ^3F_3 - 4d5p\ ^3F°_3$ |
| *668.32 | 10 | 149,629 | $4d^2\ ^3F_3 - 4d5p\ ^3D°_2$ |
| 668.09 | 10 | 149,680 | $4d^2\ ^3F_4 - 4d5p\ ^3D°_3$ |
| 665.14 | 6 | 150,344 | $4d^2\ ^3F_2 - 4d5p\ ^3F°_2$ |
| *661.40 | 4 | 151,193 | $4d^2\ ^3F_2 - 4d5p\ ^3F°_3$ |
| *661.33 | 4 | 151,209 | $4d^2\ ^3F_2 - 4d5p\ ^3D°_2$ |
| 660.28 | 1 | 151,451 | $4d^2\ ^3F_3 - 4d5p\ ^3D°_3$ |
| 659.31 | 7 | 151,674 | $4d^2\ ^3F_4 - 4d5p\ ^3F°_4$ |
| 651.68 | 2 | 153,450 | $4d^2\ ^3F_3 - 4d5p\ ^3F°_4$ |
| 639.95 | 2 | 156,262 | $4d^2\ ^3F_3 - 4d5p\ ^3P°_2$ |
| 638.51 | 0 | 156,615 | $4d^2\ ^3F_2 - 4d5p\ ^3P°_1$ |
| 434.52 | 6 | 230,139 | $4d^2\ ^3F_3 - 4d4f\ ^3F°_2$ |
| 431.55 | 6 | 231,723 | $4d^2\ ^3F_2 - 4d4f\ ^3F°_2$ |
| 428.63 | 3 | 233,301 | $4d^2\ ^3F_3 - 4d4f\ ^3F°_3$ |
| 425.77 | 0 | 234,869 | $4d^2\ ^3F_2 - 4d4f\ ^3F°_3$ |
| 420.61 | 5 | 237,750 | $4d^2\ ^3F_4 - 4d4f\ ^3F°_4$ |
| 417.49 | 6 | 239,527 | $4d^2\ ^3F_3 - 4d4f\ ^3F°_4$ |
| 414.11 | 0 | 241,482 | $4d^2\ ^3F_4 - 4d4f\ ^3G°_4$ |
| 413.11 | 0 | 242,055 | $4d^2\ ^3F_3 - 4d4f\ ^3G°_3$ |
| 412.42 | 5 | 242,471 | $4d^2\ ^3F_4 - 4d4f\ ^3G°_5$ |
| *411.08 | 8 | 243,255 | $4d^2\ ^3F_3 - 4d4f\ ^3G°_4$ |
| 410.35 | 5 | 243,665 | $4d^2\ ^3F_2 - 4d4f\ ^3G°_3$ |

several of the principal lines belonging to these groups were not resolved on the plates.

The identification of the remainder of the lines was facilitated by determining the narrow region in which they must lie by use of diagrams similar to Fig. 1 for the corresponding transitions in the other members of the sequence.

The singlets were identified by finding the transitions of $4d5p\ ^1(P°D°F°)$ into $4d5s\ ^3D$. After these lines had been identified, it was possible

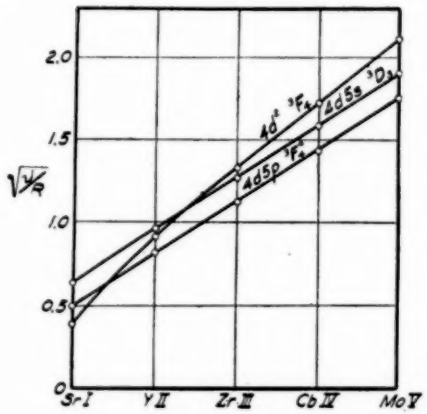


FIG. 2. Moseley diagram.

to determine the $4d5s\ ^1D$ and $4d5d\ ^1(PD)$ terms by their combinations with the $4d5p$ singlets. The $4d^2\ ^1(FP)$ terms were not found, as the lines yielded by the combinations they make with the $4d5p$ singlets lie at shorter wavelengths than it was possible to photograph successfully.

Table I gives a list of the classified lines, with their relative intensities and wave numbers. The lines not completely resolved from other lines very near them are marked with asterisks.

Approximate absolute term values were assigned from extrapolations on a Moseley diagram, Fig. 2. The values found by extrapolation

TABLE II. *Term values for Mo V.*

| CONFIG. | TERM | RELATIVE TERM VALUES | APPROXIMATE ABSOLUTE TERM VALUES | CONFIG. | TERM | RELATIVE TERM VALUES | APPROXIMATE ABSOLUTE TERM VALUES |
|---|---|---|---|---|---|---|---|
| $4d^2$ | $^3F_2$ | 0 | 493,359 | $4d5p$ | $^3F^\circ_4$ | 155,033 | 338,326 |
| | $^3F_3$ | 1,585 | 491,774 | | $^3P^\circ_1$ | 156,616 | 336,743 |
| | $^3F_4$ | 3,359 | 490,000 | | $^3P^\circ_0$ | 157,060 | 336,299 |
| | $^3P_0$ | 11,165 | 482,194 | | $^3P^\circ_2$ | 157,852 | 335,507 |
| | $^3P_1$ | 11,812 | 481,547 | | | | |
| | $^3P_2$ | 13,413 | 479,946 | $4d5d$ | $^1D_2$ | 212,620 | 280,739 |
| | | | | | $^3D_3$ | 213,840 | 279,517 |
| $4d5s$ | $^1D_2$ | 83,971 | 409,388 | | $^3D_2$ | 214,671 | 278,688 |
| | $^3D_1$ | 92,381 | 400,978 | | $^3D_1$ | 214,786 | 278,571 |
| | $^3D_2$ | 93,113 | 400,246 | | $^1P_1$ | 215,874 | 277,485 |
| | $^3D_3$ | 94,837 | 398,522 | | $^3F_2$ | 236.714 | 256,645 |
| | | | | | $^3F_3$ | 239,071 | 254,288 |
| $4d5p$ | $^1F^\circ_3$ | 141,150 | 352,209 | | $^3F_4$ | 242,104 | 251,255 |
| | $^1P^\circ_1$ | 147,209 | 346,150 | | | | |
| | $^3D^\circ_1$ | 148,950 | 344,409 | $4d4f$ | $^3F^\circ_2$ | 231,724 | 261,635 |
| | $^3F^\circ_2$ | 150,346 | 343,013 | | $^3F^\circ_3$ | 234,886 | 258,473 |
| | $^3F^\circ_3$ | 151,196 | 342,163 | | $^3F^\circ_4$ | 241,112 | 252,247 |
| | $^3D^\circ_2$ | 151,212 | 342,147 | | $^3G^\circ_3$ | 243,665 | 249,694 |
| | $^1D^\circ_2$ | 151,760 | 341,599 | | $^3G^\circ_4$ | 244, 41 | 248,518 |
| | $^3D^\circ_3$ | 153,041 | 340,318 | | $^3G^\circ_5$ | 245,830 | 247,529 |

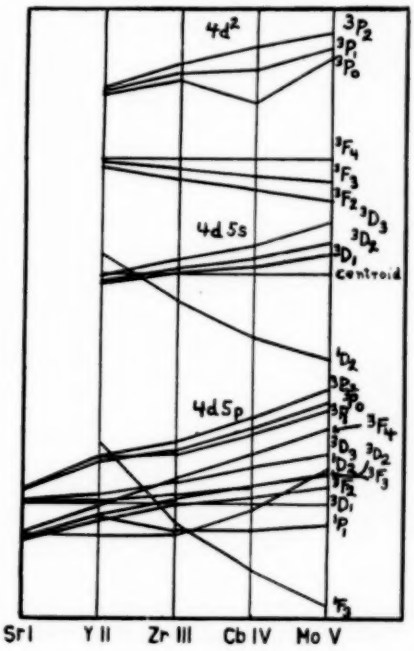


FIG. 3. Relative positions of terms in the configurations.

of $(4d^2\ ^3F_4/R)^{\frac{1}{2}}$, $(4d5s\ ^3D_3/R)^{\frac{1}{2}}$, and $(4d5p\ ^3F^\circ_4/R)^{\frac{1}{2}}$ gave the most consistent results and are the only ones shown in Fig. 2. The absolute term values estimated by this method and referred to $4d\ ^2D_{1\frac{1}{2}}$ of Mo VI along with the term values relative to $4d^2\ ^3F_2$, the lowest term actually found, are given in Table II.

Fig. 3 shows the terms of each configuration throughout the sequence plotted relative to one of the terms of that configuration or to the centroid of the configuration in the case in which all the terms of that configuration were found. The terms for Mo V seem to be related to each other and to the terms of the preceding elements in a manner to be expected, except for an apparent irregularity in the Cb IV $4d^2\ ^3P_{0,\ 1}$.

The writer wishes to thank Professor R. C. Gibbs for suggesting the problem and for giving much helpful advice in connection with the work. He is deeply indebted to Professor R. J. Lang for his kindness in supplying Professor Gibbs with his unpublished data on Cb IV which have been utilized in the composition of Figs. 1, 2 and 3.

# The Hyperfine Structure of the Mercury Triplet $6^3P_{012}-7^3S_1$ in Optical Excitation

EMILY E. BOGGS AND HAROLD W. WEBB, *Columbia University*

(Received May 31, 1935)

The relative intensities of the hyperfine structure components of λ5461, λ4358 and λ4047 in optically excited mercury vapor were computed by using the energy level scheme and intensity distribution calculated by Schüler and Keyston, with the assumption of complete absorption of λ2537 and slight absorption of λ4358. Since the excitation is in two steps, the ratio of the intensities of the components due to the less abundant isotopes to those due to the more abundant is much less than in the normal low pressure arc, in which the excitation of each isotope is proportional to its concentration These calculations were checked experimentally. Mercury vapor in a quartz resonance cell was excited optically by a low pressure mercury glow discharge in a helical quartz tube. This source was found to have the energy distribution predicted by Schüler and Keyston indicating small reversal. The hyperfine structure was photographed with a Lummer plate and the intensities determined from microphotometer records. The intensities from the optically excited vapor were found to agree within experimental error with the computed values.

VARIOUS experimenters[1] have observed that the lines of the sharp series triplet $6^3P_{012}-7^3S_1$ of mercury showed marked differences in the relative intensities of their hyperfine structure under different conditions of excitation. These differences were due in the most part to self-absorption in the radiating sources. E. Hobart Collins[2] investigated with a Lummer plate the relative intensities of the hyperfine structure when the triplet was excited optically[3] at low pressures by absorption of λ4358 following the absorption of λ2537. The mercury vapor in a quartz resonance tube was excited by light from water-cooled, magnetically deflected quartz mercury arcs. Conspicuous differences were observed between the radiation excited by electron impact and that excited optically. λ5461, which in the unreversed arc has 12 components, showed only one in the optical excitation. In λ4358 and λ4047 some but not all the components which appear in the arc were found in the optically excited radiation. Since the intensities were estimated by assuming that the blackening of the photographic plate was proportional to the intensity and no calibration marks or intensity standards were used, the results were only qualitative. In each case the central component was relatively much stronger than the other components. Later Mrozowski[4] found only the central component present in the optically excited radiation. Still more recently Pool and Simmons[5] in similar experiments found the relative intensity of the central component much enhanced in the optical excitation, although the other components were observed.

Very careful measurements of the wavelengths of these lines have been made by Nagaoka[6] and others.[7] Several attempts to explain the structure[8] were made but none were very satisfactory until Schüler and Keyston[9] in 1931 developed a system of energy levels for these hyperfine structures based upon the assignment of the components to the various isotopes of mercury. It was assumed that the even isotopes (196, 198, 200 and 204) had a nuclear moment $I=0$ and that the odd isotopes (199 and 201) had nuclear moments of $I=1/2$ and $I=3/2$, respectively. These assumptions, together with the sum rule of Burger and Dorgelo[10] and the data determined by Aston on the abundance of the various

[1] H. Luneland, Ann. d. Physik **34**, 505 (1911). (This article gives a résumé of work previous to this date.) H. Nagaoka, Proc. Tok. Math. Soc. [2] **8**, 229 (1915); J. L. Snoek, Zeits. f. Physik **35**, 883 (1926); R. Brunetti, Acad. Lincei. Atti, 496 (1923).

[2] E. H. Collins, Phys. Rev. **32**, 753 (1928).

[3] C. Füchtbauer, Physik. Zeits. **21**, 635 (1920); R. W. Wood, Phil. Mag. **50**, 775 (1925).

[4] S. Mrozowski, Zeits. f. Physik **78**, 826 (1932).

[5] M. L. Pool and S. J. Simmons, Phys. Rev. **44**, 744 (1933).

[6] H. Nagaoka, reference 1.

[7] L. Janicki, Ann. d. Physik **19**, 36 (1906); **39**, 439 (1912); J. C. McLennon and A. R. McLeod, Proc. Roy. Soc. **A90**, 243 (1914).

[8] H. Nagaoka, Proc. Tok. Math. Soc. [2] **5**, 1 (1909); Physik. Zeits. **10**, 609 (1909); J. C. McLennon and A. R. McLeod, reference 7.

[9] H. Schüler and J. Keyston, Zeits. f. Physik **72**, 423 (1931); H. Schüler and E. G. Jones, Zeits. f. Physik **74**, 631 (1932).

[10] H. C. Burger and H. B. Dorgelo, Zeits. f. Physik **23**, 258 (1924).

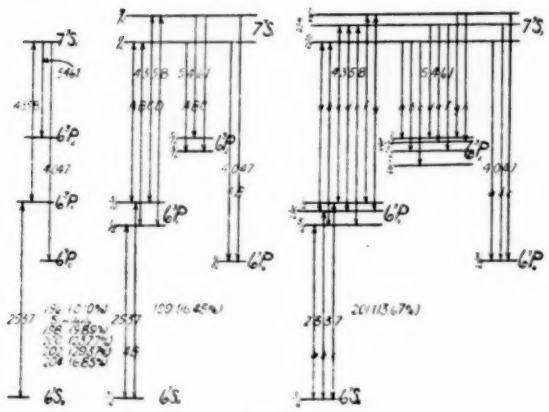

FIG. 1.

isotopes, enabled them to calculate the relative intensities of the hyperfine structure components of each of the lines as excited by electron impact, i.e., in an arc or glow discharge free from the effects of self-reversal. Observations made on a specially designed water-cooled mercury arc checked these observations quite satisfactorily. Fig. 1 shows the energy level system devised by Schüler and Keyston for λ2537 and the three lines of the triplet $6^3P_{012}-7^3S_1$. Since the hyperfine energy levels of all the even isotopes are single, the system of levels shown at the left represents any one of the even isotopes. Throughout this paper, the components arising from the even isotopes will be denoted by $X$, the isotope to which the particular component belongs being denoted by the subscript. The components arising from the isotope 199, as shown in the system of energy levels in the center of the diagram, will be denoted by upper case letters and those from isotope 201, shown on the right, by lower case letters. The figures in the parentheses beside the number designating the isotope give the abundance of the isotope as determined by Aston.

In the research described in this paper the intensity distribution of the hyperfine structure components of the lines of this triplet was measured under carefully controlled conditions of optical excitation and the results compared with those computed from the Schüler and Keyston scheme. The intensity distribution was also examined in an "unreversed arc" and found to agree with that predicted by Schüler and Keyston. By an unreversed arc is meant an arc or glow discharge in which the intensity distribution produced by electron impact is not appreciably altered by self-absorption.

In calculating the relative intensity distribution to be expected from optical excitation, we have, in general, to consider the absorption process as though we had seven distinct substances having different concentrations. For any substance the total excitation by electron impact depends upon its concentration and upon the excitation probability. Since the latter is the same for each isotope, we find for this type of excitation, under conditions for which there is no self-absorption, that the total radiation from each isotope is proportional to its relative abundance, $N$. With optical excitation, on the other hand, since this results in the case of the triplet under consideration from two-step absorption, the problem is quite different. In at least one of the steps the absorption is small so that it depends in amount upon the number of absorbing atoms $n$, the intensity of the impressed radiation $I$ and the atomic absorption coefficient $B$, being approximately equal to $nIB$.

Now $n$ for a resonance line, such as λ2537, depends directly upon the abundance of the isotope and $I$ depends upon the same, if an unreversed arc is the exciting source. In the case of the even isotopes, which have only a single component in each line, for very weak absorption the relative absorption for λ2537 by any two of these would be in the ratio of the squares of their abundances. If now these isotopes absorb λ4358 from the same source and this absorption is also weak, since $n$ is now proportional to $N^2$ we would have the relative number of atoms optically excited to the $7^3S_1$ level in these two even isotopes proportional to $N^3$. If, however, the first step in the excitation, i.e., the absorption of λ2537 is very large, the relative amount of excitation of these isotopes would be proportional to the relative values of $I$ from the two isotopes, so that the relative values of the final excitation to the $7^3S_1$ level and the subsequent emission of the triplet would be proportional to $N^2$, as in the case of a single step. This illustration assumes that the absorption lines of the isotopes in question do not overlap, that is, one isotope can not absorb the radiation of the other.

TABLE I. *Absorption of λ2537.*

| ISOTOPE 1 | N 2 | COMPONENT 3 | I 4 | UPPER LEVEL 5 |
|---|---|---|---|---|
| 201 | 13.67 | *a* | 6.84 | 5/2 |
| | | *b* | 4.56 | 3/2 |
| | | *c* | 2.28 | 1/2 |
| 199 | 16.45 | *A* | 5.48 | 1/2 |
| | | *B* | 10.96 | 3/2 |
| 196 | .10 | $X_{196}$ | .10 | 1 |
| 198 | 9.89 | $X_{198}$ | 9.89 | 1 |
| 200 | 23.77 | $X_{200}$ | 23.77 | 1 |
| 202 | 29.27 | $X_{202}$ | 29.27 | 1 |
| 204 | 6.85 | $X_{204}$ | 6.85 | 1 |

TABLE II. *Absorption of λ4358.*

| COMPONENT 1 | LOWER LEVEL ($f_1$) 2 | I 3 | $\frac{I}{N}$ 4 | $\frac{A}{A_e}$ 5 | k'B 6 | n IN LOWER LEVEL 7 | I ABSORBED 8 | UPPER LEVEL ($f_2$) 9 | n IN UPPER LEVEL 10 |
|---|---|---|---|---|---|---|---|---|---|
| *a* | 3/2 | 2.05 | .15 | .30 | .45 | 4.56 | 4.21 | 5/2 | 27.14 |
| *b* | 5/2 | 4.79 | .35 | .70 | .70 | 6.84 | 22.93 | 5/2 | |
| *c* | 1/2 | 1.90 | .14 | .42 | .83 | 2.28 | 3.61 | 3/2 | 8.19 |
| *d* | 3/2 | .61 | .04 | .13 | .13 | 4.56 | .37 | 3/2 | |
| *e* | 5/2 | 2.05 | .15 | .45 | .30 | 6.84 | 4.21 | 3/2 | |
| *f* | 1/2 | .38 | .03 | .17 | .17 | 2.28 | .14 | 1/2 | 3.78 |
| *g* | 3/2 | 1.90 | .14 | .84 | .42 | 4.56 | 3.64 | 1/2 | |
| *A* | 3/2 | 1.83 | .11 | .33 | .17 | 10.96 | 3.35 | 1/2 | 16.73 |
| *B* | 1/2 | 3.66 | .22 | .67 | .67 | 5.48 | 13.38 | 1/2 | |
| *C* | 3/2 | 9.15 | .56 | .84 | .84 | 10.96 | 83.70 | 3/2 | 87.04 |
| *D* | 1/2 | 1.83 | .11 | .17 | .33 | 5.48 | 3.34 | 3/2 | |
| $X_{196}$ | 1 | .10 | 1 | 1 | 1 | .10 | .01 | 1 | .01 |
| $X_{198}$ | 1 | 9.89 | 1 | 1 | 1 | 9.89 | 97.81 | 1 | 97.81 |
| $X_{200}$ | 1 | 23.77 | 1 | 1 | 1 | 23.77 | 565.01 | 1 | 565.01 |
| $X_{202}$ | 1 | 29.27 | 1 | 1 | 1 | 29.27 | 856.73 | 1 | 856.73 |
| $X_{204}$ | 1 | 6.85 | 1 | 1 | 1 | 6.85 | 46.92 | 1 | 46.92 |

In the case of two odd isotopes the calculation is, however, more complex since each of these lines is made up of several components. The calculations for one of these isotopes, 199, will be considered in detail below. Those for the other are omitted for lack of space.

In making the following calculations it is assumed that all the components of λ2537 are completely absorbed, an assumption which corresponds well with the experimental conditions of these tests. The radiation from the exciting source used is further taken as unreversed, that is, as having the energy distribution given by Schüler and Keyston. The details of the computation are shown in Table I for the absorption of λ2537. Column 1 shows the various isotopes of mercury and column 2 the abundance of each isotope as given by Aston: column 3 lists the components of λ2537, column 4 the intensity of each component according to Schüler and Keyston and column 5 the quantum number $f$ of the upper hyperfine energy levels of each component. Since λ2537 is taken as completely absorbed the concentration $n$ of atoms excited by absorption to the $6^3P_1$ state in all the isotopes will have the same relative values as the corresponding emission lines in the source, that is $n=kN$, where $k$ is a constant of proportionality. Table II shows the details of the computation for the subsequent absorption of λ4358. It is assumed that the components of λ4358 are only slightly absorbed, the absorption and therefore the contribution of each component to the number of excited atoms in the upper level being given by $BIn$. Column 1 shows the components of λ4358, column 2 the hyperfine quantum numbers $f_1$ for the lower levels, column 9 gives the corresponding values $f_2$ for the upper levels, column 3 the intensities of the lines according to Schüler and Keyston and column 4 $I/N$. In column 5 are the values of the Einstein atomic emission coefficients, $A$ divided by a constant $A_e$, the value of the coefficient for the components from the even isotopes. These values of $A$ were obtained from the relationship $A=(I/\Sigma I)A_e$, where the summation is over all the components originating at the upper level in question. In column 6 are the atomic absorption coefficients $B$, multiplied by a convenient constant $k'$ obtained by the relationship $B=\text{const.}\,(p_2/p_1)A$, where $p_2=2f_2+1$ and $p_1=2f_1+1$. Column 7 gives the relative concentrations $n$ of electrons in the lower level for each component of λ4358, resulting from the absorption of λ2537. For example, the absorption of component $C$ of λ4358 in isotope 199 is $nIB=0.84\times9.15\times10.96$, since it arises from the 3/2 hyperfine level of the $6^3P_1$ state. Again, the absorption of component $D$ of λ4358 is given by $0.33\times1.83\times5.48$ since it arises from the 1/2 level of the $6^3P_1$ state. These products are recorded in column 8. Both of these absorption processes result in excited atoms in the 3/2 level of the $7^3S_1$ state so that the sum, 87.04, of the quantities absorbed gives a measure of the optical excitation of this level. Similarly, absorption of $A$ and $B$ results in the excitation of the 1/2 level of the $7^3S_1$ state of isotope 199, the calculated value of which is 16.73. (See column 10.)

The optical excitation of the 5/2, 3/2 and 1/2 levels of the $7^3S_1$ state of isotope 201 was computed in a similar manner, the process being more complex since for this isotope there are

three hyperfine lower levels ($6^3P_1$) and three hyperfine upper levels ($7^3S_1$) for λ4358. The calculations for the even isotopes follow the same scheme except that all the levels are single and, therefore, each level is filled by absorption of only one component. The excitation of each upper level (column 9) for all the isotopes is given in column 10.

From the computed concentrations of atoms excited to the various levels of the $7^3S_1$ state of the various isotopes and the previously calculated values of the emission coefficients ($A$), the relative intensities of the hyperfine structure components for the optical excitation of each of the lines of the triplet are found. These calculated values, expressed as percentages of the total radiation from all the isotopes for each line of the triplet, are given in Table III column 7 for λ5461, in Table IV column 7 for λ4358, and in Table V column 7 for λ4047.

The above calculations were made on the assumption that each component was absorbed separately, i.e., that the wavelengths of no two components were so close that there was appreciable overlapping of their line structure and a consequent mutual absorption. Since, however, there are extremely small differences between the recorded wavelengths of several components, the effect of this overlapping was considered. An outstanding example of such groups of components is $a$, $A$ and $X_{204}$ in λ2537; in λ4358 all the components emitted by the even isotopes form such a group. The above calculations were repeated assuming that such components overlapped completely, that is, that the wavelengths were exactly the same. The results gave the same general type of distribution of the intensities but did not agree as well with the experimental results as the simpler calculation, indicating that the effect of mutual absorption due to overlapping was small.

Calculations were also made neglecting overlapping and assuming that there was small absorption of λ2537 followed by a small absorption of λ4358. As pointed out above, the absorption of λ2537 would then be similar to that of λ4358 and there would be a still greater difference between the intensities of the components from the more abundant and less abundant isotopes. The results given by these calculations

TABLE III. *Hyperfine structure of λ5461.*

| Isotope 1 | Upper level 2 | Component 3 | $d\nu$ (cm$^{-1}$) 4 | Unreversed Arc Calc. 5 | Unreversed Arc Expt. 6 | Optical Excitation Calc. 7 | Optical Excitation Expt. 8 |
|---|---|---|---|---|---|---|---|
| 201 | 5/2 | *a* | −0.728 | 0.14 | * | 0.03 | * |
| | | *b* | −.431 | 1.23 | 1.3 | .29 | 0.32 |
| | | *c* | 0 | 5.44 | 5.4† | 1.27 | 1.27† |
| | 3/2 | *d* | −.247 | .23 | .23‡ | .024 | .026‡ |
| | | *e* | 0 | 1.46 | 1.5† | .16 | .16† |
| | | *f* | +.232 | 2.87 | 3.1 | .30 | .37 |
| | 1/2 | *g* | +.158 | 1.14 | 1.2 | .11 | .12 |
| | | *h* | +.342 | 1.14 | 1.2 | .11 | .11 |
| 199 | 1/2 | *A* | −.278 | 5.50 | 5.4‡ | .98 | 1.04‡ |
| | 3/2 | *B* | 0 | 9.88 | 9.9† | 4.60 | 4.60† |
| | | *C* | +.790 | 1.10 | 1.1 | .51 | .51 |
| 196 198 200 202 204 | | *Central* ($X$'s) | 0 | 69.88 | 69.75† | 91.62 | 91.64† |

* Component *a* was not observed because of its low intensity and unfavorable overlapping of orders.

† A procedure similar to that described in the previous note was followed for components *B*, *c*, *e* and the *X*'s, which are completely merged.

‡ *A* and *d* are not well resolved and *d* is very small. They were treated as one in measurement and in the table given the relative proportions determined by the calculated values.

TABLE IV. *Hyperfine structure of λ4358.*

| Isotope 1 | Upper level 2 | Component 3 | $d\nu$ (cm$^{-1}$) 4 | Unreversed Arc Calc. 5 | Unreversed Arc Expt. 6 | Optical Excitation Calc. 7 | Optical Excitation Expt. 8 |
|---|---|---|---|---|---|---|---|
| 201 | 5/2 | *a* | −0.555 | 2.05 | 2.4 | 0.48 | 0.47 |
| | | *b* | −.099 | 4.79 | 4.9 | 1.10 | 1.04 |
| | 3/2 | *c* | −.164 | 1.90 | 2.0 | .20 | .25 |
| | | *d* | +.106 | .61 | .62* | .064 | .064* |
| | | *e* | +.556 | 2.05 | 2.0 | .22 | .25 |
| | 1/2 | *f* | +.245 | .32 | .32 | .037 | .036 |
| | | *g* | +.505 | 1.90 | 2.0 | .18 | .25 |
| 199 | 1/2 | *A* | −.960 | 1.83 | 1.8† | .32 | .32† |
| | | *B* | −.240 | 3.66 | 4.0 | .65 | .53 |
| | 3/2 | *C* | +.106 | 9.15 | 9.3* | 4.25 | 3.91* |
| | | *D* | +.836 | 1.83 | 1.8† | .85 | .85† |
| 196 198 200 202 204 | | *Central* ($X$'s) | 0 | 69.88 | 68.9† | 91.62 | 92.04† |

* *C* and *d* are not well resolved. A procedure similar to that described in the previous note was followed in obtaining their separate values.

† *A* and *D* were merged with the central components of adjacent orders and, therefore, could not be isolated. *A* and *D* together with the central components constitute 93.18 percent of all the components and in the table this total is divided among them according to the ratios determined by the theoretical values.

TABLE V. *Hyperfine structure of λ4047.*

| Isotope 1 | Upper level 2 | Component 3 | $d\nu$ (cm$^{-1}$) 4 | Unreversed Arc Calc. 5 | Unreversed Arc Expt. 6 | Optical Excitation Calc. 7 | Optical Excitation Expt. 8 |
|---|---|---|---|---|---|---|---|
| 201 | 5/2 | *a* | −0.394 | 6.84 | 6.3 | 1.59 | 1.69 |
| | 3/2 | *b* | +.270 | 4.56 | 4.2 | .48 | .54 |
| | 1/2 | *c* | +.668 | 2.28 | 2.1 | .22 | .27 |
| 199 | 1/2 | *A* | −.743 | 5.48 | 5.0 | .98 | 1.10 |
| | 3/2 | *B* | +.330 | 10.96 | 10.0 | 5.11 | 5.18 |
| 196 198 200 202 204 | | *Central* ($X$'s) | 0 | 69.88 | 72.6 | 91.62 | 91.22 |

are very far from agreement with the experimental results and are interesting only because they justify the previously assumed conditions of absorption.

## Experimental

The resonance cell used was a straight quartz tube terminating in a curved horn. The straight portion was 20 cm long and 2.5 cm in diameter, the end toward the spectrograph being closed by a clear, polished, plane quartz window. The cell was connected to a mercury diffusion pump operating continuously during exposures. A small quantity of mercury was always present in the connecting tube which was kept at approximately 25°C giving a vapor pressure in the cell of 0.00184 mm of mercury. The exciting source was a quartz glow tube about 12 mm in diameter and 50 cm long. The electrodes of this tube were large hollow cylinders of aluminum. It was operated with a current of 100 milliamperes from a 3000 volt transformer. At this current the tube did not become very hot even after prolonged running; consequently the vapor pressure in the glow tube was low and the emitted line λ2537 was narrow and easily absorbed. This type of glow tube emits relatively little of the other lines, as for example λ4358. To increase the efficiency it was made in the form of a spiral of four turns, covering about 5.5 cm of the middle of the straight part of the resonance cell which was placed inside it with a clearance of 2 mm. To increase the amount of light available for excitation a thin cylindrical reflector was wrapped around the quartz spiral. Since ozone absorbs λ2537, strongly decreasing optical excitation, nitrogen was circulated continuously in the space between the resonance cell and the spiral during exposures. The results of observations on this tube given in columns 5 of Tables III, IV and V, showed that the hyperfine structure of the lines of the triplet emitted from this tube had very nearly the relative intensity distribution predicted by Schüler and Keyston for the intensities of lines excited by electron impact, justifying this assumption made in the above calculations.

Since the amount of λ4358 furnished by the glow tube was comparatively small, when measuring the hyperfine structure of λ5461 the radiation from the glow tube was supplemented by that from a pair of U-shaped, 5-ampere glass arcs which were placed around the quartz spiral after removing the reflector. To keep the arcs cool and prevent self-absorption, these arcs were made with large mercury pool electrodes and cooled by a draft of air from an electric fan. Measurements showed that these glass arcs provided less than half the λ4358 available for optical excitation. The energy distribution in the glass arcs varied slightly from the Schüler and Keyston distribution, so that some slight divergences from the calculated values of the relative intensities in the optical excitation of λ5461 may be attributed to this fact. To avoid complications these arcs were not used when measuring the optical excitation of λ4358 and λ4047.

The measurement of the hyperfine structure of the lines was made by means of a glass Lummer plate 4.64 mm thick and 12.0 cm long mounted between the collimating lens and the prism of a glass spectrograph. In order to avoid blurring the pattern the temperature of the Lummer plate and spectrograph was kept constant to better than 0.01°C during the exposures by lagging the spectrograph with layers of felt and by enclosing the entire spectrograph except for the slit in an asbestos walled enclosure in which the temperature was controlled thermostatically to 0.01°C. During the summer cold water from a tank kept at a constant temperature by an electric refrigerator was pumped through the coils inside the enclosure. During cooler weather the temperature of the room was thermostatically controlled at a temperature somewhat lower than that of the enclosure. In order to prevent vibration, all fan and pump motors connected with the temperature control system were run as slowly as possible and the supports for the moving apparatus, the spectrograph and the table upon which it rested were insulated with sponge rubber.

The lengths of exposure were from 5 minutes, when studying the structure from the glow tube, to 55 hours when studying the optical excitation. Eastman type G IV plates were used for λ5461 and Eastman 33 plates for λ4358 and λ4047. A fine grain developer was employed. Calibration marks were put on each photographic plate by

exposing it for a time equal to that used for the Lummer plate pattern in a second spectrograph on the slit of which was focused the image of a calibrated platinum step wedge. The wedge was illuminated with light from a glass mercury arc, the intensity of this source being varied as necessary by placing colored celluloid filters before the arc. The density measurements were made from records taken by a Moll microphotometer. By means of the records and the calibration data, intensity-wavelength curves of the hyperfine structure patterns were constructed.

In each order on each plate used for calculation the shape of a typical component was determined from that of a strong well-resolved component. When it was possible, this component was selected from the exposure under consideration. If the exposure under examination was too weak or too strong to enable the shape of some well-resolved component to be determined accurately, a second exposure of suitable density was made on the same plate with the same exposure time to provide a suitable shape curve. Since the position of each component was accurately known, it was possible to build up a synthetic intensity distribution curve, adjusting the magnitudes of the curves for each separate component until the best fit with the experimental intensity curve was obtained. The area under each component curve, measured with a planimeter, was taken as proportional to the intensity of that component.

An estimate of the precision of such determinations was made by altering the intensity curve for any one component by a specific amount and readjusting the other components to obtain the best fit for the experimental curve. The estimated precision of the determination is of the order of 10 percent for strong moderately well-resolved components and 20 percent for weaker less well-resolved components. Since an exposure which gave the weak components a density suitable for measurement produced overexposure of the strong ones, it was found best to determine the relative intensities of the very strong and very weak ones by first determining their intensities relative to that of a component of intermediate intensity by using several exposures. For example, component $A$ in λ5461 had a convenient intermediate intensity and was used as a reference component for that line. In the measurements of λ5461 the comparison of strong and weak components was expedited by use of a silvered filter of known transmission. A thin layer of silver was chemically deposited on a cover glass, one-half of which was then wiped clear leaving a sharp edge. This filter was placed against the slit face with the edge of the silvering in the center of the slit and parallel to its edges. In this manner two Lummer plate spectra of different densities and the same exposure time were taken together. Knowing the relative amounts of light transmitted by the clear and by the silvered glass, comparisons could be made between the weak components in the dense spectrum and the strong components in the less dense spectrum, with the same calibration marks.

In these measurements there was no appreciable error due to the scattered light. To decrease the amount of light reflected from the sides of the absorption cell, the entire cell was blackened except for the space covered by the exciting quartz spiral and a small portion of the window at the end where the light passed out to the spectrograph, the slit of which was about 5 cm from the window. To test for scattered light, a soft glass tube which eliminated the optical excitation by cutting out λ2537, was slipped between the resonance cell and the exciting quartz spiral. When this tube was in position, exposures made with the glow tube running showed no detectable blackening of the photographic plate for exposure times equal to those used for photographing the optical excitation.

## Results

The results of the calculations and the corresponding measurements are summarized in Tables III, IV and V for the lines λ5461, λ4358 and λ4047. In each of these tables, in column 3 are listed the components due to the isotopes listed in column 1. Column 2 gives the $f$ number of the corresponding hyperfine $7^3S_1$ level, the upper level of the transitions involved; column 4, the wave number separation of each component from the main component; column 5, the calculated distribution of intensity among the components for an unreversed arc according to the

Schüler and Keyston scheme; and column 6, the corresponding experimentally determined values from the quartz glow tube used in these experiments. Column 7 gives the calculated values for the optical excitation under the conditions assumed above and column 8 the values experimentally determined. It should be noted that for each line the intensities are expressed as percentages of the total radiation of this line including all the components.

A comparison of columns 5 and 6 shows that the energy distribution in the exciting source is sufficiently close to that given by Schüler and Keyston to justify the use of their intensity distribution in the computation of the intensities in the optical excitation. All the values check within 10 percent except for component *a* in λ4358 which is 2.05 as given by Schüler and Keyston and 2.4 as measured here.

That the optical excitation observed agrees well with that calculated is seen from a comparison of columns 7 and 8. The differences except in the case of *f* in λ5461; *c*, *e*, *g* and *B* in λ4358; and *b* and *c* in λ4047 are within 10 percent. In λ4358 these components are so situated in the pattern and of such a size as to make their measurement somewhat less precise than the measurement of the other components. As for the components *b* and *c* of λ4047, it may be noted that the measured values of the components due to isotope 201 are a little high in all three lines. These components, however, are the weakest and are less easily measured, partly due to the difficulty of estimating the continuous background in the Lummer plate spectrum.

The results for λ5461 should be somewhat more reliable than those for either λ4358 or λ4047. A larger number of measurements on more exposures were made for this line than for the other two and therefore a somewhat greater precision was obtained. The measurement of λ4358 was also complicated by the overlapping of orders and the fact that many of the components of this line are of approximately the same intensity and unfavorably grouped in the structure.

It should be noted that the components of the even isotopes of λ5461 are combined in the actual measurement with component *B* from isotope 199 and components *c* and *e* from 201, as these are practically identical in wavelength and, therefore, not separable. The values listed in the table were obtained from the total measured intensity of the central component which was divided in the proportions given by the calculations.

The experimental results verify the interesting conclusion derived from the calculations that the central component is remarkably enhanced as compared with the other components, due to the fact that the sum of the concentrations of the even isotopes which account for the major part of the central component is so much larger than the concentration of the odd isotopes which account for the other components; this increase is from approximately 70 percent of the total radiation in the case of the unreversed arc to approximately 91.5 percent in the case of optical excitation. For short exposures only the central component appears in the optical excitation which probably accounts for the failure of Mrozowski and other earlier experimenters to observe the weaker lines. The intensities found by Collins for those of the weaker lines which he observed are not checked in this work. The enhancement of the central component in the optical excitation was observed by Pool and Simmons who found in λ4047 the ratios of the intensities of components *A*, *a* and *B*+*b* to that of the central component in the optical excitation when divided by the corresponding ratios for the arc to be 2.9, 2.8 and 2.9, respectively; for the same components, this research gives 5.7, 4.6 and 3.1, respectively. These differences might arise from slight differences in the intensities in the exciting light.

The close agreement between the calculated and the measured values of the intensities of the components of these lines in the optical excitation and a comparison of these with measurements on the radiation from the unreversed arc gives an independent check on the correctness of the Schüler and Keyston scheme. Since the relative decrease in the intensities in the former type of spectra with respect to the latter depends both upon the isotope concentration and upon the multiplicities of the levels in each isotope, a comparison of the two types of spectra is in most cases sufficient to determine definitely which components belong to each of the isotopes and to which hyperfine structure level each should be attributed.

# Hyperfine Structure in Silver

HARRY HILL, *Ryerson Physical Laboratory, University of Chicago*

(Received May 31, 1935)

Twenty lines in the visible spectrum, λ7688 in the infrared, and the two resonance lines λ3383 and λ3281 were studied by means of a hollow cathode source and Fabry-Perot interferometers. All lines in the visible were found to be simple in agreement with the findings of other investigators. λ7688 was found to be a very broad line and lines λ3383 and λ3281 were each found to be double with the weaker component on the longer wavelength side. Photographic plates measured gave an average of 0.055 $cm^{-1}$ for the separation in λ3383 and 0.056 $cm^{-1}$ in λ3281. It is concluded that the doubling of these lines is due to a splitting of the 5*S* level because of nuclear spin which is probably 3/2.

SEVERAL attempts have been made recently to find hyperfine structure in the spectrum of silver. Frisch,[1] using a Schüler hollow cathode source and the fourth order of a large concave grating, found no indication of hyperfine structure in the resonance lines. Shenstone[2] stated that silver shows no hyperfine structure. Mohammad and Sharma[3] used the Mohammad vacuum tube source with a Wehnelt oxy-cathode of platinum and an anode of silver. They used thermionic currents of from 1.5 to 2.5 amperes thinking that it was necessary to melt the silver. By means of a Lummer-Gehrke plate, they studied eighteen lines of the silver spectrum, and found all of them simple except the resonance lines. In each of these they got three components, two about equally intense and a third, on the short wavelength side, much weaker. They believed the 5*S* level of silver to be a triplet with term separations of 0.218 $cm^{-1}$ and 0.166 $cm^{-1}$.

Williams and Middleton[4] used a liquid-air cooled hollow cathode source and a reflection echelon. In order to avoid the reversal that was supposed to have given the two intense components in the results of Mohammad and Sharma, their hollow cathode was made of 95 percent cadmium and 5 percent silver. Jackson's[5] source consisted of silver chloride in the capillary portion of a fused silica tube containing neon at a pressure of 0.5 mm Hg. He also used a reflection echelon. After calculating line widths he concluded that any separation in the resonance lines must be less than 0.07 $cm^{-1}$ and that any separation in the other lines must be less than 0.04 $cm^{-1}$. Tolansky[6] used a water-cooled hollow cathode with fairly low currents and a silvered Fabry-Perot interferometer to study lines in the visible and infrared parts of the silver spectrum. He used interferometer spacings up to 25 mm and found all the lines studied to be simple, however, he mentioned in a note in his paper that λ7688 was broadened and that a narrow doubling due to the term $6s^2S_{\frac{1}{2}}$ was suspected. He believed Williams' plates to show that any doubling in the resonance lines is less than 0.05 $cm^{-1}$.

Before the papers mentioned in the preceding paragraph were published work was started on the spectrum of silver at Ryerson Laboratory. This was continued in order to see if sufficient resolution could be obtained to detect any structure in the 5*S*, 6*S* or possibly the *P* terms. The first source used was a simple uncooled graphite hollow cathode 8 cm long and 1.5 cm in diameter, in helium at a pressure of 3 mm Hg with current supplied by a 2000-volt d.c. generator. A small amount of metallic silver was placed inside the cathode. Exposures were made from the first to the fifth orders inclusive in the visible and near ultraviolet, on a 21-foot grating with 15,000 rulings to the inch. Currents first used were of the order of one ampere. All lines studied appeared to be simple except the resonance lines which showed reversals faintly on third order plates and quite strongly on plates of the fifth order. Another set of exposures made with the current reduced to 0.5 ampere showed no reversals and no structure in the fifth order. Eastman Process plates were used for exposures to the resonance lines.

[1] R. Frisch, Zeits. f. Physik **71**, 89 (1931).
[2] A. G. Shenstone, Phys. Rev. **37**, 1023 (1931).
[3] W. Mohammad and C. Sharma, Ind. J. Phys. **6**, 75 (1931 and 1932).
[4] W. E. Williams and A. Middleton, Nature **131**, 692 (1933).
[5] D. A. Jackson, Nature **131**, 691 (1933).
[6] S. Tolansky, Proc. Phys. Soc. London **45**, 559 (1933).

Later a larger water-cooled hollow cathode was substituted for the uncooled one. This consisted of a very thin graphite tube inserted tightly inside a thick-walled, cylindrical aluminum block that was cooled by water flowing through copper tubing around it. The anode was a nickel cylinder three inches long and one inch in diameter. The cathode was placed at the center of a three-liter flask and the anode in a side tube sealed on to the flask. The helium used was purified by allowing it to flow slowly through a charcoal trap in liquid nitrogen into a reservoir on the apparatus. Then what was used in the discharge tube was circulated through another flask where magnesium was vaporized by a heating coil. A large Fabry-Perot interferometer with silver surfaces on glass constituted the dispersive apparatus and this was mounted between the collimator and prism of a large aperture prism spectrograph.

Exposures were made with interferometer plate separations ranging from 3.5 mm to 45 mm, with currents of 1 ampere, 0.7 ampere and 0.46 ampere. Twenty lines in the visible spectrum and one in the infrared were studied. These involved terms up to $8s^2S_{\frac{1}{2}}$, $5p^2P_{1\frac{1}{2}}$, and $7d^2D_{2\frac{1}{2}}$. No structures were found.

The green lines λ5209 ($5p^2P_{\frac{1}{2}}-5d^2D_{1\frac{1}{2}}$), λ5465 ($5p^2P_{1\frac{1}{2}}-5d^2D_{2\frac{1}{2}}$), and λ5471 ($5p^2P_{1\frac{1}{2}}-5d^2D_{1\frac{1}{2}}$) were studied very carefully. The most satisfactory exposures were obtained with an interferometer separation of 25 mm and a current of 0.46 ampere, but there was no indication of structure on the plates. Microphotometer traces were made of λ5209 and λ5465. The peaks in these traces were very symmetrical and showed no indications of structure. Hence it was to be concluded that if there is any structure in the $P$ terms the line component separations due to it are entirely unresolved with the apparatus used. Number VI in Fig. 1 is an example of a trace of λ5465. Ilford Soft Gradation Panchromatic plates were used for photographing these lines.

Many exposures were made of λ7688 ($5p^2P_{\frac{1}{2}}-6s^2S_{\frac{1}{2}}$) at the currents given above with an interferometer separation of 25 mm in an attempt to show whether or not the broadening of this line is due to a doubling. Only the broadening mentioned in the note of Tolansky's[6] paper was observed. Eastman type N plates were used in the study of this line.

Preliminary work on the resonance lines was reported in a letter to *The Physical Review*.[7] The same water-cooled hollow cathode source already described was used in the study of these lines but it was found that very low currents had to be used on account of self-reversals. The silver surfaced glass interferometer was replaced by one with quartz plates coated with aluminum by the evaporation process. This quartz-aluminum etalon was used with a Zeiss spectrograph having quartz lenses and a quartz prism which gave very good dispersion in the region of the resonance lines of silver. These lines were separated by approximately 1.5 millimeters on the

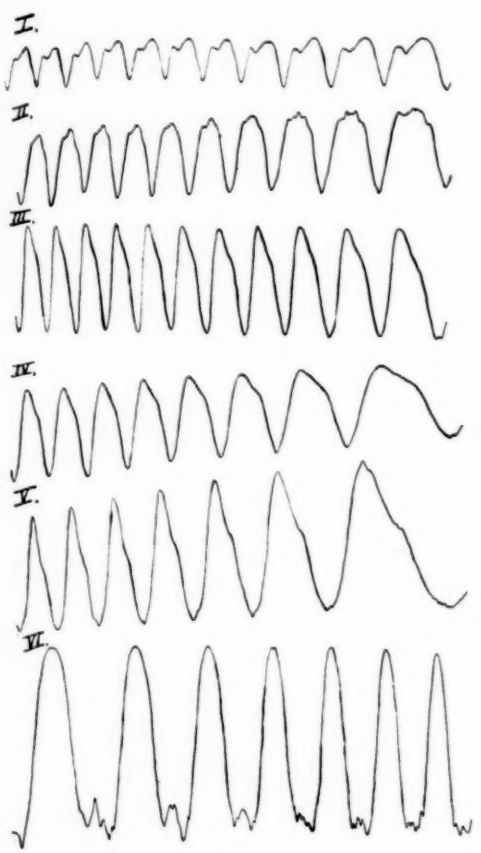


FIG. 1. Microphotometer traces of fringe systems. I, λ3383 at 0.34 ampere, showing reversal. II, λ3383 at 0.17 ampere, showing both the reversal and the hfs components. III and IV, λ3383 at 0.1 ampere but each from a different series of exposures. V, λ3281 at 0.05 ampere. VI, λ5465 at 0.46 ampere, with λ5471 showing faintly between the peaks of λ5465.

[7] H. Hill, Phys. Rev. **46**, 536 (1934).

plates. Etalon separators used were 32.5 mm, 26 mm, 23 mm (more accurately 22.965), 15 mm and 10 mm.

The first complete series of exposures was described in the letter referred to above. This series was made with the 23 mm spacer as the current was changed by small steps from 0.7 ampere to 0.05 ampere. At 0.7 ampere both lines are much reversed and the wing of the reversal on the longer wavelength side of each line is broader and more intense than the wing on the shorter wavelength side. The wings of the reversal of λ3281 ($5s^2S_{\frac{1}{2}}-5p^2P_{1\frac{1}{2}}$) are much farther apart than those of λ3383 ($5s^2S_{\frac{1}{2}}-5p^2P_{\frac{1}{2}}$) at the same current, as might be explained by the larger $J$ value of the $P$ term of λ3281, and the wing on the shorter wavelength side in one order is very near the wing on the longer wavelength side of the next lower order in the interferometer pattern.

At 0.34 ampere the reversal of λ3383 is much reduced and a hyperfine structure component begins to show on the longer wavelength side of the line. This reversal is shown by microphotometer trace I in Fig. 1. Trace II shows that the reversal has practically disappeared at 0.17 ampere and the component on the longer wavelength side is definitely visible on the original plate. Trace III was made from an exposure at 0.1 ampere, and trace IV from another at about the same current in a later series. Traces III and IV show broadening but no sign of reversal. These and other series of exposures show quite definitely that the weaker component on the longer wavelength side of each fringe appears as the reversal disappears. It is not possible to confuse the weaker component with the weaker wing of the reversal since they appear on opposite sides of the fringes. The presence of the weaker component is probably the cause of the great lack of symmetry in the reversal. After the preliminary results were reported by letter, many other exposures were made with different currents and different helium pressures. Best results were always obtained with the 23 mm separator.

At 0.34 ampere λ3281 has about the same appearance as λ3383 at 0.7 ampere. At 0.17 ampere it is about the same as λ3383 at 0.34 ampere. At 0.1 ampere it is comparable to

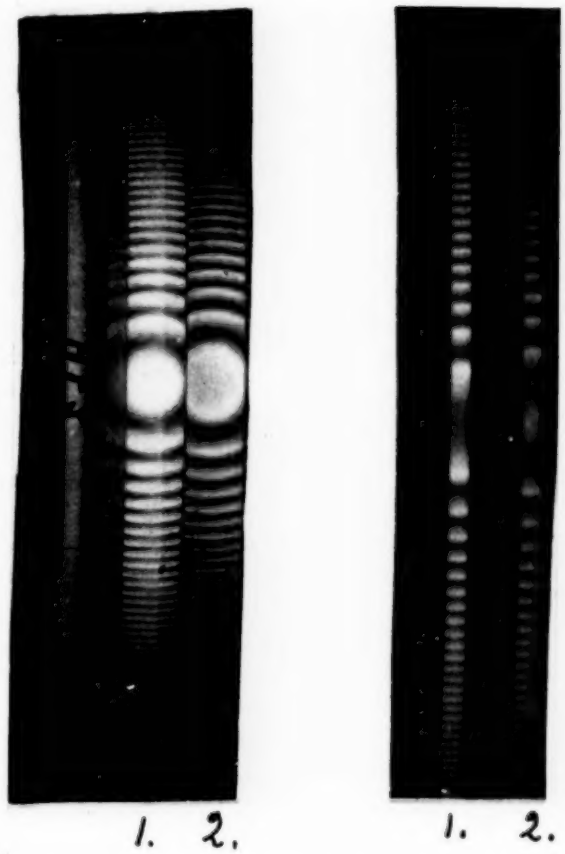


FIG. 2. 1. shows HFS of λ3281. 2. shows HFS of λ3383.

λ3383 at 0.17 ampere. Microphotometer trace V of λ3281 was made from a plate of a later series exposed at a current of 0.05 ampere. The component is shown in approximately the same manner as that shown by λ3383 exposed at a current of 0.1 ampere or lower. The intensity at this current is naturally quite low.

The reversals did not disappear at the same currents when the helium pressure was changed. In one current-series of exposures when the pressure was reduced to about half of that used at first, one wing of the reversal of λ3281 overlapped the other wing in the next lower order and the appearance was that of an unreversed line. Good reversals of both lines were obtained at 0.25 ampere, and that of λ3281 persisted down to a current of approximately 0.1 ampere, however, it was not determined in this case whether or not the cooling of the cathode was the same as it had been in the first series of

TABLE I. *Line component separations.*

| λ3383 | λ3281 |
|---|---|
| 0.053 $cm^{-1}$ | 0.057 $cm^{-1}$ |
| 0.056 | 0.055 |
| 0.056 | 0.053 |
| 0.057 | 0.058 |
| 0.052 | 0.056 |
| 0.052 | |
| 0.054 | 0.056 $cm^{-1}$ Average. |
| 0.053 | |
| 0.058 | |
| 0.055 $cm^{-1}$ Average. | |

exposures described. The time of exposures ranged from 20 minutes to four hours.

For the preliminary results comparator measurements were made of four different plates of λ3383 and two different ones of λ3281. Later measurements were made of nine additional plates of λ3383 and five of λ3281, and separations calculated according to the methods outlined by Tolansky[8] and Ritschl.[9] These measurements which were made more carefully than the first gave values somewhat lower than the approximate values given in the letter. The maximum number of orders measured on any one plate was 35 and the minimum number 12. Table I shows these data.

Finally another series of exposures was run repeating results obtained with the different etalon spacers available. The two components were observed with the 32.5 mm and the 26 mm spacers but these spacers were not very stable and no good exposures were obtained. Good exposures were obtained with the 15 mm and the 10 mm spacers. The components of λ3383 are still quite well resolved at an etalon separation of 15 mm, but the resolution of λ3281 is hardly detectable. At 10 mm separation λ3383 only indicates a double line while λ3281 appears to be unresolved. It is evident that smaller etalon separations yield patterns not sufficiently resolved, while larger ones spread the components so far apart that the orders overlap sufficiently to mask the true effect. These facts may account for the failure of earlier investigators to obtain the true doubling of the lines.

These results differ from those of Mohammad and Sharma who used such high currents that reversals of the lines were certainly present but they are not inconsistent with the conclusions of Tolansky and Jackson concerning the upper limit for structure.

Since no structure was found in the green lines which involve the $P$ and $D$ terms, and it was found in the resonance lines involving the $S$ and $P$ terms, the conclusion that the effect is due to a splitting of the $5S$ term seems to be justified. It could also be concluded that the broadening of λ7688 is due to a splitting in the $6S$ term. The fact that the doubling effect shows only in the $5S$ term and not in the $P$ terms indicates that it is due to a nuclear spin and not to an isotope shift. Silver has two isotopes, 87 and 89, about equally abundant. Tolansky[6] considered that the mass isotope shift would be too small to be observed and need not come into consideration. If the separation is due to a nuclear spin it would be expected that the separation of the $6S$ level is smaller than that of the $5S$ level, and that separations in the $P$ terms are very small compared to the separation in the $5S$ level in agreement with the observed results. Since the separation in the $5S$ level is small, resolution of the smaller $P$ term separations cannot be expected with our present resolving power. The higher $J$ value of the $P$ term of λ3281 leads one to expect more broadening of the two components of this line than of the two components of λ3383 also in agreement with observed results. Resolution of the two components of λ3281 was more difficult to secure than the resolution of the two components of λ3383. The above conclusions have to rest on the assumption that the observed hyperfine structure is due to a superposition of nearly identical patterns belonging to the two isotopes of silver.

A few attempts were made toward measuring intensity ratios of the components of the silver resonance lines but the difficulties are at present too great to warrant a very definite conclusion. Many calibrations of the Eastman Process plates were made following approximately the method used by Granath and Van Atta[10] in their work on the resonance lines of sodium. The etalon was removed from the apparatus, the collimator slit

[8] S. Tolansky, J. Sci. Inst. **8**, 223 (1931).
[9] R. Ritschl, Zeits. f. Physik **79**, 3 (1932).
[10] L. P. Granath and C. M. Van Atta, Phys. Rev. **44**, 935 (1933).

was made wider and a series of exposures at different times made on the same plate. Microphotometer traces of these were run on the same paper with traces of corresponding interferometer patterns, but the plate calibrations in the case of silver were only used in selecting the peaks of the traces to be analyzed. The greater lack of resolution in the microphotometer traces of the silver lines made the analysis of the peaks more difficult than the example shown by Granath and Van Atta for sodium. The resolution of the silver resonance lines obtained to date does not justify making such corrections as are mentioned by Tolansky and Heard[11] in their work on the fine structure multiplet of As II. The intensity calibrations and the microphotometer traces showed that possibly the fourth to eighth fringes inclusive might give approximately the intensity ratio of the two components of λ3383. Traces of λ3281, taken from exposures of very low intensity due to the very low currents that had to be used, showed too much variation and hence were not measured. Traces from seven plates of λ3383 were measured giving the following averages: 1.87, 1.54, 1.80, 1.85, 1.64, 1.76, 1.72; with a general average of 1.74. This average lies between 3, the theoretical value for the intensity ratio when I is ½ (if it is supposed that the spectral line has only two components, in this case originating from the $^2S$ lower level), and 1.67 the theoretical value when I is 3/2. If the structure is due to a spin, and half integral values only are to be considered because the mass numbers of both isotopes are odd, then 1.74 suggests that the nuclear spin of silver is 3/2.

The writer wishes to acknowledge the interest and assistance of Professor George S. Monk who suggested the problem, and under whose direction the work was done. It is also a pleasure to thank Professor Carl Eckart and Professor R. S. Mulliken for helpful advice.

[11] S. Tolansky and I. F. Heard, Proc. Roy. Soc. **A146**, 818 (1934).

---

AUGUST 1, 1935 PHYSICAL REVIEW VOLUME 48

# The Electro-Optical Kerr Effect in Ammonia, Nitrogen and Oxygen

WILLIAM M. BREAZEALE, *University of Virginia*

(Received June 7, 1935)

Absolute values for the Kerr constant in anhydrous ammonia, nitrogen and oxygen have been determined. Measurements in $NH_3$ were made at wavelengths of 6500A and 5750A, pressures from 13 to 30 atmospheres, and temperatures from 40° to 80°C. In $N_2$ and $O_2$ the wavelength used was 6500A, pressures in the neighborhood of 100 atmospheres and temperatures from 20° to 65°C. The absolute value for the Kerr constant reduced to N. P. T. and 6500A is for $NH_3$ $(62.3\pm1.8)10^{-12}$, for $N_2$ $(4.64\pm0.10)10^{-12}$ and $O_2$ $(6.94\pm0.30)10^{-12}$.

## INTRODUCTION

WHEN certain isotropic substances are placed in an electric field they acquire the optical properties of a uniaxial crystal with the optic axis in the direction of the electric field. The law governing this phenomenon, first determined by Kerr, states that the phase difference $D$, in radians, between the two components of the light beam is given by

$$D=2\pi l(n_p-n_s)/\lambda=2\pi BlE^2, \qquad (1)$$

where $n_p$ and $n_s$ are the refractive indices corresponding to electric vectors parallel and perpendicular to the electric field, respectively, $l$ the length of the light path through the electric field, λ the wavelength, $E$ the field strength in e.s.u., and $B$ the so-called Kerr constant.

If plane polarized light is passed through the field, the electric vector making an angle of 45° with the direction of the field, the relation between the intensities of the components is given by

$$D=2 \text{ arc sin } (I_k/I_0)^{\frac{1}{2}}. \quad (2)$$

Here $I_0$ is the total intensity of the light passing through the Kerr cell and $I_k$ the intensity of the Kerr beam which, when the polarizer and analyzer are parallel, will appear only when the electric field is applied.

A combination of (1) and (2) gives

$$B=(1/\pi lE^2)(I_k/I_0)^{\frac{1}{2}}. \quad (3)$$

This is the equation used to determine $B$ from the quantities measured in this experiment. Here the argument is set equal to the arc sine, but since $D$ is small in these experiments, the error introduced is negligible.

From the Langevin-Born theory of the Kerr effect[1, 2] the Kerr constant $B$ for a nonpolar gas such as oxygen or nitrogen is given by

$$B=[(n^2-1)(n^2+2)(\epsilon+2)^2/n\lambda]\cdot C_1/T \quad (4)$$

and for a polar gas such as ammonia,

$$B=[(n^2-1)(n^2+2)(\epsilon+2)^2/n\lambda] \times(C_1/T+C_2/T^2). \quad (5)$$

Here $n$ is the index of refraction, $\epsilon$ the dielectric constant, $\lambda$ the wavelength, and $C_1$ and $C_2$ constants independent of density, temperature and wavelength. These equations have been tested experimentally and found to hold for gases; they are used to reduce the value of $B$ measured at any particular density, temperature and wavelength to that at N. P. T. and the desired wavelength. Quantum-mechanical treatment by Serber[3] merely adds a correction term which becomes appreciable only in the ultraviolet.

Ammonia and nitrogen were measured directly but fire hazard prevented doing this with oxygen. Instead the Kerr constant of a mixture of nitrogen and oxygen was measured and the Kerr constant for oxygen determined from this and the known value for nitrogen. The relation used in determining the value for oxygen is obtained as follows. For constant temperature and wavelength Eq. (4) reduces to

$$B=(n^2-1)(n^2+2)(\epsilon+2)^2C/n, \quad (6)$$

where $C$ is another constant. Now $(\epsilon-1)$ and $(n^2-1)$ and, to a sufficient degree of accuracy for our purposes, $(n-1)$ are additive in a mixture of nitrogen and oxygen. Hence for the mixture

$$B_m=\frac{[(n_1^2-1)+(n_2^2-1)][n_1^2+n_2^2+1][\epsilon_1+\epsilon_2+1]^2}{n_1+n_2-1}\cdot C_m. \quad (7)$$

Here the subscripts 1, 2 and $m$ distinguish the properties of the first and second gases and the mixture. (7) can be rewritten

$$B_m=(n_1^2-1)\frac{(n_1^2+n_2^2+1)(\epsilon_1+\epsilon_2+1)^2}{n_1+n_2-1}C_m + (n_2^2-1)\frac{(n_1^2+n_2^2+1)(\epsilon_1+\epsilon_2+1)^2}{n_1+n_2-1}C_m. \quad (8)$$

Setting the first half of the right-hand member equal to a new constant $B_1'$ and dividing by the value for $B_1$ given by (6) gives

$$B_1'=B_1\frac{n_1(n_1+n_2+1)(\epsilon_1+\epsilon_2+1)^2C_m}{(n_1+n_2-1)(n_1^2+2)(\epsilon_1+2)^2C_1}. \quad (9)$$

A similar expression can be written for $B_2'$. Substituting in (8) gives

$$B_m=B_1'+B_2'. \quad (10)$$

The value for $C$ obtained from the theory of the Kerr effect[2] is

$$C=\frac{(\epsilon-1)(n-1)}{36\pi NkT\lambda(n^2-1)}\cdot\frac{\Delta}{6-7\Delta}. \quad (11)$$

Here $N$ is the number of molecules per cc, $k$ is Boltzmann's constant, $\Delta$ is the light scattering coefficient and $\epsilon$ and $n$ are values of the dielectric constant and refractive index at N. P. T. However, all that is necessary for calculation is the ratio of $C_1$ to $C_2$. This is given by

$$\frac{C_1}{C_2}=\frac{\Delta_1(\epsilon_1-1)(n_1-1)(n_2^2-1)(6-7\Delta_2)}{\Delta_2(\epsilon_2-1)(n_2-1)(n_1^2-1)(6-7\Delta_1)}. \quad (12)$$

[1] Langevin, Le radium **7**, 249 (1910); Born, Ann. d. Physik **55**, 177 (1918).

[2] For a résumé of the derivation of this theory see Beams, Rev. Mod. Phys. **4**, 133 (1932), or Stuart, *Molekulstruktur* (Julius Springer, 1934).

[3] Serber, Phys. Rev. **43**, 1011 (1933).

TABLE I. *Kerr constant in ammonia.*

| 1 PRESSURE (ATMOS.) | 2 TEMP. (°C) | 3 WAVE-LENGTH (A) | 4 FIELD (E.S.U.) | 5 $B$ STD. DEN. ($\times 10^{12}$) | 6 $B$ N.P.T. AND 6500A ($\times 10^{12}$) |
|---|---|---|---|---|---|
| 13 7 | 40.8 | 5750 | 75.5 | 54.0 | 63.2 |
| 13.6 | 41.1 | 5750 | 76.9 | 53.4 | 62.5 |
| 22.0 | 59.8 | 5750 | 76.4 | 46.5 | 61.2 |
| 21.8 | 61.1 | 5750 | 82.1 | 46.5 | 61.6 |
| 32.2 | 81.0 | 5750 | 79.7 | 41.0 | 61.0 |
| 30.6 | 79.7 | 5750 | 89.8 | 43.8 | 64.7 |
| 13.5 | 41.4 | 6500 | 72.3 | 48.4 | 64.1 |
| 13.7 | 39.7 | 6500 | 75.1 | 46.8 | 61.4 |
| 14.3 | 60.5 | 6500 | 72.4 | 42.0 | 62.6 |
| 22.2 | 60.7 | 6500 | 83.0 | 42.0 | 62.8 |
| 15.1 | 78.1 | 6500 | 72.4 | 38.1 | 63.0 |
| 31.1 | 81.8 | 6500 | 94.5 | 36.9 | 62.4 |
| | | | | Mean | 62.6 |

Since $C$ is a function of the molecular structure, it is safe to assume that

$$C_m = f_1 C_1 + f_2 C_2, \tag{13}$$

where $f_1$ and $f_2$ are the fractional number of molecules of the first and second gases in the mixture. This, then, provides a means of calculating the ratios $C_m/C_1$ and $C_m/C_2$.

Since $B_m$ is measured and $B_1$ is known, $B_1'$ can be calculated from (9) and (12). Eq. (10) then gives $B_2'$ and by using an equation similar to (9) $B_2$ can be deduced.

## EXPERIMENTAL METHOD

The experiments were performed using a method developed by Stevenson and Beams[4] and improved by Bruce[5] and Quarles.[6] The principal advantage of this method is that it permits the use of high gas pressures and higher electric fields with a consequent increase in the magnitude of the effect.

The apparatus used was essentially the same as that described by Bruce and Quarles. The only major change was the substitution of a more sensitive amplifier.

The anhydrous ammonia was obtained by evaporation from a commercial tank of the liquid. Conductivity tests of the liquid indicated that it contained less than 0.01 percent water. The nitrogen and oxygen were taken from commercial cylinders of these gases. The manufacturers' analysis gave about 0.5 percent impurities, mainly rare gases. A correction was made to the pressure for these. In all cases the Kerr cell was evacuated and dried before the gases to be measured were admitted.

TABLE II. *Kerr constant in nitrogen.* Wavelength = 6500A.

| 1 PRESSURE (ATMOS.) | 2 TEMP. (°C) | 3 FIELD (E.S.U.) | 4 $B$ STD. DEN. ($\times 10^{12}$) | 5 $B$ N.P.T. AND 6500A ($\times 10^{12}$) |
|---|---|---|---|---|
| 106.6 | 20.1 | 360 | 4.22 | 4.53 |
| 101.5 | 20.0 | 357 | 4.27 | 4.58 |
| 108.1 | 45.0 | 344 | 3.95 | 4.60 |
| 110.7 | 65.1 | 358 | 3.90 | 4.83 |
| | | | Mean | 4.64 |

[4] Stevenson and Beams, Phys. Rev. **38**, 133 (1931).
[5] Bruce, Phys. Rev. **44**, 689 (1933).
[6] Quarles, Phys. Rev. **46**, 692 (1934).

## RESULTS

The results of the measurements of the Kerr constant $B$ in anhydrous ammonia are shown in Table I. The first four columns give the experimental conditions under which the measurements were made. The fifth column gives the Kerr constant at standard density but at the temperature and wavelength of measurement computed with the aid of Eq. (5). This column then shows the variation of $B$ with temperature for two wavelengths. The sixth column gives $B$ reduced to its value at N. P. T. and 6500A again by the use of Eq. (5). The constancy of this column is a measure of the precision of the measurements and the reduction formulae. The variation of $B$ with temperature is shown graphically in Fig. 1. The experimental points are shown by circles while the solid line is the theoretical curve plotted from Eq. (5).

TABLE III. *Kerr constant in oxygen.* Wavelength = 6500A

| 1 PRESSURE NITROGEN (ATMOS.) | 2 PRESSURE MIXTURE (ATMOS.) | 3 TEMP. (°C) | 4 FIELD (E.S.U.) | 5 $B$ STD. DEN. ($\times 10^{12}$) | 6 $B$ N.P.T. AND 6500A ($\times 10^{12}$) |
|---|---|---|---|---|---|
| 43.1 | 106.5 | 20.1 | 334 | 6.52 | 7.00 |
| 45.3 | 108.1 | 20.1 | 335 | 6.38 | 6.83 |
| 67.3 | 109.7 | 20.1 | 333 | 6.21 | 6.67 |
| 66.8 | 110.3 | 20.1 | 335 | 6.47 | 6.94 |
| 51.3 | 107.1 | 44.9 | 334 | 6.10 | 7.10 |
| 52.8 | 111.3 | 65.0 | 334 | 5.75 | 7.12 |
| | | | | Mean | 6.94 |

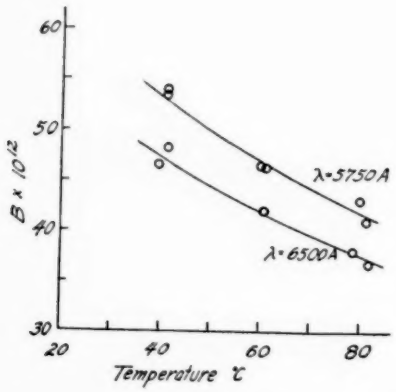


FIG. 1. Temperature variation Kerr effect in ammonia.

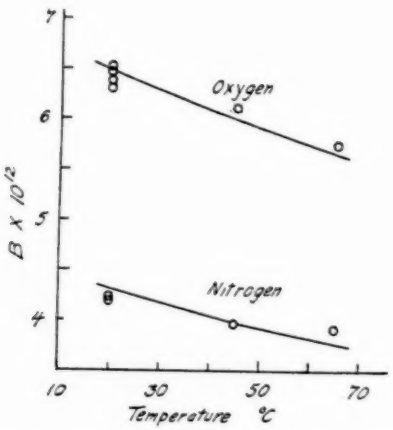


FIG. 2. Temperature variation Kerr effect in nitrogen and oxygen.

Table II shows the results of the measurements in nitrogen. The fourth and fifth columns were determined with the aid of Eq. (4). Since it has been well established that gases obey the Langevin-Born theory, effort was concentrated on determining absolute values of the Kerr constant rather than its variation with density, temperature, etc. To this end measurements were made under only a few different conditions, but a large number of readings were taken at each point.

The value for the Kerr constant of oxygen as determined from measurements in the nitrogen-oxygen mixtures is shown in Table III. $B$ for oxygen was determined as previously described and the results reduced to N. P. T. using Eq. (4). The density of the individual gases in the mixture was computed with the aid of the Beattie-Bridgman equation of state using a linear combination of constants as described by Beattie and Ikehara.[7]

Values of the index of refraction for these calculations were determined with the aid of the Lorentz-Lorenz relation which, Occhialini[8] has shown, holds with sufficient accuracy for these experiments. Zahn[9] has measured the variation of $(\epsilon-1)$ with temperature and density for ammonia and shows that it follows Debye's equation, $(\epsilon-1)\,vT=AT+B$. Debye's equation with Zahn's experimental values for $A$ and $B$ was used to calculate $\epsilon$ for ammonia at the various points.

Fig. 2 shows graphically the variation of $B$ with temperature for nitrogen and oxygen. Again the circles are experimental points and the solid lines theoretical curves calculated this time from Eq. (4).

The absolute value of the Kerr constant for these three gases at N. P. T. and 6500A is for ammonia $(62.6\pm1.8)10^{-12}$, for nitrogen $(4.64\pm0.10)10^{-12}$, and for oxygen $(6.94\pm0.30)10^{-12}$. Szivessy[10] gives $59\times10^{-12}$ for $B$ in ammonia at one atmosphere, 17.5°C and 5890A. Reduced to N. P. T. and 6500A this would be $64\times10^{-12}$. Bruce,[5] from an indirect comparison with carbon dioxide, obtained $5.7\times10^{-12}$ for $B$ in nitrogen at one atmosphere, 34.6°C and 4550A. This corresponds to $5.1\times10^{-12}$ at N. P. T. and 6500A. The author knows of no experimental value for $B$ in oxygen. The theoretical value calculated on the basis of the Langevin-Born theory is $6.49\times10^{-12}$ at N. P. T. and 6500A.

## ACKNOWLEDGMENTS

The author wishes to express his appreciation to Dr. J. W. Beams under whose direction this work was done, to Dr. L. G. Hoxton for assistance in preparation of the manuscript, and to Dr. W. E. Deming of the Fixed Nitrogen Laboratory for valuable suggestions in computing densities of mixtures.

[7] Beattie and Ikehara, M. I. T. publications, Serial No. 239.
[8] Occhialini, Nuovo cimento (6) **8**, 123 (1914).
[9] Zahn, Phys. Rev. **27**, 455 (1926).
[10] Szivessy, Zeits. f. Physik **26**, 323 (1924).

# The Production and Focusing of Intense Positive Ion Beams

M. A. TUVE, O. DAHL AND L. R. HAFSTAD, *Department of Terrestrial Magnetism, Carnegie Institution of Washington*

(Received June 13, 1935)

Based on a suggestion by Dr. F. L. Mohler, a high intensity source of positive ions utilizing a gaseous low voltage arc constricted by a metal capillary has been developed. With 250 watts input and 10–cc gas flow per hour, this source delivers controllable positive ion currents up to 1.5 *milliamperes* through a probe canal 1 mm in diameter. The focusing of weak and intense positive ion beams by various electrostatic lens arrangements has been empirically investigated, giving additional data on quantitative design concerning the multiple section high voltage tubes long in use in the laboratory of the Department of Terrestrial Magnetism of the Carnegie Institution of Washington, and indicating the requirements met in delivering the total ion current from the source onto a target at the far end of such a tube.

## (A) INTRODUCTION

WE have described[1] the technique developed in the laboratory of the Department of Terrestrial Magnetism of the Carnegie Institution of Washington for studies of nuclear transmutation, utilizing electrostatic generators and cascade type high voltage tubes. The focusing characteristics of multiple section high voltage tubes have been rather strikingly demonstrated, and in spite of the limitations of the low voltage arc ion source used in the experiments with a poorly aligned tube provisionally installed it has been possible to concentrate currents of 5 to 10 microamperes of protons or deuterons (after magnetic analysis) on targets less than 1 cm in diameter for hours at a time. However, the ordinary type of ion source used here has given us a certain amount of trouble and inconvenience, and has been proved incapable of delivering more than 10 to 25 microamperes total ion current into the tube (frequently less) even with a comparatively high gas flow (deuterium consumption). Above 1000 kilovolts, currents of one to ten microamperes are ample or even excessive for the study of many transmutation problems, but for the study of relatively infrequent processes, and especially for investigations at lower voltages, higher currents are necessary and a trouble-free ion source capable of delivering hundreds or even thousands of microamperes has been sought in various laboratories as well as here. A low voltage arc, such as used at this Department for nearly three years, can readily supply ion currents of some milliamperes to a probe several cm² in area immersed in the plasma and, if the probe is a simple gauze or mesh or is perforated with a large hole, such currents can be projected into an apparatus for further acceleration or use.[2] However, if the current density to the probe is such that a hole 5 to 10 mm in diameter is required to pass the desired ion current, not only are the pumping requirements formidable if a low pressure is to be maintained in the apparatus beyond the probe, but the gas consumption itself becomes so enormous as to prohibit the use of deuterium, and deuterium ions are perhaps the most important of all bombarding particles for transmutation experiments. In the course of numerous tests here a new type of low power ion source has been evolved, delivering large ion currents with very modest gas consumption as described below (section B).

The production of an intense stream of ions is only half the task, however. The problem of concentrating the ions into a beam and then preventing this beam from diverging unduly between the source and the target or other point where the ions are utilized, is of equal importance. Especially at high current densities (many milliamperes per cm²) space-charge effects influence the beam, as well as the aberrations of the simple electrostatic lenses ordinarily used for this purpose; both factors constitute limitations requiring empirical study. In our experience at this Department with several multiple section high voltage tubes of very dissimilar design we have consistently obtained at the

[1] M. A. Tuve, L. R. Hafstad and O. Dahl, Phys. Rev. **48**, 315 (1935).

[2] E. S. Lamar and O. Luhr, Phys. Rev. **46**, 87 (1934); R. D. Fowler and G. E. Gibson, Phys. Rev. **46**, 1075 (1934).

target, after a crude but obviously necessary adjustment of the available focusing parameters (adjustment of voltages on those tube sections through which the ion beam is traveling slowly), practically the entire ion current which enters the tube from the ion source. Workers in other laboratories, using high voltage tubes having similar cylindrical electrodes but with only one or two sections, have reported a much smaller effectiveness in focusing the ion beam entering the tube, most of which is lost before reaching the target. Bombardment of the walls of the tube by this "lost" portion of the initial ion current is undesirable for several reasons in addition to the simple loss of intensity at the focal spot. Before constructing a more permanent tube to replace the provisional one used, it appeared desirable to examine the relative importance of the numerous factors which determine the focusing of an ion beam by a system of cylindrical electrodes, with particular reference to numerical magnitudes (voltage ratios, dimensions, electrode designs) and to the extent to which space-charge effects and the aberrations of the electrostatic lenses are important in the focusing of large ion currents into small area beams without loss. A tendency toward poorer focusing had apparently been observed with our tubes at currents above 2 microamperes, and this tendency might be exceedingly important at currents of 100 to 1000 microamperes. Although a considerable amount of theoretical and experimental work has been done in recent years on the problems of "electron optics," very little of the material is directly applicable to this ion focusing problem until experimentally tested, especially because of space-charge effects; furthermore, the case of cylindrical electrodes has evidently not been treated in detail. Consequently an empirical study of the most important factors in tube design for proper focusing has been made as described in the latter part of this paper.

### (B) The Capillary Arc Ion Source

Knowing of the difficulties experienced here due to ion source limitations, Dr. F. L. Mohler of the National Bureau of Standards kindly described to us last summer some preliminary experiments he had made with the ultimate aim of studying the $(H^2+H^2)$ reactions. In these experiments he had obtained very high current density to a negative probe inserted from one side into a low voltage (hot cathode) hydrogen arc in a quartz tube which was provided with a short constriction or capillary (5-mm diameter) at the location of the probe; high ion density, and hence high probe current density, evidently was obtained because of the high arc current density in the constriction. With the help of Dr. C. M. Van Atta, temporarily a guest investigator in this laboratory, we developed[3] an ion source in the autumn of 1934 on this basis which provides positive ion currents of more than one milliampere, if desired, with modest power requirements and low gas consumption (small diameter probe canal). This source in fact gives such high ion current densities (certainly exceeding 200 milliamperes per $cm^2$) that a major problem is to overcome the divergence of the beam arising in part from the mutual repulsion effects of space charge, tending to disperse the ions before and as they are accelerated to form a high speed beam. We had previously anticipated and experienced such effects with ion densities of only a few microamperes per $mm^2$ at low voltages, and it is of importance in various applications to have empirical data on the extent to which space-charge effects and other causes of divergence can be prevented from limiting the formation of ion beams under specified conditions (voltages, distances, size and shape of electrodes). The limitation of a proton current, due to mutual repulsion effects, to a "theoretical maximum" of 10 milliamperes per square centimeter in the ideal case of plane parallel electrodes with a gradient of $10^5$ volts/cm, mentioned[4] at the London Conference, thus appears to be greatly modified by the conditions in this source.

In many applications, as well as in our own, it is impossible to utilize an ion source requiring many kilowatts of power—with its attendant necessity of artificial cooling—especially if large and bulky auxiliary apparatus such as a 50-kv rectifier set is essential to its operation. In these

[3] M. A. Tuve, O. Dahl and C. M. Van Atta, Phys. Rev. **46**, 1027 (1934).
[4] M. L. E. Oliphant, Int. Conf. Phys. London, 1934 **1**, 144 (1935).

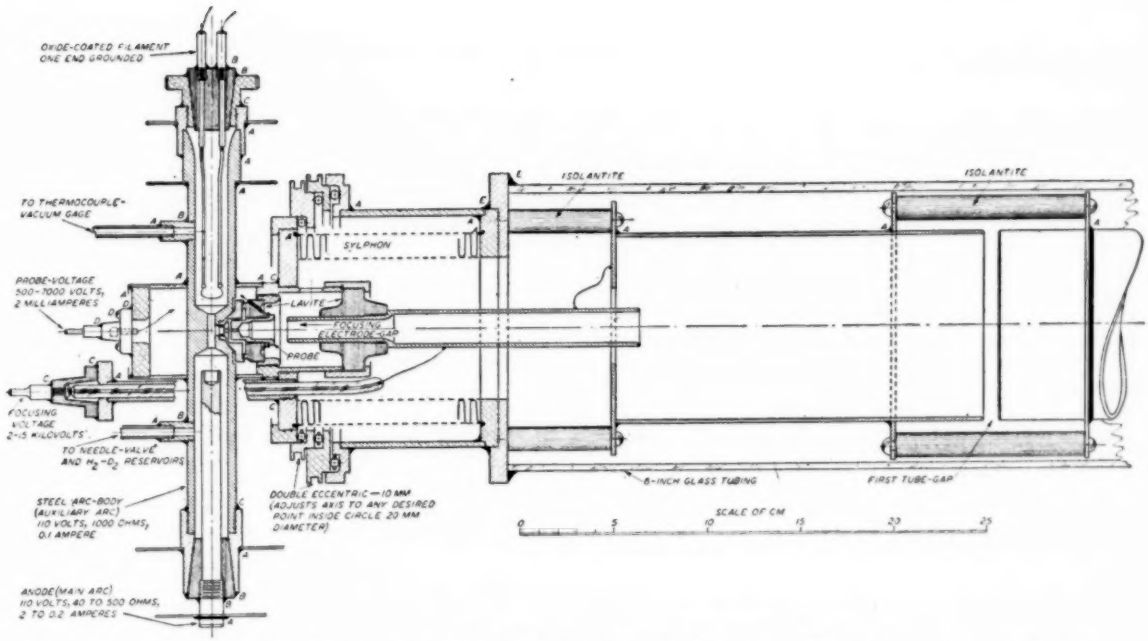
OXIDE-COATED FILAMENT ONE END GROUNDED
TO THERMOCOUPLE-VACUUM GAGE
PROBE-VOLTAGE 500-7000 VOLTS, 2 MILLIAMPERES
FOCUSING VOLTAGE 2-15 KILOVOLTS
TO NEEDLE-VALVE AND $H_2$-$O_2$ RESERVOIRS
STEEL ARC-BODY (AUXILIARY ARC) 110 VOLTS, 1000 OHMS, 0.1 AMPERE
ANODE (MAIN ARC) 110 VOLTS, 40 TO 500 OHMS, 2 TO 0.2 AMPERES
SYLPHON
LAVITE
FOCUSING ELECTRODES
PROBE
DOUBLE ECCENTRIC — 10 MM (ADJUSTS AXIS TO ANY DESIRED POINT INSIDE CIRCLE 20 MM DIAMETER)
ISOLANTITE
ISOLANTITE
6-INCH GLASS TUBING
FIRST TUBE-GAP
SCALE OF CM
0 5 10 15 20 25

FIG. 1. Ion source with first focusing gap of high voltage tube. *A*—Tin solder; *B*—rock cement and glyptal or De Khotinsky cement; *C*—picein; *D*—De Khotinsky cement; *E*—Apiezon plasticene "*Q*".

respects and in its simplicity of control, the capillary arc ion source has fortunately proved advantageous.

### (1) Construction

The complete ion source as attached to the high voltage tube is shown in Figs. 1 and 2 in which the important features of the arc, probe and focusing electrodes are shown to scale. Referring to Fig. 2, the arc is confined by a steel capillary, bored out of the solid steel cylinder *A*, the arc capillary *B* (3.5-mm diameter, 18 mm long) joining the arc spaces containing the oxide-coated filament *C* and the steel anode *D*. A side volume *E* (diameter 5 mm) was bored out as shown for the diffusion of ions from the capillary arc to the probe, and the conical steel insert *J* serves to provide flat gas seal surfaces between the arc space and the evacuated high voltage tube. The steel probe *F* is mounted on the lavite[5] insulator *K* and is provided with a canal *H*, 1 mm in diameter by 4 mm long, through which the ion current (as well as gas flow) passes into the evacuated high voltage tube. The steel "button" *G* is inserted to act as a partial diaphragm at the lower end of the space *E*. Introduction of this button diaphragm reduced the total current to the face of the probe *F* (including secondaries) by a factor of

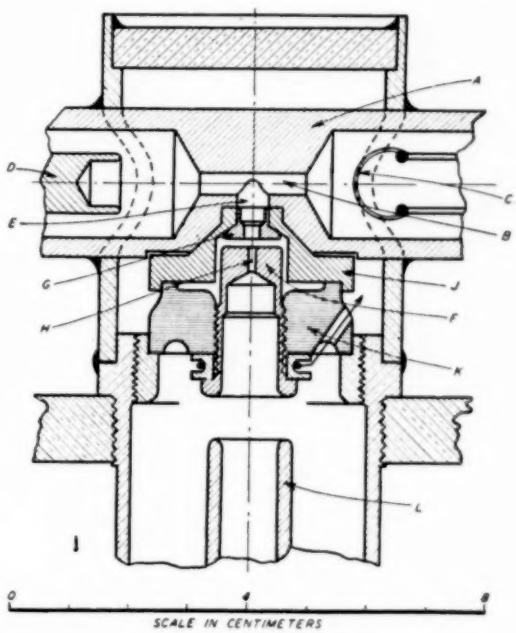


FIG. 2. Ion source detail.

[5] Finest grade unfired imported steatite, purchased from American Lava Corporation, 1420 Williams Street, Chattanooga, Tennessee. Insulators of any shape are readily fabricated from this material; they expand slightly on firing at about 1000°C for one hour.

4 or 5, and, evidently by causing a more favorable curvature of the space-charge sheath separating the negative probe from the arc plasma, it also served to concentrate the probe current on the canal *II*, increasing the current through the probe canal by a factor between 2 and 3 at various voltages. The ion stream projected through the probe canal *II* rapidly diverges (the initial ion paths, due to the space-charge sheath, are not parallel), and an initial "focusing gap" very near to the probe canal is incorporated as a part of the ion source, to deliver to the first section of the high voltage tube, in the form of an ion beam of the proper characteristics (speed, divergence, beam area) to suit the focusing-parameters of that tube section and those which follow, the total ion current which emerges from the probe canal. This initial "focusing gap" is formed by the cylindrical end of the probe and the cylindrical electrode *L*, which is held at a controlled direct-current potential of 2 to 15 kv —the correct voltage depending on the probe voltage and the focusing properties (voltage is the chief variable) of the first tube sections. The probe voltage (100 to 4000 volts, see Table I) is supplied, through the connection indicated by arrows in Figs. 1 and 2, by a filtered rectifier using type '66 tubes, and the focus voltage (2 to 15 kv serves for all but the extremely high currents, see below) is supplied by a half-wave unit using a ZP-85 kenotron. Protective resistors (50,000 ohms) are essential in the probe and focus voltage leads to prevent "blowing out" the arc (possibly by oscillations). The ease of accurate control of the tube current (probe voltage) and spot focus (focus voltage) by autotransformers of the Variac[6] type is important enough to mention. The complete ion source is mounted on a large sylphon and provided with a double eccentric arrangement to make it possible to move the point-source of ions with respect to the lens system, thus providing an optical lever arrangement for moving the focal spot.

### (2) Operating characteristics

The total power consumption of an ion source is an important factor in many applications; in the range of currents covered by our tests the power required for this source is of the order of 250 watts or less. The cooling-fins shown in Fig. 1 keep the temperature low enough for the wax seals without it, but we usually direct the breeze of a "toy" electric fan on the source when in use. The arc readily operates on 110 volts direct current, with an external resistor controlling the arc current (0.2 to 2.0 amperes—usually 1.0); the voltage drop across the arc itself is about 55 volts, the "floating" arc body assuming a potential 22 to 30 volts above the filament, which is grounded. The filament power is appreciable, a 4-mm by 14-mm strip of 2-mil platinum drawing 16 amperes at 3 to 6 volts. The oxide coating[7] of the filament requires occasional replacement, but lasts for more than a month of daily use with hydrogen. The power requirements for the probe and focus voltages are almost negligible (except for the losses in the rectifier units). The arc through the capillary can be struck by the application of a "leak tester" (spark coil) to the floating arc body; it will continue to run at a pressure somewhat lower than that required for striking. A self-striking auxiliary arc (0.2 ampere) to the steel arc body surrounding the filament will operate at a slightly lower pressure than will the main capillary arc, and it serves to restrike the latter arc, if it goes out for some cause (too low pressure, too high probe voltage), as soon as the cause is removed, except when extreme purity of the hydrogen makes the arc difficult to strike. This may be of importance in certain applications requiring intermittent bursts of ions. The auxiliary arc reduces the ion current output of the source at the higher probe voltage values, however, and should be omitted if maximum ion currents are desired.

The actual pressure of the hydrogen in the arc and the rate of flow of gas through the probe canal have not been ascertained with precision. Crude records of the number of hours à 1-liter flask of gas will operate the source indicate a flow of about 10 cc per hour (normal pressure and temperature), allowing the use of deuterium without recovery at nominal cost. An Apiezon

[6] Supplied in three sizes by General Radio Company, Cambridge A, Massachusetts.

[7] The regular oxide mixture of the radio tube trade, purchased in liquid suspension from Callite Products Company, Union City, New Jersey, is used.

pumping-system with a speed (for air) of about 30 liters per second maintains a pressure of about $2\times10^{-5}$ mm in the high voltage tube (Western Electric ionization gauge, type No. D-79510, reads 6 to 10 microamperes at 20-ma emission) when the pressure in the arc is perhaps $2\times10^{-3}$ (General Electric thermocouple vacuum gauge, catalog No. 3850264-G1, with 50-ma heater-current, reads 90 to 60 microamperes at arc pressure and 200 microamperes for zero pressure). The arc appears to operate at lower pressures if the hydrogen in the arc space is not 100 percent pure; this is usually insured by the gas evolution of the oxide-coated filament, but we have also introduced small amounts of air or helium into the hydrogen reservoir with apparently a similar result, although our experience with the older form of low voltage ion source used here for several years definitely shows that the introduction of small amounts of air with the hydrogen reduces the numbers of hydrogen-ions (of various kinds) by as much as a factor of 10.

### (3) Output ion currents

The ion current output from the 1-mm by 4-mm probe canal shown in Fig. 2 has been measured, as a function of probe voltage, arc current, pressure and other variables, by utilizing the cylindrical electrode $L$ and all subsequent electrodes (larger diameter) as a very deep Faraday cage. Some effect of secondary electrons is obvious, but making the Faraday cage successively 45 volts plus and minus with respect to the probe shows that the usual equal potential measurement indicates approximately the true ion current, as indicated below. [Note: The focus gap $FL$ was shortened to 3.5 mm during most of these measurements, later left at about 7 mm; these changes were of practically no effect on the focusing-characteristics of the gap.] A typical series of measurements of the total ion current output from the probe canal is given in Table I. Many of the current values were duplicated within about 10 percent after focusing (by application of the proper potential to electrode $L$) into a similar Faraday cage beyond $L$ and at its potential, a further indication of the absence of very large secondary emission errors in the current measurements.

TABLE I. *Total ion current output of probe canal as a function of probe voltage and arc current.* (Arc pressure, 100μA on thermo-gauge; hydrogen plus 10 percent air; auxiliary arc, 0.13 ampere.)

| ARC CURRENT (AMP.) | PROBE VOLTAGE 700 (μA) | 1000 (μA) | 1500 (μA) | 2000 (μA) | 4000 (μA) | 7000 (μA) |
|---|---|---|---|---|---|---|
| 0.25 | **50** | 75 | 82 | 70 | 52 | 40 |
| 0.5 | 40 | **94** | **161** | 200 | 150 | 110 |
| 1.0 | 19 | 50 | 157 | **290** | 450 | 410 |
| 1.5 | 14 | 30 | 90 | 260 | **770** | 990 |
| 2.0 | 12 | 22 | 58 | 170 | 750 | 1410 |
| 2.5 | .. | .. | ... | ... | 710 | **1600** |

We have evidence indicating a secondary electron emission of from 100 percent to 500 percent of the ion current itself when a flat metal electrode is used to measure the current instead of a deep Faraday cage, a source of serious errors not always fully appreciated in work of this kind.

The ratio of atomic to molecular ions is undoubtedly dependent on the hydrogen pressure, impurities and other operating factors, but in our experience with a great variety of low voltage arc arrangements used as ion sources we never have observed fewer than 50 percent, and never more than 90 percent atomic ions, the balance of the hydrogen ions being often largely triatomic. This source shows the same behavior.* [We have had occasion so far to make relatively few measurements of ion ratios with the capillary type source and these have not been made at the very highest currents, but there is no reason to suppose that the number of atomic ions should decrease with higher probe voltages.] The exact ratio of atomic to molecular ions

* *Note added in proof:* We have recently had opportunity to make more extended measurements on the ion varieties emitted by the capillary-arc source. With the probe-canal shown in Fig. 1 and using tank-hydrogen, only 20 to 30 percent of the hydrogen ions are atomic; as with our other sources, the hydrogen ions constitute one-half to three-fourths of the total. With 2000 volts on the probe and 70 kilovolts on a single-section tube, typical currents in the separate spots after magnetic analysis are: Mass 1, 22 microamperes; mass 2, 32 microamperes; mass 3, 36 microamperes; mass 4, less than 0.1 microampere; masses 16, 17 and 18, 36 microamperes; total (measured before entering the long analysis-chamber), 162 microamperes; sum of all measurable spots, 126 microamperes. The distances in this arrangement were known to be too great to prevent the loss of part of the ion current at this low tube-voltage before it reached the target, placed in a deep Faraday cage beyond the magnet. Ordinary tank-hydrogen gives a better proton-ratio than hydrogen diffused through palladium, or hydrogen mixed with air, helium or water vapor. By collision-dissociation of the molecular ions after attaining appreciable speeds, a longer probe-canal gives a better proton-ratio, although the total currents for a given probe-voltage are much reduced. Modifications should be possible to enhance this dissociation effect.

TABLE II. *Variability of output current—effects of secondary electrons.*

| PROBE VOLTAGE (VOLTS) | CAGE VOLTAGE (VOLTS) | ARC = 1 AMPERE THERMO-GAUGE PRESSURE 60μA NO AUX. ARC (μA) | 90μA NO AUX. ARC (μA) | 90μA AUX. ARC, (0.3 AMP.) (μA) | ARC = 2 AMPERES THERMO-GAUGE PRESSURE, 90μA NO AUX. ARC (μA) | AUX. ARC, (0.3 AMP.) (μA) |
|---|---|---|---|---|---|---|
| 100 | 100 | 1.5 | ... | ... | .... | ... |
| 200 | 200 | 2.3 | ... | ... | .... | ... |
| 500 | 500 | 7.2 | ... | ... | .... | ... |
| 1000 | 1000 | 28 | 32 | ... | 22 | ... |
| 2000 | 2000 | 230 | 250 | 250 | 155 | 230 |
| 4000 | 4000 | 600 | 570 | 280 | 800 | 740 |
| 6000 | 6000 | 680 | 590 | 210 | 1110 | 810 |
| 6000 | 6045 | ... | 460 | ... | 940 | ... |
| 6000 | 5955 | ... | 850 | ... | 1500 | ... |

coming from the source is of no importance in our experiments since magnetic analysis is used at the target, as it always should be if the variety of ion is of importance. If capture and loss phenomena take place after acceleration and before magnetic analysis, there will of course be an overlapping of ion varieties. Such capture processes occur only to a negligible extent in our high voltage tubes, as indicated by the lack of any ions at the target more readily deflected than the full speed protons.

It is to be noted that an optimum value of arc current (for maximum output current) exists for each probe voltage, increasing with the latter, as indicated by the current values in bold face type. These current values do not duplicate exactly on different occasions with slightly changed conditions, but the extent of the variation, as well as the effects of secondary electrons, may be seen by comparison with Table II.

The output currents do not appear to vary greatly with pressure over the working range of pressures used. The pressure is usually set at a value not much higher than is necessary to prevent extinction of the arc. Much larger output currents undoubtedly can be obtained, if desired, by increasing the size of the probe canal at the expense of increased gas consumption, or as indicated by Table I by increasing the arc current through the capillary and raising the probe voltage to its corresponding optimum value.

### (4) Dependence on configuration and other variables

The effect of the auxiliary arc on the output current from the probe canal has been mentioned above, as well as the changes brought about by

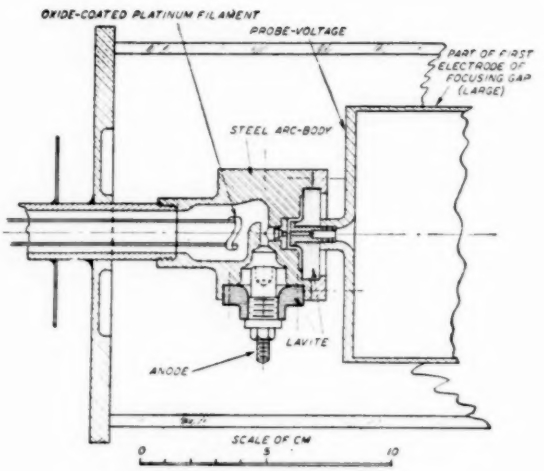


FIG. 3. Right-angle capillary—ion source.

the diaphragm button *G* ahead of the probe. Before the introduction of the latter, the position of the probe face was varied in steps from 1 mm inside the arc capillary itself to its final position as shown in Fig. 2. Except for the fact that the arc was extinguished by probe voltages as low as 500 to 1000 volts, no great dependence on probe position was observed. The current to the probe face (4-mm diameter) was roughly constant at about 8 milliamperes for all probe voltages from 20 volts to extinction. The diaphragm button *G* allowed much higher probe voltages to be applied without extinguishing the arc. The few brief tests which have been made with probe canals of diameters differing from the standard 1-mm diameter indicate that the output current increases somewhat more than in proportion to the area of the probe canal. It must be remembered that the gas flow increases with the cube of the diameter of this canal, however. The gas flow is inversely proportional to the length of the canal, but the dependence of the ion current on the canal length is a function of the probe voltage in question, probably on account of changes in curvature of the space-charge sheath, giving different degrees of divergence to the initial ion stream. For medium values of probe voltage it varies more rapidly than the inverse square of the length of the canal. This is a crude statement but may be of assistance in adapting this design to other conditions. For low probe voltages the "best" probe canal is a diaphragm in a thin

plate; for higher voltages the canal profitably can have appreciable length, thereby decreasing the gas flow without seriously decreasing the output current by loss to the sides of the canal.

For reasons of convenience (removal of filament) in a particular application we constructed a modified form of the capillary arc source, differing from that of Fig. 1 by the fact that the arc was struck "around a corner" as shown in Fig. 3. It was astonishing to discover that this source had characteristics rather widely different from those of the original design. Because of a slip, the side volume $E$ at first was bored out slightly off-center with respect to the arc capillary, which was 3.5 mm by 18 mm as before. When the arc required 75 volts and showed an anode drop (with respect to the capillary) equal to the former total arc voltage (50 volts) with the total probe current only 200 microamperes, it was thought that no arc was passing through the capillary. The latter was consequently shortened to 9 mm with but slight effect. The arc capillary was then bored out to 6.5 mm diameter and centered with respect to the probe axis. With an arc current of 1 ampere (low density because large capillary) a probe canal 1 mm by 4 mm as before gave an output current of only 38 microamperes at 2000 volts instead of about 230 microamperes with the source of Fig. 1. The output current was found to show rather sharp maxima with increasing probe voltage and arc current, and even the optimum values were only about one-eighth of the normal output of the original source at a given voltage. The arc capillary was then plugged and rebored to a diameter of 3.5 mm and length of 10 mm, centered on the probe axis. The probe canal output current was raised by this to about one-third of the value for the straight capillary but it still showed a strong dependence on arc current and sharp maxima with the latter and with probe voltage, as indicated in Table III.

TABLE III. *Right-angle capillary arc: Dependence of probe canal output current on arc current and on probe voltage.*

| Probe canal, 1 by 4 mm Thermo-gauge pressure, 75μA | | | Probe canal, 0.51 by 9.5 mm Thermo-gauge pressure, 70μA | | |
|---|---|---|---|---|---|
| Probe voltage (volts) | Arc current (amp.) | Output current (μA) | Arc current (amp.) | Probe voltage (volts) | Output current (μA) |
| 2000 | 0.25 | 6 | 0.9 | 4000 | 11 |
| | 0.5 | 16 | 1.2 | 2000 | 5 |
| | 1.0 | 68 | | 3000 | 16 |
| | 1.25 | 62 | | 4000 | 21 |
| | 1.50 | 46 | | 5000 | 12 |
| | 3.0 | 28 | 2.2 | 2000 | 4 |
| | 5.0 | 22 | | 3000 | 9 |
| | | | | 4000 | 28 |
| | | | | 5000 | 50 |

Thus, although the behavior of the ion source of Fig. 1 has been consistent throughout months of use and a great variety of changes (exceeding 30) of various associated parts, the behavior of the right-angle arc of Fig. 3 remains an interesting but unimportant mystery. It is described solely to indicate the extent of our recommendations for changes in the source shown in Fig. 1 on the basis of the few variations we have tried.

### (5) Tests of various electrostatic lens arrangements: The focus gap *FL* of the ion source

On the assumption that it might be important, because of space charge and initial divergence of

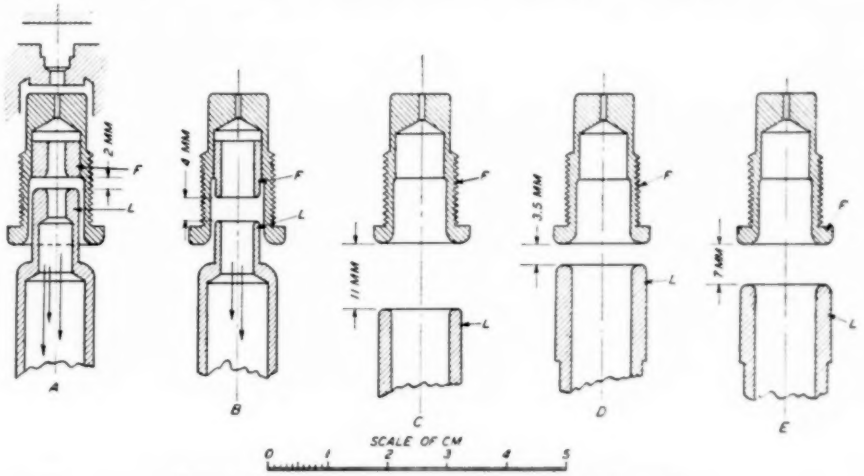


FIG. 4. Electrostatic lenses adjacent to probe canal.

TABLE IV. *Variation of current into Faraday cage with 2000 volts in probe F and canal output 230 microamperes (case a of Fig. 4).*

| FOCUS VOLTAGE ON *FL* (VOLTS) | CURRENT INTO FARADAY CAGE (μA) |
|---|---|
| 4000 | 6 |
| 6000 | 10.5 |
| 7000 | 13.5 |
| 8000 | 3.2 |
| 10000 | 0.5 |

the ion paths, to place a focusing lens as near as possible to the output end of the probe canal early tests were made of the arrangements shown in Figs. 4*a* and 4*b*. As a test of the focusing, the currents were measured which passed into a long Faraday cage (50 cm long by 6 mm diameter) through a 5-mm hole in a diaphragm at the lower end of electrode *L*. For the first case (4*a*) this 5-mm hole was 20 cm below the arc capillary (18 cm below the lens *FL*), and it was found that a peculiar "over-focusing effect" occurred; only 5 percent of the total current could be passed as a beam through the hole. This was erroneously thought to be a space-charge effect leading to an "excluded" zone at a distance as large as 20 cm, the ion paths switching sharply from "under-focused" to "over-focused" (crossing axis) at a value far below that (virtually) necessary for focusing. The 5-mm diaphragm was consequently moved nearer to the lens, to a position 14 cm below the capillary, and the larger lens 4*b* was tested. This was much better, although still delivering only about 35 percent of the ions into the cage, as shown in Table V.

It is probable that both lenses per Fig. 4*a* and Fig. 4*b* failed to form good ion beams because their dimensions were comparable to the dimensions of the incident divergent ion stream. The probe canal, as in all subsequent measurements, was 1 mm in diameter by 4 mm long, thus permitting initial ion paths throughout a cone of rather large angle from an initial area 1 mm in diameter. The aberrations of a simple lens for a beam as large as one-third its own diameter are probably large, but it is also desirable (unless initial side components of velocity are negligible) for the lens to be far enough removed, from a source of finite area which emits ions in a variety of initial directions, to permit the ion paths to separate, so that those ion paths entering a given (circular) zone of the lens all make the same angle with the axis. When this condition is fulfilled, the requirements on the lens are obviously much less stringent.

Adopting lens electrodes of still larger diameter, further removed from the ion emitting area (end of the probe canal), the arrangements *c*, *d* and *e* of Fig. 4 were tested. With the 5-mm diaphragm (into the Faraday cage) at the original distance of 20 cm, the lens 4*c* gave a fairly satisfactory beam, 11 kilovolts serving to focus through the 5-mm hole the total output of the probe canal at 2000 volts (230 microamperes). A wider gap (14 mm) required the application of a slightly higher voltage (15 percent) before complete focusing was attained (at any given probe voltage) and with the narrow gap 4*d* (3 mm) a slightly (20 percent) lower voltage sufficed, but otherwise little variation with electrode spacing could be observed. The medium gap of 4*c* (7 mm) was chosen for further tests (this lens was adopted in the final arrangement as now used).

It was observed that as the output current of the probe canal was increased by increasing the probe voltage, the voltage required on the lens *FL* to focus the ions in a beam through the 5-mm diaphragm was also higher. To determine whether this was in part due to increased mutual repulsion and consequent space-charge dispersion at the higher beam currents or simply to the increased "stiffness" of the beam (higher initial velocity of ions as they enter the lens) with increasing probe voltages, measurements were made of the focus voltages required to concentrate the total output current from the probe canal through the 5-mm hole at 14 cm into the

TABLE V. *Variation of current into Faraday cage (case b of Fig. 4).*

| PROBE VOLTAGE (VOLTS) | CANAL OUTPUT (μA) | CAGE CURRENT (μA) | REQUIRED FOCUS VOLTAGE (KV) |
|---|---|---|---|
| 2000 | 230 | 105 | 14 (max. available) |
| 1500 | 93 | 34 | 10–14 |
| 1000 | 28 | 10 | 5 |

TABLE VI. *Observations showing focus voltage proportion to voltage (energy) of incident ion beam.*

| PROBE VOLTAGE (VOLTS) | OUTPUT CURRENTS (μA) | REQUIRED FOCUS VOLTAGE (KV) | FARADAY CAGE CURRENT (μA) |
|---|---|---|---|
| 100 | 1.5 | 1.0 | 1.4 |
| 200 | 2.3 | 1.5 | 2.3 |
| 350 | 4.5 | 2.5 | 4.3 |
| 700 | 12 | 6.0 | 13.3 |
| 1000 | 28 | 8.0 | 33 |
| 1200 | .... | 10 | 55 |

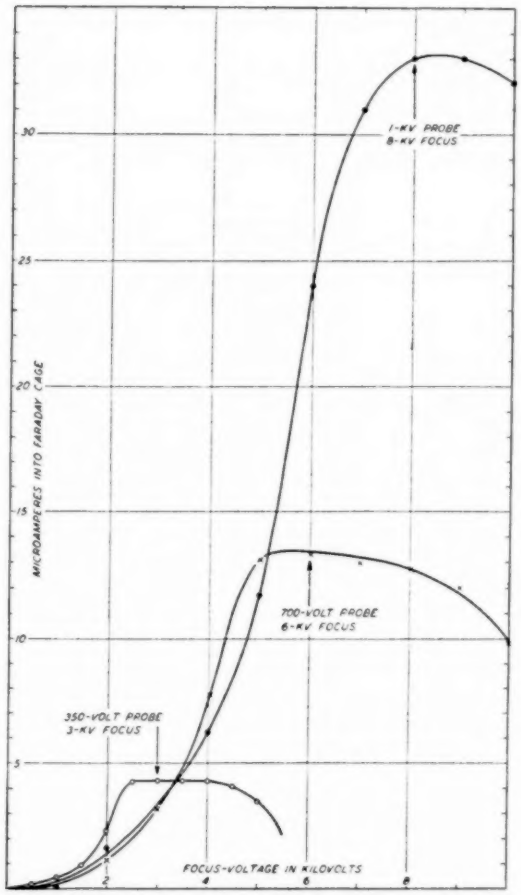


FIG. 5. Typical curves showing importance of initial ion beam "stiffness."

Faraday cage. Typical curves are shown in Fig. 5, and the results are summarized in Table VI.

The approximate proportionality of the probe voltages and required focus voltages indicates the lack of space-charge effects and the importance of the "stiffness" of the ion beam.

Tests of the distances which the ion beam could be made to travel without undue dispersion were next inaugurated. The Faraday cage tests using the 5-mm diaphragm hole as well as corroborative tests with a fluorescent screen, showed that the lens 4*c*, at a distance from the probe canal as shown, was able to concentrate all of the ions from the probe canal (at least up to 350 microamperes) into a beam which would travel a distance of 20 cm without much dispersion, most of the ions striking an area about 2 mm in diameter when the focus voltage was correctly adjusted. A large (8-cm) fluorescent

TABLE VII. *Observations on focusing with single lens and 85-cm target distance (case e of Fig. 4).*

| PROBE VOLTAGE (VOLTS) | OUTPUT CURRENT (μA) | REQUIRED FOCUS VOLTAGE (KV) | FARADAY CAGE CURRENT (μA) | DIAMETER FOCAL SPOT (MM) |
|---|---|---|---|---|
| 350 | 4.5 | 2.8 | 5 | 8 |
| 500 | 7.2 | 3.9 | 9 | 7 |
| 700 | 12 | 5.4 | 15 | Diffuse >10 |
| 1000 } >1000 | No focal spot—annular rings and background | | | |

screen was installed at a distance of 85 cm from the arc capillary in a crude Faraday cage of wire mesh. When projected this distance through an equipotential cylinder extending to the cage and screen, the lens 4*e* gave a definite but rather large focal "spot" for currents under 10 microamperes, but the beam spread over the whole screen with larger currents (higher voltages) as shown by Table VII.

That this failure to give a good focal spot at higher currents would not be overcome to any large extent if the lens 4*e* had considerably less "curvature" and hence projected a higher speed beam toward the screen (coming to a focus at the same distance) was unintentionally determined by the introduction of a "negative lens" a short distance beyond the lens 4*e*. This came about in one experiment by neglecting to shield the beam at all points inside a cylinder at the focus voltage, a gap in this shielding permitting lines of force from the surrounding parts at zero potential to enter the cylinders and affect the beam as shown in Fig. 6. This lens combination required a much higher focus voltage (for a given probe voltage) but the spot became diffuse at similar currents under 10 microamperes.

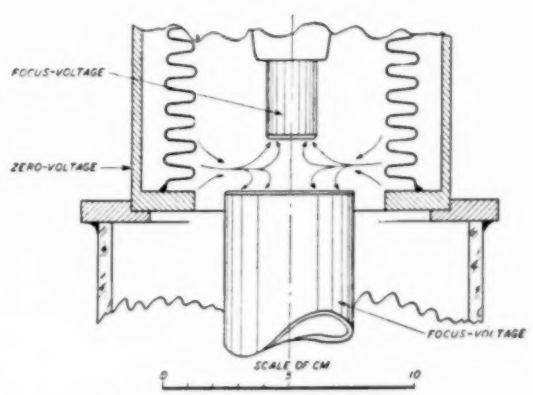


FIG. 6. Accidental negative lens.

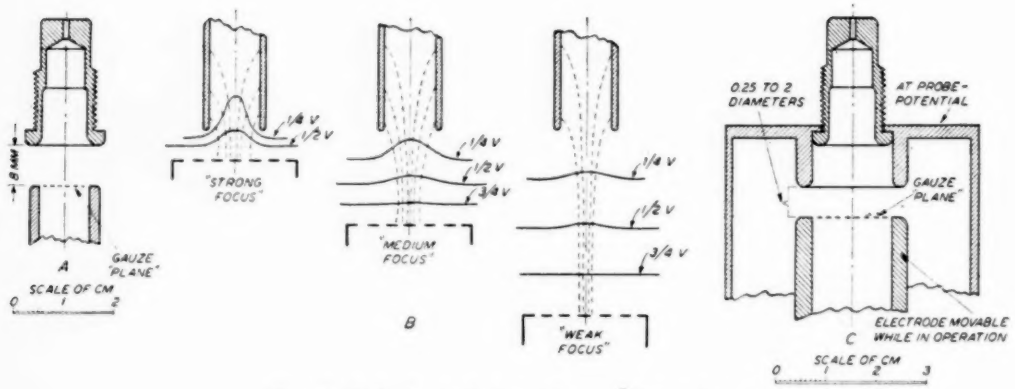


FIG. 7. Cylinder and plane—lens configurations.

The conclusion was reached that either the aberrations of a simple lens having the dimensions (and position) of 4*e* were too great to permit concentrating an ion beam to a distance of 85 cm without large dispersion, or else that this limitation was due to an insufficiently large ratio of the focus voltage to the probe voltage, permitting the side components introduced by curvature of the space-charge sheath in front of the probe to be too important.

Before turning to multiple acceleration through a succession of lenses as a means for carrying a concentrated ion beam to considerable distances, a series of brief tests was made with lens electrodes of other types. The focusing effect of a cylinder and plane arrangement was tested as shown in Fig. 7*a*. This gave a greatly magnified and somewhat distorted image on the screen (×30 at probe 1500 volts, focus 10 kv, screen at 85 cm) of an annular 100-mesh ring used for the plane, the center of the screen remaining dark and the pattern moving outward and enlarging as the focus voltage was increased (or the probe voltage decreased). Blanking off half the mesh by a sheet of metal foil showed that the effect was due to a very strong "over-focusing," the ions passing through the lens on one side of the beam crossing the axis on their way to the screen, and only a narrow (0.1-mm) annular ring or zone in the lens having the proper "focal length" for the screen at a given voltage. It was thought possible that control of the curvature of the lens zones might be effected by varying the gap between cylinder and plane as indicated by the equipotentials sketched in Fig. 7*b*. Installation of an electrode movable by rack and pinion as indicated in Fig. 7*c* showed that this was not the case, no focal spot whatever being obtainable with this arrangement on a screen at a distance of 140 cm, whereas the lens of Fig. 4*e* gave a spot 2 to 3 cm in diameter for currents up to 10 microamperes, even at this long distance.

TABLE VIII. *Observations on focusing with single lens and incidental negative lens (case of Fig. 6).*

| PROBE VOLTAGE (VOLTS) | OUTPUT CURRENT (μA) | REQUIRED FOCUS VOLTAGE (KV) | FARADAY CAGE CURRENT[a] (μA) | DIAMETER FOCAL SPOT (MM) |
|---|---|---|---|---|
| 100 | 1.5 | 2.5 | 1.6 | <10 |
| 200 | 2.3 | 4.5 | 3.7 | 10 |
| 350 | 4.5 | 7 | (7.8) | Some background |
| 500 | 7.2 | ... | (14 ) | Mostly background |
| 700 | 12 | 13 | (28 ) | No spot |

[a] Secondaries bad.

With the movable-electrode apparatus several other electrode arrangements were tested. Two modifications of the "negative lens" were tested, as shown in Figs. 8*a* and 8*b*; neither gave a satisfactory spot, although the much higher focus voltages required (22-kv focus for 1000-volt probe gave an annular spot 20 mm in diameter) permitted somewhat better definition at the expense of impracticable voltage requirements. The arrangement of two equal cylinders with variable spacing, shown in Fig. 8*c*, was similar to the standard lens in Fig. 4*e* and behaved similarly, giving a spot 20 to 30 mm in diameter without much background at currents under 10 microamperes but showing bad aberrations at higher currents (probe voltages). A spacing of 18 mm required 50 percent greater voltage for focusing than one of 14 mm, although the variation was less marked as the gap was decreased below this

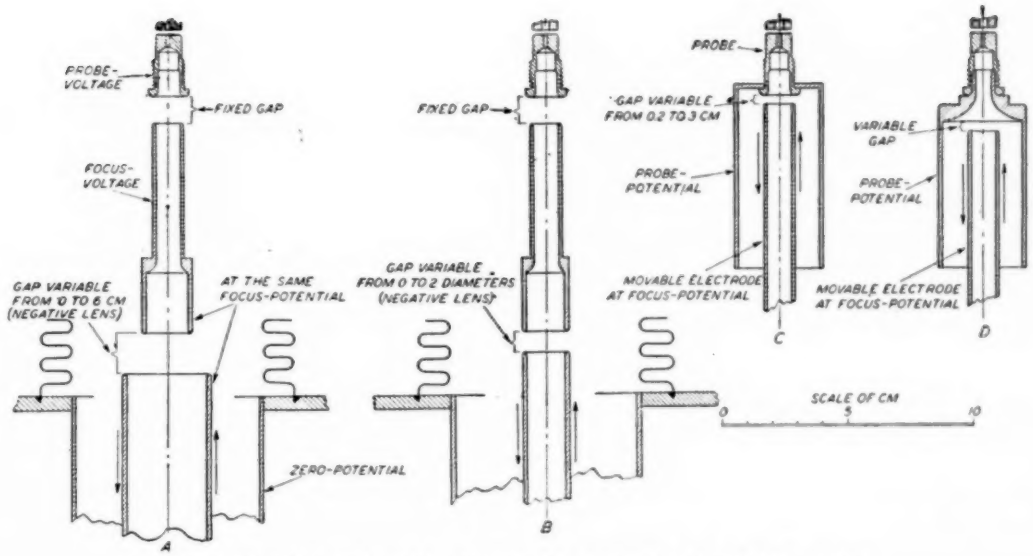


FIG. 8. Negative and positive lenses with electrodes of variable spacing.

to 1-mm spacing, the voltage required for focusing with the latter gap being only about 25 percent less than for the 14-mm gap. The arrangement of a cone and a movable electrode, shown in Fig. 8*d*, was similar in behavior to the cylinders of Fig. 7*c* when the cone-cylinder spacing exceeded 15 mm (the spot was very poor for smaller gaps), and required a somewhat lower voltage for the same focusing effect.

Thus no simple arrangement of electrodes was found which might serve with applied voltages under 25 kv to project a well-concentrated ion beam to distances much greater than 20 cm, especially with beam currents exceeding a few microamperes. Consequently the lens of Fig. 4*e* was adopted for the ion source focus control and tests of the important factors governing the behavior of multiple lens arrangements were begun.

## (C) The Electrostatic Focusing of Positive Ion Beams in High Voltage Tubes

In a brief investigation undertaken for the practical purpose of obtaining numerical information on the major factors involved in cascade type high voltage tube design, and which has proved a rational basis for a previously utilized empirical solution of the problem, which is not necessarily a unique solution, no attempt was made at completeness in the academic sense. In view of the scarcity (or absence) of information and data on this problem in the literature, however, it is thought that data on some of the rather poor electrode arrangements tested here may be of nearly as much interest as the simple specification of an electrode system which functions satisfactorily in a high voltage tube. Many discussions, largely innocent of experimental information, have been held regarding the desirability of one electrode arrangement or another for focusing of ion beams; these experiments outline certain features which are important and indicate the relative unimportance of others.

### (1) Focusing parameters

Among the variables more or less subject to choice or specification in the problem of ion beam focusing, the following may be listed for discussion and empirical examination.

(*a*) The $e/m$ of the ions should be of no influence in the case of simple electrostatic focusing. If the ions have fallen through the same total potential-difference before entering the "lens," electrons and heavy (negative) ions should describe the same paths, provided space charge can be neglected. This is a serious proviso however. With relatively slow moving ions and until data were obtained on high current densities at specified (low) voltages, no predictions could be made with confidence. It appears from our experiments that space-charge effects in the

ion beam itself as it travels are of less importance than the aberrations of the electrostatic lenses, which of course may be in part due to space-charge effects. If the latter is true, however, our experiments indicate that the lens aberrations are of practical importance even with the smaller ion currents. For distances of the order of 100 cm and beam currents above 10 microamperes, mutual repulsion (space-charge) effects in the beam itself probably become important.

(*b*) For the initial speed (voltage) of the ions entering the focusing field (electrostatic lens), the expected linear relationship between the initial voltage of the ions and the voltage required across a given lens to produce a given convergence of the beam is experimentally verified. The importance of lenses introduced where the beam is traveling slowly, and conversely the difficulty of altering the divergence of a high speed beam, are obviously indicated, as is also the clear-cut necessity for controlling the initial speed or the applied voltage, or both, if a beam is to be rendered parallel or brought to a focus at a given distant point by a given lens.

(*c*) The initial divergence of the ion stream affects its path through the lens and beyond and, unless the compensation by the lens is correctly adjusted for all angles of incident cones, we encounter the analog of spherical aberration. In this study we deal with ions of uniform energy emerging from a point, to be focused to a distant point; the analogs of chromatic aberration and off-axis astigmatism consequently are of no concern.

(*d*) The total beam current becomes important if thereby the space charge becomes sufficiently high, as indicated above, altering the field of the lens system and spreading the beam along its path due to mutual repulsion of the ions. Space-charge effects from our experiments appear somewhat less important than other disturbing factors.

(*e*) The beam area must not be too large, if serious aberrations are to be avoided, in comparison with (*f*).

(*f*) The dimensions of the lens (sizes of the electrodes) are important.

(*g*) The distance from the ion source to the lens, implicitly involved in several items above, is important enough to mention explicitly.

(*h*) The distance from the lens to the target or to the next lens is also important.

(*i*) The additive effects of multiple focusing gaps or lenses allow only a limited optical analogy, because of the change in speed or "stiffness" of the beam as it is accelerated by the successive lenses. In general, however, the division of the total voltage among a series of lenses placed at intervals along the total path of the beam probably results in much less aberration or spreading than is evidenced with a single lens using the same voltage and same path length. Our chief information on the behavior of multiple lens arrangements has come from our experience with cascade tubes, described in the paper on our high voltage technique.[1]

(*j*) The quantitative characteristics of various types and sizes of electrodes used for the lenses are of importance in problems of design. The actual voltages required with given electrodes to accomplish a desired focusing of a given ion current are of interest, as well as data concerning the importance of shape and dimensions of various possible electrode arrangements. We have examined to some extent each of the following electrode types:

(1) Equal cylinders—small, medium, large diameter; variable spacing (gap).

(2) Unequal cylinders—beam progressing from small diameter cylinder into large diameter cylinder and *vice versa*.

(3) Cone and cylinder, with variable spacing.

(4) Cone and plane (gauze), with variable spacing.

(5) Cylinder and plane (gauze), with variable spacing.

Our results may be summarized by the statement that if the ion source of Fig. 1 is attached as shown to the first lens (electrode gap) of a cascade type high voltage tube having additional sections exactly the same as the first, spaced not more than 40 or 50 cm apart and carrying 100 to 125 kv each at full voltage, with a beam travel beyond the final lens not exceeding 1 meter per 100 total kilovolts, then with proper adjustment of voltages on the lenses practically all of the ion current output of the source will be concentrated by the tube in an excellent focal spot not more than 2 or 3 mm in diameter.*

* *Note added in proof:* The short Isolantite insulators shown in Fig. 1 were used for spacing the tube-gap in these focusing tests only and will fail if the proportions shown are duplicated in a multiple-section tube for high

Currents as high as 1.0 milliampere from the capillary arc ion source have been concentrated on a 3-mm focal spot with a two-section tube having an applied voltage of 110 kv. Multiple-section tubes have been used at higher voltages but only for small currents.

### (2) Characteristics of individual lenses

Although our use of such tubes in transmutation experiments for more than two years had amply demonstrated that simple cascade type tubes having 4-inch diameter cylindrical electrodes separated by gaps of 2 inches, each section being $10\frac{1}{2}$ inches in total length, gave excellent focusing, and the recently developed capillary arc ion source with its focusing lens provided a highly satisfactory means for introducing an ion stream under control into such a tube, it appeared desirable to have further information for purposes of design. For example, information is needed concerning the properties of large and small diameter electrodes, of re-entrant electrodes (possibly desirable from the standpoint of shielding), on the effect of electrode spacing, and on the importance of target distance at low voltages and at high beam currents.

(*a*) *Large diameter equal cylinders, narrow spacing.* Tests were first made of the arrangement shown in Fig. 9*a* with the first "tube lens" at 40 cm from the arc capillary and a fluorescent screen (in a very crude Faraday cage) at a distance of 1 meter (from the arc). This lens was formed by two 4-inch cylinders separated 3/8 inch. It was immediately found that this arrangement gave an excellent (2- or 3-mm) focal spot on the screen provided the voltage on the tube lens was sufficient to prevent dispersion of the ion beam. With a good focal spot the whole of the ion current from the probe canal was concentrated on the screen. The probe voltage was found to have little or no effect on the focusing, the latter being controlled, with a fixed voltage across the tube lens, by the voltage across the lens *FL* of the ion source. The probe voltage consequently served to vary the beam current without appreciably changing the focusing. Tests were carried only to 2000 volts on the probe as another rectifier unit was not available. The data of Table IX show the behavior of this combination.

With the screen at the same distance (1 meter from arc capillary) an identical lens (4-inch diameter, 3/8-inch gap) was tried at a distance of 60 cm from the source as shown in Fig. 9*b*. This lens required the same focus voltages as the source lens *FL* and gave similar red hot focal spots (probably due to incandescent carbon from the material used for mounting the fluorescent salts) but the accompanying "background" was distinctly worse. In further tests the original lens at 40 cm was used with the fluorescent screen removed to a distance of 3 meters in the tube. With no voltage on the tube lens a spot 20 to 30 mm in diameter was obtained with 500 volts on the probe (7 microamperes) and 4.5 kv on the source lens *FL*; but upon raising the probe voltage to 1000 volts the "background" covered the whole screen and the "spot" decreased to the same intensity level. Application of 33 kv to the tube lens with a probe voltage of 1500 and 7.6 kilovolts on *FL*

TABLE IX. *Observations on focusing with ion source lens and one tube lens (case a of Fig. 9).* [Tube lens, 4-inch electrodes, 3/8-inch spacing; tube pressure 12$\mu$A (ionization-gauge).]

| Tube lens voltage (kv) | Probe voltage (volts) | Output current from probe ($\mu$A) | Required focus voltage (kv) | Faraday cage current ($\mu$A) | Diameter of focal spot and ring (mm) |
|---|---|---|---|---|---|
| 17 less focus voltage $\leqq$14 on lens | 300 | 4 | 2.4 | 5 | 3 |
| | 500 | 7 | 2.6 | 7.5 | 3; ring 6 |
| | 700 | 12 | 2.8 | 10 | Strong ring, 10 |
| | 1000 | 28 | 2.9 | 22 | Strong ring, 10 |
| | 1500 | 93 | 3.0 | 34 | Annular ring, 15 |
| | 2000 | 230 | 3.1 | 52 | Annular ring, 20 |
| 33 less focus voltage $\leqq$29 on lens | 500 | 7 | 4.0 | .. | .. |
| | 700 | 12 | 5.0 | 16 | 1, red hot spot |
| | 1000 | 28 | 5.2 | 38 | 1, red hot spot |
| | 1500 | 93 | 4.8 | 116 | 1, very red spot |
| | 2000 | 230 | 4.8 | 163 | 1, very red spot; ring, 30 |
| 50 less focus voltage $\leqq$43 on lens | 500 | .. | 3.8(?) | 8 | Poor spot; background (?) |
| | 700 | .. | 5.0(?) | .. | (?) |
| | 1000 | .. | 5.0 | .. | 20 |
| | 1000 | 28 | 7.2 | (24 to 30) | 2, red hot spot |
| | 1500 | 93 | 7.1 | ($\leqq$200) | *Bright* red spot |
| | 2000 | .. | .. | ($\leqq$300) | 2, *yellow* hot spot |
| 50 less focus voltage $\leqq$43 on lens | 1000 | .. | 5.0 | .. | 12 |
| | 1000 | .. | 6.0 | .. | 5 |
| | 1000 | .. | 7.1 | .. | 2, red hot spot |
| | 1000 | .. | 8.0 | .. | 4, not red |
| | 1000 | .. | 9.0 | .. | 10 |

voltages, due to the "cascading effect." The latter causes very high transient voltages to be impressed on subsequent sections if a tube-flash starts in one section. Such transients have extremely steep wave fronts. The electrodes of our multiple-section tubes are supported by the glass tube itself, with the metal parts so disposed as to prevent unduly high electric fields at metal surfaces adjacent to the glass, in spite of its high dielectric constant, and with spark-over in air between the tube-shields providing a "by-pass" of low impulse-ratio.

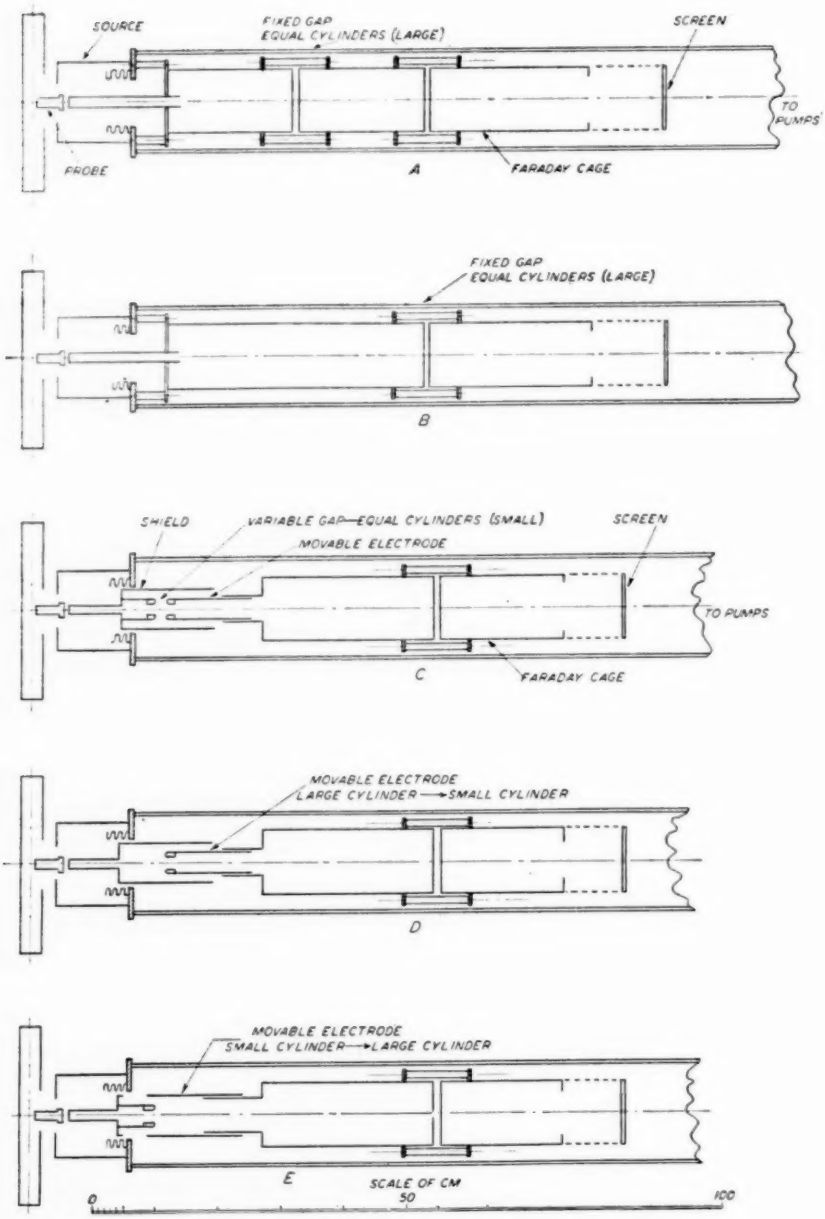


FIG. 9. Dimensions and positions of various electrodes used in tests of focusing effect of first tube gap.

gave 30 microamperes on the screen, but the "spot" spread over the whole screen and no adjustments gave any improvement. It was concluded that the distance was too great for a small diameter ion beam exceeding 10 microamperes at these voltages. In all of these tests at currents above 100 microamperes the ion beam was faintly visible in the tube beyond the tube lens, provided the voltages were set to make its diameter less than 10 mm.

(*b*) *Small diameter equal cylinders, variable spacing.* To determine the effect of variations in the diameter and spacing of the cylindrical electrodes used as the tube lenses, tests were next made, for the arrangement shown in Fig. 9*c*, with small diameter cylinders as electrodes one of which was movable by rack and pinion to vary the spacing or gap of the lens. The fluorescent screen was left at one meter from the arc capillary, but it was thought more nearly

TABLE X. *Observations on focusing with ion source lens and small diameter tube lens (case c of Fig. 9).* [Tube lens electrodes about 25-mm diameter (rounded), variable spacing or gap.]

| TUBE LENS VOLTAGE (KV) | GAP BETWEEN ELECTRODES OF TUBE LENS (MM) | PROBE VOLTAGE (VOLTS) | OUTPUT CURRENT FROM PROBE (μA) | REQUIRED FOCUS VOLTAGE (KV) | FARADAY CAGE CURRENT (μA) | DESCRIPTION OF SPOT |
|---|---|---|---|---|---|---|
| 17 LESS FOCUS VOLTAGE ≦12 ON LENS | 4 | 2000 | 230 | 5.7 | 70 | Hardly visible |
| | 15 | 2000 | 230 | 5+ | 50 | |
| | 40 | 2000 | 230 | 4+ | 42 | |
| | 15 | 1000 | 28 | 5.2 | 22 | |
| 33 LESS FOCUS VOLTAGE ≦23 ON LENS | 2 | 2000 | 230 | 11.7 | 160 | Red hot spot; annular rings; background |
| | 7 | 2000 | 230 | 10.9 | .. | |
| | 15 | 2000 | 230 | 10.0 | .. | Red; less background |
| | 24 | 2000 | 230 | 9.5 | 160 | Red |
| | 40 | 2000 | 230 | 8.4 | .. | Yellow hot spot; no visible background |
| | 15 | 1000 | 28 | 10.0 | 25 | Very faint spot still focused |
| 50 LESS FOCUS VOLTAGE ≦40 ON LENS | 4 | 2000 | 230 | 15 | 225 | Red hot spot; strong background |
| | 15 | 2000 | 230 | 13.5 | 225 | Bright red spot; much less background |
| | 24 | 2000 | 230 | 12 | 225 | Yellow hot spot |
| | 40 | 2000 | 230 | 11 | 225 | Bright yellow spot |
| | 15 | 1000 | 28 | 13.5 | (40) | Still focused |

correct for comparison with the 4-inch lens to have this smaller tube lens nearer the source, and it was placed at 20 cm instead of 40 cm as before. The measurements with this lens showed that these smaller diameter electrodes concentrated the total ion current from the source onto the screen nearly as completely as did the 4-inch electrodes, although below 50 kv both large and small lenses failed to focus the total current entering the tube for the higher currents. It is probable that there is no great difference between the two lenses as regards the completeness of focusing, both sizes focusing the total available current onto the target, but the smaller electrodes at close spacings gave definite evidence of worse aberrations, as indicated by the general background accompanying the focal spot. The aberrations are less at the larger spacings, which require a lower speed of the incident beam for the same focusing effect, the focusing effect of the lens itself being smaller at the wider spacings.

TABLE XI. *Observations on focusing with ion source lens and reentrant tube lens, from large cylinder into small cylinder (case d of Fig. 9).*

| TUBE LENS VOLTAGE (KV) | PROBE VOLTAGE (VOLTS) | OUTPUT CURRENT FROM PROBE (μA) | REQUIRED FOCUS VOLTAGE (KV) | FARADAY CAGE CURRENT (μA) | DESCRIPTION OF SPOT |
|---|---|---|---|---|---|
| 50 LESS FOCUS VOLTAGE ≦40 ON LENS | 2000 | 230 | 10.3 | 160 | Yellow hot, 2-mm. diam. |
| | 1500 | 98 | 10.4 | 70 | |
| 33 LESS FOCUS VOLTAGE ≦10 ON LENS | 2000 | 230 | 7.2 | 110 | Red hot |
| 17 LESS FOCUS VOLTAGE ≦4 ON LENS | 2000 | 230 | 4.2 | 60 | |
| | 1000 | 28 | 4.1 | 25 | |

In general, these electrodes $1\frac{1}{4}$ inches in diameter have nearly twice the focusing effect of the 4-inch electrodes (require nearly twice the voltage on lens *FL* of the ion source to prevent overfocusing of the beam by the tube lens).

(*c*) *Reentrant electrodes.* Because of the possibility that reentrant electrodes might be desirable to shield the ion beam from deflection by charges on the glass walls of the high voltage tube, brief tests were made of two such arrangements, although the fact that closely spaced electrodes of large diameter also had been found satisfactory largely eliminated any possibility that reentrant electrodes might be necessary.

The arrangement of Fig. 9*d*, in which the ion beam is accelerated from a large cylinder into a small cylinder, was first tested. Although excellent (2-mm) focal spots were again obtained, the total output ion current did not reach the screen even at 50 kilovolts. The focusing effect of this arrangement (required "stiffness" of incident beam) was comparable to that of two equal cylinders the size of the smaller one used.

TABLE XII. *Observations on focusing with ion source lens and reentrant tube lens, from small cylinder into large cylinder (case e of Fig. 9).*

| TUBE LENS VOLTAGE (KV) | PROBE VOLTAGE (VOLTS) | OUTPUT CURRENT FROM PROBE (μA) | REQUIRED FOCUS VOLTAGE (KV) | FARADAY CAGE CURRENT (μA) | DESCRIPTION OF SPOT |
|---|---|---|---|---|---|
| 50 LESS FOCUS VOLTAGE ≦13 ON LENS | 2000 | 230 | 13.4 | 185 | Bright yellow, 2-mm diam. |
| | 1500 | 98 | 13.3 | 75 | Yellow |
| 33 LESS FOCUS VOLTAGE ≦9 ON LENS | 2000 | 230 | 8.1 | 125 | Bright red |
| | 1500 | 98 | 9.0 | 70 | Red; visible background |

The reverse of this arrangement was also tested, the ion beam being accelerated from a small cylinder into a larger cylinder as indicated in Fig. 9*e*. This lens also appeared to give an excellent focal spot, although again focusing less than 100 percent of the probe canal output current.

(*d*) *Conclusions.* It is clear from the above tests that almost any arrangement of electrodes can be used with fair or even excellent success in a cascade type, multiple lens, high voltage tube, focusing most or all of the ion current entering the lens system onto a distant target *provided* the various voltages (including the ion source) are adjusted in relation to each other. Such considerations as the desirability for some problems of working with an ion beam spread uniformly over a comparatively large area (for example, 10-cm diameter) serves to indicate that electrodes of fairly large diameter are desirable, at least in the sections of the tube nearest the target. Again, if it is desired to apply a voltage of the order of 100 kv to the first section of the high voltage tube (nearest the ion source), it is also desirable to select fairly large diameter electrodes for this section (and those adjacent) in order that an inconveniently high voltage will not be required on the lens *FL* of the ion source to provide a beam of the requisite "stiffness" on entering the first tube lens.

### (3) Successive lenses

Our knowledge of multiple lens arrangements is chiefly the qualitative information we have obtained during the past several years in using tubes having from 6 to 23 lenses for focusing ion currents up to 20 microamperes on distant targets at voltages from 200 to 1200 kv. That it is possible with such tubes to focus on the target all or nearly all of the ion current entering the tube, by proper control of the voltages applied to the first several lenses, already has been mentioned. In connection with the experiments described in this paper we have made only one set of observations with voltage applied to more than one tube lens. Using the arrangement of Fig. 9*a* with a potential of 70 kv on the tube lens nearest the ion source, currents up to 1000 microamperes were satisfactorily concentrated on a 3-mm focal spot on the screen. With 60 kv on the lens 700 microamperes was the maximum current which could be concentrated on the focal spot at the given distance and this current was correspondingly less at lower voltages. A second rectifier unit was then connected across the second tube lens, hitherto used as part of the Faraday cage for the target. Because of secondary electron emission the target currents were very unreliable, but it was interesting to find that when the ion source and first tube gap were left at given voltage settings, the indicated target current and the shape and size of the focal spot changed very little or not at all when the voltage across the second tube lens was changed from 10 kv to 65 kv. Some change in the brilliance of the focal spot was noticeable, due to the increase of 55 kv in the total tube voltage. This experiment again demonstrated the relative unimportance of the subsequent tube lenses after the ion beam has once attained an energy equal to or exceeding that corresponding to the voltage across a single tube lens. It also served to emphasize the importance of giving the initial ion beam the proper characteristics before introducing it into the lens system of the tube, since the focus voltage of the ion source continued to control the size of the focal spot.

The writers take pleasure in recording their indebtedness to Dr. F. L. Mohler and to Dr. C. M. Van Atta for their contributions to this work.

# The Variation with Magnetic Field and Temperature of the Thermoelectric Properties of Ferromagnetics*

F. E. LOWANCE AND F. WOODBRIDGE CONSTANT, *Duke University*

(Received May 28, 1935)

It was first shown by Sir Wm. Thomson that a thermocouple may be composed entirely of iron or nickel provided part is in a magnetic field and part not. A survey of the work previously done on this subject and an experimental investigation of a more extended nature than any heretofore have been attempted in order to clear up existing confusion and render the subject more available to theoretical interpretation. Measurements on iron, nickel, cobalt and permalloy from room temperature to above the Curie point indicate that the e.m.f. produced by a magnetic field in these thermocouples is conditioned by (1) the crystal structure and (2) the change in direction of the resulting spins or intrinsic magnetization in separate crystal regions, and that this effect is related to the change in length on magnetization.

## INTRODUCTION

IT was first shown by Sir Wm. Thomson[1] in 1856 that a thermocouple may be constructed entirely of iron or of nickel provided the two parts are in different states of magnetization. Numerous investigations have since been made of the effect with conflicting results. Thomson,[1] Battelli[2] and Broili[3] found the e.m.f. opposite for iron and nickel, but Strouhal and Barus,[4] Chassagny,[5] Bidwell,[6] Cohen,[7] Grondahl and Karrer,[8] Bordoni,[9] T'Ao and Band,[10] Ross[11] and finally Perrier and Kousmine[12] have found the e.m.f. positive, i.e., from magnetized to unmagnetized metal at the cold junction, in both cases. (Here and elsewhere reference is to a longitudinal field; a transverse field generally gives the opposite direction to the effect.) In the case of iron the e.m.f. was sometimes observed to decrease for strong magnetic fields and Bidwell,[6] Houllevigue,[13] Rhoads,[14] Smith[15] and Broili[3] actually obtained a reversal, although Smith applied tension and Broili "recrystallized" his specimen. This decrease or reversal in strong fields suggested to some[6, 15, 16] a connection with the similar change in length on magnetization, but in the case of cobalt[6] and Heusler alloys[8] no relationship was found. Others[15, 17, 18] have postulated a connection between this effect and the change of resistance in a magnetic field, but the analogy is close only for nickel. Finally the state of confusion in regard to this effect has recently been exemplified by Gerlach[17] and by Ross[11] and Williams[19] who have reported a "new effect" which is in reality only that discovered by Thomson.

In view of the present confused state of the subject of Thomson's thermomagnetic effect the present attempt has been made first to review all the previous work done, and second, to repeat experimental measurements. In previous work

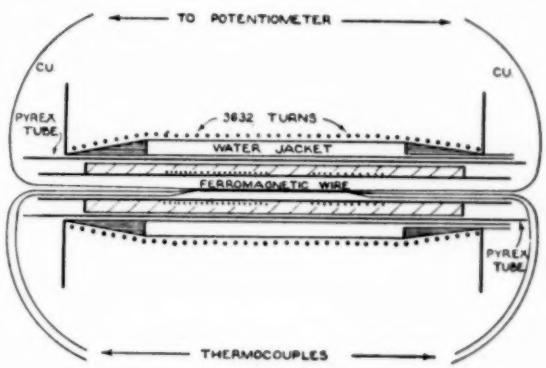


FIG. 1. Cross section of furnace and solenoid.

* Part of a thesis submitted by F. E. Lowance in partial fulfilment of the requirements for the Ph.D. degree in the Graduate School of Arts and Sciences of Duke University.

[1] Wm. Thomson, Phil. Trans. London **146**, 709 (1856).
[2] A. Battelli, Rend. Acc. Linc. (5) **2**, 162 (1893).
[3] H. Broili, Ann. d. Physik **14**, 259 (1932).
[4] V. Strouhal and C. Barus, Wied. Ann. **14**, 54 (1881).
[5] Chassagny, Comptes rendus **116**, 977 (1893).
[6] S. Bidwell, Proc. Roy. Soc. **A73**, 413 (1904).
[7] F. Cohen, Ann. Fac. Sci. Marseille (II) **18**, 51 (1909).
[8] Grondahl and S. Karrer, Phys. Rev. **33**, 531 (1911); (2) **4**, 325 (1914).
[9] U. Bordoni, Nuov. Cim. (6) **2**, 245 (1911).
[10] S. C. T'Ao and W. Band, Proc. Phys. Soc. **44**, 166 (1932).
[11] W. H. Ross, Phys. Rev. **38**, 179 (1931).
[12] A. Perrier and T. Kousmine, Comptes rendus **198**, 810, 920 (1934).
[13] L. Houllevigue, J. de physique (3) **5**, 53 (1896).
[14] E. Rhoads, Phys. Rev. **15**, 321 (1902).
[15] A. W. Smith, Phys. Rev. **19**, 285 (1922).
[16] Bachmetjew, Wied. Ann. **43**, 723 (1891).
[17] W. Gerlach, Proc. Phys. Soc. **42**, 418 (1930).
[18] W. Chang and W. Band, Proc. Phys. Soc. **45**, 602 (1933).
[19] S. R. Williams, Phys. Rev. **39**, 368 (1932).

the effect has been studied with only one or two substances at a time and often without uniform magnetization or a wide temperature range, whereas in this attempt the effect has been studied by comparison of the magnetized metal in a uniform field with the same metal unmagnetized, from ordinary temperatures to above the Curie points, under identical conditions for each of the metals used and for as many different substances as possible in order that the resulting data might be more available for interpretation.

## Experimental Method

Wires of iron, nickel and cobalt were secured from Baker and Co.; they had been prepared by the Taylor process and were 99.9 percent pure or better by analyses. The iron and nickel were 0.2 cm in diameter and approximately 14 cm long, while the cobalt was 0.025 cm in diameter and 10 cm long. The permalloy wires, kindly donated by the Bell Telephone Laboratories, contained 78.5 percent nickel and were 0.05 cm in diameter and 10 cm long.

To demagnetize the specimens the iron wires were heated to 800°C and two nickel wires to 450°C and allowed to cool slowly in vacuum. One nickel wire was simply demagnetized by the method of reversals but the experimental results were the same for this wire as for the other two nickel wires which were heated above the Curie point, hence thereafter all specimens were demagnetized by reversals. All specimens were eventually heated a little above their Curie points during the course of the measurements, but their properties were not affected appreciably.

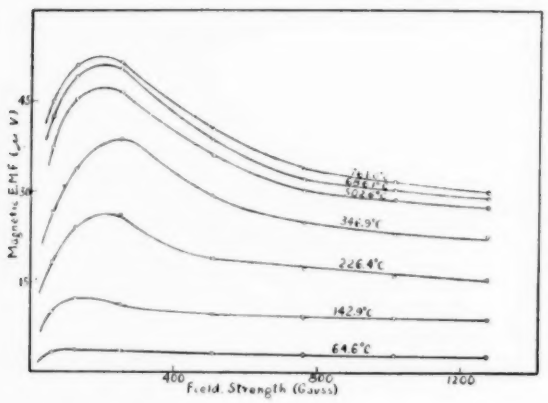


Fig. 2. Iron with cold junction temperature of 32.0°C.

In order to compare magnetized with unmagnetized materials the thermal e.m.f. of each was measured against copper, first for the demagnetized state and then when subjected to uniform longitudinal fields up to 1300 gauss. Thus the specimens could be held entirely in a uniform field and the transition regions relegated to the copper part of the circuit. The experimental arrangement is shown in Fig. 1. The specimen was welded to copper leads and copper-constantan thermocouples held in contact with the junctions by wrapping with fine copper wire. The specimen was then placed in an alundum tube carrying two noninductive windings for controlling the temperature of each end. The tube was covered with an asbestos coat and was all contained in a Pyrex tube which was sealed at the ends and evacuated, thus preventing oxidation and reducing heat conduction. This was all placed inside a water-cooled solenoid with tapered ends. A search coil showed the field produced constant within one percent over the middle third, which contained the specimen. A null method using an L. and N. type $K$ potentiometer for measuring the e.m.f.'s was sensitive to 1/10 microvolt. The temperatures of the junctions were maintained constant to 1/300°C during the interval in which measurements were made. It was necessary to insulate each part of the apparatus by using sulphur blocks for supports in order to eliminate electrical leaks and galvanometer drift.

## Results and Conclusions

Although two or three wires of each material were tested the results for the specimens of the same metal did not differ appreciably. In Figs. 2, 3, 4 and 5 is shown the change in the normal thermal e.m.f. against copper on application of magnetic fields up to 1300 gauss for iron, nickel, cobalt and permalloy, respectively. This is called $\Delta E$ or the "magnetic e.m.f." and also represents the e.m.f. of each metal magnetized against the same metal unmagnetized. In every case $\Delta E$ was positive except for cobalt when it was slightly negative unless the hot junction, $T_2$, was above 350°–400°C when it again became positive. Remembering that the normal e.m.f. against

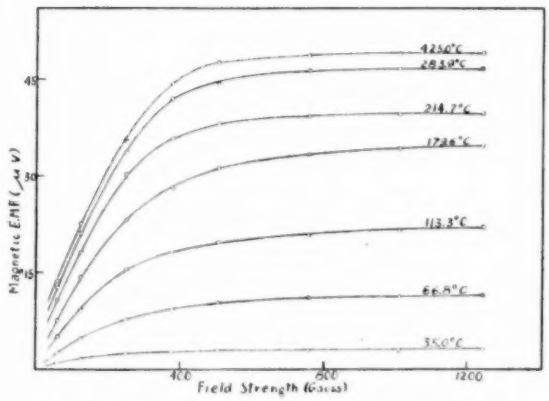


FIG. 3. Nickel with cold junction temperature of 22.5°C.

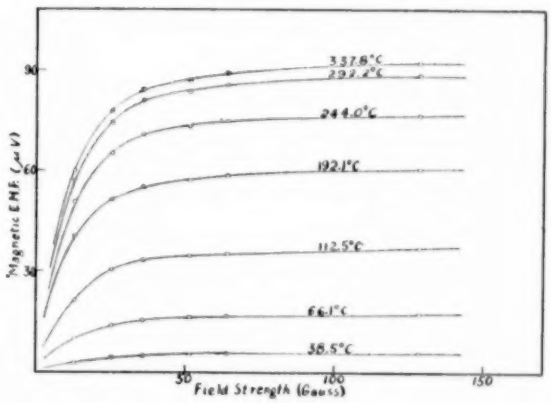


FIG. 5. Permalloy with cold junction temperature of 25.0°C.

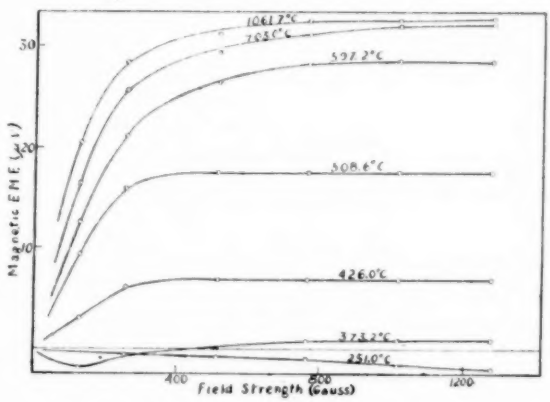


FIG. 4. Cobalt with cold junction temperature of 56.1°C.

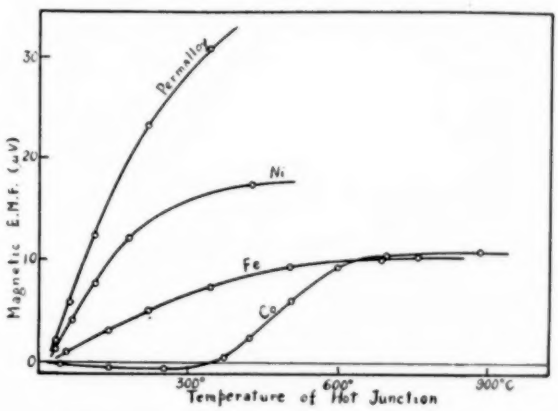


FIG. 6. Cold junction at 25°C, $H = 1018$ gauss.

copper is negative for nickel, permalloy and cobalt, and for iron above about 470°C, it is seen that $\Delta E$ represents an actual decrease in the magnitude of the total e.m.f. against copper for nickel and permalloy, for cobalt above 350°–400°C and for iron above 470°C, otherwise $\Delta E$ represents an increase in the size of $E$.

In Fig. 6 is shown the variation of $\Delta E$ with the temperature of the hot junction, $T_2$, for a field of 1018 gauss. Each curve was carried above the Curie point except for cobalt and in every case saturation was attained as the Curie point was approached. This indicated the effect was truly a ferromagnetic one. It was also noted that the direction of the field made no difference provided it was longitudinal. Finally, although demagnetization was carried out for the data shown in the figures, it was found that the data could be nearly duplicated without demagnetization between readings, indicating that the specimens were magnetically very soft (the $B$ *vs.* $H$ curves were also actually found), as was also suggested by the failure of the effect to show any hysteresis with the field.

The data show similar behavior for nickel and permalloy, and for cobalt at higher temperatures; in each of these cases the crystal structure is the same, face-centered cubic. Iron, which is body-centered cubic, and cobalt below 400°C, when it is hexagonal, gave quite different results. The conclusion is that crystal structure is one of the factors governing the effect.

The curves for change of resistance with magnetic field are of the same type for all the four metals, and although similar to the $\Delta E$ curves for nickel, cobalt above 400°C and permalloy there is no analogy in the case of iron. This indicates no close relationship between these two effects.

The change in length on magnetization shows a

closer resemblance, the curves being very similar in shape and sign to those for $\Delta E$ except in the case of nickel where $\Delta l$ is negative and $\Delta E$ positive. In the case of iron the analogy is very close, the $\Delta l$ *vs.* $H$ curves showing the type of maxima in Fig. 2. In the case of the change of length an explanation has been found by studying single crystals. For iron the (100) is the direction of easiest and the (111) of hardest magnetization, and $\Delta l$ is always positive for the former and negative for the latter.[20] A polycrystalline specimen would therefore show the combined effects for single crystals magnetized parallel to (100) and (111) directions, respectively, the direction of easy magnetization predominating for low fields. The same explanation may be advanced for the $\Delta E$ curves. The following summarizes the picture: According to Weiss' and later theories a ferromagnetic substance is regarded as containing regions or "blocks" of the order of $10^5$ atoms which are magnetized to saturation without an external field; on gradually increasing the external field the "blocks" are lined up parallel to that (100) direction in each crystal nearest that of $H$, thereby increasing $l$ and $E$, the resistance, $R$, remaining unchanged; finally in strong fields the "blocks" must turn slowly from (100) directions into more exact parallelism with $H$ or somewhat in (111) directions, thereby decreasing $l$ and $E$ and increasing $R$. A similar picture follows for the other metals. In the case of nickel $\Delta l$ is of the same sign[21] and hence also $\Delta E$ for all directions and the (111) is the direction of easiest magnetization. It would appear that $\Delta E$ and $\Delta l$ are both due to the same thing.

The above conclusions are in accord with those of Akulov[22] and Chramov and Lwowa,[23] who conclude that $\Delta E$ may be produced by magnetization or stretching and is conditioned by (1) crystal structure of specimen, (2) change of direction of resulting spins in separate crystal regions.

[20] W. L. Webster, Proc. Roy. Soc. **A109**, 570 (1925); Proc. Phys. Soc. **42**, 431 (1930).

[21] Mashiyama, Sci. Rep. Tohôku Univ. **17**, 948 (1928).
[22] N. Akulov, Zeits. f. Physik **87**, 768 (1934).
[23] P. Chramov and L. Lwowa, Zeits. f. Physik **89**, 443 (1934).

AUGUST 1, 1935 PHYSICAL REVIEW VOLUME 48

# The Relation Between the Electron Field Emission and the Work Function of Liquid Mercury

L. R. QUARLES, *Rouss Physical Laboratory, University of Virginia*

(Received June 3, 1935)

The variation in the field necessary to initiate a vacuum discharge between a mercury cathode and a molybdenum anode and the accompanying variation in the work function of the cathode have been measured. The work function variations were obtained from measurements of the contact potential between the mercury and a platinum filament. The fields were applied by an impulse circuit, the time constant of the voltage wave being very short in order to prevent distortion of the mercury. The final results show a variation of the field with work function which, while in the same direction, is more pronounced than that forecast by the Fowler-Nordheim theory. For a change of work function of one volt the field required to initiate the discharge varied from 375 kv/cm to 575 kv/cm.

## INTRODUCTION

NUMEROUS experiments[1] have been performed to study the relation between the field current and the field strengths involved. Several theories[2] have been proposed to forecast what this relation should be or to fit the experimentally found relation, the latest being that of Fowler and Nordheim. As a whole the results of various experiments on the problem have been capable, after making an assumption regarding the work function of the surface serving as cathode, of being fitted to an expression such as they have deduced.[3] The present experiments were carried out to investigate the relation con-

[1] Millikan and Eyring, Phys. Rev. **27**, 51 (1926); Eyring, Mackeown and Millikan, Phys. Rev. **31**, 900 (1928); Gossling, Phil. Mag. **1**, 609 (1926); Millikan and Lauritsen, Proc. Nat. Acad. Sci. **14**, 46 (1928).

[2] Schottky, Zeits. f. Physik **14**, 63 (1923); Richardson, Proc. Roy. Soc. **A117**, 173 (1928); Houston, Zeits. f. Physik **47**, 33 (1928); Fowler and Nordheim, Proc. Roy. Soc. **A119**, 173 (1928).

[3] Stern, Gossling and Fowler, Proc. Roy. Soc. **A124**, 699 (1929).

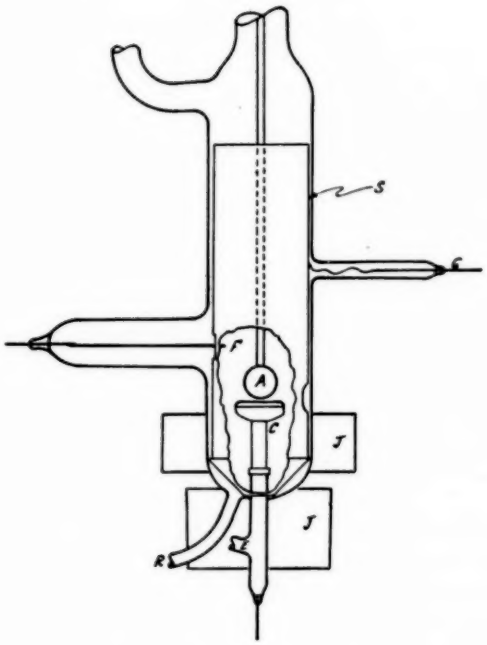


FIG. 1. The discharge tube.

necting the work function and the field with a fixed current density.

It has been shown[4] that a vacuum spark is initiated by field emission from the cathode. The rapid variation of the current density with field justifies the assumption that the density to start the discharge is practically constant, or if not constant, at least the variation of field will be small over the range of variation of the required current, on the assumption the criterion used for the field emission was the passage of a discharge between the cathode being studied and the anode. This does away with the need of measuring the current and thereby simplifies the use of impulsive fields which have a decided advantage in the experiment as described below.

Mercury was chosen as the cathode material both on account of the ease with which its work function could be varied by vacuum distillation and because it would automatically assume a plane surface, free of polish imperfections. However, this eliminated the possibility of using steady fields, since a steady field would very seriously distort the surface and thus make impossible a fair calculation of the field strength from the value of the applied voltage. This called for impulsive potentials of short duration to avoid any appreciable movement of the mercury.

The method adopted for measuring the work function was to measure the contact potential between the mercury and some fixed standard. It has been shown by several investigators[5] that the contact potential difference between two metals is equal to the difference of their work functions except for a negligible correction. Cassel and Glückauf[6] have shown that mercury vapor has no effect on the work function of a platinum filament, so platinum was chosen as the standard for measuring the contact potential.

## APPARATUS

The discharge tube is shown in Fig. 1. In addition to the part shown here, there was an extension of the upper part with an enclosed armature by means of which the spherical anode could be drawn into the upper part of the tube. The Pyrex glass envelope, $6.5 \times 25$ cm, was lined with a nickel shield to reduce disturbing effects in the electrometer circuit used for measuring the contact potential. The platinum filament $F$, 0.2 mm diameter and 2.5 cm long, was inserted from the side, supported by leads of 100 mil nickel wire. The cathode consisted of the mercury contained in the iron cup $C$, 3.5 cm diameter and about 1.2 cm deep, and which was sealed to the glass with silver chloride. Iron was chosen to eliminate the accumulation of electric charges by the overflowing mercury. The condition of the mercury surface could be altered by distillation similar to the method described by Beams.[4] The mercury entered from the still at $E$, flowed up to the cup, overflowed and returned to the still through the tube $R$. A two cm molybdenum sphere $A$ was suspended above the mercury to form the anode for the field emission measurements. The support for this was the iron rod shown extending into the upper part of the tube. The sections $J$ were jackets for packing dry ice to lower the vapor pressure of the mercury.

[4] Snoddy, Phys. Rev. **37**, 1678 (1931); Beams, Phys. Rev. **44**, 803 (1933).

[5] Richardson, Phil. Mag. **23**, 261, 615 (1912); see also Darrow, Phys. Rev. Supp. **1**, 147 (1929); Richardson and Compton, Phil. Mag. **24**, 575 (1912); Millikan, Phys. Rev. **18**, 236 (1921); Richardson and Robertson, Phil. Mag. **43**, 557 (1922); Van Voorhis, Phys. Rev. **30**, 318 (1928).

[6] Cassel and Glückauf, Zeits. f. physik. Chemie **18**, 347 (1932).

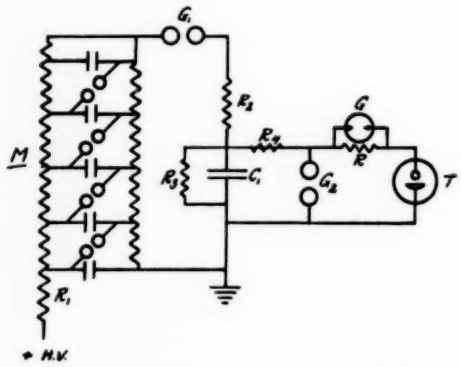


FIG. 2. Method of applying impulse potential.

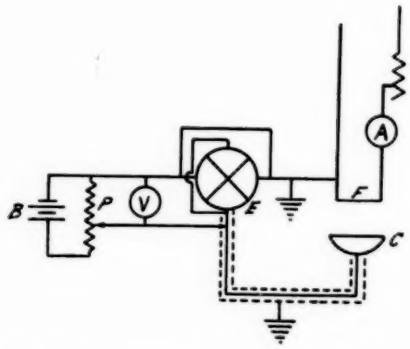


FIG. 3. Circuit for measuring contact potential between the mercury and platinum.

The vacuum system was standard with liquid air trap, McLeod gauge, two-stage mercury pump with the oil fore pump. However, no stopcocks were used except at the fore pump, all other cutoffs being of the mercury type. There was one, which was kept closed except when the pumps were operating, between the diffusion pump and the stopcock in order to decrease the danger of grease vapors getting into the system. The entire system except for the fore pump was mounted on a heavy table which was set on automobile inner tubes to eliminate transmission of building vibrations to the mercury surface serving as cathode.

Fig. 2 shows the high voltage impulse circuit. This circuit was charged by an x-ray transformer and synchronous rectifier system adjusted to supply about 28 kv to ground. The impulse circuit itself consists of the Marx circuit $M$, the isolating gap $G_1$ (12.5 cm brass hemispheres) charging resistor $R_2$ and condenser $C_1$, measuring gap $G_2$ (10 cm brass spheres), resistor $R$ and glow tube $G$, and the discharge tube $T$. The glow tube was used to indicate the presence of oscillations and to show the polarity of the discharge. The resistors in the various circuits were adjusted to values to prevent oscillations. The Marx circuit was set to deliver about 85 kv peak. $G_2$ was irradiated with ultraviolet light from an iron arc during all measurements.

The electrical connections used in determining the contact potential difference of the filament and mercury are shown in Fig. 3. Here $F$ is the filament and $G$ the cup of mercury of the discharge tube. $E$ is a Swann electrometer which was operated heterostatically. The lead from the tube to the electrometer insulated quadrants consisted of a wire surrounded by 2.5 cm brass tubing, the wires being insulated by sealing wax in the ends of the tube. The quadrants and mercury system were charged from the $B$ battery and potentiometer arrangement $P$. All connections in the electrometer system were soldered to prevent changes of their contact potentials.

Before any measurements were taken the tube and mercury still were baked about 5 hours at 300–350°C, the rest of the vacuum system being torched out in the meantime. The first part of this baking was done with no liquid air on the trap and the latter part with it. Liquid air was then kept on the trap continuously until all measurements were completed. After baking out the system the mercury, which had been cleaned by the Roller[7] process, was put in and the system immediately re-evacuated. All parts of the system which enclosed moving mercury had to be painted with "Aquadag" on the outside and wrapped in tin foil to prevent disturbing charges as much as possible.

Before making any tests the platinum filament of the tube was heated for several minutes at a current higher than that needed for the tests, and heating continued for a half-hour at the test current. Before each measurement the filament was again heated for a few minutes to drive off any mercury which might have condensed on it.

## PROCEDURE

The sphere $A$ of Fig. 1 was drawn up to the upper part of the tube and held there while

[7] Roller, J. O. S. A. and R. S. I. **18**, 357 (1929).

making contact potential measurements. The sphere and shield of the tube were grounded and the filament energized at constant current. For the contact potential determinations the electrometer quadrant and mercury system were charged to a definite voltage with respect to ground. Then this system was isolated by raising the key of the electrometer for five seconds. The deflection of the electrometer needle for this period gave a measure of the current which had passed between the filament and the mercury. Several values of the voltage applied to the mercury then gave enough points to plot a curve of the thermionic characteristic of the diode formed by the filament and the mercury. Displacements of these characteristics along the voltage axis between different runs gave the change of contact potential difference between the tube elements, and since the platinum does not change its surface condition this gives the change in the mercury surface. Another method of determining this change of contact potential was to charge the electrometer to a given potential as before and then raise the key and let the system discharge to equilibrium. This point gave the value of the voltage when the potential still applied to the mercury was equal and opposite to the contact potential difference of the mercury and platinum, thus the net voltage across the tube was zero and there was no passage of electrons from the filament to the mercury. These two methods checked almost exactly. These changes in contact potential difference are equal to changes in work function of the mercury.

The surface condition having been determined, the sphere was lowered into position just above the mercury surface and the field necessary to initiate a vacuum discharge was taken. The Marx circuit, Fig. 2, was energized and the measuring gap $G_2$ set to a small value. When the impulse circuit fired, the condenser $C_1$ charged, at a rate determined by $R_2$, until the voltage across $G_2$ was sufficient for breakdown, when it removed the potential from the tube. The next impulse was applied with $G_2$ set a little wider and so on until a value of $G_2$ spacing was reached when the discharge went through the tube instead of to the measuring gap. This value of the gap spacing then gave the value of the voltage necessary to initiate the discharge between the sphere and the mercury. The actual field at the surface could then be calculated from the expression[8]

$$E=2V/(f+1)x,$$

where $E$ is the field, $V$ the impressed voltage, $f$ a function of $x$ and the radius of the sphere, is found from tables, while $x$ is the spacing between the sphere and the mercury. This latter quantity was determined by means of a telescope with movable cross-hairs.

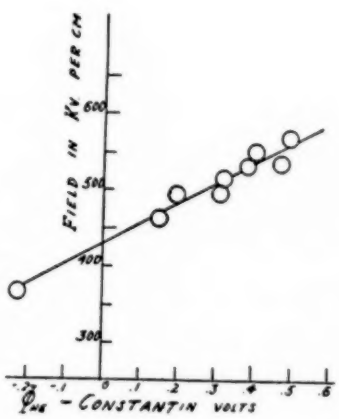


FIG. 4. Breakdown field as a function of the work function of the mercury.

Having obtained a complete set of data in this way, the mercury surface was altered. This was done in several ways and the result was uncontrollable. Sometimes the mercury was distilled, a new set of data being taken just after it overflowed in the cup. At others it was allowed to stand for long periods without distilling. These usually changed the surface condition but a given treatment did not always give the same sort of change. This, however, was unimportant since the surface condition was actually measured and a change of some sort was all that was wanted. After changing the surface new data were taken for the surface and the field, giving another point on the curve.

## RESULTS

The curve of Fig. 4 summarizes the results. The fields necessary to initiate the vacuum discharge are plotted as ordinates and the changes in work function as abscissae. These values give the straight line within the precision of the data

[8] Peek, *Dielectric Phenomena* (Van Nostrand, 1929).

which is about 3 percent. Before considering the comparison with the theory, let us consider the consistency of the data themselves. These points do not represent a progressive change from day to day, as the uncontrollable changes of the mercury surface made the location of the points a random process with time. No adjacent points represent data taken on consecutive runs. This rules out any change of a progressive drift due to something else. The manner in which these randomly determined points all fall on the same curve is strong support for the reliability of the results.

When these results are compared with those forecast by the theory of Fowler and Nordheim, we note two differences. The first of these is the marked difference in the order of the fields, those forecast being of the order of $10^7$ volts/cm. This is in agreement with the results of Beams.[4] A possible explanation of this might be a distortion of the mercury either by the field or by mechanical disturbances. The first was prevented by the short time of application of the voltage pulse ($10^{-7}$ sec. time constant) and was checked by applying pulses of different wave fronts. Since any distortion by the field would grow with increased time of application of the voltage, this time was varied and the breakdown measured. For a variation of the time from $10^{-7}$ to $10^{-6}$ sec. there was no observable change in the field necessary for breakdown. A second check was made by putting ripples on the surface of the mercury. A coil containing a loose iron core was placed on the table with the vacuum system and connected to the 60-cycle supply, thus giving the mercury a 120-cycle agitation. The effect of this was to decrease the field needed by about 6 percent for the wave front used in the experiment and somewhat more for the slower waves. The effect under the conditions of the experiment is very close to that calculated for the intensification of the field by the ripple. This would not have been true if irregularities had been present.

The second difference with the theory is in the difference in the influence of the work function. The effect found here for this quantity, while in the same direction, is more than forecast by the Fowler-Nordheim equation. The equation gives a 30 percent change of field for 1 volt variation of work function while the experiment gives about 60 percent change.

We are thus led to the conclusion that, while the work function has a marked effect on the field emission, the theory fails quantitatively to fit the experimental results. To simplify the mathematics a sharp potential barrier at the surface of the metal was assumed—that is, the barrier was represented as a rectangular step, the effect of the external field being assumed to change this to a sort of triangular barrier, the edge of the metal still being represented by a vertical rise. This picture is no doubt too simplified, the actual barrier probably being some sort of irregular affair before the application of the field, and the effect of the applied field penetrating slightly into the metal. Both of these would have the result of increasing the effect of any work function variation on the field emission as was observed.

### Acknowledgments

In conclusion I wish to express my appreciation to Dr. J. W. Beams for guidance and encouragement in the course of the work, and to Dr. C. M. Sparrow for discussions of the results and for aid in computing the effect of the ripples on the mercury. I am also indebted to Mr. D. D. Knowles of the Westinghouse Research Laboratories for the loan of apparatus.

# Interaction of Neutrons with Matter

J. R. DUNNING, G. B. PEGRAM, G. A. FINK AND D. P. MITCHELL, *Pupin Physics Laboratories, Columbia University*

(Received June 8, 1935)

The interaction of fast neutrons with matter has been studied through their transmission out of spheres of various materials. Of the order of 90 percent or more of the collisions with atomic nuclei were found to be approximately elastic, probably around 10 percent of the neutrons which make collisions with nuclei being captured or suffering energy losses which make them undetectable through projected protons. The interaction of "slow" neutrons with matter has been studied largely through the ionizing particles ejected with high efficiency from Li (or B) by slow neutrons, with very sensitive ionization chambers whose inner surfaces are entirely of Li metal, the ionization being detected through amplifier systems using thyratron or photographic oscillograph recorders. The anomalous effects characteristic of slow neutrons, such as high absorption in Cd, are not observable with the lowest energy neutrons detectable through projected protons. The use of a Cd shutter with the Li ion chamber permits separation of fast and slow neutrons effects. Cd is used as shielding against slow neutrons, and serves as effective material for slits to define beams of slow neutrons. The production of slow neutrons through collisions of fast neutrons with H nuclei has been studied by using paraffin, $H_2O$ and $D_2O$. The slow neutron production curve with paraffin and $H_2O$ shows a maximum with spheres of about 10 cm radius and the decrease in the number of slow neutrons emerging from larger spheres is attributed largely to absorption processes such as combination with H to form deuterium. The presence of large numbers of neutrons with energies already below 100,000 e.v. in Rn-Be neutron sources appears necessary to account for this and other effects. Li also detects neutrons having energies intermediate between fast and slow. $H_2O$ is about 5.5 times as effective as $D_2O$ in producing slow neutrons, as determined through the relative enhancement of the artificial radioactivity produced in Ag. The question of thermal equilibrium of slow neutrons was investigated, and in the range from about 95° to 373°K, the change in the number of disintegrations of Li was found to be very small and the change in the absorption of Cd was found to be of the order of 5 percent, the results probably indicating that many of the neutrons approach thermal equilibrium but that these effects are not sensitive functions of the neutron energy in this region. The absorption of Cd for slow neutrons has been found to be very nearly exponential when measured with a reasonably parallel beam of slow neutrons. The neutron-nucleus collision cross sections for fast neutrons lie on a fairly smooth curve, indicating increasing nuclear radii with atomic weight in fair accord with other data, although all the lower atomic weights have about the same cross section for fast neutrons. The neutron-nucleus collision cross section for slow neutrons has been investigated over a wide range of elements with an approximately parallel slow neutron beam, and varies from values which may be slightly smaller than the comparison values for fast neutrons in such cases as Al and S, to values several thousand times larger, in the case of Gd, Sm and Cd, the first two having the largest absorption coefficients for slow neutrons yet measured. Studies of the amount of elastic scattering of slow neutrons from Cd show that, compared to Cu, less than 1 percent of the slow neutrons are elastically scattered, indicating that the large neutron-nucleus cross sections for slow neutrons are due to neutron capture and not elastic scattering. The same appears to be true for other elements of high absorbing power.

## HIGH ENERGY NEUTRONS

THE interaction of fast neutrons, having energy of the order of 1 MEV, with matter has now been studied from a number of standpoints[1, 2, 3, 4, 5, 6, 7] and it appears that most of the phenomena associated with the passage of such neutrons through matter arise from the scattering of the neutrons by elastic collisions with atomic nuclei, rather than from the less frequent capture of neutrons by nuclei. The interaction of fast neutrons with nuclei, expressed in terms of neutron-nucleus collision cross section, gives values for nuclear radii which vary quite smoothly over the range of elements[4, 8] and which agree well with nuclear radii inferred from other types of measurements[9] and from theoretical considerations. The disintegration of various nuclei by neutrons,[10, 11, 12, 13] the dis-

[1] Chadwick, Proc. Roy. Soc. **A136**, 702 (1932); **A142**, 1 (1933), London Conf., Solvay Conf.
[2] Curie-Joliot, J. de phys. et rad. **4**, 21 (1933); **4**, 278 (1933).
[3] Dunning and Pegram, Phys. Rev. **43**, 497 (1933); **43**, 775 (1933).
[4] Dunning, Phys. Rev. **45**, 586 (1934).
[5] Meitner and Phillip, Naturwiss. **21**, 286 (1933).
[6] Bonner, Phys. Rev. **44**, 235 (1933); **45**, 601 (1934).
[7] Dee, Proc. Roy. Soc. **A135**, 727 (1932).
[8] Rabi, Phys. Rev. **43**, 838 (1933).
[9] Pollard, Phys. Rev. **47**, 611 (1935).
[10] Feather, Proc. Roy. Soc. **A141**, 194 (1933); **A142**, 3 (1933); **A142**, 689 (1933).
[11] Harkins, Gans and Newson, Phys. Rev. **43**, 208 (1933); **44**, 945 (1933); Harkins, Phys. Rev. **47**, 702 (1935); **44**, 529 (1933); **46**, 397 (1934).
[12] Kurie, Phys. Rev. **43**, 771 (1933); **47**, 97 (1935); **45**, 904 (1934); **46**, 324 (1934).
[13] Meitner and Phillip, Zeits. f. Physik **87**, 484 (1934).

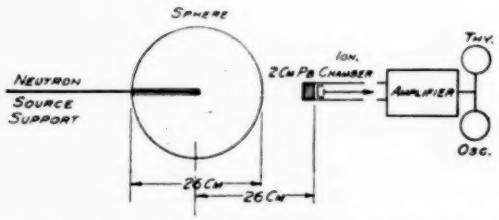


FIG. 1. Apparatus for the measurement of the absorption of fast neutrons in spheres of various materials.

covery by Fermi and his colleagues[14] of artificial radioactivity produced by neutrons, which is well explained as due to the capture of the neutron by the struck nucleus, and the suggestion of possible energy losses by neutrons through noncapture processes,[15, 16, 15a, 15b, 15c] make it desirable to have measurements of the absorption of neutrons as contrasted with scattering.

## ABSORPTION OF FAST NEUTRONS

The amount of actual absorption of high energy neutrons, i.e., capture or large reduction in energy, has been studied[16] by observing the number of detectable neutrons emerging through spheres, surrounding the neutron source, of various materials and graded sizes.

Fig. 1 shows the general experimental arrangement. A Rn-Be neutron source of about 500 mc strength, encased in a platinum container of the form shown, with about 5 mm wall thickness, was placed in the position shown, and surrounded successively by spheres of 3.8, 6.3, 10.2 cm radius, of $H_2O$, C (coal), Al, $SiO_2$ (sand), Cu (shot) and Pb (shot). Spherical shells of about 1 mm thick Cu were used as containers for all except the Al which was solid. The number of neutrons emerging from the various spheres was measured through the number of projected protons (from paraffin front), plus projected nitrogen and oxygen nuclei (from chamber gas), detected in an ionization chamber connected to an amplifier system with thyratron and photographic oscillograph recorders.[16a]

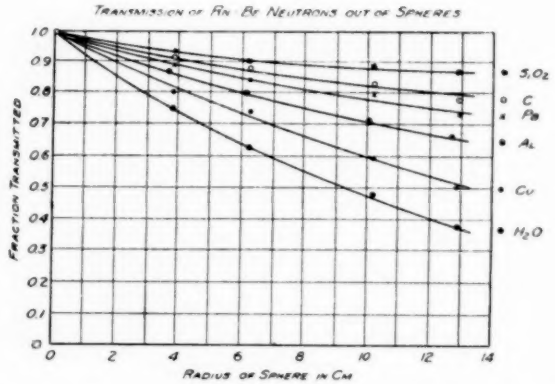


FIG. 2. Transmission of fast neutrons out of spheres of various materials and sizes.

Fig. 2 shows the decreasing number of neutrons detected as the sphere size was increased. If there were no absorption, or some process making the neutrons undetectable through projected nuclei, every neutron would emerge and the number observed with increasing sphere size should be practically constant. The obliquity of neutron paths in the case of larger spheres was not a factor since the chamber was shown in a test experiment to decrease in sensitivity by only a few percent at most when neutrons entered it from the largest angles that are possible in this arrangement.

Two general processes can account for these results: (1) capture of the neutron, and therefore removal from the beam, or (2) loss of energy by the neutrons so that some no longer have sufficient energy to project H, N or O nuclei with detectable ionization. The first process would appear to apply in the case of Al or Si, the neutron capture giving rise to artificial radioactive elements, and this undoubtedly accounts for at least part of the decrease. Capture may also play some part in the case of all the other materials tested, if the production of stable nuclei by fast neutron capture occurs (or perhaps radioactive nuclei of period so long or so short that it has not been observed), or if the reaction ${}_0n^1+{}_1H^1\rightarrow{}_1D^2+\gamma$ occurs, as has been suggested by Lea.[15] Only rather crude estimates can be made of the number of neutrons and the number of radioactive atoms produced in such cases as Al and Si but on the basis of such estimates, to account for the amount of artificial radioactivity observed, the ratio of the probability of capture

[14] Fermi, Amaldi, D'Agostino, Rasetti, Segrè, La Ricerca, Proc. Roy. Soc. **A146**, 483, 34 (1934).
[15] Lea, Nature **133**, 24 (1934); London Conference.
[15a] Fleischmann, Naturwiss. **22**, 839 (1934).
[15b] Auger, Comptes rendus **198**, 365 (1934).
[15c] Kurtchatov, Kurtchatov, Myssowsky, Roussinow, Comptes rendus **200**, 1201 (1935).
[16] J. R. Dunning, G. B. Pegram, G. A. Fink, Phys. Rev. **47**, 325 (1935).
[16a] J. R. Dunning, Rev. Sci. Inst. **5**, 387 (1934).

to the probability of elastic scattering need certainly not be greater than 1 to 10, while theory[16, 17] indicates that the ratio is very much smaller than this.

In regard to the second process, neutrons becoming undetectable through loss of energy, it is obvious that in the case of H particularly, large energy losses will occur in purely elastic collisions, and this undoubtedly accounts for the major part of the reduction with $H_2O$. The loss of energy in elastic collisions must be an appreciable factor even in the cases of C, O and Al. In addition, it may well be that there is some loss of energy through non-elastic nuclear collisions that result in excitation and subsequent gamma-radiation or nuclear rearrangement without neutron capture.[15a] Such evidence as there is[7, 5, 18, 19] indicates that neutron-electron interaction is too small to give a measurable part of the absorption observed in these experiments. A similar statement may be made as to more speculative processes such as neutron disintegration or neutron-neutrino interaction.

From our previous work,[4] we know the approximate mean free path of fast neutrons in the materials of these spheres (for collisions resulting in about 15° mean scattering of the neutrons) and it should be possible to arrive at some value for at least the maximum probability of capture (or large energy loss) per collision. An exact calculation of the probable number of collisions has not been attempted but the tabulation in Table I indicates the minimum possible number of collisions (for neutrons coming nearly straight out) and hence the maximum fraction of the neutrons lost per collision. The figures in the adjacent columns indicate more probable numbers of collisions (perhaps still too low) and hence a more probable value for the ratio of the fractional loss of neutrons to the probable number of collisions made by a single neutron in getting out of the sphere. The estimate of this ratio is if anything too high. This probability of neutron loss per collision is of about the same order of magnitude for each of these materials, around 10 percent and it seems quite certain that at least 90 percent of the collisions of high energy neutrons with these nuclei are approximately elastic.

TABLE I. *Transmission of fast neutrons out of spheres.*

| MATERIAL | FRACTION TRANS. | FRACTION ABS. | RADIUS SPHERE | EXPER. M.F.P. | EST. MIN. NUMBER COLLIS. | EST. NUMBER COLLIS. | MAXIMUM FRACTION ABS./COLL. | ESTIMATED FRACTION ABS./COLL. |
|---|---|---|---|---|---|---|---|---|
| $H_2O$ | .38 | .62 | 12.85 | 5.9 cm | 2.2 | 3.3–4. | 0.28 | 0.19–0.15 |
| C (coal) | .74 | .26 | 12.85 | 14.0 cm | 1.0 | 1.4–1.9 | .26 | .17– .13 |
| $SiO_2$ | .852 | .148 | 12.85 | 30 cm | .43 | .65–1.0 | .32 | .23– .14 |
| Al | .662 | .338 | 12.65 | 6.5 cm | 1.95 | 2.9–4. | .17 | .117–.085 |
| Cu | .55 | .45 | 12.85 | 7.05 | 1.82 | 2.8–3.6 | .22 | .16–.125 |
| Pb | .731 | .269 | 12.85 | 8.85 | 1.46 | 2.2–2.9 | .18 | .12–.092 |

## SLOW NEUTRONS

Fermi and his co-workers[14] observed that neutrons from an ordinary source, such as radon-beryllium, when surrounded by a substance containing hydrogen, such as paraffin or water, show much increased interaction with atomic nuclei, including enhanced production of radioactive atoms, great variation in absorption from element to element, and the immediate disintegration of certain light elements. Since the effect on neutrons of passing through hydrogen is certainly to slow them down, the term slow neutrons is applied to neutrons showing these enhanced interactions with nuclei. The stopping power of cadmium for these slow neutrons is so great that we may approximately describe the slow neutrons as those that do not go through a sheet of cadmium, say half a mm thick. It may be remarked here that the question of whether or not the range of neutron velocity in which cadmium absorption is very high coincides with the velocity range of neutrons showing the other characteristic slow neutron effects will be touched upon later in this paper.

A fundamental question regarding slow neutrons is that of the range of velocities involved. It was readily found that no measurable fraction of the neutrons detected through projected protons showed any anomalous effects characteristic of slow neutrons, such as the increased absorption in Cd, although the sensitivity of the apparatus for slow projected protons was increased to the limit. This would indicate that slow neutrons have much lower energies than could be detected by the projected proton method, i.e., probably well below 100,000 e.v.

[17] (*a*) Wigner, Phys. Rev. **43**, 252 (1933); (*b*) Bethe, Proc. Roy. Soc. **A149**, 176 (1935).
[18] Massey, Proc. Roy. Soc. **A138**, 460 (1932).
[19] N. F. Mott, *Handbuch der Physik*, Vol. **24**, p. 834.

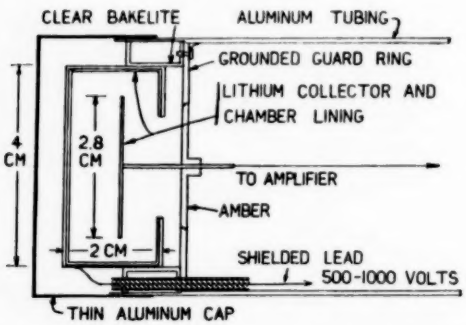


FIG. 3. Lithium ionization chamber for the detection of slow neutrons.

The nuclear transformations produced by slow neutrons resulting in the immediate ejection of heavy particles, as with boron[21] or lithium,[22, 23] which particles can be detected with an ionization chamber and amplifier system, afford for many purposes a more direct and convenient method of studying slow neutrons than the production of artificial radioactivity. We have used chiefly the lithium disintegration, for which the reaction is probably:

$$_3Li^6 + _0n^1 \rightarrow _2He^4 + _1H^3 + K.E.,$$

resulting in two groups of particles of about 1.5 and 5–6 cm range in air, which have the characteristic ionization of alpha-particles and hydrogen nuclei, respectively. This nuclear transformation seems to take place with such high efficiency that practically every slow neutron in traversing a distance of not more than about a mm in Li is captured by a Li nucleus with the formation of a helium and a hydrogen (isotope) nucleus and with an energy liberation of about 2 or 3 MEV.

The earlier experiments discussed in this paper were performed with ionization chambers having a Li front only. In the later work, chambers of the type shown in Fig. 3 have been used, which make use of nearly the full possibilities of Li as a detector, since nearly all the internal surfaces are Li. The external parts of the chamber, with the thin clear Bakelite support, amber insulation, guard ring and thin aluminum shell, are assembled and sealed at the joints with picein or glyptal. The walls and the collector, made of Li metal rolled out to about 0.015 cm thickness (just sufficient to absorb the longest range particles ejected in the reaction) are then put in place, being securely held by a conducting cement, and chamber front sealed up under a $N_2$ or A atmosphere. Since the two particles are ejected in opposite directions,[24, 24b] one particle will usually get into the chamber, if it has enough energy to emerge from the thin Li. Hence practically the whole chamber is effective and the detection efficiency is high. A chamber lined with powdered boron is about equally effective.

A 500 mc, Rn-Be source in a 6 cm radius paraffin sphere 30 cm from the chamber gives about 1600 counts a minute. In contrast as to detection efficiency, a similar paraffin front chamber for detecting fast neutrons from the same source at the same distance gives about 20 counts a minute. Most of the work was done with counting at a much lower rate, such as 200 per minute. The Li walls, of low atomic weight, also reduce gamma-radiation disturbance to a minimum. We estimate that the lithium chamber may detect $\frac{1}{4}$ or more of the slow neutrons falling on it.

Although a Li lined chamber responds most effectively to slow neutrons, it is also affected by higher energy neutrons. Detection with Li makes it comparatively easy to separate out high and low energy neutron effects, by making use of the anomalous absorption of slow neutrons by Cd. As will be seen from the absorption curve of Cd in a later section, the introduction of 0.030 to 0.075 cm of Cd as a shutter in front of the chamber is sufficient to absorb practically all of the slow neutrons which lie within the absorption band of Cd and within the efficient disintegration region of Li. From such a chamber there is always a residual number of counts (about 10 percent) due to higher energy neutrons that have not been entirely slowed down, so that they still have sufficient energy to project nitrogen nuclei from the chamber gas, to project occluded H from the Li, to project Li nuclei directly and, in addition, they may also disintegrate Li nuclei. The residual count left when Cd is interposed is

[21] Amaldi, D'Agostino, Fermi, Pontecorvo, Rosetti, Segrè, Ricerca Scient. V, vol. 1 (1935).
[22] Chadwick and Goldhaber, Nature **135**, 65 (1935).
[23] J. R. Dunning and G. B. Pegram, Phys. Rev. **47**, 640 (1935).
[24] Taylor and Goldhaber, Nature **135**, 341 (1935).
[24b] Kurtchatov, Kurtchatov, Latychev, Comptes rendus **200**, 1199 (1935).

then called the high energy neutron residual component (although it might possibly be that a few of these counts are due to neutrons lying below the Cd absorption region) but in any case the use of Cd permits studying the effects of slow neutrons lying within a fairly definite region. There is some evidence to be noted later that the lithium detection region extends to higher velocities than the Cd absorption region.

As will be shown later, Cd really absorbs practically all the slow neutrons incident, for the number of slow neutrons elastically scattered from it is almost undetectable. Cd thus offers unusual possibilities for defining beams of slow neutrons, since very thin sheets may serve to define slits etc., and it may also be used as shielding against slow neutrons, as is indicated in the accompanying figures of apparatus for the various experiments. A combination of a hydrogen containing material, such as paraffin or water, and a material having a high absorption coefficient for slow neutrons, such as Cd, B, Hg, etc. serves as an effective shield for both high and low energy neutrons. The combination of a paraffin sphere with a canal and defining diaphragms of Cd serves fairly well to collimate a beam of slow neutrons and has been used in a few experiments.

## Production of Slow Neutrons

A number of problems, concerning the initial and final energies of the neutrons, the number of collisions necessary and the combination of slow neutrons with H, C or O arise in considering the production of slow neutrons through the process of allowing fast neutrons to lose energy in collisions with hydrogen nuclei in such substances as water or paraffin.

Fig. 4 shows the experimental arrangement used to investigate some of these questions. A 500 mc Rn-Be source bulb, about 4 mm in diameter with about 0.75 mm lead foil around it, was suspended as far from floor, ceiling, walls or other objects as possible, at 64 cm from the Li lined ionization chamber. This source was then successively surrounded by a series of ten paraffin spheres of sizes up to 23 cm radius, and the number of slow neutrons emerging was measured for each sphere. With a sphere surrounding the

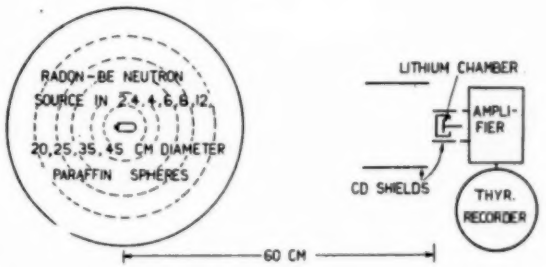


Fig. 4. Arrangement of apparatus to investigate the production of slow neutrons.

source, the number of neutrons detected should be a constant fraction of the number emerging from the sphere, regardless of the size of the sphere. The ionization chamber in the earlier experiments had a Li front only[25] but in the later work an all Li chamber was used.[26] Sheet Cd cylinders 0.040 cm thick were suitably placed to protect the detecting chamber from slow neutrons scattered back from the floor, etc., and from high speed neutrons, which have been scattered back into the chamber as slow neutrons, after being slowed down due to impacts with H in the floors, walls, etc. This latter effect is quite appreciable and may account for some of the artificial radioactivity ascribed to fast neutrons if the experiments are done near wooden table tops, etc. Readings were taken with and without Cd interposed to block the beam of slow neutrons out of the chamber, so as to follow both the change in the number of slow neutrons diffusing out of the spheres and the change in the number of higher energy neutrons emerging which were outside of the Cd effective absorption region.

Fig. 5 shows the observed results. The upper solid curve shows the results without Cd and the lower curve the results with Cd shutter interposed, the intermediate dashed curve being the difference between them, or the "slow" neutron component. For comparison, the lower dashed curve shows the data from Fig. 2, for high energy neutrons emerging from spheres of water, when detected through projected protons.

The number of slow neutrons present in the original beam is apparently zero and until a fairly considerable amount of paraffin surrounds

[25] J. R. Dunning, G. B. Pegram, Phys. Rev. **47**, 640 (1935).
[26] J. R. Dunning, G. B. Pegram, G. A. Fink, D. P. Mitchell, Phys. Rev. **48**, 970 (1935).

the source, the number of slow neutrons produced is still practically zero. After adding a thickness of paraffin sufficient to cause enough neutron-proton collisions to bring the lowest velocity neutrons present in the original source down to the "slow" region, the number of slow neutrons climbs rapidly, reaches a maximum at around 10 cm radius and then drops off quite rapidly as the amount of paraffin is still further increased. Water in thin Cu spherical shells of 10, 12.8 and 17.5 cm radii gave about the same results as paraffin.[25a]

Previous experiments with paraffin samples, using fast neutrons detected through projected protons,[4] show mean free paths in paraffin of the order of 4–5 cm, for collisions with H (or C) which result in scattering of the neutrons through about 15° mean angle. Attempts to measure changes of the neutron MFP in paraffin with lower energy neutrons, by making the detection system favor the lower velocity projected protons, in order to provide some comparison of neutrons above 2 MEV with neutrons of the order of 500,000 e.v. down to the limit of detection (possibly 100,000 e.v.) have failed to show a significant change of MFP in that region. On the other hand, the MFP of slow neutrons in paraffin is of the order of 2 to 3 mm, as shown later. Thus there seems to be a large difference in the neutron-proton interaction at the lowest "fast" neutron energy we can measure with one method, perhaps around 100,000 e.v. and in the "slow" neutron region which may be near thermal energies. Since the lower solid curve in Fig. 5 with the Cd shutter interposed actually shows a slight rise with Li detection for the smaller paraffin spheres, whereas when projected proton detection is used, the number of "fast" neutrons steadily decreases, Li must be detecting some of the neutrons in the intermediate range between fast and slow which are not highly absorbed by Cd. This appears to explain the small angle observed between the tracks of the ejected particles in the experiments of Taylor and Goldhaber.[24] Experiments with these intermediate energy neutrons have been performed by absorbing the slow neutrons in the beam with Cd and then measuring the proton cross section with the high and intermediate energy neutrons remaining. These results indicate a neutron-proton cross section of the order of $7\times10^{-24}$ cm$^2$, and a MFP in paraffin of the order of 8 to 15 mm. The transition to higher neutron-proton cross sections and shorter MFP thus takes place above the Cd absorption range and this factor should considerably increase the slowing down of the neutrons, once they are down in this region.

It hardly seems likely that high energy neutrons, of the order of 2 to 5 MEV with MFP of about 4–5 cm in paraffin could make enough impacts in a sphere of 3 cm radius to become slowed down to thermal velocities, even though the factor mentioned above is operative. However, there seems to be good evidence that in this type of Rn-Be source there are already a large number of neutrons which have energies so low that they can no longer be detected through projected protons.[4] The simplest way to explain the 2 to 1 difference in the number of fast neutrons detected with "forward" and "backward" neutrons in the work mentioned is that half or more of the backward neutrons have energies already too small to detect with this method. The continued rise at the low energy end of the curve in the same paper showing number of projected protons *versus* range also lends point to this view. From this standpoint, the presence

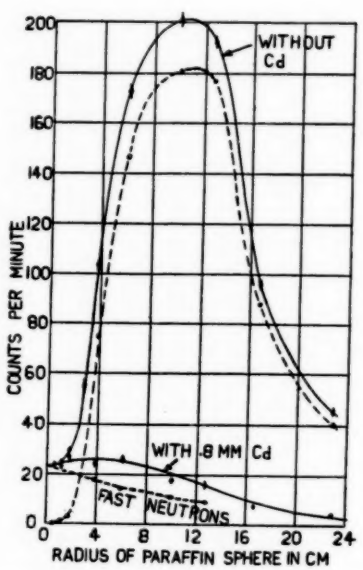


FIG. 5. Production of slow neutrons.

[25a] Westcott and Bjerge, Proc. Camb. Phil. Soc. 145 (1935).

of a considerable number of quite low energy neutrons in the source, whose MFP may already have decreased appreciably, makes it seem reasonable that some of these neutrons can make a sufficient number of collisions in a sphere of 3 cm radius to be brought down into the near thermal region, for Fermi has shown,[14] that the neutrons lose $1/e$ of their energy per collision, on the average. As the sphere size is further increased, more and more of the fast neutrons are of course slowed down and, with a sphere of 12–15 cm radius, most of the higher energy neutrons might be slowed down and the growth curve might simply flatten out, if there were no absorption.

As to the decrease in observed number with the largest spheres, since the chamber showed practically no difference in sensitivity with neutrons coming at it from the largest angles possible with the big sphere, the obliquity of entrance from the sides of the larger spheres is proved unimportant. To account for this decrease two postulates are available; (1) either the neutrons have been dropped in energy below the Li detection region or (2) some process is removing neutrons from the beam. There is no evidence that suggestion (1) is reasonable; from the viewpoint of Bethe's theory this should not be possible. The evidence for (2), however, is not entirely conclusive either. Reactions involving capture of the neutrons such as:

$$_1H^1+{}_0n^1\rightarrow{}_1D^2+\gamma$$

or similar reactions involving $O^{16}$ or $C^{12}$ or their isotopes, might occur.[15] There seems to be no reason for excluding these reactions at present but, since the MFP of the neutron with respect to the H in the paraffin is so small, the number of collisions with H has increased enormously for the two largest spheres and the experiment proves that the probability of capture per collision with protons must be very small. However, it might well account for the decrease. The number of collisions with C or O, from the neutron-nucleus cross section measurements in a following section, is much smaller than with protons and it is not considered likely that these play much part but here, also, the experiment shows that probability of capture cannot be very large, certainly less than 10 percent per collision and, furthermore, O cannot be very much different from C. It may well be that the slowest neutrons are being continually removed from the beam through combination with H, C or O, which might prevent the emerging neutrons from ever reaching a near thermal equilibrium. The more speculative possibilities of the disintegration of the neutron or combination with neutrinos may also deserve some consideration.

## Production of Slow Neutrons by Deuterium

The relative efficiency of $H_2O$ and $D_2O$ in enhancing artificial radioactivity produced by neutrons was studied with the experimental arrangement shown in Fig. 6.[26a]

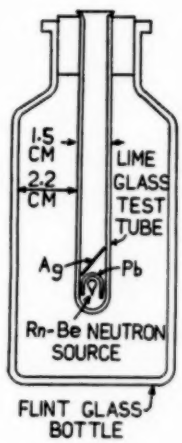


FIG. 6. Apparatus for studying the relative enhancement of artificial radioactivity by $H_2O$ and $D_2O$.

A piece of silver 1.5×2.5 cm by 0.025 cm thick was activated by suspending it above a 200 mc Rn-Be neutron source encased in about 2 mm of lead at the bottom of a thin soft glass test tube, first in an empty 200 cc bottle, next with the bottle filled with 200 cc of $H_2O$ and then with 200 cc of $D_2O$ (99.8 percent), kindly supplied by Professor H. C. Urey. The radioactivity of the silver was tested by placing it under a thin-walled tube counter of Dow metal (Mg alloy), 0.025 mm thick. The data are summarized in Table II. The number per minute in the table is the average number for the first 4 minutes after placing the silver under the counter. Subtracting for the effects of the naturals and the number from the direct beam with nothing but air

[26a] J. R. Dunning, G. B. Pegram, G. A. Fink, D. P. Mitchell, Phys. Rev. **47**, 416 (1935).

TABLE II. *Enhancement of artificial radioactivity by $D_2O$ and $H_2O$.*

| | $H_2O$ | $D_2O$ | Air | Naturals |
|---|---|---|---|---|
| Runs | 5 | 8 | 7 | 21 |
| Number per minute | 107 | 35.2 | 19.3 | 3.7 |
| Net | 103.3 | 31.5 | 15.7 | |
| Enhancement | 87.6 | 15.8 | | |
| Relative effect | 6.5 : 2 : 1 | | | |
| Relative enchancement | 5.5 : 1 | | | |

surrounding the material, the results indicate that $H_2O$ is about 5.5 times as effective as $D_2O$ in enhancing the artificial radioactivity from Ag under these conditions.[27, 28] This enhancement by $D_2O$ is little more than might be expected from the back-scattering of high energy neutrons from any material placed around the source and sample.[29] Since the average energy lost by a neutron in an elastic collision with the deuteron is only slightly (1/8 in the case of direct impact) less than in a proton collison, the comparatively small production of slow neutrons by $D_2O$ must be ascribed to a lower probability of collision, that is a much smaller interaction between neutron and deuteron than between neutron and proton. This accords with absorption results discussed in another section.

## ENERGIES OF SLOW NEUTRONS

The question of whether or not the "slow" neutrons do have approximately thermal velocities is of fundamental importance. Fermi[30] and his colleagues first attacked this problem using hydrocarbon mixtures to slow the neutrons down, and studying the artificial radioactivity produced first at room temperatures, then with the hydrocarbon mixture raised to about 200°C. No significant effects on the properties of the neutrons were observed.

In our experiments[31, 32] we have used the temperature range from liquid air to boiling water in order to get a greater change in energy of the neutrons, if the neutrons are in thermal equilibrium with the hydrogenic materials used to slow them down and we have used the Li chamber detection system.

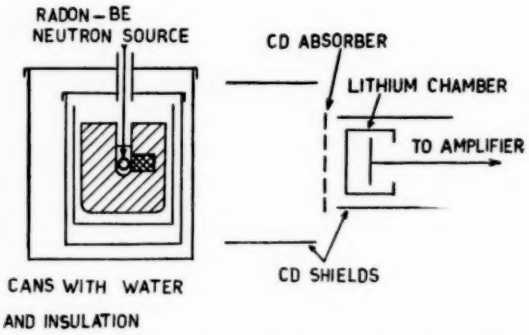


FIG. 7. Apparatus for investigation of the effect of temperature on the properties of slow neutrons.

Fig. 7 shows the general arrangement of the apparatus. The Rn-Be neutron source encased in a platinum container was placed in a cylindrical vessel of water, which was in turn placed inside of several thin concentric polished cans. This permitted cooling the $H_2O$ down to liquid air temperatures, by pouring liquid air over the inner container, and with the insertion of a small electric heater, allowed heating to the boiling point. The temperature was measured with thermocouples. The neutrons, after being slowed down in the water or ice by impacts with the H nuclei, were detected in the usual manner, with a Li lined ionization chamber. Two major groups of runs were made. In the first series, the chamber had a Li front only; in the second group, runs 4 and 5, the chamber walls were entirely of Li, increasing the counting efficiency and reducing the high energy neutron background from 35 to 11 percent. In the first group, runs 1, 2 and 3, the Rn-Be bulb was at the same temperature as the $H_2O$. It was subsequently found, in a separate test listed at the bottom of Table III, that when the bulb alone was cooled, the radon could condense on or near the Be so as to increase the recorded number of neutrons by 3 to 8.6 percent. To eliminate this effect, in runs 4 and 5 the platinum source container was placed inside a small soft glass Dewar with a heater coil and thermocouple attached to it, by which the bulb was held at about room temperature. The inner vessel was of thin Cu with 1100 g of $H_2O$ in

[27] Libby, Long, Latimer, Phys. Rev. **46**, 424 (1935).
[28] Herszfinkill, Rotblat, Zyw, Nature **135**, 654 (1935).
[29] Danyz, Rotblat, Wertenstein, Zyw, Nature **134**, 970 (1934).
[30] Amaldi, D'Agostino, Fermi, Pontecorvo, Rasetti, Segrè, Proc. Roy. Soc. **A149**, 522 (1935).
[31] Dunning, Pegram, Fink and Mitchell, Phys. Rev. **47**, 796 (1935).
[32] Dunning, Pegram, Fink and Mitchell, Phys. Rev. **48**, 888 (1935).

runs 1 and 2. In runs 3, 4 and 5, a larger thin Al vessel containing 3400 g of $H_2O$ was used, in order to bring the number of slow neutrons produced up to about the maximum value. Cd shields were used to reduce room scattering to the detection chamber in the last two runs. In most cases, the $H_2O$ was first frozen and a series of readings taken at about 273°K. The temperature was then lowered to the liquid air point, about 95°K, and the series of readings taken only after the liquid air had almost completely evaporated, small amounts of liquid air being added between readings. Readings were taken at the 273°K point again and the temperature was then raised to near 373°K for a series of readings where loss by evaporation was replaced when necessary.

Table III shows the results of the 5 runs in terms of the percentage change in the observed number of counts (about 65 percent from Li disintegrations in the first group, about 90 percent from Li in the second group) and in the last column, the percentage change in the absorption of Cd as the temperature was lowered from 373°K in the first group and 273°K to about 95°K in the second group. Runs 1 and 2 consisted of about 5000 to 7000 counts on each point; run 3 of about 10,000 to 12,000 counts on each point and runs 4 and 5 of about 12,000 to 20,000 counts on each point. The last two runs are considered the most reliable from all standpoints and the accuracy from the point of view of statistical fluctuations should be better than ±1.5 percent.

In regard to the change in the total number of counts observed at the various temperatures, as shown in column 2, a number of factors must be taken into consideration. The condensation of the radon mentioned previously, which may cause increases of the order of 3 to 8.6 percent, is probably sufficient to explain the increase in the counts, due largely to Li disintegrations, in the first series of 3 runs. As to the apparent decrease in runs 4 and 5, the possibility of a slight amount of frost absorbing some of the neutrons, the possibility of increased absorption of slower neutrons within the walls of the all Li chamber, the possibility of a small amount of liquid air not having evaporated before the beginning of the run or the possibility of increased combination with H in the $H_2O$ at low temperature may be sufficient to explain the apparent decrease. In view of this, we cannot conclude that the emission from Li is definitely increased by the decrease in temperature of the water.

TABLE III. *Change in the number of observed counts (chiefly Li disintegrations) and in the absorption of Cd as the temperature was lowered to about 95°K.*

| RUN | CHANGE IN LI DISINTEGRATIONS | CHANGE IN CD ABSORPTION |
|---|---|---|
| *Source at $H_2O$ temperature, 95°–373°K* | | |
| 1 | +7.8 percent | + 2.6 percent |
| 2 | +4.1 | +10.7 |
| 3 | +8.9 | + 2.7 |
| *Source at constant temperature, $H_2O$ at 95°–273°K* | | |
| 4 | −1.46 percent | + 3.8 percent |
| 5 | −2.8 | + 2.4 |
| *$H_2O$ at constant temperature, source at 95°–273°K* | | |
| | +3 to 8.6 percent | |

The change in the absorption of Cd, as measured by introducing a sheet of about 0.005 cm of Cd (sufficient to absorb about 50 percent of the slow neutrons) is a test of the properties of the neutrons which should be little affected by factors that may change the total number. The results in column 3 of Table IV indicate that "cold" neutrons are slightly more easily absorbed by Cd. While the effect is small, of the order of 5 percent, it is considerably larger than the probable error, and the probability that the apparent consistency of the 5 runs is fortuitous should be very small.

There are a number of interpretations which can be made of these results. (1) No large fraction of these slow neutrons is actually in thermal equilibrium. (2) A considerable fraction of these neutrons may be in thermal equilibrium but the absorption of Cd, and the disintegration of Li, are not sensitive functions of the neutron energy in this region. (3) The removal of the slowest neutrons from the beam by combinations with H or O as suggested before, may keep any large number from emerging with thermal energies. There is likewise the possibility that the Li detection region may not extend down to near zero energy or that the small differences between the Li and Cd regions suggested by the data on the production of slow neutrons may be influencing the results. The fact that the absorption curve of Cd, when measured with a reasonably parallel beam of slow neutrons, is very nearly exponential seems to show that the absorption of

Cd is not a sensitive function of the neutron energy. In experiments such as these, in which a wide range of neutron energies must be present, if the Cd curve is singly exponential, then once the neutrons are below the threshold where abnormal absorption effects set in, the absorption of the slow neutrons will not be a sensitive function of the neutron energy and the temperature effects will be small. If the high absorption by Cd extends up to neutrons well above thermal velocities, say above 0.1 e.v., the shift in the thermal velocities caused by changing the temperature of the water would make little change in the effect of the neutrons.

## Interaction of Slow Neutrons with Matter

The interaction of high energy neutrons, i.e. neutrons which have energies above 100,000 e.v., with atomic nuclei has already been investigated by various methods and as shown previously, most of the phenomena associated with their passage through matter are accounted for by more or less elastic scattering in about 90 percent or more of the nuclear impacts. The variation in neutron-nucleus collision cross section with atomic weight, investigated under fairly good geometrical conditions as discussed in one of our earlier papers[4] is shown in Fig. 8. The variation in cross section for the elements of lower atomic weights, has been studied more carefully and, as the curve shows, H, D, Li, Be and C, all appear to have very nearly the same cross section but beyond this point the heavier elements show cross sections which increase about as the (atomic weight)$^{2/3}$. The nuclear radii, as calculated by Professor Rabi and Mr. Clark from these data, agree quite well with nuclear radii inferred from other types of measurements, if the neutron radius is taken as about $1.2\times 10^{-13}$ cm.

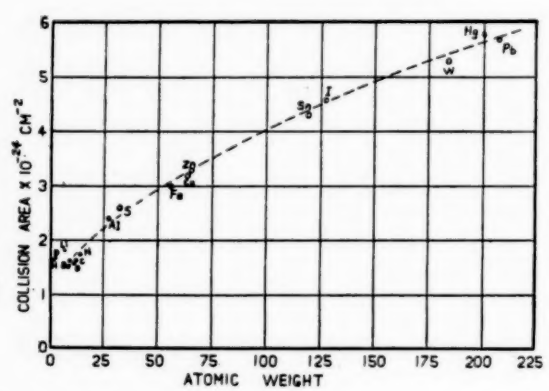


Fig. 8. Neutron-nucleus collision cross sections of the various elements for fast neutrons.

As neutrons are slowed down by impacts with H nuclei, no great differences have been observed as yet in their properties as long as they have sufficient energy to be detected through projected protons, although there may be resonance phenomena which are not observed because of the wide range of energies present. The borderline region where neutrons can no longer be detected through projected protons is not very well defined, being dependent on amplifier sensitivity and disturbances, and the nature of the interaction in this region, but it is probably somewhere in the neighborhood of 100,000 e.v. We have not succeeded in detecting in this energy range any of the effects peculiar to slow neutrons. The region where the effects characteristic of slow neutrons set in is probably far below this region, possibly down to near thermal energies.

It is possible to make some measurements in the intermediate region between fast and slow with Li as a detector but the fast neutron residual component is difficult to allow for.

## Absorption of Cadmium

The remarkably high absorption of slow neutrons in cadmium makes its absorption curve of especial interest. It requires only about 0.005 cm thickness of Cd to absorb 50 percent of the slow neutrons, which is of the order of $\alpha$-particle absorption, although it still requires about 2.5 cm of lead to absorb one-half of the slow neutrons. In earlier experiments,[33] the absorption curve was shown to be very nearly exponential but in those experiments the chamber had a Li front only and the large high energy neutron background made accurate measurements difficult. There was also some question as to the effect of room scattering.

Fig. 11 in the next section shows the general arrangement for a more recent series of measurements. The all Li chamber, with Cd shields to protect against room scattering, was used. Fig. 9 shows the absorption curve for the slow neutrons. As the amount of cadmium interposed is in-

[33] Dunning, Pegram, Fink and Mitchell, Phys. Rev. **47**, 796 (1935).

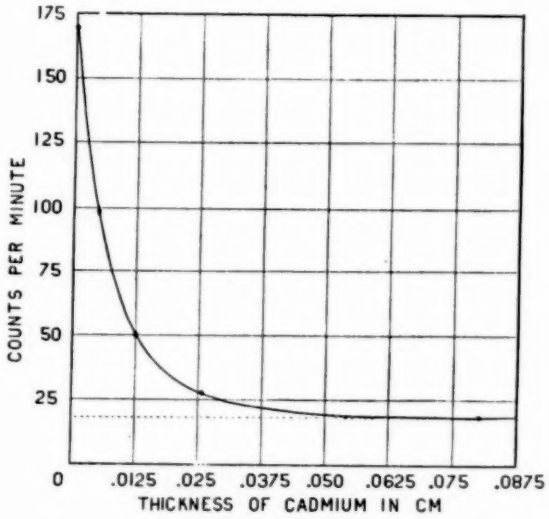


FIG. 9. Absorption of slow neutrons by cadmium.

creased, the number of counts drops off rapidly and the curve flattens out until with about 0.04 cm of Cd it is almost asymptotic, the slope from there on being about what one would expect for high energy neutrons, practically all of the slow neutrons having been absorbed.

Fig. 10 shows the absorption curve plotted on logarithmic scale, with the high energy neutron component subtracted, in order to obtain the absorption of the slow neutrons only. The deviation from a straight line is only a few percent. If the neutron beam were more nearly parallel, the curve should more nearly approach a straight line. Fermi and his collaborators obtained an absorption curve for Cd by using artificial radioactivity as a detector but it was necessary to

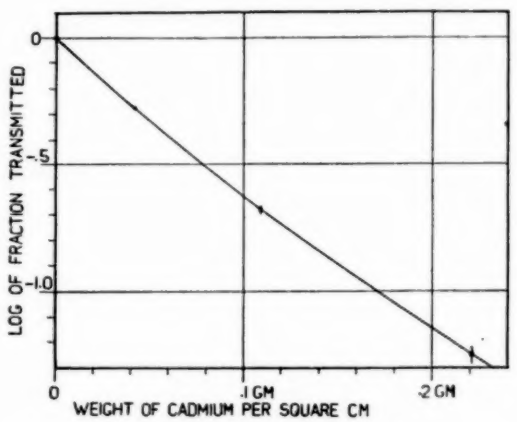


FIG. 10. Absorption of slow neutrons by cadmium-logarithmic plot.

place the Cd and the detector close to the paraffin blocks used to slow down the neutrons.[30] The large number of slow neutrons entering the Cd at oblique angles would naturally show a higher absorption than those entering near the normal and would give a different absorption curve from that obtained with a nearly parallel beam. Fig. 10 indicates that the absorption of Cd for the slow neutrons which disintegrate Li can be closely expressed by a single exponential curve. Considering the wide range of neutron energies undoubtedly present, this must mean that the absorption of Cd is not a sensitive function of the neutron energy in this region. It is not clear how Bethe's theory[24, 35, 36] of the interaction of slow neutrons with nuclei can adequately explain this exponential absorption curve for Cd. There must be some compensating factors not taken into account in the theory which make the absorption more independent of energy than the theory indicates. This absorption curve may also suggest that if these neutrons do have approximately thermal energies, either this abnormal absorption sets in at a quite sharp threshold and does not come in gradually over a wide velocity region, or else that abnormal absorption extends above the main group of slow neutrons so that no large number of the slow neutrons lie within the region where the absorption coefficient varies. Any of these interpretations would indicate that the temperature effect should not be large. One might expect the change in temperature to affect only those neutrons which are responsible for the departure from exponential absorption, or those near the threshold of the abnormal cross section change, if that threshold is quite low. There is always some question as to whether some peculiar characteristic of the Li detection region may not be influencing these results but, except for the indication in Fig. 5 that Li is slightly affected by neutrons which are above the Cd absorption region, Li seems to be entirely satisfactory.

## ABSORPTION OF SLOW NEUTRONS BY VARIOUS ELEMENTS

In order to investigate the neutron-nucleus interaction for slow neutrons over a wide range of

[34] Bethe, Phys. Rev. **47**, 747 (1935).
[35] Perrin and Elsasser, Comptes rendus **200**, 450 (1935).
[36] Beck and Horsley, Phys. Rev. **47**, 510 (1935).

elements, we have made several series of absorption measurements by interposing test samples between source and detector, using the experimental arrangement shown in Fig. 11, for the later measurements. In the earlier measurements[23, 26] the chamber had a Li front only and the source and chamber were unshielded. The necessity for subtracting a large high energy neutron background and the uncertain scattering from the room made these earlier measurements only approximate. The arrangement in Fig. 11 greatly improves the situation. The source and 12 cm diameter paraffin ball are contained in a cylindrical box of Cd, so that slow neutrons emerge in the forward direction only, so as to minimize room scattering, and Cd shields protect the chamber. A Cd diaphragm with a 4 cm hole further defines the beam to the size of the test sample. The neutron beam striking the sample is only approximately parallel but it is much better than can conveniently be used with artificial radioactivity as a detector, with this type of source. Geometrical conditions are very important in determining the cross section values obtained from experiment, as noted in the preceding section. Apparently for this reason our cross section estimates are lower than those of Professor Fermi and his group.

The test samples were cylinders 4 cm in diameter, with the thickness adjusted to give about a 40 percent decrease in the slow neutrons, when interposed. Pure elements were used if available, and in solid form where possible. The powders, finely divided metals, etc. were held in very thin Dow metal (Mg alloy) containers, which have practically no absorption. Where pure elements were not available, the oxides were in general used, since the absorption of O is small and its effect can be allowed for. Since many elements exhibit high cross sections, their presence in small amounts as impurities might seriously affect the results. Practically all the elements tested showed analyses that indicated very little impurity of high cross section elements but analyses were not available for some of the elements tested. Particularly in the case of the rare earths the purity was in most cases uncertain, and since a small admixture of samarium or gadolinium would give a large increase in the absorption a number of the results must be considered rather rough estimates. Where the amount of absorbing material in powdered form necessary to absorb 40 percent is very small, as with gadolinium or samarium, it is difficult to get a very uniform thin layer, and some uncertainty in their large cross sections results from this. The water content of the slightly hygroscopic substances may possibly influence the results somewhat in those cases.

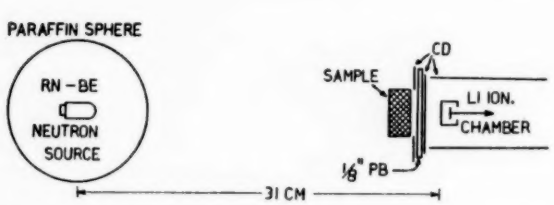


FIG. 11. Experimental arrangement for slow neutron absorption measurements.

A new sample of uranium oxide has given a much lower absorption than a sample previously reported.[32]

In computing these results, it is convenient to express them in terms of neutron-nucleus collision cross section. If $N_0$ is the original number of counts per minute with no absorber and $N$ the number with absorber interposed, then for the fraction transmitted, we have

$$p = N/N_0 = e^{-\lambda/d} \qquad \text{where} \qquad \lambda = 1/N\pi\sigma^2$$

is the mean free path of the neutrons, $d$ is the thickness of the sample, $N$ the number of nuclei per cm$^3$, and $\pi\sigma^2$ is the neutron-nucleus collision cross section, $\sigma$ being the sum of the "radii" of the neutron and of the nucleus. In order to determine the cross section for slow neutrons only, all readings were taken with and without cadmium, in order to eliminate the high energy neutron component. The readings for the high energy neutron components were subtracted to make $N$ and $N_0$ refer to the slow neutrons only. These cross sections have been computed without taking into account the thermal velocities of the neutrons, which would be of significance only if there were a considerable number of neutrons near thermal equilibrium with one of the lighter elements.

Table 4 shows the various elements tested, their atomic weights, the compound used if the element was not feasible, the g/cm$^2$ used, the fraction transmitted, $P$ computed for slow

TABLE IV. *Neutron-nucleus collision cross sections.*

| ELEMENT | ATOMIC NO. | ATOMIC WT. | COMPOUND USED | G/CM² | FRACTION TRANSMITTED $P$ | CROSS SECTION $\times 10^{24}$ CM$^{-2}$ SLOW NEUTRONS | CROSS SECTION $\times 10^{24}$ CM$^{-2}$ FAST NEUTRONS |
|---|---|---|---|---|---|---|---|
| H | 1 | 1.008 | $(CH_2)_n$ | 0.131 | 0.673 | 35 | 1.68 |
| D | 1 | 2.014 | $D_2O$ | 1.36 | .631 | 4.0 | 1.71 |
| Li | 3 | 6.94 | LiF | .24 | .765 | 45 | 1.84 |
| Be | 4 | 9.02 | Be | .703 | .780 | 5.3 | 1.65 |
| B | 5 | 10.82 | $B_4C$ | .0557 | .418 | 360 | 1.60 |
| C | 6 | 12.00 | C | 2.86 | .549 | 4.1 | 1.65 |
| N | 7 | 14.01 | $NaN_3$ | 1.30 | .630 | 11.3 | 1.76 |
| O | 8 | 16.00 | $SiO_2$ | 3.78 | .709 | 3.3 | |
| F | 9 | 19.00 | NaF | 1.94 | .827 | 2.5 | |
| Na | 11 | 23.00 | Na | 1.48 | .847 | 4.2 | |
| Mg | 12 | 24.32 | Mg | 4.67 | .669 | 3.5 | |
| Al | 13 | 26.97 | Al | 7.24 | .788 | 1.5 | 2.4 |
| Si | 14 | 28.06 | Si | 2.23 | .867 | 2.5 | |
| P | 15 | 31.03 | P | 1.69 | .615 | 14.7 | |
| S | 16 | 32.06 | S | 6.6 | .840 | 1.4 | 2.6 |
| Cl | 17 | 35.46 | NaCl | 1.35 | .541 | 39 | |
| K | 19 | 39.10 | K | 1.60 | .816 | 8.2 | |
| Ca | 20 | 40.07 | CaO | 1.87 | .751 | 11.0 | |
| Ti | 22 | 48.1 | $TiO_2$ | 1.97 | .760 | 11.9 | |
| V | 23 | 50.96 | $V_2O_5$ | 2.41 | .751 | 10 | |
| Cr | 24 | 52.01 | Cr | 5.82 | .718 | 4.9 | |
| Mn | 25 | 54.93 | Mn | 3.69 | .558 | 14.3 | |
| Fe | 26 | 55.84 | Fe | 3.87 | .605 | 12.0 | 3.0 |
| Co | 27 | 58.94 | Co | 1.41 | .602 | 35 | |
| Ni | 28 | 58.69 | Ni | 3.03 | .637 | 15.4 | |
| Cu | 29 | 63.57 | Cu | 6.22 | .642 | 7.5 | 3.2 |
| Zn | 30 | 65.38 | Zn | 10.7 | .627 | 4.7 | 3.3 |
| Ge | 32 | 72.60 | $GeO_2$ | .08 | .93 | *est.* 75 | |
| As | 33 | 74.96 | As | 5.28 | .692 | 8.6 | |
| Se | 34 | 79.2 | Se | 3.47 | .606 | 19 | |
| Br | 35 | 79.92 | KBr | 3.43 | .705 | 11.8 | |
| Sr | 38 | 87.63 | $SrCrO_4$ | 2.21 | .832 | *est.* 9 | |
| Y | 39 | 88.9 | $Y_2O_3$ | .18 | .463 | 800 | |
| Zr | 40 | 91 | $ZrO_2$ | 1.87 | .807 | 16.7 | |
| Cb | 41 | 93.1 | $Cb_2O_5$ | 1.01 | .90 | *est.* 14 | |
| Mo | 42 | 96.0 | Mo | 1.70 | .926 | 7.1 | |
| Ru | 44 | 101.7 | Ru | 6.1 | .647 | 12.5 | |
| Rh | 45 | 102.9 | Rh | 0.62 | .664 | 115 | |
| Pd | 46 | 106.7 | Pd | 6.2 | .715 | 10– | |
| Ag | 47 | 107.88 | Ag | 1.88 | .557 | 55 | |
| Cd | 48 | 112.41 | Cd | .0416 | .524 | 3300 | |
| Sn | 50 | 118.70 | Sn | 18.8 | .678 | 4.0 | 4.3 |
| Sb | 51 | 121.77 | Sb | 7.26 | .745 | 8.1 | |
| Te | 52 | 127.5 | Te | 5.52 | .790 | 8.2 | |
| I | 53 | 126.93 | I | 6.78 | .738 | 9.4 | 4.6 |
| Ba | 56 | 137.37 | BaO | .662 | .680 | 140 | |
| La | 57 | 138.90 | $La_2O_3$ | .214 | .933 | 80 | |
| Ce | 58 | 140.25 | $CeO_2$ | .98 | .896 | *est.* 25 | |
| Pr | 59 | 140.9 | $Pr_2O_3$ | 2.43 | .77 | 25 | |
| Nd | 60 | 144.27 | $Nd_2O_3$ | .72 | .559 | 220 | |
| Sm(Sa) | 62 | 150.43 | $Sa_2O_3$ | .04 | .525 | 4700 | |
| Eu | 63 | 152 | Eu-Gd-Al | .02 | .647 | *est.* <1000 | |
| Gd | 64 | 157.6 | $Gd_2O_3$ | .0068 | .590 | 30,000 | |
| Tb | 65 | 159.2 | Tb-Al | .06 | .919 | *est.* <1000 | |
| Dy | 66 | 162.5 | Dy-Al | .27 | .685 | 700 | |
| Ho | 67 | 163.4 | Ho-Al | .144 | .877 | *est.* 400 | |
| Er | 68 | 167.7 | $Er_2O_3$ | .666 | .780 | 120 | |
| Tm | 69 | 169.4 | Tm-Al | .07 | .987 | *est.* 500 | |
| Yb | 70 | 173.6 | $Yb_2O_3$ | .315 | .912 | 90 | |
| Lu | 71 | 175.0 | Lu-Al | .045 | .93 | *est.* 400 | |
| Ta | 73 | 181.5 | Ta | 4.56 | .663 | 27 | |
| W | 74 | 184.0 | W | 7.05 | .592 | 23 | 5.3 |
| Re | 75 | 186.31 | Re | 2.39 | .501 | 89 | |
| Os | 76 | 190.8 | Os | 5.35 | .643 | 27 | |
| Ir | 77 | 193.1 | Ir | .785 | .509 | 285 | |
| Pt | 78 | 195.2 | Pt | 4.30 | .769 | 25 | |
| Au | 79 | 197.2 | Au | 2.52 | .508 | 88 | |
| Hg | 80 | 200.61 | HgO | .545 | .556 | 380 | 5.8 |
| Tl | 81 | 204.39 | Tl | 10.5 | .710 | 11 | |
| Pb | 82 | 207.20 | Pb | 22.7 | .568 | 8.6 | 5.7 |
| Bi | 83 | 209.00 | Bi | 9.07 | .805 | 8.2 | |
| Th | 90 | 232.15 | $ThO_2$ | 2.75 | .772 | 32 | |
| Ur | 92 | 238.17 | $UrO_2$ | 2.52 | .83 | 43 | |

neutrons only, and the values for the slow neutron-nucleus cross section. The slow neutron cross sections vary all the way from values apparently below those for fast neutrons to enormous values in such cases as Cd, Sm and Gd. The samarium and gadolinium samples are probably quite pure. Previous measurements on a sample of terbium, known to contain possibly 40 percent impurities, indicated a cross section of about $6000\times10^{-24}$ cm², but measurements on a terbium-aluminum alloy show a cross section probably less than $1000\times10^{-24}$ cm. Gadolinium as an impurity was doubtless the cause of the high absorption by the earlier sample of terbium. We estimate that in most cases the values given are accurate to within $\pm10$ percent for the smaller cross sections and probably within $\pm25$ percent for the larger values, except in the Cd case, where it should be within $\pm10$ percent. In some cases where only a small amount of material was available or other factors made the result only approximate, the estimated cross sections are labelled "est." A number of the rare earths tested were in the form of alloys with aluminum of which the composition was known to be between 40 and 60 percent aluminum. In the final column, the comparison values for high energy neutrons from the curve in Fig. 8 are included.[33b]

The geometrical conditions were much better for the high energy neutron measurements and the ratio of fast neutron to slow neutron cross section is modified somewhat by this and by the fact that what is measured here is a combination of elastic-scattering cross section, and capture cross section. Either elastic scattering of the neutron by the struck nucleus through a sufficient angle, or capture of the neutron by the struck nucleus, would remove it from the beam. In the high energy neutron case, the cross section computed is almost entirely due to elastic scattering of the neutrons through angles of about 15° or more. In the slow neutron case, however, both elastic scattering and capture play a part. From the evidence in the following section on scattering of slow neutrons, it appears that in cases in which the slow neutron cross section is about the same as that for fast neutrons, elastic scattering plays the major part. For intermediate

[33b] Preiswerk, Comptes rendus **200**, 827 (1935).

cross sections, both elastic scattering and capture are involved, while for the large cross sections, capture seems to be the major factor. Since the neutron must be scattered as much as 30° to be scattered out of the chamber with the geometrical arrangement as in Fig. 11, the small cross section values for slow neutrons, where elastic scattering is the main factor, are a little too small in comparison with the fast neutron values. Some measurements with fast neutrons, using copper spheres and detection through projected protons, indicate that this geometrical factor may be of the order of 1.25, i.e., the smaller cross sections for slow neutrons such as Al and S should be multiplied by about 1.25. Even so, this factor is not sufficient to bring the slow neutron cross section of Al and S up to the value for fast neutrons and, while these correction factors are not certain, it seems that the slow neutron interaction with such nuclei as Al and S is probably less than with fast neutrons. This may be reasonable from Bethe's theory.

The nuclear cross section values for slow neutrons from our earlier data have been tabulated by Bethe.[34] At that time it seemed that, in terms of his theory, a random distribution of phase angles among the various elements might account for the distribution in observed cross section values. Since samarium and gadolinium as well as Cd have now been shown to have enormous cross sections, the point may need to be examined again. The question of whether all or only one of the isotopes of these elements is responsible for the large interaction is not quite clear as yet. Cd has 6 to 9 isotopes, the most abundant of which is 35 percent; Sm has about 7 isotopes, with the most abundant about 25 percent; and gadolinium has probably five isotopes, the most abundant being around 23 percent. If only one of the isotopes in Gd or Sm is responsible, then the cross section of that isotope must be very much larger yet, approximating the size of the K shell of electrons or even larger.

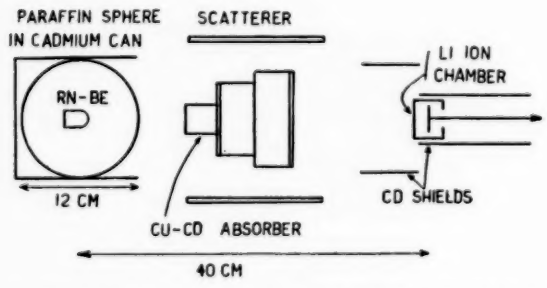


FIG. 12. Experimental arrangement for the measurement of the scattering of slow neutrons.

## CAPTURE AND SCATTERING OF SLOW NEUTRONS

The question of what is actually happening to the neutron in the cases where large neutron-nucleus collision cross sections indicate large interaction between nucleus and neutron is not entirely clear as yet. The work of Fermi has shown that in a number of cases where the cross sections are large, the amount of artificial radioactivity is greatly increased, indicating capture of the neutron, but in other cases such as cadmium where capture is quite certain, the radioactivity is small or absent. The elastic scattering cross section, from Bethe's theory, should be at least as large or larger than the capture cross section. If the neutron is captured, we may expect the production of an immediately unstable combination, such as in the Li or Al cases, resulting in the emission of heavy particles with or without subsequent radioactivity; or we may expect the production of an unstable radioactive isotope of the struck nucleus, with subsequent beta-emission and gamma-emission; or the production of a stable isotope, with gamma-ray emission, as has been indicated in a number of cases.

In order to obtain experimentally an estimate of the ratio of scattering to capture of slow neutrons in the case of cadmium we have made some experiments using the arrangement in Fig. 12. The Rn-Be source with paraffin sphere and chamber are enclosed in Cd to reduce the room scattering, while the direct beam to the chamber of the order of 500 per minute is reduced to about 15 per minute by a Cd disk to eliminate the slow neutrons and by a Cu or paraffin cylinder to reduce the high energy neutrons. The scattering of various materials was then observed by placing them, in cylindrical form in most cases, in the position shown, so that the neutrons could be scattered back into the chamber. The results in Table V show the approximate relative scattering of the various materials. The results are not very

TABLE V. *Scattering of slow neutrons from various materials.*

| Material | No. per min. |
|---|---|
| Background | 16.7 |
| Cu cylinder | 45 |
| Cd cylinder | 14.1 |
| NaCl | 22.3 |
| MgO brick | 43.4 |

exact since the Mg was in brick form, while the NaCl and $CaCO_3$ were in flat form, but these were taken largely as a rough comparison to Cd.

Cd shows so little elastic scattering of slow neutrons that introducing a cylinder of it does not increase the number of neutrons recorded but actually decreases it, since it screens out some of the neutrons scattered back from the floor, etc., into the chamber. It is certain from this experiment that, even though practically every slow neutron incident on the Cd is stopped, only a few percent could possibly be scattered, but the limit is hard to set and the experiment described in the following section was designed to measure this more accurately. NaCl does show some scattering but the scattering is little more than might be expected from the low cross section Na, the high cross section Cl probably absorbing most of the neutrons that fall on it. Cu, $CaCO_3$ and MgO, all of which show rather ordinary cross sections, show quite large elastic scattering. Apparently the large cross sections of various elements are due to capture then, rather than scattering, although from these experiments we cannot express the ratio of scattering to capture very quantitatively.[37]

Fig. 13 shows the arrangement designed to determine the residual elastic scattering of slow neutrons by Cd more accurately. In effect, the experiment is done inside of a cylindrical Cd box to eliminate room scattering and the experiment measures the scattering from the interior walls of the Cd cylinder itself. The direct beam of slow neutrons to the chamber is cut out by a disk of Cd 0.1 cm thick, and the direct fast neutron beam is greatly reduced by some paraffin directly behind the Cd disk. The only slow neutrons that can enter the chamber, then, are those scattered from the walls of the Cd cylindrical box or from the air itself in the box. By interposing a Cd shutter in front of the chamber opening, the slow neutrons scattered from the walls or air are stopped and the decrease measures the number of scattered slow neutrons. A series of measurements (2000 counts total) gave 13.4 per minute as the number of neutrons detected with the shutter removed and 12.7 per minute with the Cd shutter interposed, the difference, 0.7 per minute, representing the number of scattered slow neutrons. This is not much more than the probable error from statistical fluctuations. Had the cylindrical box been made of copper, the number scattered to the detecting chamber would have been about 100 a minute. The elastic scattering of slow neutrons from a sheet of cadmium is then very small, certainly less than 1 percent of the number captured. The neutron-nucleus cross section of Cd as usually computed is therefore to be regarded as a capture cross section and not an elastic collision cross section. Rough experiments with other highly absorbing elements also indicate small scattering.

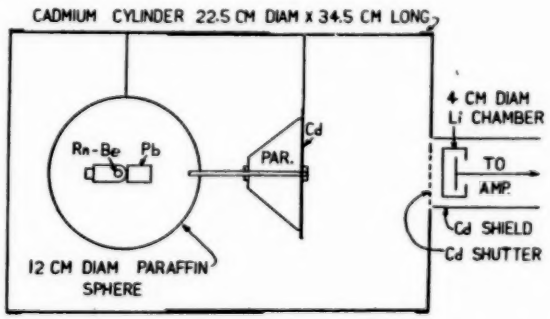


FIG. 13. Arrangement for the measurement of the residual scattering of slow neutrons from cadmium.

We are much indebted to the American Platinum Company for fabricating the platinum and supplying the metals of the platinum group used in these experiments and to Mr. Sigmund Cohn for fabricating the cadmium used in this work. We appreciate very much the cooperation of Mr. J. P. Alexander of the General Electric Company, Mr. J. G. Troxel of the Fansteel Company, our colleagues, Professors H. T. Beans, S. J. Kiehl, P. E. Kerr, Colin G. Fink, V. K. La Mer, E. F. Kern and Dr. G. H. Walden, who have supplied us with a number of elements, Dr. A. F. Daggett who has supplied us with many of the rare earths and Mr. H. H. Goldsmith who has helped with specimens and assistance. The National Lead Company, The Aluminum

[37] Mitchell and Murphy, Phys. Rev. **47**, 812 (1935).

Company of America, The U. S. Metals Refining Company, The Callite Company and The Pennsylvania Glass Sand Corporation have furnished us many of the samples tested. In particular, Dr. J. S. Miner, The Maywood Chemical Company and the Bell Telephone Laboratories, Inc., have supplied us with many rare earth specimens. The International Nickel Company has kindly supplied us with the special magnetic alloys for the moving light beam oscillograph used for photographic recording. Most of all we are indebted to the cooperation of the Memorial Hospital which has supplied the necessary radon for this work, through the helpful interest of Dr. G. Failla, Dr. J. J. Duffy and members of the technical staff of the hospital.

---

AUGUST 1, 1935 PHYSICAL REVIEW VOLUME 48

# Band Spectra of AgO and CuO

F. W. LOOMIS AND T. F. WATSON, *University of Illinois*

(Received June 10, 1935)

Band spectra of AgO and CuO, obtained by arcing between metal electrodes in oxygen at reduced pressure, have been photographed in the first order of a 21-foot grating. An ultraviolet and a blue system of AgO are subjected to vibrational analysis and are attributed respectively to $^2\Sigma \rightarrow {}^2\Sigma$ and $^2\Pi \rightarrow {}^2\Sigma$ transitions, with a common lower state. A third system in the far red was too faint for measurement. It is found that the red system of CuO is due to something more complicated than the $^2\Sigma \rightarrow {}^2\Sigma$ transition attributed to it by Mahanti.

THE arc source previously used[1] for the study of the spectrum of SnO has here been applied to AgO and CuO. It is simply an arc between metal electrodes operating in a stream of oxygen at some 5 cm pressure and has proved to be a rather intense and stable source for oxide spectra.

## Silver Oxide Bands

Hulthén and Zumstein,[2] while studying the spectrum of AgH observed a group of bands near 2600A which they attributed to the AgO molecule. These bands were not found in the present investigation, although three other systems were observed. One of these is in the ultraviolet between 3400 and 3700A and degrades to higher frequencies, a second is in the blue and degrades toward the red, and the third is in the red and degrades in the direction of decreasing frequencies. The bands in the red are of very low intensity and have not been photographed with sufficient dispersion to permit a vibrational assignment. The other two systems have been photographed in the first order of a 21-foot grating with an average dispersion of 1.3A/mm. A vibrational analysis of these two systems has been made and it is found that the frequencies of their heads can be represented by the following expressions:

$$\nu = 28{,}074.6 + \{534.7(v'+\tfrac{1}{2}) - 6.10(v'+\tfrac{1}{2})^2\} - \{493.2(v''+\tfrac{1}{2}) - 4.10(v''+\tfrac{1}{2})^2\}, \quad (1)$$

$$\left.\begin{matrix}\nu = 24{,}139.9 \\ 24{,}310.9\end{matrix}\right\} + 233.0(v'+\tfrac{1}{2}) - \{493.2(v''+\tfrac{1}{2}) - 4.10(v''+\tfrac{1}{2})^2\}. \quad (2)$$

These indicate, of course, that the two systems have a common lower state.

The frequencies and roughly estimated intensities of these bands, together with vibrational quantum assignments and deviations of observed frequencies from those calculated from Eqs. (1) and (2) are given in Tables I and II.

Since the vibrational spacings in the upper and lower states of the ultraviolet system are nearly equal, the bands are grouped into non-overlapping sequences and are comparatively easy to assign.

[1] Loomis and Watson, Phys. Rev. **45**, 805 (1934).
[2] Hulthén and Zumstein, Phys. Rev. **28**, 13 (1926).

TABLE I. *Ultraviolet system of AgO.*

| INTENSITY | $v'$ | $v''$ | FREQUENCY | FREQUENCY OBS.–COMP. |
|---|---|---|---|---|
| 0 | 3 | 1 | 29140.1 | −0.7 |
| 1 | | | 28716.2 | |
| 1 | 5 | 4 | 28693.3 | −1.1 |
| 1 | 4 | 3 | 28680.0 | −1.2 |
| 3 | 3 | 2 | 28662.7 | −1.2 |
| 3 | 2 | 1 | 28643.5 | 0.9 |
| 2 | 1 | 0 | 28615.7 | −1.6 |
| 5 | 1 | 1 | 28133.2<br>(28130.0)* | 0.9 |
| 4 | 0 | 0 | 28093.9 | −0.9 |
| 2 | 2 | 3 | 27698.0 | 0.8 |
| 2 | 1 | 2 | 27655.4<br>(27652.4)* | −0.1 |
| 2 | 0 | 1 | 27610.7<br>(27607.3)* | 0.9 |
| 0 | | | 27229.0 | |
| 0 | 1 | 3 | 27185.3 | −1.6 |

* Some of the bands show a double-headed structure. The frequency of the second head is given in parentheses.

TABLE II. *Blue system of AgO.*

| INTENSITY | $v'$ | $v''$ | FREQUENCY | FREQUENCY OBS.–COMP. | INTENSITY | $v'$ | $v''$ | FREQUENCY | FREQUENCY OBS.–COMP. |
|---|---|---|---|---|---|---|---|---|---|
| 5 | 1 | 0 | 24415.6 | 0.8 | 0 | 1 | 3 | 22982.5 | −1.8 |
| 5 | | | 24243.9 | 0.1 | 2 | | | 22812.0 | −1.0 |
| 4 | 1 | 1 | 23930.7<br>(23930.2)* | 0.9 | 3 | 0 | 3 | 22753.2 | 1.9 |
| 4 | | | 23760.3<br>(23759.6)* | 0.3 | 1 | | | 22580.0 | 0.0 |
| 2 | | | 23518.2 | | 1 | | | 22741.5 | |
| 3 | 1 | 2 | 23451.9<br>(23450.7)* | −1.4 | 2 | 0 | 4 | 22292.0 | 1.0 |
| 2 | | | 23281.7 | −0.6 | 1 | | | 22119.5 | −0.4 |
| 2 | 0 | 2 | 23223.8 | 3.8 | 1 | | | 22134.8 | |
| 2 | | | 23049.5 | 0.5 | 1 | | | 22107.3 | |
| | | | | | 1 | 0 | 5 | 21838.5 | 0.0 |
| | | | | | 1 | | | 21664.0 | −2.0 |

* In bands where double heads were observed due to the isotope effect, the second head has been included in parentheses.

TABLE III. *Intensities of bands of ultraviolet system of AgO as functions of $v'$ and $v''$.*

| $v'$ \ $v''$ | 0 | 1 | 2 | 3 | 4 |
|---|---|---|---|---|---|
| 0 | 4 | 2 | | | |
| 1 | 2 | 5 | 2 | 0 | |
| 2 | | 3 | – | 1 | |
| 3 | | 1 | 3 | – | |
| 4 | | | | 1 | – |
| 5 | | | | | 1 |

TABLE IV. *Intensities of the bands of the blue system of AgO as functions of $v'$ and $v''$.*

| $v'$ \ $v''$ | 0 | 1 | 2 | 3 | 4 | 5 |
|---|---|---|---|---|---|---|
| 0 | – | – | 2 | 1 | 1 | 1 |
| | – | – | 2 | 3 | 2 | 1 |
| 1 | 5 | 4 | 2 | 2 | | |
| | 5 | 4 | 3 | 0 | | |

The estimated intensities of these bands are entered as functions of $v'$ and $v''$ in Table III and, as is to be expected, lie along a narrow Franck-Condon curve.

The bands of the blue system occur in pairs, the bands of each pair being of apparently equal intensity and separated by a constant interval of 171 $cm^{-1}$. This must be the doublet interval of the upper state, since the lower state is common to both systems and no doubling is observed in the ultraviolet system.

The intensity distribution of the bands of the blue system is shown in Table IV. The system terminates abruptly after two $v''$ progressions, presumably indicating predissociation of the upper state for $v' > 1$.

Although the resolution available was inadequate for a rotational analysis of either system, it is possible to ascertain the nature of the states involved by the following argument. A rough approximate calculation, assuming that $\omega/B$ is of the order of 1000 in both states, as is the case with monoxides which have been studied, leads to some 6 $cm^{-1}$ for the order of magnitude of the separation between heads and origins of the bands of the ultraviolet system. If $Q$ heads were present at anything like this separation from the $P$ heads, they should be clearly visible, but they are not. Moreover, in two favorably situated bands, the dip in intensity corresponding to the origin can actually be seen at about the expected location. It may be concluded that the ultraviolet system is a $\Sigma - \Sigma$ transition. A similar calculation shows that one would not expect to be able to resolve the $R$ and $Q$ heads of the blue system.

Hence the fact that $Q$ heads are not observed in that system either is not in contradiction with the conclusion, drawn from the occurrence of pairs of bands of equal intensity, that the upper state of that system is a doublet with $\Lambda > 0$. Hence from the rule that $\Delta\Lambda = \pm 1$ or 0 and the assumption that these strong systems are not likely to be transitions between states of different multiplicity one may deduce that the blue system is $^2\Pi \rightarrow {}^2\Sigma$ and the ultraviolet system $^2\Sigma \rightarrow {}^2\Sigma$.

According to Aston,[3] silver has two isotopes of masses 107 and 109 in nearly equal abundance. The bands of the ultraviolet system are all so near the system origin that the calculated isotope effect is small, and the effect was in fact not observed. In the blue system, however, certain favorably situated bands were observed to have a double-headed structure, with separations which agree, within the accuracy of measurement, with those calculated from the usual expressions for the vibrational isotope effect. This observation serves to confirm the vibrational assignment and the identification of the emitting molecule.

### Copper Oxide Bands

Incidentally to the above, we have taken occasion to photograph the red bands of CuO in the oxygen arc. These bands have often been observed[4] in various flame and arc sources. In 1930 Mahanti[5] published a note on them, attributing them to a $^2\Sigma \rightarrow {}^2\Sigma$ transition, with vibrational intervals of 620 and 345 $cm^{-1}$. Our 21-foot grating measurements of the frequencies of the heads, and sub-heads, of these bands can indeed be fitted into Mahanti's scheme, with only slightly different constants, but when this is done it appears that the two halves of the so-called doublet have obviously very different intensities. The bands are degraded to the red and the fainter heads are 40 $cm^{-1}$ to the violet of the stronger ones. It seems to us more likely that these fainter heads belong to satellite branches and hence that the transition is something more complicated than $^2\Sigma \rightarrow {}^2\Sigma$. Other vibrational arrangements than Mahanti's also appear to be possible, including one with a doublet interval about 275 $cm^{-1}$, if one is willing to assume slight variation from band to band of the separation between heads and origins. It seems unlikely that the matter can be cleared up without a rotational analysis, which promises to be difficult.

[3] Aston, *Mass Spectra and Isotopes* (1933).

[4] Hertenstein, Zeits. Wiss. Phot. **11**, 69, 119 (1912); Eder and Valenta, *Atlas Typischer Spectren* (1924); Mulliken, Phys. Rev. **26**, 1 (1925).

[5] Mahanti, Nature **125**, 819 (1930).

# LETTERS TO THE EDITOR

*Prompt publication of brief reports of important discoveries in physics may be secured by addressing them to this department. Closing dates for this department are, for the first issue of the month, the twentieth of the preceding month; for the second issue, the fifth of the month. The Board of Editors does not hold itself responsible for the opinions expressed by the correspondents.*

## Evidence for the Existence of an Isotope of Potassium of Mass 40

Recently Klemperer[1] and Newman and Walke[2] have suggested that the facts about the radioactivity of potassium could best be correlated by assuming the existence of a rare radioactive isotope of potassium of mass 40. There was no direct evidence for this isotope and Bainbridge[3] had estimated that if such an isotope existed the ratio of its abundance to that of $K^{39}$ must be less than 1/300. It occurred to me that with the mass spectrograph at my disposal it would be possible either to detect such an isotope or to set a much lower limit on its abundance ratio.

The mass spectrograph used by Tate and Smith[4] has been rebuilt to give greater resolving power. One of the vacuum tube amplifiers described by Distad and Williams[5] was used to measure the analyzed positive ion current.

The potassium was prepared by heating KCl with metallic Ca. It was repeatedly distilled before being introduced into the spectrograph.

Fig. 1 shows the interesting portion of one of many mass spectrographic analyses of the region around $m/e=40$. As may be seen there is a very definite peak due to an ion with an $m/e$ value of 40. The rising portions on either side of this peak are the feet of the very much larger peaks due to $K^{39}$ and $K^{41}$. The sensitivity and resolving power of the spectrograph is indicated by the fact that if these latter peaks were plotted on the same scale as Fig. 1 they would have heights of 44,300 and 3190 units, respectively.

The average value of the ratio of the height of the peak due to the ion at 40 to that of the peak due to $K^{39}$ is 1/8600 with a probable error of approximately 10 percent. The ratio of the heights of the peaks due to $K^{39}$ and $K^{41}$ is $13.96\pm0.1$ which agrees well with the abundance ratio of $K^{39}/K^{41}=13.88\pm0.4$ given by Brewer and Kueck.[6]

There remains the problem of identifying the ion at $m/e=40$. The following considerations lead definitely to the conclusion that it is a rare isotope of potassium, $K^{40}$.

**1.** By varying the potential applied to the electrons producing the ion in question its ionization potential was directly compared to that of $K^{41}$. Fig. 2 shows the results. The ionization potential of the ion at 40 is the same as that of potassium (4.32 volts) with an uncertainty which appears to be less than 0.5 volt. Consequently the ion at 40 cannot be due to any element or compound the ionization potential of which is greater than 5 volts. In particular it cannot be $Ca^{40}$ or $A^{40}$. The possibility that it might be $Ca^{40}$ was given particular consideration because of the method of preparing the potassium and because Ca might come from the heated glass walls, although calculation showed that the vapor pressure of Ca would be too low at the temperatures used to account for the magnitude of the peak observed.

**2.** The ratio of the heights of the peaks at 39, 40 and 41 remained constant, within experimental error, over a sixfold variation of the pressure of potassium vapor.

**3.** At electron energies of about 100 volts, peaks were found at $m/e$ values of $19\frac{1}{2}$, 20 and $20\frac{1}{2}$ corresponding to $K^{++}$. The ratios of their heights were the same, within experimental error, as for the singly charged ions.

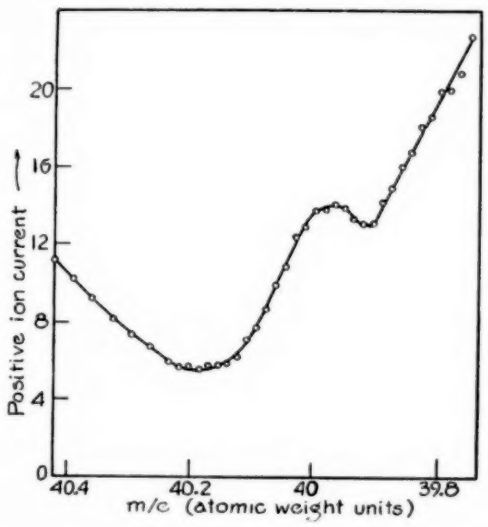


FIG. 1. Typical mass spectrographic analysis of region around mass 40. Potassium vapor in tube, 8.4 volts applied to electrons. Height of peak at 39, 44,300; at 41, 3190 units.

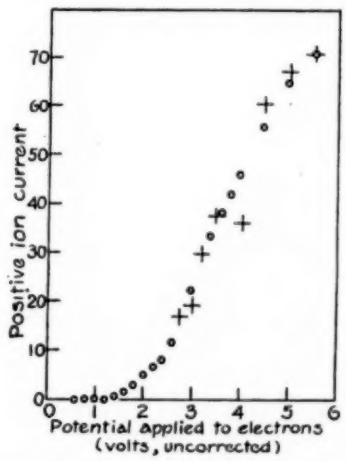


FIG. 2. Comparison of ionization efficiency curves for $K^{41}$ (circles) and ion of mass 40 (crosses). The points at potential 5.5 volts are made to coincide.

**4**. Na was present as an impurity. Because of the slight chance that the ion at 40 might be $(NaOH)^+$ a search was made at 56 and 58 for $(KOH)^+$. No trace was found.

**5**. If the peak at 40 were due to $K^{39}H$ a corresponding one at 42 due to $K^{41}H$ should have been present in abundance 1/14 as great. None was present in abundance greater than 1/150,000 of $K^{39}$. Neither $(H_2O)^+$ nor $H_2^+$ could be detected in the tube.

**6**. At the higher pressures peaks were found at masses 78 and 80 corresponding to $(K^{39}K^{39})^+$ and $(K^{39}K^{41})^+$. The peak at 40 could not, however, be due to $(K^{39}K^{41})^{++}$ because at the lower pressures the peak at 80 disappeared completely, as it should, while that at 40 remained.

It is estimated that the apparatus had sufficient sensitivity and resolving power to detect a peak at 40 of magnitude 1/45,000 compared to $K^{39}$. In the region of masses 42 and 43 there is less background than at 40. One can safely say that $K^{42}$ and $K^{43}$, if present, were each present in abundance less than 1/150,000 relative to $K^{39}$.

I wish to express my appreciation to Professor John T. Tate for his valuable suggestions and interest in this work.

ALFRED O. NIER

Department of Physics,
University of Minnesota,
July 15, 1935.

[1] Klemperer, Proc. Roy. Soc. **A148**, 638 (1935).
[2] Newman and Walke, Phil. Mag. **19**, 767 (1935).
[3] Bainbridge, J. Frank. Inst. **212**, 338 (1931).
[4] Tate and Smith, Phys. Rev. **46**, 773 (1934).
[5] Distad and Williams, Rev. Sci. Inst. **5**, 289 (1934).
[6] Brewer and Kueck, Phys. Rev. **46**, 894 (1934).

---

## Remarks on the Theory of Protons and Neutrons

In a recent paper[1] the author attempted to write the equations of the proton and the neutron (considered as two quantum states of one heavy particle) in close analogy with Dirac's equations for the electron and Pauli's equations for the neutron.[2] Eight values of the spin-variable were used and two additional terms in the Hamilton-operator were introduced. These latter represented (1) the interaction of the tensor of the electromagnetic field with the electric and magnetic moment of the particle and (2) the interaction of the heavy particle with the quantized field of electrons and neutrinos. (This second interaction is analogous to that introduced by Fermi[3] in his theory of $\beta$-rays.)

We write:

$$(p_0 - H/c)\psi = 0,$$

where

$$H = H_{PN} + H' \tag{1}$$

and $H_{PN}$ is the Hamilton-operator of the heavy particle:

$$\frac{1}{c}H_{PN} = \frac{e}{c}A_0\gamma - \alpha_4 Mc - \Sigma\alpha_k\left(p_k - \frac{e}{c}A_k\gamma\right) - \frac{e\hbar}{Mc}\Sigma\epsilon_{kl}\frac{\partial A_l e}{\partial x_k}. \tag{2}$$

Here $\epsilon_{kl}$ represents the components of the antisymmetrical tensor of the magnetic and electric moment of the heavy particle: $\epsilon_{23} = i\alpha_2\alpha_3\alpha_4\cdots$, $\epsilon_{01} = i\alpha_1\alpha_4\cdots$. $\gamma$ is a matrix introduced in our previous paper in such a manner that the potentials $A_k$ do not appear in the equations for a neutron. $H'$ represents the interaction between the heavy particle and the electrons and neutrinos. It must be written so that the conservation laws of the energy and of the spin are respected; that is, every transition of a neutron into a proton must be accompanied by the emission of an electron and a neutrino (as by Fermi[3]). In the present paper we remark that the values of the magnetic moment of the proton ($3e\hbar/2Mc$) and of the neutron ($2e\hbar/2Mc$), which we obtain from (2) by introducing only one numerical factor $e\hbar/Mc$ (as a coefficient of $\epsilon_{kl}$), are both in a satisfactory agreement with the values recently deduced by G. Kruger (2.7 and 1.75 nuclear magnetons) and with the measurements of the magnetic moment of the proton.

It seems also noteworthy that the interaction of the heavy particles with the electrons (represented, for instance, by the Dirac "density matrix") and neutrinos makes it possible to understand the oriign of the exchange forces between the proton and the neutron (considered by Heisenberg and E. Majorona).

A more detailed account of this question will be published shortly.

G. WATAGHIN

University of San Paulo (Brazil),
Department of Physics,
July 22, 1935.

[1] Lincei R. (in press).
[2] J. F. Carlson and J. R. Oppenheimer, Phys. Rev. **41**, 63 (1932).
[3] Fermi, Zeits. f. Physik **88**, 162 (1934).

---

## The Relation Between Internuclear Distances and the Force Constants of Diatomic Molecules

Some time ago the writer called attention to the close relation, in diatomic molecules, between the internuclear distance, $r_e$, and the "bond force constant," $k_e$ (defined as $d^2V/dr^2$ at the equilibrium separation) and proposed an equation expressing this relation,[1] which may be written as follows:

$$r_e = (C/k_e)^1 + d_{ij}. \qquad \text{Relation I.}$$

This equation gives satisfactory agreement with experimental data if $C$ is taken as a universal constant and $d_{ij}$ is constant for all molecules made up of two atoms found in the $i$th and $j$th *rows* of the periodic table, respectively.

The writer has recently observed another relationship which may be expressed in an equation of just the same form:

$$r_e = (C_{mn}/k_e)^1 + d_{mn}. \qquad \text{Relation II.}$$

In this case $d_{mn}$ and $C_{mn}$ are constant for the analogous electronic states of all molecules made up of two atoms found in the $m$th and $n$th *groups* of the periodic system, respectively. In other words a given pair of constants will fit the ground states, for example, of all molecules in such a set as $Cl_2$, $Br_2$, IBr, ICl and $I_2$; or CO, SiO, CS, TiO and PbO. Relation II gives even more satisfactory agreement

TABLE I. *Test of Relation II.*

| MOLCULE | $r_e$ (obs.) | $r_e$ (calc.) | CONSTANTS OBTAINED FROM DATA ON |
|---|---|---|---|
| ICl | 2.310A | 2.31A | $Cl_2$ and $I_2$ |
| $PF_2$ | 2.28 | 2.28 | " " " |
| PN | 1.487 | 1.50 | $N_2$ and $P_2$ |
| SO | 1.489 | 1.47 | $O_2$ and $S_2$ |
| HCl | 1.272 | 1.26 | HF and HBr |
| HI | 1.600 | 1.60 | " " " |
| SiO | 1.505 | 1.48 | CO and TiO |
| CS | 1.53 | 1.52 | " " " |
| PbO | 1.918 | 1.91 | " " " |

with experiment than Relation I, as may be seen from Table I in which, for the ground states of several molecules, the observed $r_e$ is compared with the value calculated from $k_e$ (obtained from vibrational data) with the use of constants determined from the data on two other similar molecules.

Because of lack of data Relation II can at present only be well tested for the ground states of molecules, but there is an indication that it also applies, but with different values of the constants, to analogous excited states of molecules within sets of the type described, and may possibly be a test as to whether excited states of two molecules are similar or not.

It is interesting to note that in case the constants $d_{ij}$, $d_{HR}$ and $C_{mn}$ can be determined from other molecules, it is possible by means of the two relations together to predict both $r_e$ and $k_e$ for molecules for which no data at all exist.

RICHARD M. BADGER

Gates Chemical Laboratory,
California Institute of Technology,
June 22, 1935.

[1] R. M. Badger, J. Chem. Phys. **2**, 128 (1934).

# THE AMERICAN INSTITUTE OF PHYSICS

INCORPORATED


## GOVERNING BOARD

*For The American Physical Society:*

KARL T. COMPTON, *Chairman*
Massachusetts Institute of Technology

GEORGE B. PEGRAM, *Secretary*
Columbia University

JOHN T. TATE
University of Minnesota

*For The Optical Society of America:*

E. C. CRITTENDEN
Bureau of Standards

PAUL D. FOOTE
The Gulf Companies

F. K. RICHTMYER
Cornell University

*For The Acoustical Society of America:*

HARVEY FLETCHER
Bell Telephone Laboratories

VERN O. KNUDSEN
University of California at Los Angeles

WALLACE WATERFALL
The Celotex Company

*For The Society of Rheology:*

E. C. BINGHAM
Lafayette College

A. STUART HUNTER
du Pont Rayon Company

S. E. SHEPPARD
Eastman Kodak Company

*For The American Association of Physics Teachers:*

HOMER L. DODGE
University of Oklahoma

PAUL E. KLOPSTEG
Central Scientific Company

FREDERIC PALMER
Haverford College



## ADMINISTRATIVE STAFF

HENRY A. BARTON, *Director* JOHN T. TATE, *Adviser on Publications*

MADELINE M. MITCHELL, *Editorial Secretary*

*Office:* 11 East 38th Street, New York, New York


---

## JOURNALS

### THE PHYSICAL REVIEW

### REVIEWS OF MODERN PHYSICS

### PHYSICS

JOHN T. TATE, *Editor*
J. W. BUCHTA, *Assistant Editor*
E. C. BINGHAM, *Rheology Editor*

### THE JOURNAL OF THE OPTICAL SOCIETY OF AMERICA

### THE REVIEW OF SCIENTIFIC INSTRUMENTS WITH PHYSICS NEWS AND VIEWS

F. K. RICHTMYER, *Editor*

### JOURNAL OF THE ACOUSTICAL SOCIETY OF AMERICA

F. R. WATSON, *Editor*

### THE JOURNAL OF CHEMICAL PHYSICS

HAROLD C. UREY, *Editor*

### THE AMERICAN PHYSICS TEACHER

DUANE ROLLER, *Editor*

The American Institute of Physics is a membership corporation of which five societies are the founding members. These five societies are the principal national societies devoted to pure and applied physics in America. Their names, and those of their representatives who form the Governing Board of the Institute, are given above. The principal work of the Institute is the publication of journals sponsored by the societies or by itself. The names and the editors of the journals are also listed above.

The broad purpose of the Institute is to represent, in all matters of wide or common interest, the five thousand or more members and subscribers associated with the Founder Societies and the journals. It aims to advance the science and profession of physics, and to promote cooperation between pure research, the applied sciences and the industries. To achieve these aims, it is greatly in need of an endowment and is empowered by law to administer grants and funds of any kind.

# CONTENTS

PHYS. REV. 48 (1935) AUGUST 1

Radioactivity of the Earth's Crust and Its Influence on Cosmic-Ray Electroscope Observations Made Near Ground Level. . . . . ROBLEY D. EVANS AND RUSSELL W. RAITT 171

Ionization Currents Produced by Radon, RaA and RaC′ in Cylindrical Ionization Chambers . . . . . ROBLEY D. EVANS 177

Double Electron Transitions in X-Ray Spectra . . . . . F. BLOCH 187

Size and Arrangement of Bismuth Microcrystals Formed from Vapor . . . . . C. T. LANE 193

Dilatations in Rochelle Salt . . . . . IRWIN VIGNESS 198

Radiative Capture of Protons by Carbon . . . G. BREIT AND F. L. YOST 203

Formation of Electron-Positron Pairs by Internal Conversion of $\gamma$-Radiation . . . . . MORRIS E. ROSE AND GEORGE E. UHLENBECK 211

Spectrum of Molybdenum V . . . . . M. W. TRAWICK 223

Hyperfine Structure of the Mercury Triplet $6^1P_{012}-7^3S_1$ in Optical Excitation . . . . . EMILY E. BOGGS AND HAROLD W. WEBB 226

Hyperfine Structure in Silver . . . . . HARRY HILL 233

Electro-Optical Kerr Effect in Ammonia, Nitrogen and Oxygen . . . . . WILLIAM M. BREAZEALE 237

Production and Focusing of Intense Positive Ion Beams . . . . . M. A. TUVE, O. DAHL AND L. R. HAFSTAD 241

Variation with Magnetic Field and Temperature of the Thermoelectric Properties of Ferromagnetics . F. E. LOWANCE AND F. WOODBRIDGE CONSTANT 257

Relation Between the Electron Field Emission and the Work Function of Liquid Mercury. . . . . L. R. QUARLES 260

Interaction of Neutrons with Matter . . . . . J. R. DUNNING, G. B. PEGRAM, G. A. FINK AND D. P. MITCHELL 265

Band Spectra of AgO and CuO . . . F. W. LOOMIS AND T. F. WATSON 280

Letters to the Editor:

Evidence for the Existence of an Isotope of Potassium of Mass 40. . . . . ALFRED O. NIER 283

Remarks on the Theory of Protons and Neutrons. . . . . G. WATAGHIN 284

Relation Between Internuclear Distances and the Force Constants of Diatomic Molecules. . . . . RICHARD M. BADGER 284

LANCASTER PRESS INC., LANCASTER, PA.